SUPERCONDUCTIVITY, HIGH TEMPERATURE SUPERCONDUCTIVITY

On competition between *s*- and *d*-symmetry types of the order parameter in high-temperature superconductors

È. A. Pashitskiĭ, V. I. Pentegov, and A. V. Semenov

*Institute of Physics, National Academy of Sciences of the Ukraine, 252650 Kiev, Ukraine**
(Submitted August 19, 1996; revised October 21, 1996)
Fiz. Nizk. Temp. **23**, 140–145 (February 1997)

It is shown that strong anisotropy of the quasi-two-dimensional electron spectrum in high-temperature superconductors and the competition between attraction and repulsion in the electron–electron interaction can lead either to anisotropic *s*-, or *d*-type of Cooper pairing depending on the system parameters. In the case when attraction prevails on the entire Fermi surface (e.g., due to electron–phonon interaction), the s_{xy}- or s^*-symmetry in the superconducting order parameter is advantageous from the energy point of view. At the same time, the $d_{x^2-y^2}$-symmetry of the gap is observed in the case of repulsion in the entire Brillouin zone (which is typical, for example, of the electron–magnon interaction) as well as in the case of effective attraction on the regions of Fermi surface with the maximum density of states. In the latter case, the superconducting transition temperature T_c is always higher than in the former case, indicating the important role of additional attraction in the mechanism of high-temperature superconductivity. © *1997 American Institute of Physics.* [S1063-777X(97)00202-8]

1. Experimental data on the observation of spontaneous Josephson currents in SQUID-type systems with two tunnel junctions at mutually perpendicular faces of Y(123) single crystals[1–3] as well as the generation of half-integral magnetic flux quanta observed in superconducting (SC) rings made of Y(123) and Bi(2212) films with an odd number of weak links[4,5] speak in favor of the $d_{x^2-y^2}$-type symmetry in the SC order parameter $\Delta_d(\mathbf{k})\sim(\cos k_x-\cos k_y)$ in high-temperature superconductors. New results of experiments on photoelectron spectroscopy with angular resolution (ARPES method), which were reported recently,[6,7] refute previous conclusions drawn by these authors[8–10] on the s_{xy}-type symmetry of $\Delta_s(\mathbf{k})\sim\cos k_x \cos k_y$ and confirm the $d_{x^2-y^2}$-symmetry in Bi(2212) single crystals.

It should be emphasized, however, that the $d_{x^2-y^2}$-symmetry of the SC gap does not indicate unambiguously a specific mechanism of Cooper pairing of charge carriers. For example, it cannot serve as a proof of the magnon mechanism of high-temperature superconductivity (HTS) due to exchange by virtual quanta of collective spin-density excitations (by paramagnons) in a nearly antiferromagnetic Fermi liquid, in which the electron–electron repulsion prevails in the entire volume of the Brillouin zone (BZ).

In this paper, we prove that a strong anisotropy of the quasi-two-dimensional electron spectrum in high-temperature superconductors[14,15] combined with a competition between the attraction (e.g., due to the electron–phonon interaction (EPI) and repulsion of the Coulomb or magnon origin) can lead either to the anisotropic *s*-, or the *d*-type of Cooper pairing depending on the electron–electron interaction constants. In the case of prevailing attraction on the entire Fermi surface (FS), the s_{xy} symmetry in the superconducting order parameter or the s^*-symmetry of $\Delta_s(\mathbf{k})\sim(\cos k_x+\cos k_y)$ is advantageous from the energy point of view. At the same time, the $d_{x^2-y^2}$-symmetry of the gap is observed in the case of repulsion in the entire volume of the BZ as well as in the case of effective attraction on the FS regions with the maximum density of states (DS). In the latter case, the superconducting transition temperature T_c is always higher than in the former case, indicating the important role of additional attraction in the HTS mechanism.

2. It was proved in Refs. 16 and 17 that the strong hybridization of overlapping wide and anomalously narrow $2D$ energy bands in the electron spectrum of a layered crystal leads to the formation of extended saddle regions which were observed in ARPES experiments with a high energy resolution.[14,15] As a result, the anisotropic cylindrical FS splits into four pairs of ''electron'' regions and four ''hole'' regions in the case when the Fermi level (FL) lies above the bottom of the saddles (see Fig. 1). The curvature $\partial^2E/\partial k_\perp^2$ of the spectrum in these regions (the ''transverse'' effective mass) is accordingly positive or negative.[1)] It is important for further analysis that these regions have essentially different densities of states and characteristic energy scales (see below). In this case, the DS on quasi-one-dimensional (flat) ''electron'' regions has a Van Hove root singularity, which might facilitate the enhancement of the electron–electron interaction and elevate the superconducting transition temperature T_c.[15,18]

It should be noted that the presence of an anomalously narrow band with a high DS near the FL facilitates the emergence of the electron–plasmon interaction (EPI) due to ex-

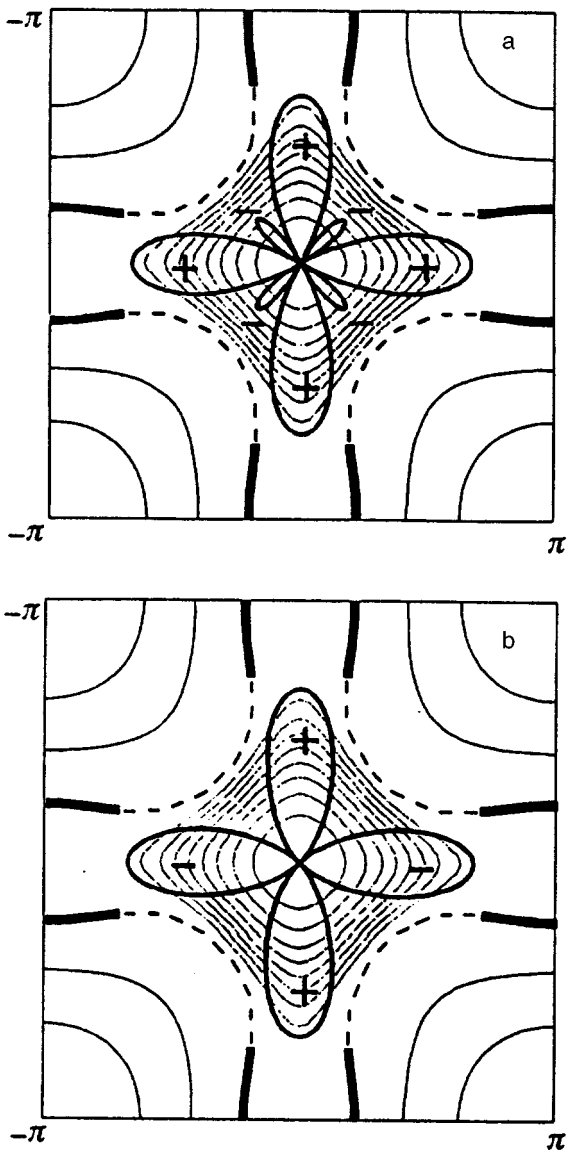

FIG. 1. (a) The structure of an anisotropic superconducting gap in the case of the s_{xy}-symmetry of the order parameter. The cross section of the cylindrical Fermi surface in a layered Bi(2212) single crystals in the first Brillouin zone (bold curves correspond to ''electron'' regions with a positive curvature and dashed curves to ''hole'' regions with a negative curvature. (b) The gap structure in the case of the $d_{x^2-y^2}$-symmetry of the order parameter.

change of virtual quanta of low-frequency (LF) collective charge-density excitations (acoustic plasmons).[19]

Bearing in mind the possibility of FS splitting into regions with essentially different properties, we shall use the model of anisotropic superconductor with a multicomponent SC order parameter, which was developed in Refs. 16, 17 and 20. In this case, the equation for the superconducting order parameter can be presented in the form

$$\Delta_{ij}(\mathbf{k},\omega)=T\sum_{\omega'}\int\frac{d^2k'}{(2\pi)^2}\sum_{l,m}W_{ij,lm}(\mathbf{k},\mathbf{k}',\omega-\omega')F_{lm}(\mathbf{k}',\omega'),\qquad(1)$$

where ω and ω' are discrete Matsubara frequencies, $W_{ij,lm}$ the matrix elements of the retarded electron–electron interaction, F_{lm} anomalous Green's functions, and the subscripts i and j label different regions on the FS.

If we disregard ''cross'' Cooper pairing of electrons from different regions of an anisotropic FS and put $\Delta_{ij}=0$ for $i\neq j$, the system of equations (1) for the gaps $\Delta_i=\Delta_{ij}$ assumes the following form after averaging over momenta (within each region on the FS):

$$\Delta_i(\omega)=-T\sum_{\omega'}\int d\xi\sum_j\nu_j(\xi)\widetilde{W}_{ij}(\omega-\omega')F_{jj}(\xi,\omega'),\qquad(2)$$

where ξ is the electron energy measured from the common FL, and ν_j and $\widetilde{W}_{ij}$ are the values of DS and matrix elements $W_{ii,jj}$ describing the retarded electron–electron attraction near the FS due to the EPhI as well as due to screened Coulomb repulsion, which are averages over area of the jth surface element of the FS for $i\neq j$, $\widetilde{W}_{ij}$ defines the probability of virtual two-particle transitions between different regions of the FS. Naturally, such an approach cannot lead to an explicit angular dependence of the anisotropic gap $\Delta(\theta)$, but reflects the basic symmetry properties of the order parameter taking into account only the mean values of the magnitude of the gap and its signs on different regions of the FS depending on interaction constants (see below).

If we neglect the violation of the $C_{\nu 4}$ symmetry in the initial spectrum, which can be associated, for example, with the formation of a superlattice in the $\Gamma-Y$ direction in a Bi(2212) single crystal,[8] the system of equations (2) for a multicomponent order parameter has the following types of solutions:

(1) in all ''electron'' regions of the FS, the gaps Δ_1 have the same magnitude and sign, while the gaps Δ_2 are smaller than Δ_1 in the ''hole'' regions and can have either the same sign as Δ_1, or the opposite sign; this solution corresponds to the s-type of symmetry of the SC order parameter (Fig. 1a);
(2) in mutually perpendicular ''electron'' regions of the FS, the gaps have the same absolute values, but opposite signs, while in the ''hole'' regions (along the diagonals of the BZ), the gaps are equal to zero; this solution corresponds to the $d_{x^2-y^2}$-wave Cooper pairing (Fig. 1b). Besides, a d_{xy}-type solution with $\Delta_d(\mathbf{k})\sim\sin k_x\sin k_y$ is also possible, but it has a low probability in view of a low DS in the ''hole'' regions.

In the first case (s-pairing), the system of equations for the gaps Δ_1 and Δ_2 in the BCS approximation can be reduced to

$$\Delta_1=\Delta_1(\lambda_{11}+2\lambda'_{11}+\lambda''_{11})L_1+2\Delta_2(\lambda_{12}+\lambda'_{12})L_2;\qquad(3)$$

$$\Delta_2=\Delta_2(\lambda_{22}+2\lambda'_{22}+\lambda''_{22})L_2+2\Delta_1(\lambda_{21}+\lambda'_{21})L_1,\qquad(4)$$

where

$$L_1=\frac{1}{2}\int_{-E_{F1}}^{E_{F1}}\frac{d\xi}{\sqrt{\xi^2+|\Delta_1|^2}}\left(\frac{E_{F1}}{\xi+E_{F1}}\right)^{1/2}\tanh\frac{\sqrt{\xi^2+|\Delta_1|^2}}{2T};$$

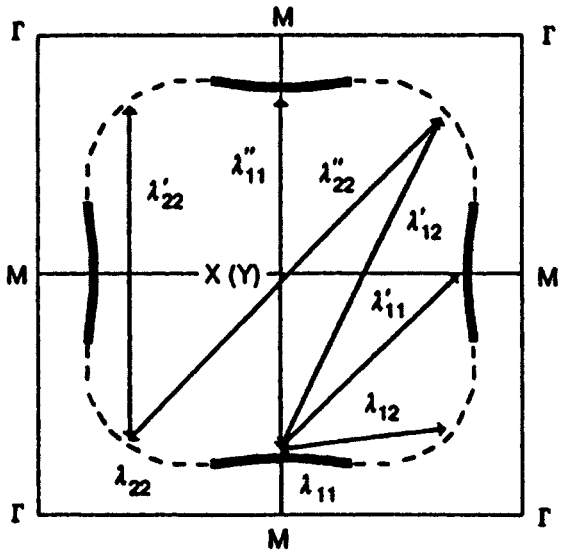

FIG. 2. Cross section of a cylindrical FS centered at the X (or Y) point of the BZ. The arrows indicate the interaction between electrons from different regions of the FS, corresponding to different coupling constants, λ_{ii}, λ'_{ii} and λ''_{ii} $(i=1,2)$, and $\lambda'_{ij}(i \neq j)$.

$$L_2 = \int_0^{\widetilde{\Omega}} \frac{d\xi}{\sqrt{\xi^2+|\Delta_2|^2}} \tanh \frac{\sqrt{\xi^2+|\Delta_2|^2}}{2T}; \tag{5}$$

E_{F1} and λ_{11} are the Fermi energy and the dimensionless coupling constant in the quasi-one-dimensional ''electron'' region of the FS with a root singularity of the DS,[15,17] $\widetilde{\Omega}$ and λ_{22} are the cutoff energy of interaction and the coupling constants in the ''hole'' regions of the FS, λ'_{ii} and λ''_{ii} are the constant of interaction between different ''electron'' $(i=1)$ and ''hole'' $(i=2)$ regions, and λ_{ij} and λ'_{ij} are the constants of cross interaction $(i \neq j)$ between ''electron'' and ''hole'' regions of the FS. We assume that the Fermi energy in the ''hole'' regions is $E_{F2} > \widetilde{\Omega}$ so that the constants λ_{22}, λ'_{22}, and λ''_{22} contain, along with the EPhI and EPI, the Coulomb pseudopotential:

$$\mu_c^* = \frac{\mu_c}{1+\mu_c \ln(E_{F2}/\widetilde{\Omega})}, \tag{6}$$

while λ_{11}, λ'_{11}, and λ''_{11} contain the nonrenormalized constant $\mu_c > \mu_c^*$ of Coulomb repulsion since $E_{F1} < \widetilde{\Omega}$. Figure 2 shows schematically electron–electron interactions in different regions of the FS corresponding to different coupling constants.

Equations (3) and (4) show that in the case of prevailing attraction in the entire volume of the BZ owing to strong EPhI and EPI, when all the coupling constants are positive, a quasi-isotropic solution of the s-type with the same signs (phases) of the parameters Δ_1 and Δ_2 is advantageous from the energy point of view. On the other hand, for negative values of cross constants λ_{ij} and λ'_{ij} with $i \neq j$ $(i,j=1,2)$, the solution with opposite signs of the gaps Δ_1 and Δ_2 is realized (e.g., $\Delta_1 > 0$ and $\Delta_2 < 0$), which corresponds to the s_{xy}- or s-type symmetry.

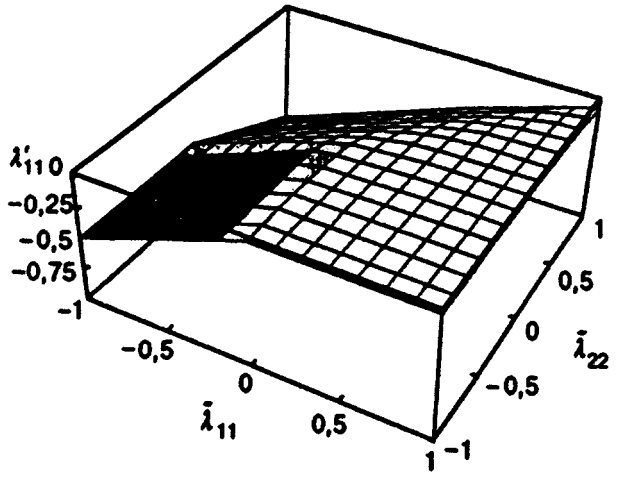

FIG. 3. Interface between the regions with s- and d-types of Cooper pairing in the space of the parameters $\widetilde{\lambda}_{11}$, $\widetilde{\lambda}_{22}$ and λ'_{11} for $\widetilde{\lambda}_{12}\,\widetilde{\lambda}_{21}=0.04$.

In the latter case (d-pairing), we obtain a single equation for the gap modulus Δ_1 in the saddle (''electron'') regions of the FS:

$$1 = (\lambda_{11} - 2\lambda'_{11} + \lambda''_{11}) L_1. \tag{7}$$

It should be noted that the magnon mechanism of Cooper pairing[11–13] corresponds to negative signs of all constants $(\lambda_{11}<0,\ \lambda'_{11}<0,\ \lambda''_{1111}<0)$ so that a SC transition can take place only for a strong anisotropy of interaction, when the magnitude of the coupling constant along a BZ diagonal satisfies the inequality $(|\lambda'_{11}| > 1/2(|\lambda_{11}| + |\lambda''_{11}|)$. On the other hand, if the electron–electron attraction due to the EPhI and EPI dominates in the ''electron'' regions of the FS, when $\lambda_{11}>0$, while Coulomb repulsion between electrons from neighboring regions dominates ($\lambda'_{11}<0$ and $\lambda''_{11}<0$), the d-pairing can take place under a much less stringent condition $(\lambda_{11} + 2|\lambda'_{11}| - |\lambda''_{11}|) > 0$.

3. A comparison of the superconducting transition temperatures T_c^s and T_c^d calculated on the basis of relations (3)–(5) on one hand and (7) on the other hand allows us to find the ranges of the parameters for which either s- or d-symmetry of the gap is observed. Such a comparison can be carried out analytically by using a simple model of the BCS type without taking into account the root singularity of the DS in L_1 and for the same values of cutoff interaction energy $\widetilde{\Omega}$, when $L_1 = L_2$ for $T \to T_c$. In this case, relations (3), (4), and (7) lead to $T_c^{s,d} = \widetilde{\Omega} \exp(-1/\Lambda_{s,d})$, where the effective coupling constants Λ_s and Λ_d are given by

$$\Lambda_s = \frac{\Lambda_{11}+\Lambda_{22}}{2} + \left(\frac{(\Lambda_{11}-\Lambda_{22})^2}{4} + \widetilde{\lambda}_{12}\widetilde{\lambda}_{21} \right)^{1/2},$$

$$\Lambda_d = \Lambda_{11} - 4\lambda'_{11}, \tag{8}$$

where

$$\Lambda_{ii} = \lambda_{ii} + 2\lambda'_{ii} + \lambda''_{ii} \quad \widetilde{\lambda}_{ij} = 2(\lambda_{ij} + \lambda'_{ij}), \quad (i,j=1,2). \tag{9}$$

Figure 3 shows the surface defined by the condition $\Lambda_s = \Lambda_d$ which can be reduced to the form

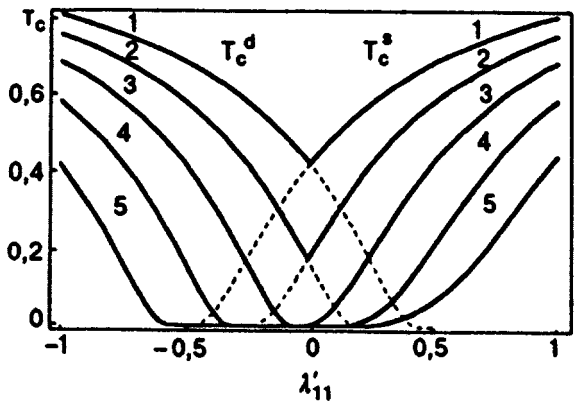

FIG. 4. Dependences of T_c^s and T_c^d on λ'_{11} for $\tilde{\lambda}_{22}=0.5\tilde{\lambda}_{11}$ and $\tilde{\lambda}_{12}$ $\tilde{\lambda}_{21}=0.04$ for various values of $\tilde{\lambda}_{11}$: 1 (curves *1*), 0.5 (curves *2*), 0 (curves *3*), -0.5 (curves *4*), and -1 (curves *5*). The dashed curves show continuations of curves *1* and *2* to the region where the corresponding values of T_c^s and T_c^d are smaller than the maximum value of T_c.

$$2\lambda'_{11}=\frac{\tilde{\lambda}_{11}+\tilde{\lambda}_{22}}{2}-\left(\frac{(\tilde{\lambda}_{11}-\tilde{\lambda}_{22})^2}{4}+\tilde{\lambda}'_{12}\tilde{\lambda}_{21}\right)^{1/2}. \tag{10}$$

This surface separates the regions of *s*- and *d*-pairing in the space of parameters $\tilde{\lambda}_{11}\equiv(\lambda_{11}+\lambda''_{11})$, $\tilde{\lambda}_{22}\equiv\Lambda_{22}$ and λ'_{11} for a fixed value of the constants of cross interaction between ''electron'' and ''hole'' regions of the FS, i.e., $\tilde{\lambda}_{12}$ $\tilde{\lambda}_{21}=0.04$.

The region of *d*-pairing in which $T_c^d>T_c^s$ lies below this interface, while the region of *s*-pairing in which $T_c^s>T_c^d$ lies above the interface. A region in which neither *s*- nor *d*-pairing is observed exists above the darkened region of the surface (corresponding to the plane $\tilde{\lambda}_{11}=2\lambda'_{11}$ in which T_c^d vanishes) in the range $\tilde{\lambda}_{11}<2\lambda'_{11}<(\tilde{\lambda}_{12}\tilde{\lambda}_{21}/\tilde{\lambda}_{22}-\tilde{\lambda}_{11})$. Numerical calculations show that the inclusion of the root singularity of the DS in the expression for L_1 [(see Eq. (5)] in the ''electron'' regions of the FS does not lead to qualitative changes in the structure of regions of *s*- and *d*-pairing.

It can be seen that *d*-pairing is possible only for negative values of the constant λ'_{11} describing the interaction between neighboring ''electron'' regions of the FS with the transferred momentum $q\approx\pi\sqrt{2}/a$. In this case, a weak repulsion between electrons from different regions ($\lambda'_{11}<0$) is sufficient for the emergence of *d*-pairing even in the case of attraction between electrons in the same quasi-one-dimensional (saddle) region of the FS due to the EPhI and EPI ($\sim\tilde{\lambda}'_{11}>0$). Such a repulsion can be a consequence of the electron–magnon interaction (EMI) or of an incomplete compensation of Coulomb attraction due to the EPhI and EPI.

On the other hand, in the case of prevailing repulsion in the saddle region ($\tilde{\lambda}_{11}<0$), *d*-pairing is possible only for large in absolute value negative values of the coupling constant λ'_{11}, which corresponds to anisotropic interaction of charge carriers with paramagnons.[11–13]

Figure 4 shows the dependences of T_c^s and T_c^d on λ'_{11}, calculated on the basis of Eqs. (3)–(5) and (7) for various values of $\tilde{\lambda}_{11}$ for $\tilde{\lambda}_{22}=0.5\tilde{\lambda}_{11}$ and $\tilde{\lambda}_{12}$ $\tilde{\lambda}_{21}=0.04$. It can be seen that for $\tilde{\lambda}_{11}<0$ there exists an interval of values of the constant λ'_{11} in which T_c^s and T_c^d are equal to zero (curves *4* and *5*). At the same time, attraction in ''electron'' regions of the FS ($\tilde{\lambda}_{11}>0$) leads to elevation of T_c as compared to the case of the EMI for which $\tilde{\lambda}_{11}<0$ even against the background of repulsion forming the *d*-symmetry of the gap ($\lambda'_{11}<0$).

Thus, the existence of additional attraction in the FS regions with a high DS, which facilitates the attaining of high values of T_c irrespective of the type of Cooper pairing and gap symmetry, is important for the HTS. It should be noted that the values of coupling constants can change significantly with the concentration of doped charge carriers; this follows from the strong concentration dependence of T_c in cuprate metal oxide compounds (see, for example, Ref. 21). This means that in the course of doping in high-temperature superconductors, a transition from one type of the order parameter symmetry to another can occur in principle. It should also be noted that the violation of the initial symmetry C_{v4} of the electron spectrum [due to the formation of a superlattice in Bi(2212) in the direction of one of the diagonals of the BZ[8] or due to the ordering of chains in Y(123)] leads to a more complex anisotropic structure of the SC gap[20,22,23] and to an anomalous temperature dependence of the gap,[16,24] which differs radically from the standard dependence $\Delta(T)$ in the BCS theory.

This research was carried out under the project No. 2.4/561 of the Ukrainian State Foundation on Fundamental Studies.

*E-mail: pashitsk@physics.kiev.ua

[1)]These regions coincide approximately coincide with the regions on the FS characterized by a positive and negative curvature (see Fig. 1).

[1] D. A. Wollman, D. J. Van Harlinger, W. C. Lee *et al.*, Phys. Rev. Lett. **71**, 2134 (1993).
[2] I. Iguchi and Z. Wan, Phys. Rev. **B49**, 12388 (1994).
[3] D. A. Browner and H. R. Ott, Phys. Rev. **B50**, 6530 (1994).
[4] S. S. Tsuei, J. R. Kirtley, C. C. Chi *et al.*, Phys. Rev. Lett. **73**, 593 (1994).
[5] J. R. Kirtley, S. S. Tsuei, M. Rupp *et al.* Phys. Rev. Lett. **76**, 1336 (1996).
[6] M. R. Norman, M. Randeria, J. C. Campuzano, and A. F. Bellman, Phys. Rev. **B52**, 15107 (1995).
[7] H. Ding, M. R. Norman, J. C. Campuzano, and A. F. Bellman, Preprint Cond. Mat. No. 9603044 (1996).
[8] H. Ding, J. C. Campuzano, A. F. Bellman *et al.*, Phys. Rev. Lett. **74**, 2784 (1995).
[9] R. Ferenbacher and M. R. Norman, Phys. Rev. Lett. **74**, 3884 (1995).
[10] M. R. Norman, M. Randeria, H. Ding, and J. C. Campuzano, Phys. Rev. **B52**, 615 (1995).
[11] A. J. Millis, H. Monien, and D. Pines, Phys. Rev. **B42**, 167 (1990).
[12] P. Monthoux, A. V. Balatsky, and D. Pines, Phys. Rev. **B46**, 14803 (1992).
[13] P. Monthoux and D. Pines, Phys. Rev. **B47**, 6069 (1993).
[14] D. M. King, Z.-X. Shen, D. S. Dessau *et al.*, Phys. Rev. Lett. **73**, 3298 (1994).
[15] V. Gofron, J. C. Campuzano, A. A. Abricosov *et al.*, Phys. Rev. Lett. **73**, 3302 (1994).
[16] È. A. Pashitskii and V. I. Pentegov, Pis'ma Zh. Éksp. Teor. Fiz. **63**, 553 (1996) [JETP Lett. **63**, 583 (1996)].
[17] È. A. Pashitskii, V. I. Pentegov, and A. V. Semenov, Fiz. Nizk. Temp. **22**, 479 (1996) [Low Temp. Phys. **22**, 367 (1996)].
[18] A. A. Abrikosov, Physica **C214**, 107 (1993); *ibid*. **C222**, 191 (1994); *ibid*. **C244**, 243 (1995).
[19] È. A. Pashitskii, Zh. Éksp. Teor. Fiz. **55**, 2387 (1968) [Sov. Phys. JETP **28**, 1267 (1968)]; *ibid*. **103**, 867 (1993) [JETP **76**, 425 (1993)].

[20] È. A. Pashitskii, Pis.ma Zh. Éksp. Teor. Fiz. **61**, 264 (1995) [JETP Lett. **61**, 603 (1995)].
[21] J. L. Tallon, R. G. Buckley, and E. M. Haines, Physica **C185–189**, 855 (1991).
[22] A. A. Golubov and I. I. Mazin, Physica **C243**, 153 (1995).
[23] R. Combescot and X. Leyronas, Phys. Rev. Lett. **75**, 3732 (1995).
[24] Jian Ma, G. Quitman, R. J. Kelley *et al.*, Physica **C235–240**, 1875 (1994).

Translated by R. S. Wadhwa

Residual low-temperature resistivity and peculiarities of infrared absorption of $YBa_2Cu_3O_{6+x}$ superconductor as manifestations of the long-distance potential relief

V. V. Eremenko, I. S. Kachur, V. G. Piryatinskaya, A. M. Ratner, and V. V. Shapiro

*B. Verkin Institute for Low Temperature Physics and Engineering, National Academy of Sciences of the Ukraine, 310164 Kharkov, Ukraine**

(Submitted July 9, 1996; revised September 16, 1996)
Fiz. Nizk. Temp. **23**, 146–158 (February 1997)

Various physical phenomena connected with long-distance potential relief created by negative oxygen impurity ions in a conducting plane are considered. The long-distance potential generates a secondary electron structure responsible for these phenomena. The relation between the residual low-temperature resistivity and the secondary structure is established experimentally. The high sensitivity of the residual resistivity to photoillumination, modifying the long-distance potential, and its increase with decreasing temperature suggest the low-temperature localization of holes in long-distance potential wells. Optical transitions between energy levels of the secondary structure differing from other optical transitions in a much higher probability and a high sensitivity to the shape of the long-distance potential well are analyzed. The results of analysis are in qualitative agreement with the available data on optical absorption spectra. [S1063-777X(97)00302-2]

INTRODUCTION

The electron properties of the copper-oxide superconductor $YBa_2Cu_3O_{6+x}$ are determined to a considerable extent by its structural peculiarity associated with the spatial distribution of the oxygen acceptor impurity.[1–3] The O^{2-} impurity ions supplying holes to the conducting CuO_2 plane are located in a parallel plane of CuO_x separated from the CuO_2 plane by a comparatively long distance in the conducting plate 4.15 Å. For this reason, impurity charges create Coulomb potential wells in the conducting plate with a width much larger than the atomic spacing in the lattice. Such potential wells bend the bottom of the band of hole carriers moving in the conducting plane and create a long-distance secondary potential relief for these carriers (the primary, or fundamental potential of the conducting plane with the period of the lattice is taken into account in terms of the effective mass).

The secondary potential relief with a modulation depth significantly exceeding the Fermi energy of holes (~ 1 eV) affects the electron properties of the superconductor. This is manifested in the conductivity anisotropy that is enhanced upon an increase in the oxygen index, together with anisotropy in the secondary relief,[2,4] as well as in anomalies of Raman scattering.[2,5] The correlation interaction (Van der Waals attraction) of holes moving at adjacent minima of the secondary relief can be sufficient for the formation of a superconducting gap having a width of the order of several or even tens of millielectronvolts.[2]

The form of the long-distance relief is determined by the oxygen index x. With increasing x, the average length of copper–oxygen chains formed in the CuO_x plane increases, while the fraction of oxygen impurity contained in the plane in the form of isolated O^{2-} ions decreases. The negative charge of the chain plane per oxygen impurity ion increases (in magnitude) in this case. The charge of this plane does not change with the emergence of an isolated O^{2-} ion in it since the charge of the ion is compensated by an increase in the charges of two adjacent copper ions from $+1$ to $+2$; on the contrary, the attachment of an ion O^{2-} to a chain changes the charge of the chain plane by -1.[2,6]

It follows from what has been said above that the number of holes in the conducting plane (which is equal in magnitude to the negative charge of the chain plane) increases even for a fixed oxygen index if the average length of copper–oxygen chains increases as a result of a certain external effect (e.g., photoillumination).[2,7] The long-distance potential relief increases simultaneously (and even to a larger extent). This makes it possible to control experimentally the superstructure, viz., the long-distance relief easily. Such a possibility was used in Ref. 1 for establishing experimentally the relation between the superconductivity mechanism and the long-distance potential.

Thus, the electron properties of the superconductor $YBa_2Cu_3O_{6+x}$ are determined to a considerable extent by the long-distance potential relief. New manifestations of this relief are considered in this article.

In Sec. 1, the residual low-temperature resistivity of the superconductor, displaying a high sensitivity to photoillumination, is studied. Such a clearly manifested photoinduced effect is incommensurate with a small photoinduced change in the number of charge carriers and can be attributed only to more significant photostimulated changes in the long-distance relief. The observed increase in the residual resistance upon a decrease in temperature and during photostimulated deepening in the minima of the long-distance potential suggests a blurred low-temperature transition to the insulating phase with the localization of holes at these minima.

In Sec. 2, spectroscopic manifestations of the secondary electron structure, i.e., the energy levels of the long-distance potential, are considered. The frequencies of optical transitions between these levels correspond to the near infrared region. It will be proved below that transitions between the energy levels of the secondary structure differ from other optical transitions in the same crystal in a much higher prob-

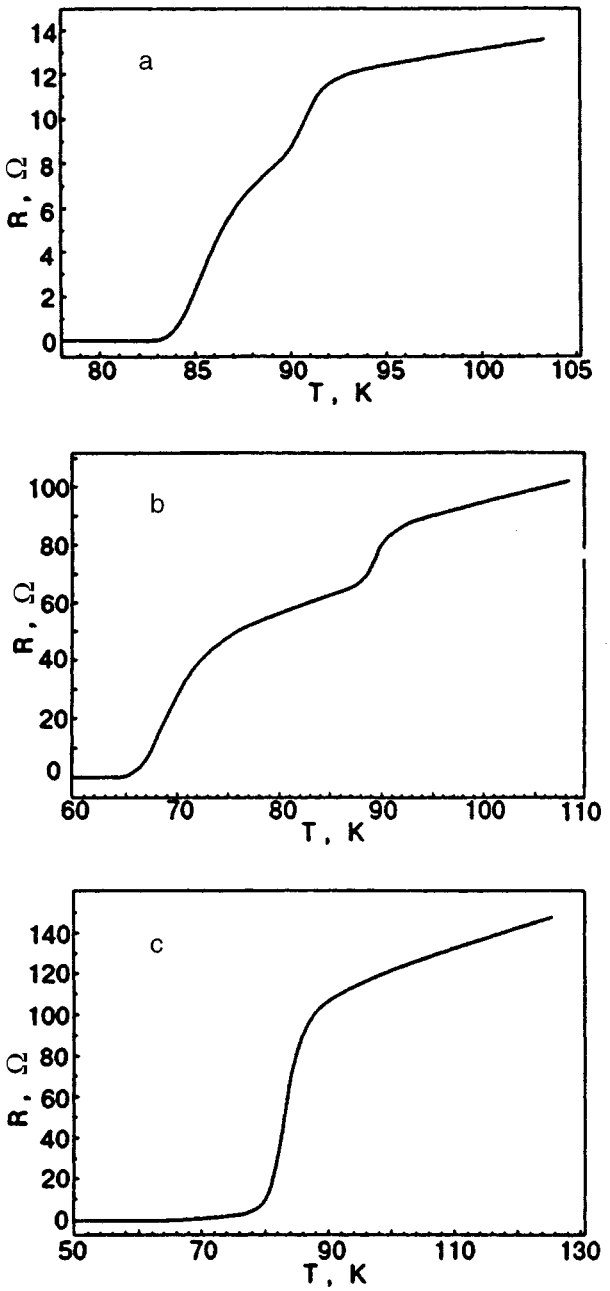

FIG. 1. Temperature dependence of the resistance of samples (films) measured with a low sensitivity over a wide temperature interval: sample No. 1 (a), 2 (b) and 3 (c).

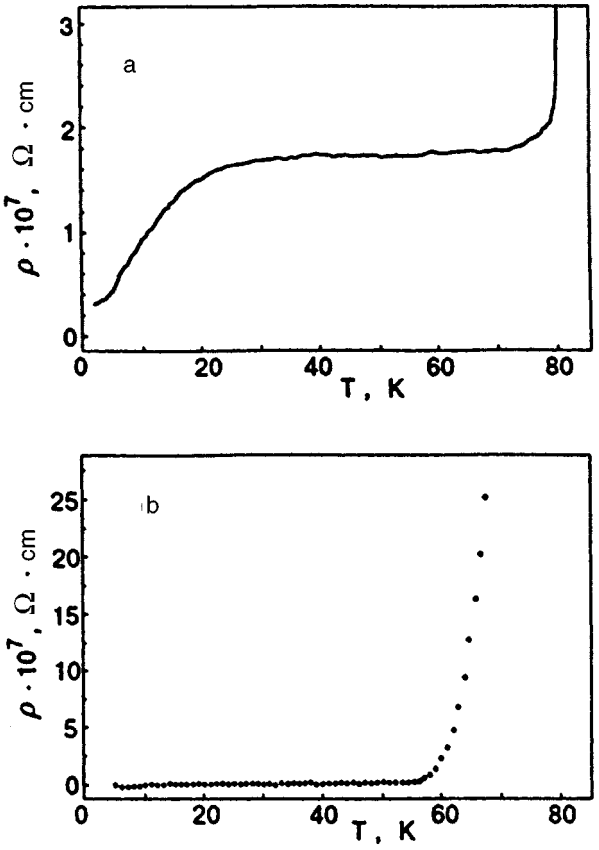

FIG. 2. Temperature dependence of the resistance of samples (films) measured with a high sensitivity in a temperature range below T_c: sample No. 1 (a) and 2 (b).

ability and in a high sensitivity to the shape of the long-distance potential relief. The experimental data[8] confirm this conclusion qualitatively.

1. RESIDUAL LOW-TEMPERATURE RESISTIVITY AND ITS RELATION TO THE LONG-DISTANCE POTENTIAL RELIEF

1.1. Experiment

The objects of investigations were three $YBa_2Cu_3O_{6+x}$ epitaxial films with various extents of phase homogeneity. The measurements were made by using the high-sensitivity four-probe technique. The temperature dependences of the resistance R of the samples are presented in Fig. 1. These dependence reflect the presence of two phases with different oxygen indices and accordingly with different superconducting transition temperatures T_c in samples No. 1 (Fig. 1a) and No. 2 (Fig. 1b) ($T_{c1}\simeq 90$ K, $T_{c2}\simeq 83$ K for sample No. 1 and $T_{c1}\simeq 90$ K, $T_{c2}\simeq 65$ K for sample No. 2). The characteristic $R(T)$ for sample No. 3 is typical of a one-phase material with the superconducting transition temperature $T_c=80$ K (Fig. 1c).

The high-sensitivity measurements have made it possible to observe a weak residual resistivity in samples No. 1 and 2 below the critical temperatures T_{c2} down to $T=1.8$ K (the $R(T)$ dependence for sample No. 1 measured in the high-sensitivity mode is shown in Fig. 2a). For sample No. 3, we can indicate the temperature (~ 56 K, Fig. 2b) below which zero resistance is observed within the sensitivity of our measurements.

The temperature dependence of the residual resistance R for sample No. 1 (see Fig. 2a) is an ascending curve with a plateau in the interval from 20 to 75 K. In the interval from 5 to 20 K, the resistance R increases linearly, while near 80 K its sharp increase preceding a transition to the normal state in the low-temperature phase ($T_{c2}\simeq 83$ K) is observed. The dependence of voltage on current density J (Fig. 3a) is also characterized by a monotonic increase of the derivative, indicating a noticeable resistivity for sample No. 1 even at very low temperatures.

The residual resistance of sample No. 2 proved to be

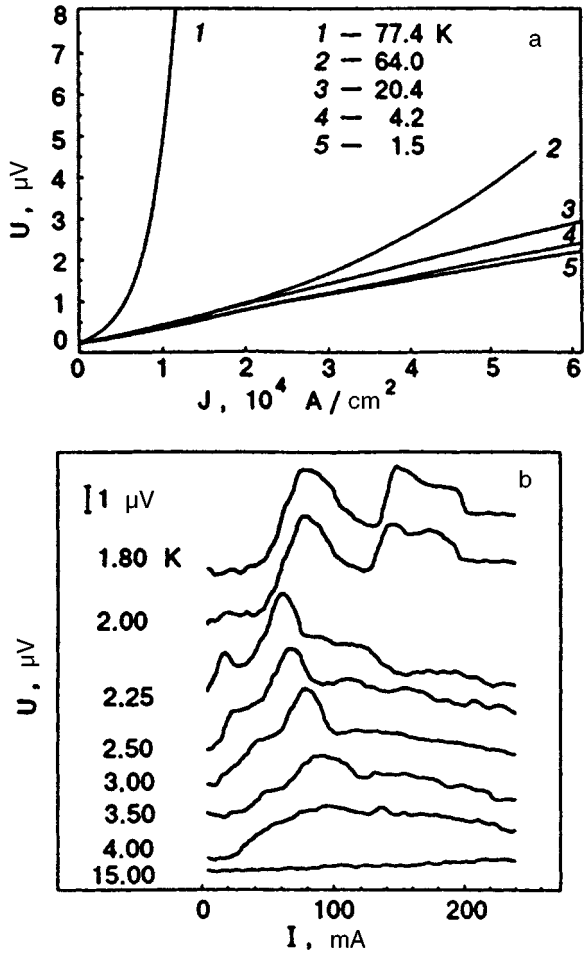

FIG. 3. Current–voltage characteristics of films measured for fixed temperatures below the superconducting transition temperature: sample No. 1 (a) and 2 (b).

smaller by 3–4 orders of magnitude; it is characterized by an anomalously decreasing temperature dependence and an oscillating dependence on current. Figure 3b shows a series of current–voltage characteristics (IVC) for sample No. 2, measured at various temperatures. It can be seen from the figure that the residual resistivity decreases upon an increase of temperature in the interval from 1.8 to 15 K. Below 15 K and for a precritical current of 200 mA ($I_{cr} > 300$ mA), the voltage across the sample is 0.2 μV, which corresponds to the sample resistance of 1 $\mu\Omega$, i.e., to the resistivity of the order of 10^{-11} $\Omega\cdot$cm.

It can be seen that the dependence of voltage on the transport current density at low temperatures is nonmonotonic (Fig. 3b). The current–voltage characteristics contain broad regions of negative dynamic resistance. In the formed ''spectrum'' of resistivity bands, the band width decreases, while the amplitude increases with decreasing temperature. At $T=3$ K, two bands with abscissas (values of transport current) of the peaks $I_1=45$ mA and $I_2=81$ mA can be singled out. With decreasing temperature, the peaks of the bands become higher and are displaced towards smaller currents, while below 2.07 K the ''spectrum'' does not change qualitatively.

In order to analyze the effect of photoillumination on the resistive parameters of the film, we used a wide-band xenon lamp DKSSh-150 as a light source. Electric contacts of the films were thoroughly protected from illumination. The exposure dose did not exceed $5\cdot 10^{21}$ photons per square centimeter of the film area. Such doses do not cause irreversible structural changes in the sample (it was established by us earlier[1] that the transport characteristics of the film relax after illumination to their initial values). It can be seen from Fig. 4 that the peaks of the current–voltage characteristics are intensified, become narrower, and are shifted toward smaller transport currents as a result of photoillumination. These changes are persistent (the relaxation time at room temperatures is of the order of several hours).

1.2. Relation between residual resistivity and the long-distance potential and its possible mechanism

The peculiarities of the current–voltage characteristics for sample No. 2 (see Figs. 3b and 4) allow us to draw certain conclusions on the mechanism of residual resistivity.

It can be seen from Fig. 4 that the maximum resistance (corresponding to the first, most intense peak on the IVC) is approximately doubled as a result of illumination for half an hour. This effect is opposite in sign to the effect of metallization of films (increase in their conductivity) under photoillumination, which was investigated earlier.[1,7] Moreover, the increase in the amplitudes of resistivity bands is incommensurate with the photoinduced increase in the number of hole carriers. Indeed, an increase in the number of holes in a $YBa_2Cu_3O_{6.5}$ sample induced by the same radiation dose was approximately 2%,[1] while in sample No. 2 with a larger x ($x=0.75$, judging from the superconducting transition temperature $T_{c2}\simeq 65$ K) it must be smaller since the photoinduced effect in $YBa_2Cu_3O_{6+x}$ is suppressed with increasing x.[7]

Thus, the photoinduced change in residual resistivity cannot be explained by the change in the number of charge carriers. According to some indications, this change is due to photoinduced ordering of the long-distance secondary potential relief.

The long-distance potential relief of the conducting CuO_2 plane changes due to photostimulated elongation of copper–oxygen chains in the CuO_x plane. We now prove that the chain length changes more strongly than the number of charge carriers. If we measure the chain length by the number ν of oxygen ions contained in it, the charge ζ increases with the chain length according to the law[2,6]

$$\zeta \approx \nu - 1. \tag{1}$$

Since the number of holes n_h in the conducting plane is equal to the total negative charge of the chain plane, we arrive at the following relation between the relative changes in the number of holes n_h and the average length $\overline{\nu}$ of the chain for a fixed amount of oxygen in the chain plane ($\Sigma\nu=$const):

$$\delta\overline{\nu}/\overline{\nu} \approx \overline{\nu}\,\delta n_h/n_h \quad (\overline{\nu} \gg 1). \tag{2}$$

In the metal phase (outside the narrow neighborhood of the concentration metal–insulator transition), the average

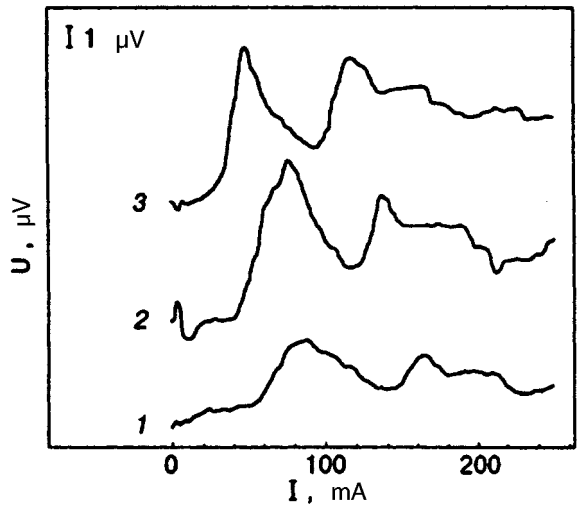

FIG. 4. Current–voltage characteristics of sample No. 2 measured at 2 K before (curve *1*) and after photoillumination for 10 (curve *2*) and 30 min (curve *3*).

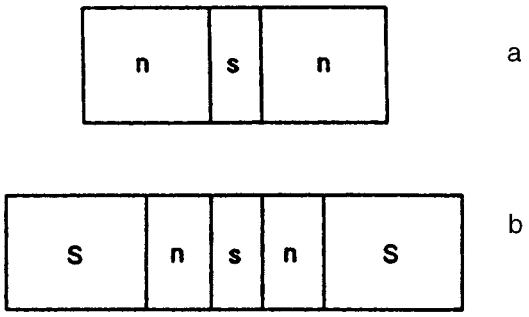

FIG. 5. (a) Compound conductor whose resistance decreases upon a transition of the short superconducting part *s* into the normal state.[9] (b) Superconductor *S* containing inclusions of type *a*, whose superconducting part is characterized by a small critical current.

length of chains is $\overline{\nu} \gg 1$. Consequently, it follows from (1) and (2) that the width and depth of a long-distance potential well increase as a result of illumination of the superconductor at a much higher rate than the number of charge carriers. This circumstance, in combination with clearly manifested photoinduced changes in the residual resistance, serves as an additional argument in favor of a decisive role of the long-distance potential relief.

Residual resistivity, which is manifested most clearly in the helium temperature range (see Fig. 3b) and is enhanced upon photoillumination together with the minima of the secondary potential relief (see Fig. 4), can be naturally explained under the assumption concerning a partial low-temperature metal–insulator transition. In the insulator phase, holes as localized at broad minima of the secondary relief, which corresponds to a small energy scale of the phase transition and its low temperature (according to Fig. 3b, this temperature is 7–8 K for sample No. 2).

Since hole carriers in a strictly periodic potential are in delocalized band states even at zero temperature, we can associate the low-temperature localization of holes with a periodicity of the long-distance potential, which is in qualitative agreement with the well-known Anderson mechanism.

It is natural to assume that the low-temperature insulator–metal phase transition associated with the irregular nature of the long-distance potential is blurred to a considerable extent. This is manifested in that the effective mass m of hole carriers increases, but not to infinitely large values, while the number n of holes decreases, but not to zero. Accordingly, the Fermi energy of holes decreases, and the superconducting gap becomes narrower, which must lead to a decrease in critical current to a certain small value I_c^*.

Figure 3b shows that residual resistivity appears at $T=1.8$ K for a current exceeding 50 mA. This value can be conditionally identified with I_c^*. The value of I_c^* is an order of magnitude smaller than the ordinary critical current observed outside the temperature range of residual resistivity.

1.3. Can IVC oscillations be explained by inclusions of normal phase?

Under the assumptions made above, we could expect a monotonic increase in resistance with current I at helium temperatures for $I>I_c^*$. In actual practice, the voltage V increases with current only up to $I_c^{**}=80$ mA, where the derivative dV/dI changes its sign. The nonmonotonic dependence $V=V(I)$ can be attributed to sample heterogeneity, i.e., microscopic inclusions of the normal phase in the superconducting phase, or to a current-induced rearrangement of the electron state of the superconductor. The analysis carried out below shows that each version is fraught with certain difficulties. Let us first consider the possible role of normal inclusions.

A thin layer of a normal substance (of thickness L_n) in contact with superconducting layers (of thickness L_s) can double its resistance as a result of a superconducting transition due to Andreev's reflection of normal charge carriers by the superconductor, which leads to interference of their wave functions.[9] If the superconducting layer thickness L_s is small, the resistance of the compound conductor (Fig. 5) decreases as a result of degradation of the superconducting state *s* since interference phenomena disappear in the absence of a superconductor.

For this reason, a descending region on the dependence $V(I)$ can be obtained in the compound superconductor presented in Fig. 5 if the critical current I_S of the superconductor *S* exceeds the critical current I_s in a thin layer of the superconductor *s*. We increase the current I in the interval $I_1<I<I_2 (I_2<I_S)$ containing the point I_s. As the value of current passes through the point I_s, the voltage decreases together with the resistance of internal *n-s-n* inclusion since the resistance of the remaining part of the conductor remains unchanged and equal to zero.

Unfortunately, this mechanism can hardly explain the shape of the IVC curves presented in Fig. 3b. In order to have such a mechanism, the inclusion of the normal substance must cover the superconducting channel of diameter D. The three dimensions of the inclusion must be of the same order of magnitude as D. For the resistivity $\rho \sim 10^{-3}$ $\Omega \cdot$cm of the normal phase, the resistance $R=\rho/D$ of the inclusion is of the order of 50 Ω or more (if the width of the

superconducting channel exceeds the thickness $d=2\cdot10^{-5}$ cm of the superconducting film, we must put $R=\rho/d$). Thus, the resistance of the normal inclusion exceeds the maximum ratio V/I observed in the low-temperature range by six orders of magnitude (it can be seen from Fig. 3b that this resistance is $5\cdot10^{-5}$ Ω for sample No. 2). The resistance of an inclusion can approach this value if it has the shape of a layer whose thickness is 5–7 orders of magnitude smaller than other dimensions of the inclusion. Apparently, such a situation is hardly possible.

Under our experimental conditions, other mechanisms[10,11] leading to a decrease in the dynamic resistance of a heterogeneous superconductor upon an increase in current cannot be manifested either. Mitin *et al.*[10] explained a similar effect observed at low temperatures and for a potential difference of the order of 10 V across the junctions by the Josephson tunneling of charge carriers between superconducting granules separated by a thin layer of the normal phase. The Josephson tunneling starts when the potential difference between adjacent granules increases to a value comparable with the superconducting gap width which is not smaller than 1 meV (the critical temperature of superconducting inclusions must be higher than the sample temperature). The IVC peculiarities presented in Fig. 3 are observed at a much smaller (by 2–3 orders of magnitude) potential difference across the junctions and hence cannot be explained by Josephson tunneling.

In our experiments, the mechanism of resistance drop due to oxygen redistribution over a heterogeneous sample under the action of current could not be manifested either.[11] The change in resistance obtained in this way is virtually preserved for an indefinitely long time at room or lower temperatures, and the current–voltage characteristics shown in Fig. 3 are successfully reproduced without any hysteresis.

1.4. Can current stimulate a change in electronic properties leading to a decrease in voltage upon an increase in current?

At first sight, such an interpretation of oscillations of low-temperature IVC (see Fig. 3b) contradicts the very small value of voltage ($\sim4\cdot10^{-2}$ K) across the superconductor. The energy of an electron or hole accelerated by such a field ($5\cdot10^{-2}$ K) is two orders of magnitude lower than the temperature of the insulator–metal transition, which determines the energy scale of the spectrum rearrangement accompanied by metallization.

Let us prove, however, that even insignificant changes in electron properties corresponding to a low applied voltage can be manifested in noticeable IVC oscillations.

If the secondary long-distance potential were strictly periodic (with a period $\tilde{a}$), the secondary electron structure would be characterized by a periodic energy–momentum relation with a quasi-momentum period $2\pi\hbar/\tilde{a}$. Our analysis is based on the assumption that the irregularity in the secondary potential is not manifested very strongly, and the periodicity of the secondary energy–momentum relation is approximately preserved.

The extent of metallization in the case of a blurred insulator–metal phase transition (marked by asterisks) is characterized by the parameter

$$\mu=mn_h^*/m^*n_h, \tag{3}$$

where n_h and m are the number of charge carriers and the effective mass in the secondary potential relief. These parameters correspond to the metal phase away from the phase transition temperature ($T>15$ K). The asterisk marks the same parameters in the region of blurred phase transition ($T\sim2$ K). In the region of the low-temperature phase transition, the parameter μ is regarded as very small; this corresponds to a low Fermi energy of holes and a small width Δ^* of the superconducting gap. In turn, the narrow gap leads to a small critical current I_c^* amounting to ~50 mA for $T=1.8$ K (see Fig. 3b).

We now interpret the IVC presented in Fig. 3b, confining ourselves to the most clearly manifested insulator phase ($T=1.8$ K). In the supercritical region ($I>I_c^*$), the voltage differs from zero and increases with current up to $I_c^{**}=80$ mA, at which the derivative dV/dI changes its sign due to a certain rearrangement of electron properties. Such a rearrangement can be associated with a limited value of current density for a small number of carriers and a large effective mass. In order to impart a preset velocity $v^*=I/Sn^*$ of directional motion to a system of holes (S is the cross-sectional area), we must transfer the directional momentum component

$$P^*=m^*v^*=m^*I/Sn_h^*=mI/\mu Sn_h, \tag{4}$$

(to the holes here and below, we use atomic units).

However, the value of P^* in relation (2) cannot exceed $\pi/2\tilde{a}$. This leads to the following constraint on current:

$$I<I_{\max}=\pi n_h S\mu/2\tilde{a}m. \tag{5}$$

Substituting $n_h\sim10^{21}$ cm$^{-3}=1.5\cdot10^{-4}$ at. units, $S\sim10^{-5}$ cm$^2=3.6\cdot10^{11}$ at. units, $\tilde{a}\simeq40$ at. units, and $m\simeq5$ into (5), we obtain $I_{\max}\approx\mu\cdot4\cdot10^5$ at. units$=\mu\cdot3\cdot10^3$ A.

Identifying $I_{\max}$ with the position of the first voltage peak $I_c^{**}=80$ mA (see Fig. 3b, $T=1.8$ K), we obtain the estimate $\mu\simeq2\cdot10^{-5}$. This means, for example, that the effective mass of the secondary hole band increases by 2–3 orders of magnitude as a result of transition to the insulator phase, and the number of charge carriers decreases in the same proportion.[1)]

The above estimate of the quantity $I_{\max}$ itself is valid both for the normal and for the superconducting state. According to Fig. 3b, however, such a small value of μ can be attained for the substance under investigation only in the helium temperature range, i.e., at temperatures much lower than T_c.

A similar mechanism of limitation of current density is known for semiconductors with a low charge carrier concentration. When the current approaches the upper boundary of the allowed interval, the resistance increases until the applied electric field becomes strong enough for the rearrangement of the electron structure (for example, new energy valleys with a smaller effective mass are filled).

In the case under investigation, the rearrangement of electron properties accompanying a decrease in effective mass is associated with a considerable deformation of the momentum distribution for charge carriers, which is induced by the transport current. At first sight, the applied potential difference of a few microvolts is too small to cause such a rearrangement of the electron properties of a superconductor. However, the rearrangement corresponding to IVC peaks at $T=1.8$ or 2 K (see Fig. 3b) can be induced even by a very weak field since it is connected with a very small increase in the metallization parameter (3). Indeed, the position of the first voltage peak identified with the value $I_{\max}$ before the rearrangement and the position of the second peak corresponding to $I_{\max}$ after the rearrangement differ by a factor of two. If we take into account (5), this means that the metallization parameter μ is doubled as a result of rearrangement, i.e., changes by $\Delta\mu \simeq 2\cdot 10^{-5}$ (from the initial value $2\cdot 10^{-5}$ to $4\cdot 10^{-5}$). Complete metallization corresponding to an increase in μ by 4–5 orders of magnitude takes place, according to Fig. 2a, at a temperature of the order of 10 K or, after recalculation for the applied voltage, for $V\sim 10^{-3}$ V. A partial (very weak) rearrangement corresponding to the voltage peaks in Fig. 3b is observed for $V\simeq 4\cdot 10^{-6}$ V. The difference between these values (which amounts to 2–3 orders of magnitude) is in qualitative agreement with the small scale of variation of the metallization parameter μ for the observed rearrangement.

In order to illustrate what has been said earlier, we write the metallization factor in the simple form as a function of voltage, using its parity and presuming its analytic nature:

$$\mu(V)=\mu(0)+\mu_{\text{tot}} f(V^2/V_{\text{tot}}^2), \tag{6}$$

where $\mu_{\text{tot}}\sim 1$; $V_{\text{tot}}\sim 10^{-3}$ V and $\mu(0)\sim 2\cdot 10^{-5}$ (the subscript ''tot'' corresponds to total metallization), and the analytic function $f(z)$ satisfies the relations

$$f(0)=0, \quad f(1)=1, \quad f'(z)\sim 1 \quad \text{for } 0<z<1.$$

Expanding (6) in the vicinity of the point $V=0$, we obtain the following expression for the first IVC minimum corresponding to partial metallization:

$$\mu(V_{\text{part}})-\mu(0)\sim (V_{\text{part}}/V_{\text{tot}})^2\sim 10^{-5} \tag{7}$$

which is in qualitative agreement with the above estimate of $\Delta\mu$.

Thus, energy considerations do not rule out the interpretation of IVC oscillations on the basis of rearrangement of electron properties due to a small change in the metallization parameter (3).

1.5. Macroscopic heterogeneities of sample as a possible reason behind the instability of residual resistivity

It was shown in Sec. 1.3 that the IVC peculiarities for sample No. 2 can hardly be explained by the presence of alternating superconducting and normal regions in the bulk of the sample. Nevertheless, the macroscopic heterogeneity of the sample can affect significantly the manifestations of the physical mechanism considered in Sec. 1.4. It has been tacitly assumed in the above analysis that the low-temperature metal–insulator phase transition and the change in the electron properties under the action of transport current occur nonuniformly in the entire sample volume. However, the observed physical pattern is preserved if we assume that the same physical phenomena occur in a small part of the volume which covers the sample cross sections completely. The role of such a volume can be played by a thin interlayer between macroscopically homogeneous regions (domains) differing, for example, in the orientation of axes (the existence of such domains in single crystals is connected with twinning). In the case of films, these can be islets of homogeneous superconducting phases with different values of T_c. Irrespective of the physical origin of such a macroscopic heterogeneity, a microheterogeneity leading to irregularity in the secondary potential (which is sufficient for the Anderson localization of charge carriers) can be formed in the transition layer between domains. The macroheterogeneity of the type under investigation, which leads to residual resistivity, is probably due to the two-phase nature of the sample (it should be recalled that samples No. 1 and 2 exhibiting residual resistivity contain two superconducting phases with different values of T_c).

The transition layer with a lower electrical conductivity, which covers the sample cross section and generates residual resistivity, is apparently macroscopically heterogeneous within this cross section. The electrical properties of the sample are obviously determined by the transition layer region with the minimum resistance. In the case of several contacting layers connected in series in the circuit, the one differing from other layers by the highest resistance of the above-mentioned layer will be manifested in experiments. Consequently, we can expect that the properties of a very small region, which can easily be changed due to oxygen diffusion caused by thermal cycling, photoillumination, passage current, or annealing, will be manifested in the residual resistance. This explains the experimental fact that sample No. 2 subjected to not very long cycle of low-temperature measurements loses its peculiar properties and becomes similar to sample No. 1 as regards its current–voltage characteristics.

The above analysis shows that the current–voltage characteristics of the residual resistance observed for different samples are different as a rule. The reproduction of the same dependence of voltage on current and temperature on different samples is accidental and has a low probability. For this reason, the accumulation of experimental statistics is required to confirm and refine the concept developed here.

2. PECULIAR PROPERTIES OF INFRARED ABSORPTION CORRESPONDING TO TRANSITIONS BETWEEN ENERGY LEVELS OF SECONDARY STRUCTURE

2.1. Two types of optical electron transitions differing in sensitivity to secondary relief

Hole are real quasiparticles in the valence band that is filled almost completely with electrons. For this reason, the subsequent analysis will be carried out in terms of hole quasiparticles, which are described as electrons for brevity.

The electron structure of the CuO_2 plane (shown sche-

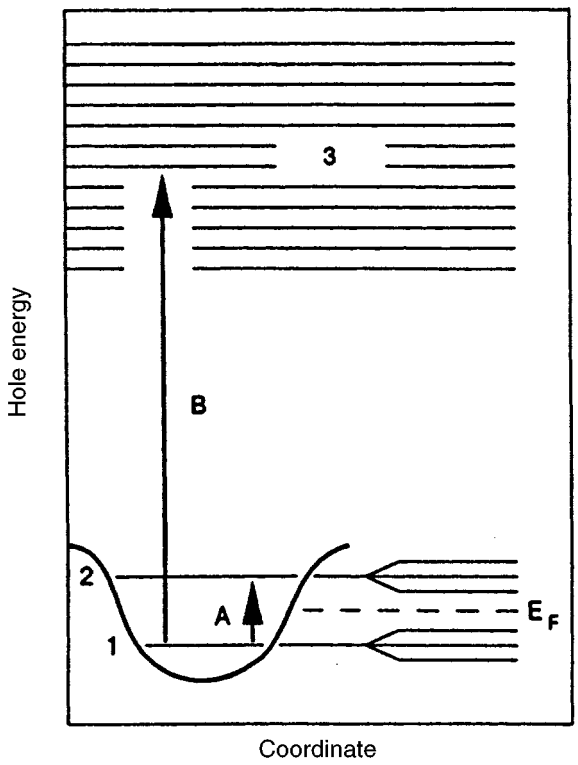

FIG. 6. Optical transitions of various types in the CuO_2 conducting plane: transition A between the energy levels of the secondary structure, belonging to the lowermost primary branch and lying on different sides of the Fermi level, and transition B between the states, belonging to different branches of the primary energy–momentum relation.

matically in Fig. 6) includes the elements of the primary structure realized in a strictly periodic lattice (in the absence of the long-distance potential) as well as the elements of the secondary structure described by the Schrödinger equation with the long-distance potential and the primary effective mass.

The primary electron structure can be considered in the strong-coupling approximation. The wave function of a hole with the two-dimensional wave vector $\mathbf{k}$ can be expanded in the orthonormal atomic basis $\chi_j(\mathbf{r}-\mathbf{n})$:

$$\psi_{\mathbf{k}j}(\mathbf{r})=N^{-1/2}\sum_{\mathbf{n}} \exp(i\mathbf{k}\cdot\mathbf{n})\chi_j(\mathbf{r}-\mathbf{n}). \tag{8}$$

Here $\mathbf{n}$ is the radius vector of a plane lattice site, running through N values, and the subscript j labels atomic states and corresponding energy branches of the primary structure. For the lowermost branch ($j=0$), the effective mass m^* and the position of energy minimum $\mathbf{k}_0$ are introduced.

Let us consider the actual electron structure of the CuO_2 plane modified by the long-distance potential modulation. The normalized wave function of a hole can be represented in the form

$$\psi_{\mathbf{k}j\alpha}(\mathbf{r})=\sum_{\mathbf{n}} \exp(i\mathbf{k}\cdot\mathbf{n})G_\alpha(\mathbf{n})\chi_j(\mathbf{r}-\mathbf{n}), \tag{9}$$

$$\sum_{\mathbf{n}} |G_\alpha(\mathbf{n})|^2=1$$

(the index α labels the levels of the long-distance potential well). The cofactor $G_\alpha(\mathbf{n})$ takes into account the long-distance potential and varies over its characteristic length L which is much larger than the lattice constant a.

Let us write the matrix element of the dipole moment $\mathbf{M}$ between the initial state i corresponding to the lowermost primary branch ($j=0$) and a certain final state f:

$$\mathbf{M}_{if}=\sum_{\mathbf{n}} \exp\{i(\mathbf{k}_f-\mathbf{k}_i)\cdot\mathbf{n}\}G_i^*(\mathbf{n})G_f(\mathbf{n})\int \chi_i^*(\mathbf{r}-\mathbf{n})e\mathbf{r}\chi_f(\mathbf{r}-\mathbf{n})d\mathbf{r}, \tag{10}$$

(e is the electron charge). This expression is written in the zeroth approximation in the overlapping of atomic functions χ centered at neighboring sites. The initial state i is presented in the effective mass approximation so that $\mathbf{k}=\mathbf{k}_0$, and $G_i(\mathbf{r})$ is the eigenstate of the Schrödinger equation with the effective mass m^* and the long-distance potential which serves as potential energy.

Figure 6 shows schematically the transitions between hole energy branches of various types. In all cases, the initial state i of the transition belongs to the energy level of the long-distance potential well, which can be expanded into a subband by overlapping hole states of the secondary structure, which are localized at neighboring wells. The A-type transitions occur, by definition, between different energy levels (1 and 2) of the long-distance well within the same lowermost primary branch. The final level (3) for B-type transitions belongs to another primary branch lying much higher and distorted slightly by the long-distance potential relief. Optical transitions of type B ($1\rightarrow 3$) belonging to the visible region were analyzed by Fugol' *et al.*[13] who called them intraband transitions. The A-type transitions ($1\rightarrow 2$) belong to the near infrared region (the depth of a long-distance potential well is 1–2 eV, while the most intense transitions between two-dimensional analogs of the s- and p- states are characterized by the energy 0.3–1 eV). In Fig. 6, different hole branches of the energy–momentum relation do not overlap; actually, they cover a wide energy interval completely, viz., the common valence band whose width is ~ 7 eV.[2,12] The low-density filling of this band with holes is characterized by the Fermi energy $E_F \simeq 0.2$ eV.

Let us prove that A-type transitions ($1\rightarrow 2$) differ in nature from the B-type transitions ($1\rightarrow 3$). This follows from the structure of the matrix element of the dipole moment (10).

We start from A-type transitions between the energy levels of a long-distance potential well corresponding to the same lowermost primary branch. The quasimomenta $\mathbf{k}_i$ and $\mathbf{k}_f$ coincide with its lower point and do not satisfy relation (10). The atomic functions χ_i and χ_f also coincide so that the integral in (10) becomes equal to $e\mathbf{n}$. Thus, for A-type transitions expression (10) assumes the form

$$\mathbf{M}_{if}(A)=\sum_{\mathbf{n}} G_i^*(\mathbf{n})G_f(\mathbf{n})e\mathbf{n}. \tag{11}$$

The functions G_i and G_f have a clear physical meaning in the opposite limiting cases $E_{\text{res}} \ll \Delta E$ and $E_{\text{res}} \gg \Delta E$, where E_{res} is the resonant energy associated with overlapping of

hole states localized at neighboring wells of the low-scale potential, while ΔE is the characteristic value of random shift of the energy level due to its transition from a long-distance potential well to a neighboring well. If $E_{\rm res} \ll \Delta E$, the quantity G_i or G_f in (11) has the meaning of the state of an individual long-distance well. In this case, we can write the total probability of transitions from a fixed state i of the well ($E_i < E_F$) to all its states $f(E_f > E_F)$ under the action of incident light having a uniform spectral density and polarized in the direction ξ:

$$P_A(i \to \text{all } f) C \sum_f |D_{if,\xi}|^2 (E_f - E_i). \tag{12}$$

Here $\mathbf{D}_{if}$ is the matrix element of the dipole moment between the states of a long-distance potential well, ξ the direction of polarization of incident light, and C denotes a certain coefficient containing the light intensity and having the same value for A- and B-type transitions.

Relation (12) can also be obtained from (11) in the opposite limiting case when $\Delta E \ll E_{\rm res}$, and the long-distance potential is almost periodic. Relation (12) is obviously observed (to within an order of magnitude) in the intermediate case also.

Let us now consider B-type transitions from the same state i belonging to the lowermost primary branch to all the states f belonging to the remaining primary branches. In view of orthogonality of the functions $\chi_0(\mathbf{r})$ and $\chi_f(\mathbf{r})$, the integral in (10) can be reduced to the atomic dipole moment $\mathbf{d}_{if}$. Using relation (10), we can find the total probability of transition from the state i to all the final states f:

$$P_B(i \to \text{all } f) = C\beta \sum_f |d_{if\xi}|^2 (E_f - E_i), \tag{13}$$

$$\beta = N \sum |G_i(\mathbf{n})|^2 |G_f(\mathbf{n})|^2 \simeq 1. \tag{14}$$

(N is the number of sites in a planar lattice). The summation in (13) is carried out over atomic states, while the summation over the wave vectors $\mathbf{k}$ of the final state is carried out without taking into account the dependence of G_f on $\mathbf{k}$ (this actually boils down to the conservation of the quasimomentum in the electron transition). Since the depth of the long-distance potential modulation is small as compared to the energy of the final state f, its envelop G_f is almost constant, which justifies this approximation from the physical point of view [which leads to the estimate (14)]. It should be noted that a weak deviation from the quasimomentum conservation law for an allowed direct transition cannot lead to a significant change in the integral intensity of absorption.

Expressions (12) and (13) give the values of areas of absorption bands of types A and B. These expressions can be used to derive a relation between the absorption coefficients κ_A and κ_B at the maxima of these bands considering that the width of each band coincides in order of magnitude with the position of its maximum:

$$\kappa_A / \kappa_B \sim (L_\xi / a)^2. \tag{15}$$

Here a is the atomic spacing and L_ξ the width of a long-distance potential well in the direction of light polarization.

Thus, A- and B-type transitions differ in nature. An A-type transition actually corresponds to the secondary electron structure, and its dipole moment is determined by the width L of the long-scale potential well. A B-type transition is actually associated only with the primary structure and is characterized by the atomic dipole moment.

Relation (15) leads to the following conclusions.

(1) The intensity of infrared optical absorption of the type A (Fig. 6) exceeds significantly the intensity of absorption of the type B occurring within the valence band and corresponding to the visible region of the spectrum. The probabilities of transitions of both types are proportional to the number of holes in the valence band; consequently, the oxygen content affects relation (15) only through the shape of the long-distance potential well [estimate (15) does not take into account interband transitions with a nonzero probability and in the absence of holes; interband transitions are limited to the spectral region $\hbar\omega > 1.8$ eV].[13]

(2) The A-type absorption is much stronger for the y-polarization of light along the copper–oxygen chains (i.e., parallel to the crystallographic axis b) than for the x-polarization (the xy plane coincides with the CuO_2 conducting plane); this follows from the relation $L_x \ll L_y$ for the dimensions of the potential well.

(3) The A-type absorption is much more sensitive (as compared to the B type) to the controllable variation of the copper–oxygen chain length, which can be achieved through photoillumination of the sample,[1,7] heating,[8,14] or by passing a strong current.[11] Indeed, the b-type absorption in all these processes changes only due to an insignificant change in the number of charge carriers n_h, while the B-type absorption is proportional to the square of the width of a long-distance potential well, which changes much more strongly than n_h according to (2).

2.2. Qualitative comparison of the theory with experimental data

Conclusions 1–3 drawn in the previous section are confirmed by the experimental data on the absorption spectrum of polarized light in a wide range from 0.05 to 2 eV.[8] Widder *et al.*[8] obtained the absorption spectrum of a single crystal from the reflection spectrum by using the Kramers–Kronig relation.

Figure 7 shows the absorption spectrum of a monocrystalline $YBa_2Cu_3O_{6.5}$ spectrum for the polarization a perpendicular to the direction of copper–oxygen chains as well as for the polarization b parallel to the chains. Two curves corresponding to sample temperatures 293 and 423 K were obtained for each polarization. Figure 8 also shows the data for a sample with a higher oxygen index (6.6) corresponding to a higher value of the average length of chains.

It can be seen from the figures that the absorption spectrum for each sample and each temperature changes significantly upon a transition through a certain frequency $\hbar\omega_c \simeq 0.8$ eV. If we identify the spectral interval $\omega < \omega_c$ with a region of predominant transitions of the A-type and the

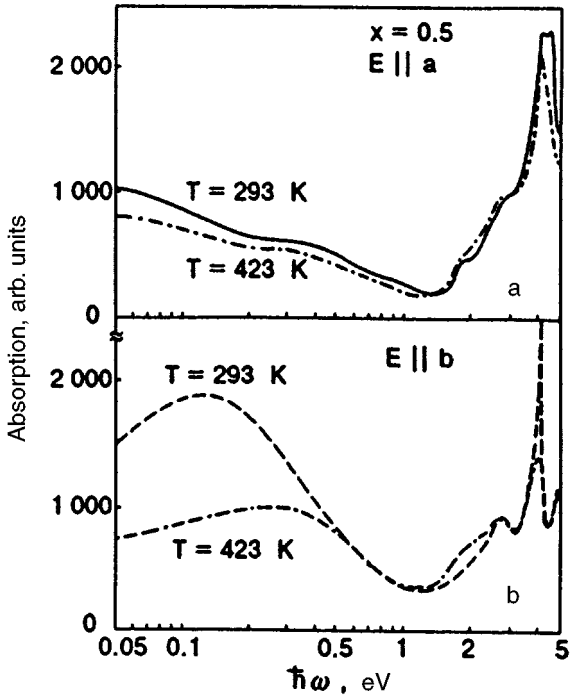

FIG. 7. Absorption spectrum of the $YBa_2Cu_3O_{6.5}$ single crystal, reconstructed in Ref. 8 according to the reflection spectrum for two values of temperature and two directions of polarization parallel to the conducting plane.

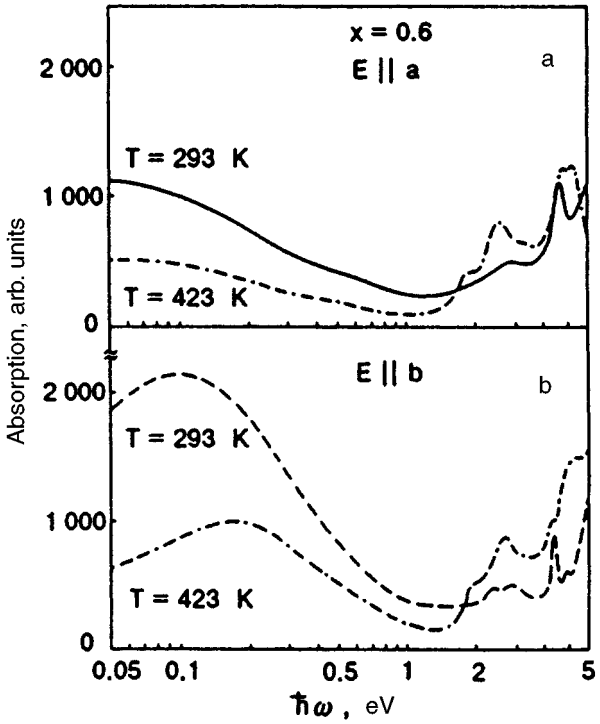

FIG. 8. The same as in Fig. 7 for $YBa_2Cu_3O_{6.6}$ (according to the results obtained in Ref. 8).

interval $\omega > \omega_c$ with the regions of B-type transitions, the experimental data presented in Figs. 7 and 8 completely confirm the conclusions 1–3 drawn in Sec. 2.1. Let us compare these conclusions with the experimental results in greater detail bearing in mind that the region of purely intraband absorption is bounded from above by the dielectric gap width[13] $E_g \simeq 1.8$ eV (in the region $\hbar\omega > E_g$, interband transitions can make a significant contribution to light absorption).

(1) It can be seen from Figs. 7 and 8 that the absorption coefficient at the maximum of the infrared band (to the left of the point $\hbar\omega_c \simeq 0.8$ eV) is 3–6 times larger than the absorption coefficient observed in the region $\hbar\omega_c < \hbar\omega < E_g \simeq 1.8$ eV for all samples, temperatures, and polarizations. According to (15), the ratio of these values of κ must be equal to $(L/a)^2 \simeq 20$; actually, it can decrease due to the additive contribution of the (Drude) plasma absorption covering a broad spectral region as well as due to the errors in the Kramers–Kronig transformation using the reflection spectrum measured in a finite frequency range.

(2) Anisotropy of the infrared absorption of the A-type is confirmed qualitatively in experiments: the absorption is approximately doubled upon a transition from the a-polarization perpendicular to the chains to the b-polarization parallel to the chains. This ratio decreases with the average length of the chain and amounts to only 1.2 for a lower oxygen index of 6.5 and at temperature 423 K (the chain length decreases with decreasing oxygen index and increasing temperature). It should be noted that, according to Figs. 7 and 8, absorption of type B in the region $\hbar\omega_c < \hbar\omega < E_g$ is almost isotropic in the ab plane.

(3) It can be seen from Figs. 7 and 8 that a decrease in the chain length upon sample heating is manifested in a considerable suppression (by a factor of 2 and more) of the type A absorption band. This effect is incommensurate with a small change in the number of charge carriers, which does not exceed a few percent even in a wider temperature interval 300–800 K.[15] According to (2), the average length of the chains changes several times more strongly, leading to a significant change in the A-type absorption in proportion to L^2.

As regards the intraband absorption of type B, it changes with temperature in proportion to the number of charge carriers by not more than a few percent in the absence of temperature phase transitions (see Fig. 7).[13] Temperature variation of the B-type absorption shown in Fig. 8 are apparently associated with certain temperature phase transitions or with errors in calculations based on the Kramers–Kronig formula near the boundary of the measuring interval.

The results obtained by Widder *et al.*[8] were interpreted from the point of view of plasma oscillations. In order to explain absorption anisotropy, the authors of Ref. 8 had to assume that the chain (CuO_x) and conducting (CuO_2) planes make comparable contributions to plasma absorption. Such an interpretation is fraught with significant difficulties. First, the charges in the chain plane in the case of oxygen indices 0.5 or 0.6 close to the insulator–metal transition point are localized, and their direct contribution to the optical conductivity is negligibly small. Second, plasma absorption in-

creases with temperature, while the absorption observed in the infrared region decreases. Plasma absorption is apparently manifested in the absorption spectrum, but does not make a dominating contribution (predicted in Ref. 8) to it, only smoothing the manifestations of the mechanism considered above and leading to the dependence of absorption on temperature and polarization.

Taking into account what has been said above, the type *A* infrared absorption band can be used for diagnostics of the average length of copper–oxygen chains in the process of its controllable variation.

CONCLUSIONS

The electron properties of the superconductor $YBa_2Cu_3O_{6+x}$ are associated with the long-distance potential relief created in the CuO_2 conducting plane by charges located in the parallel CuO_x plane. It was proved by us earlier that the motion of holes in long-distance potential wells affects the transport properties.[1–3]

Electron transitions between energy levels of a long-distance potential well are manifested in the near infrared absorption spectrum in the form of a significant contribution depending on the shape of the potential well and are sensitive to temperature, light polarization, and photoillumination which determine the well width.

A decrease in the temperature of a superconductor to a few kelvins can result in a blurred transition to the insulator phase due to localization of holes at the minima of the long-distance potential. This is manifested in residual resistivity existing at temperatures much lower than T_c; apparently, this effect is of the Anderson nature and is very sensitive to structural inhomogeneities, which can be used for their diagnostics.

The manifestations of long-distance potential relief are characterized by sensitivity to photoillumination leading to a slight increase in the number of charge carriers and to a much stronger increase in the potential well widths. If the observed photoinduced changes in physical quantities are much greater than the corresponding change in the number of charge carriers on the relative scale, a given phenomenon is apparently associated with the long-distance potential.

The authors are grateful to A. M. Kadigrobov for fruitful critical discussions.

This research was carried out under partial support of the Ukrainian State Committee on Science, Engineering, and Industrial Policy (grant No. 09.01.01/046–94).

*E-mail: shapiro@ilt.kharkov.ua

[1)]On account these circumstances, the estimate obtained in Sec. 1.5 can be too high for S and accordingly too low for μ.

[1] V. M. Dmitriev, V. V. Eremenko, I. S. Kachur *et al.*, Fiz. Nizk. Temp. **21**, 219 (1995) [Low Temp. Phys. **21**, 168 (1995)].
[2] A. M. Ratner, Fiz. Nizk. Temp. **21**, 208 (1995) [Low Temp. Phys. **21**, 159 (1995)].
[3] V. V. Erementko, I. S. Kachur, V. G. Piryatinskaya *et al.*, Physica **C262**, 54 (1996).
[4] T. Ito, K. Takenaka, and S. Uchida, Phys. Rev. Lett. **70**, 3995 (1993).
[5] A. Sacuto, M. Balkanski, and O. Gorochov, Solid State Commun. **85**, 589 (1993).
[6] G. Uimin and J. Rossat-Mignod, Physica **C199**, 251 (1992).
[7] E. Osquiguil, M. Maenhoudt, B. Wuyits *et al.*, Phys. Rev. **B49**, 3675 (1994).
[8] K. Widder, A. Zibold, M. Merz *et al.*, Physica **C232**, 82 (1994).
[9] A. M. Kadigrobov, Fiz. Nizk. Temp. **14**, 427 (1988) [Sov. J. Low Temp. Phys. **14**, 236 (1988)]; Fiz. Nizk. Temp. **19**, 943 (1993) [Low Temp. Phys. **19**, 671 (1993)].
[10] A. V. Mitin, G. M. Kuz'micheva, V.V. Murashov, and E. P. Khlybov, Zh. Éksp. Teor. Fiz. **107**, 1943 (1995) [JETP **80**, 1075 (1995)].
[11] A. V. Mitin, N. E. Alekseevskii, and E. P. Krylov, Physica **C199**, 351 (1992).
[12] M. A. Korotin, V. I. Anisimov, E. P. Butorin *et al.*, Matter. Lett. **10**, 34 (1990).
[13] I. Fugol', V. Samovarov, A. Ratner *et al.*, Physica **C216**, 391 (1993).
[14] B. W. Veal, H. You, A. P. Paulikas *et al.*, Phys. Rev. **B42**, 4770 (1990).
[15] H. Shaked, J. D. Jorgensen, B. A. Hunter *et al.*, Phys. Rev. **B51**, 547 (1995).

Translated by R. S. Wadhwa

Magnetic properties of $Ba_{1-x}K_xBiO_{3+y}$ single crystals near T_c

S. N. Barilo, V. I. Gatalskaya, and S. V. Shiryaev

*Institute of Solid State and Semiconductor Physics, Academy of Sciences of Belarus, 220072 Minsk, Belarus**

M. Baran, H. Szymczak, and R. Szymczak

Institute of Physics, Polish Academy of Sciences, 02-668 Warsaw, Poland
(Submitted May 20, 1996, revised July 31, 1996)
Fiz. Nizk. Temp. **23**, 159–166 (February 1997)

Reversible magnetization and hysteresis loops of electrochemically grown $Ba_{1-x}K_xBiO_{3+y}$ single crystals ($x=0.34, 0.37$) are studied in the vicinity of T_c. The results of measurements of reversible magnetizations are used to construct the temperature dependences of the magnetic penetration depth λ and the critical field H_{c2}. The $\lambda(T)$ dependences are described by the BCS theory more successfully than by the two-fluid model. The peak effect observed in these isotropic superconductors on magnetic hysteresis loops is associated with the presence of superstoichiometric oxygen regions. The behavior of the irreversibility line $H_{\rm irr}(T)$ for both single crystals is approximated successfully by the flux creep model. © *1997 American Institute of Physics.* [S1063-777X(97)00402-7]

1. INTRODUCTION

Single crystals of $Ba_{1-x}K_xBiO_{3+y}$ (BKBO) with $T_c \simeq 30$ K and a simple cubic structure characterized by the absence of magnetic ions in the lattice, a large coherence length, and a number of some interesting physical properties are excellent objects for experimental and theoretical investigations aimed at determining the magnetic penetration depth, upper critical field, and other important characteristics. These data lead to the conclusion concerning the magnitude of the coupling constant, and hence the mechanism of pairing in high-temperature superconductors.

It has been established that the irreversibility line $H_{\rm irr}(T)$ separating the reversible and irreversible regions of magnetization M intersects the $H-T$ phase diagram of high-temperature superconductors in the mixed state. Above the $H_{\rm irr}(T)$ line, the phase diagram displays a sharp decrease in critical current and a rapid relaxation of the diamagnetic moment. It should be noted that in spite of intense studies, the nature of the irreversibility line has not been established yet (see, for example, Ref. 1 and the references cited therein). An analysis of isothermal curves $M(H)$ near T_c in the region of reversible magnetization makes it possible to determine the London penetration depth for a magnetic field[2] since HTS materials are characterized by a wide range of magnetic fields $H_{c1} \ll H \ll H_{c2}$ in which the reversible magnetization depends linearly on the logarithm of magnetic field H:

$$4\pi M = (\varphi_0/8\pi\lambda^2)\ln(H_{c2}\beta/H), \tag{1}$$

where φ_0 is the magnetic flux quantum, $\beta \simeq 1$, H_{c2} is the upper critical field, and λ the magnetic penetration depth. In the case of accessible magnetic fields, relation (1) is applicable in a bounded temperature range close to T_c of an isotropic superconductor free of vortex lattice pinning. The magnitude and temperature dependence of the magnetic penetration depth in the BKBO system have been studied insufficiently. In Ref. 3, the $\lambda(T)$ dependence was determined for polycrystalline BKBO by using the data on magnetization and dynamic susceptibility in a varying field for the BKBO powder.

The irreversible component of magnetization $M(H)$ measured at various temperatures can be used to extract information on vortex lattice pinning (in particular, on the critical current density j_c and the irreversibility line $H_{\rm irr}$) and on the anomalous behavior of magnetization in BKBO single crystals in intermediate fields.[4] Here we consider the results of studies of reversible and irreversible magnetization of BKBO single crystals near T_c with various concentration of potassium.

2. SAMPLES AND EXPERIMENTAL TECHNIQUE

BKBO single crystals were grown electrochemically[5] and have the superconducting transition temperature $T_c = 29-30$ K depending on the potassium concentration. The concentration of potassium was determined by three methods: from x-ray measurements of the crystal lattice parameter according to the calibration curve,[6] from neutron activation analysis, and from the measurement of natural radioactivity of the isotope ^{40}K. The typical size of the crystals is $2\times2\times1$ mm. The magnetization was measured near T_c with the help of a vibrational magnetometer in fields up to 6 T and SQUID magnetometer (Quantum Design, MPMS-5) in fields up to 5 T.

3. DISCUSSION OF RESULTS

3.1. Reversible magnetization range

An analysis of the hysteresis loops $M(H)$ measured for $Ba_{1-x}K_xBiO_y$ single crystals with $x=0.34$ and 0.37 in the high-temperature range showed that the $M(\ln H)$ dependences are straight lines and are successfully described by relation (1) in the field and temperature regions under inves-

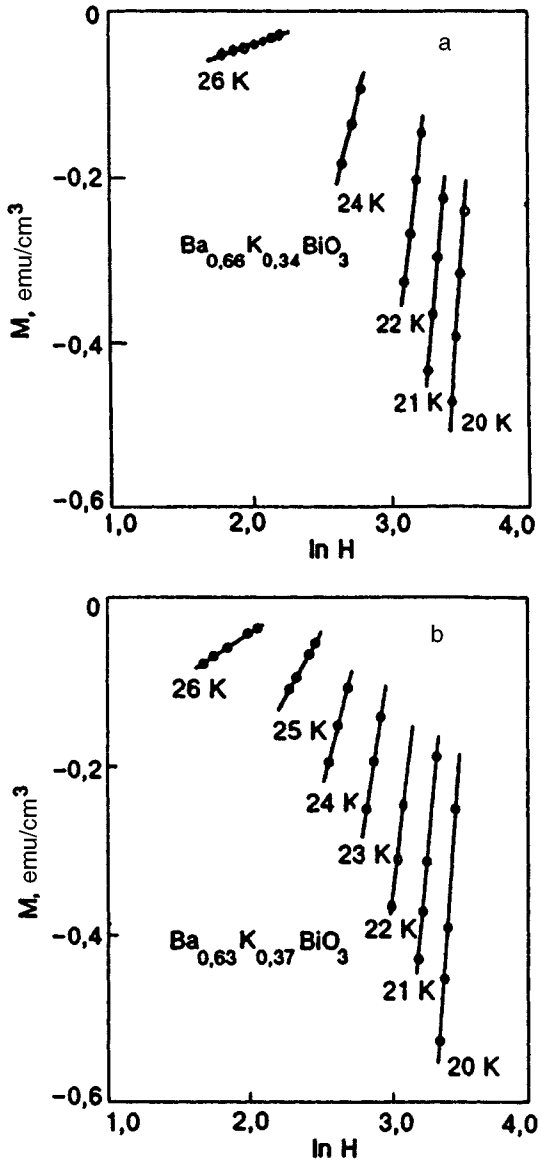

FIG. 1. Field dependence of magnetization at various temperatures of BKBO crystals with $x=0.34$ (a) and 0.37 (b).

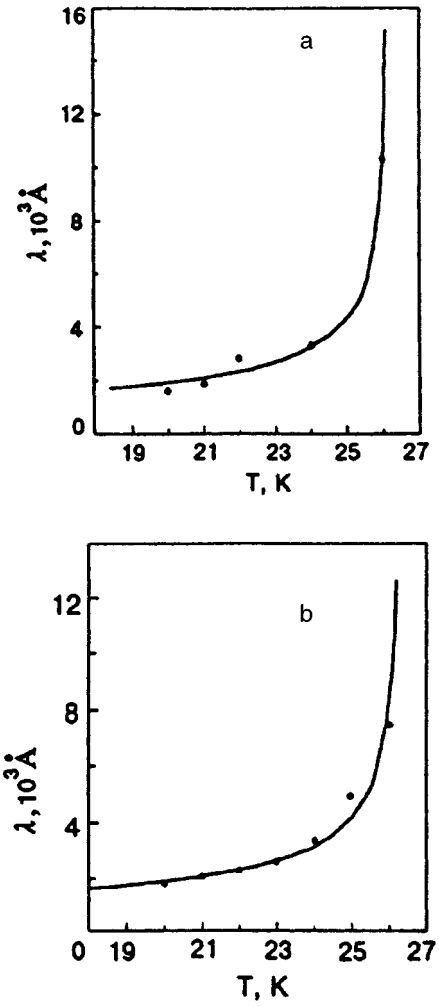

FIG. 2. Temperature dependence of penetration depth λ for BKBO crystals with $x=0.34$ (a) and 0.37 (b). Solid curves describe the approximation by the BCS theory.

tigation (Fig. 1). Figures 2 and 3 show the values of $\lambda(T)$ calculated for both crystals as well as the approximation of the experimental data by the BCS formula

$$\lambda(T)=\lambda(0)[1-(T/T_c)]^{-0.5}, \tag{2}$$

which gives a better agreement with the experimental data than the Gorter–Casimir two-fluid model

$$\lambda(T)=\lambda(0)[1-(T/T_c)^4]^{-0.5}. \tag{3}$$

The corresponding values of $\lambda(0)$ in expression (2) amount to ~924 Å ($x=0.34$) and ~935 Å ($x=0.37$). The value of T_c is of the order of 26.5 K for both samples. This value corresponds to 90% of the temperature T_c^H corresponding to the onset of the transition in weak magnetic fields $H=5$ Oe under ZFC conditions.

Expression (1) contains the upper critical field $H_{c2}(T)$ which is required for calculating the temperature dependences $\xi(T)$ and $\kappa(T)=\lambda(T)/\xi(T)$ of the coherence length and of the order parameter.[7] The values of $H_{c2}(T)$ measured for the two crystals near T_c are shown in Figs. 3 and 4. The temperature dependences of H_{c2} near T_c are described by a linear law, which is in accord with the Ginzburg–Landau theory: $H_{c2}(T)=25(1-T/T_c)^{1.13}(x=0.34)$ and $H_{c2}(T)=19.3(1-T/T_c)^{1.04}(x=0.37)$. The values of dH_{c2}/dT near T_c amount to -0.78 and -0.65 Tl/K for $x=0.34$ and 0.37 respectively. Using the WHH formalism $H_{c2}(0)=-0.693T_c\,(dH_{c2}/dT)$,[8] we can estimate the value of $H_{c2}(0)$ for the crystals under investigation: $H_{c2}^{(0)}=15.7$ Tl ($x=0.34$) and 13.1 Tl ($x=0.37$). The coherence lengths $\xi(0)$ calculated from the relation $H_{c2}=\varphi_0/(2\pi\xi^2)$ are 46 Å ($x=0.34$) and 49 Å ($x=0.37$). On the other hand, the linear extrapolation which is in accord with the Ginzburg–Landau theory led to a considerably larger values of H_{c2}:25 Tl ($x=0.34$) and 19.3 Tl ($x=0.37$), which correspond to coherence lengths 36 Å ($x=0.34$) and 41 Å ($x=0.37$) at $T=0$ K. The upper critical field $H_{c2}(0)$ for our crystals is much smaller than the values of paramagnetic critical field $H_{\rm par}=1.84T_c$ ($\simeq 55$ Tl for $x=0.34$ with $T_c=30$ K and $\simeq 53$ Tl (for $x=0.37$ with $T_c=29$ K), which means that the ''paramagnetic effect'' of

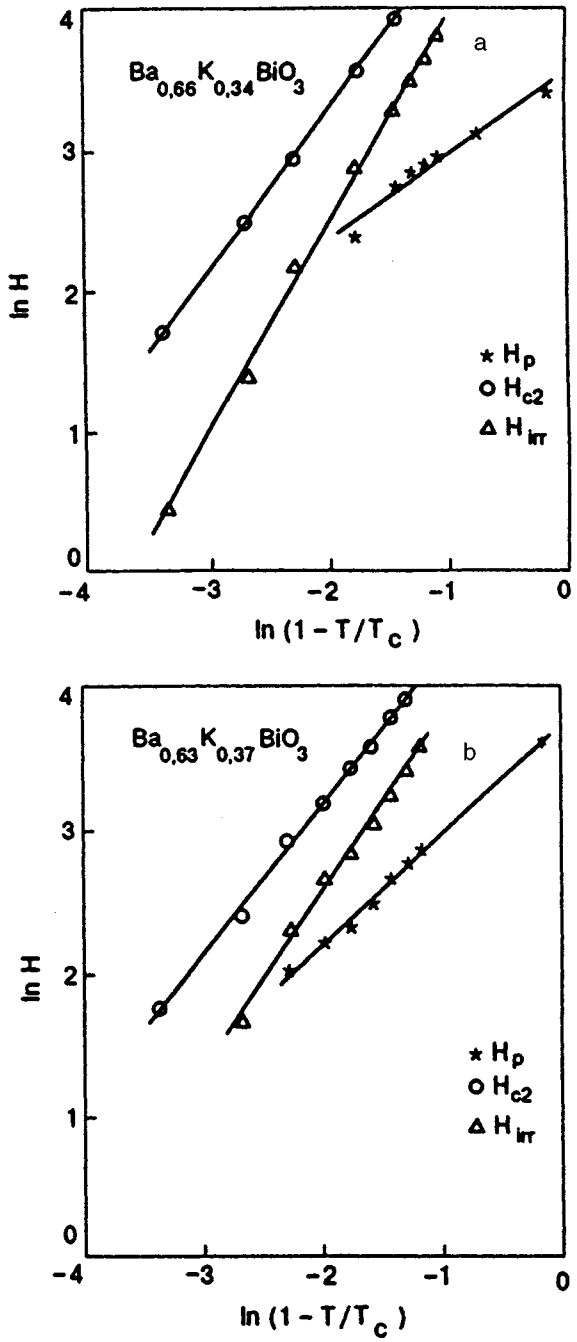

FIG. 3. Temperature dependences of H_p, H_{c2}, and $H_{\rm irr}$ for crystals with $x=0.34$ (a) and 0.37 (b).

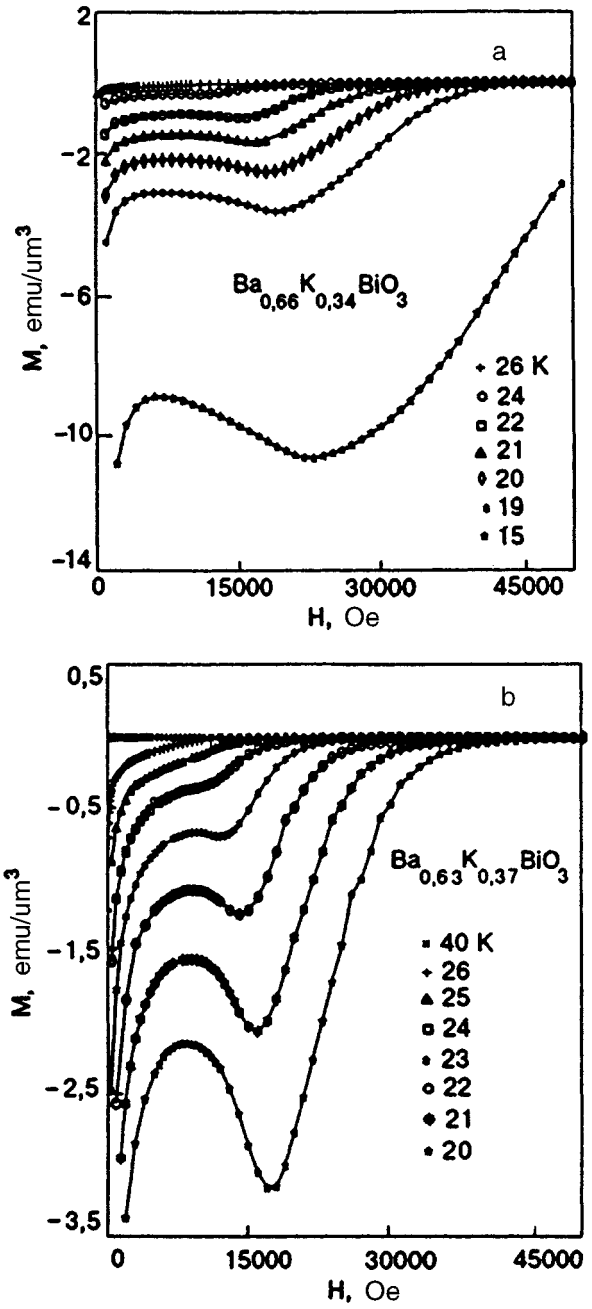

FIG. 4. Fragments of hysteresis loops for crystals with $x=0.34$ (a) and 0.37 (b) at various temperatures.

Cooper pair breaking by the magnetic field is insignificant.

The estimates obtained for coherence length, magnetic penetration depth, and upper critical field are in good agreement with the results of resistive and magnetic measurements on poly- and monocrystalline BKBO samples.[3,9–11] For example, the value of H_{c2} for single crystals grown electrochemically[9] amounts to 30 Tl (at $T=2$ K), which is twice the value of H_{c2} calculated according to the WHH theory. The coherence length $\xi(0)$ corresponding to $H_{c2}=30$ Tl is 33 Å. The order parameter $\kappa(T)$ is equal to 35 ($x=0.34$) and 26 ($x=0.37$) for $T=22$ K. Using the relation $H_{c1}/H_{c2}=(\ln\kappa)/(2\kappa^2)$, we find that for this temperature $H_{c1}=70$ and 100 Oe for $x=0.34$ and 0.37, respectively. The theoretical values of H_{c1} are in satisfactory agreement with the experimental values of H_{c1} for BKBO single crystals.[12]

3.2. Irreversible magnetization range

The peak effect in $Ba_{1-x}K_xBiO_{3+y}$ single crystals ($x>0.33$) was observed for the first time by us earlier[4] and investigated over a wide temperature range (4.2 K–T_c) in intermediate fields $H_{c1}<H_p<H_{c2}$. The shape of additional peaks on hysteresis loops depends on the temperature, while the magnitude of the peak field H_p decreases with increasing temperature. Figure 4 shows fragments of hysteresis loops

for single crystals with $x=0.34$ and 0.37 for temperatures near T_c. The values of j_c ($T=20$ K) calculated according to Bean's model were of the order of $5\cdot 10^3$ A·cm^{-2}. We analyzed the reproducibility of the $H_p(T)$ and $H_{\rm irr}(T)$ dependences for crystals with the same concentration x of potassium as well as the effect of thermal treatment, sample size, and potassium concentration on the shape of the curves. An insignificant spread in the values of H_p and a shift of the $H_{\rm irr}(T)$ line are observed for crystals having the same value of x and grown in the same experiment. The same was observed for a crystal before and after its cutting. On the other hand, sample annealing in oxidizing and reducing media affects the values of H_p and $H_{\rm irr}$ significantly even if the variations of T_c as a result of thermal treatment are small.[4] At the same time, an increase in the potassium concentration in crystals leads to a sharp decrease in H_p and to a more monotonic decrease in $H_{\rm irr}$. Such a dependence of H_p and $H_{\rm irr}$ on potassium concentration is obviously connected with the initial structure of the defects, e.g., with different distribution of oxygen in the crystals. Although the peak effect was observed only in BKBO crystals with an elevated potassium content ($x>0.33$), we concluded[4] that this effect should be attributed to its nonuniform distribution since the crystal structure of $Ba_{1-x}K_xBiO_y$ with $x>0.33$ is strictly cubical and does not exhibit a phase separation into stoichiometric phases with $x=0.08$ and 0.28 as in the case of polycrystals with $0.2<x<0.28$.[13] At the same time, single crystals acquire additional oxygen in the course of electrochemical deposition, the intensity of this process increasing with potassium concentration.[5]

An analysis of the behavior of irreversible magnetization in the temperature range close to T_c confirms our conclusions that the peak effect in BKBO is due to the presence of regions with nonstoichiometric oxygen concentration in crystals with values of H_{c2} and T_c smaller than for the matrix.[14] The models of peak effect such as anisotropy of electron properties[15] and the $3D$–$2D$ phase transition in a vortex lattice[16] are inapplicable to an isotropic cubic system like BKBO. The model of commensurability of the periods of a vortex lattice and a lattice of defects in the vicinity of the field corresponding to an additional peak on the $M(H)$ curve[15] presumes the absence of the temperature dependence of H_p, which contradicts our results (see Fig. 3). It is appropriate to mention a relatively recent publication[17] in which an attempt was made to attribute the peak effect in $YBa_2Cu_3O_{7-\delta}$ (YBCO) single crystal to the formation of irreversible regions with values of $H_{\rm irr}$ differing from that of the matrix on the basis of coincidence of temperature dependences $H_p(T)$ and $H_{\rm irr}\propto(1-T/T_c)^m$. In order to verify the possibility of application of this model to the BKBO system, we analyzed the temperature dependences $H_{\rm irr}(T)$ obtained from the hysteresis loops for YBCO and BKBO single crystals. Our results of measurements of magnetization of YBCO single crystals[4,18] give close values for the $H_p(T)$ and $H_{\rm irr}(T)$ curves near T_c: $m=1.7$ and 1.8. According to Fig. 3, the temperature dependence $H_p(T)$ for BKBO single crystals is described by the relation $H_p(T)=A(1-T/T_c)^n$, while irreversibility lines are described by the dependence $H_{\rm irr}(T)=B(1-T/T_c)^m$ (where $n<m$): $n=0.59$ ($x=0.34$) and 0.77($x=0.37$); $m=1.45$ ($x=0.34$) and 1.22($x=0.37$). Thus, there are no grounds for associating the peak effect in BKBO with the emergence of reversible regions in the crystal as a result of the passage of the magnetic field through the threshold values $H_{\rm irr}$ for regions with a nonstoichiometric oxygen concentration (we assume that such regions are present). Moreover, the values of A and B in the temperature dependence of H_p and $H_{\rm irr}$ are different: the ratio $B/A=6$ for crystals with $x=0.34$ and 4 for crystals with $x=0.37$.

The model of the ''dynamic'' nature of the peak effect presumes the existence of a mirror relation between the field dependences of the critical current density $j_c(H)$ and the magnetization relaxation rate $S(H)$,[19] for which the emergence of an additional peak on hysteresis loops is associated with a decrease in the magnetization relaxation rate due to a change in the form of flux creep. The measurements of static magnetization and magnetic relaxation in BKBO single crystals ($x=0.46$) revealed[20] that the field dependence of relaxation rate $S(H)$ has a peak corresponding to the applied magnetic field $H=H_p/2$. Besides, the peak effect does not appear in the field dependence of the density of actual critical current for this composition, which is obtained by using a generalized inversion scheme.[21] These results indicate that the ''dynamic'' interpretation of the peak effect plays a significant role in BKBO single crystals ($x=0.46$).

A systematic analysis of the pinning force as a function of magnetic field and temperature for the BKBO single crystals ($x=0.34,0.37$) carried out by us showed that at least two different mechanisms of pinning play a significant role in these compositions. Figure 5 shows experimental values of the normalized pinning force in single crystals with these compositions as functions of reduced field at different temperatures as well as their processing according to the formula[22]

$$F_p/F_{p(\max)}=A(b^*)^p(1-b^*)^q, \tag{4}$$

where $b^*=H/H_{\rm irr}$ is the reduced field in the sample, A the numerical parameter, and p and q characterize the pinning mechanism in the superconductor.[23]

The processing mentioned above gives $p=1.95$ and $q=1.52$ for $x=0.34$ at $T=19$–22 K, $p=0.48$ and $q=1.7$ at $T=25$–27 K; for $x=0.37$, $p=4.6$ and $q=3.1$ at $T=20$–22 K, and $p=0.43$ and $q=3.2$ at $T=25$–27 K. It should be noted that $q>p$ for most HTS materials.[24] However, for BKBO single crystals ($x=0.34$, 0.37), we obtained the opposite relation ($q<p$) at low temperatures. It can be seen from Fig. 5 that the experimental values of reduced pinning force are satisfactorily approximated by two different curves having a peak, according to (4), for $H_{\max}$ corresponding to

$$b^*_{\max}=p/(p+q). \tag{5}$$

It was found that $b^*_{\max}=0.56(0.22)$ for $x=0.34$ at $T=19$–22 K (24–28 K), while $b^*_{\max}=0.6(0.12)$ for $x=0.37$ at $T=20$–22 K (25–27 K). Thus, two contributions to irreversible magnetization which obviously exist for BKBO ($x=0.34$, 0.37) are manifested in a significant difference in scaling over the field at low and high temperatures. This means that the peak effect in single crystals with spatial

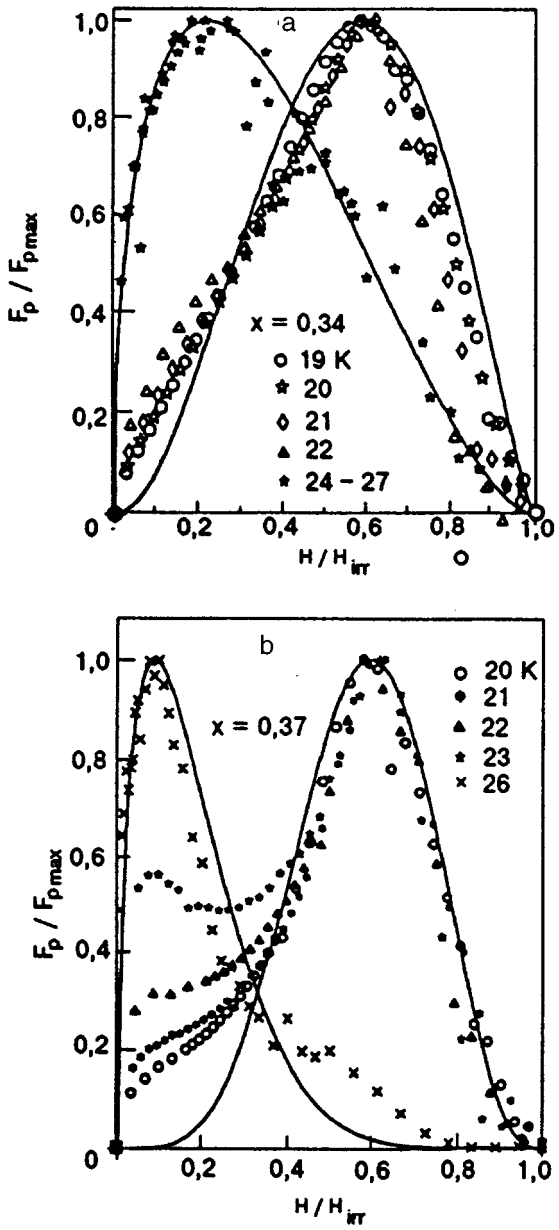

FIG. 5. Normalized pinning force $F_p/F_{p(\max)}$ as a function of the reduced field $H/H_{\rm irr}$ for crystals with $x=0.34$ (a) and 0.37 (b).

oxygen nonstoichiometry can be a consequence of the competition between two pinning mechanism each of which dominates in its own temperature region. Comparing the position of the peak of reduced pinning force with the theoretical predictions,[23] we can assume that pinning centers have a two-dimensional rather than three-dimensional geometry and that both mechanisms of pinning (the so-called δT_c- and δl-pinning) are important. In this case, the peak effect can be due to the crossover between two mechanisms of flux pinning associated with applied magnetic field and/or temperature.

It was mentioned above that complete understanding of the origin of irreversibility line has not yet been attained. It is assumed that $H_{\rm irr}$ defined as the field for which the hysteresis of the $M(H)$ curves disappears can be due to flux creep,[25] vortex lattice melting,[26] or the formation of a new thermodynamic phase of vortex glass.[27] The temperature dependence of the irreversibility field in BKBO single crystals which do not exhibit any peak effect (including those subjected to electron bombardment) was investigated by us in Refs. 12, 28, and 29. For fields above 0.1 Tl, the $H_{\rm irr}(T)$ dependence was approximated by the function $H_{\rm irr}=H_{\rm irr}(0)\times(1-T/T_c)^{3/2}$ with $H_{\rm irr}(0)\simeq 17$ Tl for the initial state. The flux creep model[25] presumes a similar dependence $H_{\rm irr}(T)$ near T_c with $m=3/2$, namely,

$$H_{\rm irr}(T)\sim\{H_c^2(0)\xi(0)\varphi_0\}(1-T/T_c)^{3/2}, \tag{6}$$

For BKBO crystals with $x<0.34$,[12,28,29] the behavior of $H_{\rm irr}(T)$ corresponds to this model. If, however, the $H_{\rm irr}(T)$ curve is due to vortex lattice melting, the irreversibility field near T_c is described by the following relation:[25,30]

$$H_{\rm irr}\sim\{c_L^4\varphi_0^5/4\pi\mu_0^2\kappa_B^2\lambda^4T_c^2\gamma^2\}(1-T/T_c)^2, \tag{7}$$

where c_L is the Lindemann criterion and γ the anisotropy parameter equal to $(m_c/m_{ab})^{1/2}$. It should be noted that the quadratic dependence (7) tends to a linear dependence upon an increase in γ on account of quantum fluctuations of the vortex lattice.[31,32] It follows from Fig. 3 that the values of m in the temperature dependence $H_{\rm irr}(T)$ decrease with increasing potassium concentration ($m=1.45$ and 1.22 for $x=0.34$ and 0.37, respectively). It should be noted that the model of vortex lattice melting correctly describes the experimentally obtained dependence $H_{\rm irr}(T)$ for an isotropic superconductor Rb_3C_{60} near T_c.[33] The fact that $m=2$ in this case unambiguously confirms the presence of a first-order phase transition of the type of vortex lattice–liquid.

If we apply the model of lattice melting to two HTS systems (isotropic BKBO and anisotropic YBCO), the irreversibility line for YBCO must lie above the irreversibility line for BKBO for the same reduced values of temperature and field, and the ratio of reduced irreversibility fields must be of the order of 25 ($\gamma=1$ and 5 for BKBO and YBCO, respectively). In actual practice, our measurements[28,29] showed that this ratio amounts to 0.3–0.5. It follows hence that the irreversibility line is still not associated with the lattice melting (at least for a YBCO single crystal). The possibility of using the model of superconducting vortex glass[27] with the temperature dependence $H_{\rm irr}(T)\propto(1-T/T_c)^{4/3}$ requires additional verification.

Since the behavior of irreversible magnetization in fields smaller than $H_{\rm irr}$ is closely connected with the critical current density of the superconductor and depends on vortex pinning at the defects, it is natural to assume that the irreversibility line is also connected with pinning centers. Electron bombardment ($E=4$ MeV) makes it possible to introduce point radiation defects into the crystal which serve as additional pinning centers. The results of our measurements of residual magnetization in BKBO single crystals exposed to fluences up to $2\cdot10^{18}$ cm^{-2} indicate[28,29] that critical currents increase by a factor of two, and the irreversibility line is shifted toward strong fields. The values of $H_{\rm irr}(0)$ amount to 20 Tl, but the nature of temperature dependence $H_{\rm irr}(T)$ remains unchanged, i.e., is determined by the simple activation model.[25] These results can be explained by a stronger pinning of vortex lattice in a crystal by radiation defects.

The thermodynamic critical field $H_c(0)=H_{c2}(0)/\sqrt{2\kappa}$ is directly related to the effective pinning force,[22] and hence the difference in vortex lattice pinning in crystals with different potassium concentrations (Fig. 5) can be explained, for example, by the difference in the values of $H_c(0)$. Indeed, using the values of the order parameter κ determined from the measurements of reversible magnetization, we find that $H_c(0)=0.93$ Tl for a crystal with $x=0.34$, while for $x=0.37$ the field $H_c(0)=0.74$ Tl. This is in accord with stronger pinning properties of the crystal with $x=0.34$ as compared to those of the crystal with $x=0.37$: the irreversibility fields are higher for the former crystal. According to (4), the values of $H_{\rm irr}$ are proportional to $H_c(0)$, but the value of $H_c(0)$ in this case decreases simultaneously with the superconducting transition temperature T_c which, in turn, decreases in our case upon an increase in x ($T_c=30$ and 29 K for $x=0.34$ and 0.37, respectively). Thus, the flux creep model explains successfully the position of the irreversibility line in the (H,T) plane for BKBO crystals.

4. CONCLUSION

We analyzed the reversible and irreversible magnetizations of $Ba_{1-x}K_xBiO_y$ single crystals with different potassium concentrations near T_c. The values of the critical current density j_c determined in Bean's model from hysteresis loops for the given system are of the order of $5\cdot10^3$ A·cm^{-2} at $T=20$ K in zero magnetic field. The peak effect observed in an isotropic high-temperature superconductor is associated with the presence of regions with superstoichiometric oxygen in the crystal. The reason behind the peak effect can be associated with the crossover δT_c- and δl-pinning mechanisms caused by the external magnetic field and/or temperature. The position of the irreversibility line $H_{\rm irr}$ in the (H,T) plane indicates a strong pinning of the vortex lattice in BKBO and is described satisfactorily by the flux creep model. The isotherms of reversible magnetization near T_c were used to estimate the most important characteristics of the superconductor: $H_{c2}(0)$, $\lambda(0)$, $\xi(0)$, $\kappa(0)$, $H_c(0)$, $H_{\rm par}(0)$. More detailed measurements of magnetization of BKBO single crystals in the reversible and irreversible regions of hysteresis loops are planned in order to determine the electron–phonon interaction constant and to clarify the mechanism of the peak effect.

This research was partly supported by the Polish State Committee on Scientific Research, grant No. KBN 2P 302 11407.

*E-mail: ifttpanb@iftt.basnet.minsk.by

[1] L. Civale, A. D. Marwick, M. W. McElfresh *et al.*, Phys. Rev. Lett. **65**, 164 (1990).
[2] V. G. Kogan, M. M. Fang, and S. Mitra, Phys. Rev. **B38**, 11958 (1988).
[3] H. C. Yang, M. H. Hsieh, D. S. Lee, and H. E. Horng, Phys. Rev. **B42**, 2551 (1990); V. F. Gantmakher, L. A. Klinkova, A. M. Neminskii, and M. V. Filatova, Zh. Éksp. Teor. Fiz. **101**, 1612 (1992) [Sov. Phys. JETP **74**, 859 (1992)].
[4] S. N. Barilo, V. I. Gatalskaya, S. V. Shiryaev *et al.*, Physica **C254**, 181 (1995).
[5] S. N. Barilo, D. I. Zhigunov, L. A. Kurochkin *et al.*, Superconductivity (SPCT) **5**, 1081 (1992).
[6] S. Pei, J. D. Jorgensen, B. Dabrowski *et al.*, Phys. Rev. **B41**, 4126 (1990).
[7] V. L. Ginzburg and L. D. Landau, Zh. Éksp. Teor. Fiz. **20**, 1044 (1950).
[8] N. R. Werthamer, E. Helfand, and P. C. Hohenberg, Phys. Rev. **147**, 295 (1966).
[9] C. Escribe-Filippini, J. Marcus, M. Affronte *et al.*, Physica **C210**, 133 (1993).
[10] M. Affronte, J. Marcus, C. Escribe-Filippini *et al.*, Phys. Rev. **B49**, 3502 (1994).
[11] W. K. Kwok, U. Welp, G. W. Crabtree *et al.*, Phys. Rev. **B40**, 9400 (1989).
[12] S. N. Barilo, V. I. Gatalskaya, D. I. Zhigunov *et al.*, Sverkhprovodimost': Fiz., Khim., Tekh. **7**, 753 (1994).
[13] A. Iyo, H. Uwe, and T. Sacudo, in *Advances in Superconductivity, IV. Proc. ISS'91*, Tokyo 211 (1992).
[14] M. Dauemlong, J. M. Seuntjens, and D. C. Larbalestier, Nature **346**, 332 (1990).
[15] V. Hardy, A. Wahl, A. Ruyter *et al.*, Physica **C232**, 347 (1994).
[16] G. Yang, P. Shang, S. D. Sutton *et al.*, Phys. Rev. **B48**, 4054 (1993).
[17] L. Klein, E. R. Yacoby, I. Yeshurum *et al.*, Phys. Rev. **B49**, 4403 (1994).
[18] V. I. Gatalskaya, G. V. Gatalskii, P. V. Gritskov *et al.*, Izv. Ros. Akad. Nauk, Ser. Fiz. **59**, 164 (1995).
[19] L. Krusin-Elbaum, L. Civale, V. M. Vinokur, and F. Holtzberg, Phys. Rev. Lett. **69**, 280 (1992).
[20] H. Szymczak, R. Szymczak, M. Baran *et al.*, JMMM (in press).
[21] H. G. Schnack, R. Griessen, J. B. Lensink, and Wen Hai Hu, Phys. Rev. **B48**, 13178 (1993).
[22] A. Campbell and J. Evetts, *Superconductors*, Taylor Francis, London (1972).
[23] D. Dew-Hughes, Phil. Mag. **30**, 293 (1974).
[24] E. J. Kramer, J. Appl. Phys. **44**, 1360 (1973).
[25] I. Yeshurum and A. P. Malozemoff, Phys. Rev. Lett. **60**, 2202 (1988).
[26] A. Houghton, R. A. Pelcovits, and A. Sudbo, Phys. Rev. **B40**, 6763 (1989).
[27] M. P. A. Fisher, Phys. Rev. Lett. **62**, 1415 (1989).
[28] V. I. Gatalskaya, G. V. Gatalskii, L. A. Kurochkin *et al.*, Phys. Status Solidi **A143**, 123 (1994).
[29] V. I. Gatalskaya, S. N. Barilo, G. V. Gatalskii *et al.*, in *Proc. 7th Workshop on Critical Currents in Supercond.*, Alpbach, Austria (1994) (ed. by H. W. Weber), World Scientific (1994).
[30] L. I. Glasman and A. E. Koshelev, Phys. Rev. **B43**, 2835 (1991).
[31] G. Blatter and B. Ivlev, Phys. Rev. Lett. **70**, 2621 (1993).
[32] P. L. Gammel, L. F. Schneermeyer, and D. J. Bishop, Phys. Rev. Lett. **66**, 953 (1991).
[33] M. F. Tai, G. F. Chang, and M. W. Lee, Phys. Rev. **B52**, 1176 (1995).

Translated by R. S. Wadhwa

Effect of magnetic flux trapped in intergranular space on magnetic field dependences of rf absorption in HTS materials

G. V. Golubnichaya, A. Ya. Kirichenko, I. G. Maksimchuk, and N. T. Cherpak

Institute of Radiophysics and Electronics, National Academy of Sciences of the Ukraine, 310085 Kharkov, Ukraine

(Submitted April 29, 1996; revised July 1, 1996)
Fiz. Nizk. Temp. **23**, 167–172 (February 1997)

Dependences of rf absorption in HTS ceramic samples on a magnetic field $H<H_{c1g}$ (H_{c1g} is the lower critical field for granules) have been investigated. Some features of these dependences cannot be described by the standard model of critical states, taking into account magnetic flux trapping only in granules. A new electrodynamic model, taking into account qualitatively the magnetic flux trapping both in granules and in the intergranular space is proposed. The modified model makes it possible to explain all the currently observed peculiarities in the magnetic-field dependences of rf absorption both for $H>H_{c1g}$ and for $H<H_{c1g}$. © *1997 American Institute of Physics.* [S1063-777X(97)00502-1]

INTRODUCTION

Electrodynamics of ceramic or polycrystalline high-temperature superconductors (HTS materials) is usually studied by using models, taking into account the coexistence of two coupled electrodynamic subsystems, viz., superconducting granules (grains, or crystallites) and weak links between them. Both these subsystems are manifested in the hysteresis dependences of critical current density, magnetic susceptibility, magnetoresistance, magnetization, and electromagnetic absorption.

Even in the first publications in this field,[1,2] the irreversibility of the dependences of critical current density J_c on the magnetic field H was explained by magnetic flux trapping in grains (first subsystem). Upon a decrease in the external magnetic field, the magnetic field of the trapped flux compensates the action of the applied field on intergranular links (second subsystem). In Ref. 2, a detailed model of the formation of the local magnetic-field in the intergranular space was developed on the basis of the model of critical state applied to granules. This model explained qualitatively the magnetic field penetration and magnetic flux trapping in HTS samples as well as the main peculiarities in the magnetic-field dependence of the critical current density in HTS samples cooled in zero magnetic field at a fixed temperature (ZFC mode).

However, subsequent analysis of the magnetic-field dependences of HTS samples cooled in a magnetic field (FC mode)[3,4] revealed a number of peculiarities which could not be explained by the model proposed in Ref. 2. In this connection, it was necessary to study local magnetic fields in the intergranular space in greater detail, taking into account their compression in order to modify slightly the model proposed in Ref. 2. Independent analysis carried out by Mishra *et al.*[5] confirmed that local fields in the intergranular space experience stronger compression in the ZFC mode than in the FC mode.

In order to explain the hysteresis behavior of the critical current density upon a change in magnetic field, a number of other physical models of formation of the local field in the intergranular space determining the current in Josephon junctions were later proposed. Among these models, we must mention above all the model taking into account the effect of Abrikosov vortices at the banks of a Josephson junction[6] and the model taking into account the magnetization of individual granules and demagnetization factor.[7] In spite of the fact that, in contrast to the model proposed in Refs. 2 and 4, these models lead to not only qualitative, but sometimes also a quantitative coincidence of the results of calculations with experimental data, the physical pattern of the processes occurring in the intergranular medium is sometimes blurred, and (which is most important) the fields trapped in the intergranular medium are ignored completely in this model.

At the same time, the magnetic flux trapping in fields $H<H_{c1g}$ was established even in the first publications on HTS ceramics,[8] and the influence of the magnetic field on the hysteresis behavior of critical current was studied in Ref. 9 (H_{c1g} is the field determining the onset of penetration of Abrikosov vortices in granules).

At the same time, a correlation between the magnetic-field dependence of dynamic magnetic susceptibility and critical current was established.[10,11] An analysis of the hysteresis behavior of electromagnetic energy absorption in HTS samples in the microwave range[12] and in the rf range[13] revealed the coincidence of the main features of the magnetic-field dependences and similar dependence of critical current. This made it possible to apply the electrodynamic model proposed in Refs. 2 and 4 in the analysis of magnetic-field dependences of magnetic susceptibility and rf absorption also.

According to the results of more detailed investigations of the rf absorption in a magnetic fields which do not disturb the Meissner state of granules ($H<H_{c1g}$), these dependences display peculiarities which cannot be explained on the basis of the model proposed in Refs. 2 and 4. These peculiarities are also responsible for the difference between the magnetic-field dependences of rf absorption and the $J_c(H)$ dependence in the same fields. For example, the field dependence of rf absorption in HTS samples with trapped magnetic flux (for $H=0$), which is obtained during zero-field

cooling, has clearly manifested regions of absorption associated with magnetic flux trapping in the intergranular medium,[14,15] which are not present on the $J_c(H)$ curves.[16,17] Peculiarities in the magnetic field penetration into a hollow cylinder[18] or the rf absorption in texturized ceramics[19] as well as in HTS samples upon a change in the orientation of the applied magnetic field for $H<20$ Oe[20,21] cannot be explained either in the standard model of critical state for granules proposed in Refs. 2 and 4.

Consequently, the electrodynamic model proposed in Refs. 2 and 4 must be modified by taking into account the dynamics of magnetic field penetration and magnetic flux trapping in the second subsystem (intergranular space) also. In order to analyze the effect of fields associated with magnetic flux trapping in current loops embracing several granules and including Josephson junctions between granules in their circuit in the intergranular medium, we analyzed the magnetic-field dependences of rf absorption in external static fields smaller than H_{c1g}.

EXPERIMENTAL RESULTS

The rf absorption at a frequency of 2.5 MHz in YBaCuO HTS ceramics was determined in our experiments from the Q-factor of the rf circuit whose inductance was loaded by the sample under investigation. The intrinsic losses in the circuit were subtracted. The measurements were made at the nitrogen boiling temperature. The measuring technique was described in detail in Ref. 11. The graphic representation of the field dependences of rf absorption in the form of reciprocal absorption $Q(H)$ facilitates their comparison with magnetic-field dependences of the critical current density[1–6] $J_c(H)$ which are basically similar.

Figures 1a and b show for comparison the dependences obtained for the samples synthesized according to traditional ceramic technology (Fig. 1a) and by using partial melting as a result of sample heating to 1050 °C during 10 min (Fig. 1b). The figures show three types of magnetic-field dependences of absorption: $Q(H)$ in a field increasing to the maximum value of the magnetic field $H=H_m>H_{c1g}$ (curve *1*), $Q(H)$ in a field decreasing after the attainment of the value $H=H_m$ (curves *2* and *2′*), and $Q_{\rm rem}(H_m)$ in the field associated with the trapped magnetic flux in the sample for $H=0$ (curve *3*). The curves *2* and *2′* differ in the value of maximum magnetic field H_m. The characteristic values of critical fields determined from the field dependences of absorption in the sample with a trapped magnetic flux, i.e., curves *3* are plotted along the abscissa axis (see Ref. 11): H_{c1j} is the lower critical field for the intergranular medium, and H_{pj} is the field corresponding to complete transition to the critical state of the sample for the intergranular medium with the conservation of the Meissner state of the granules.

It is well known that the magnetic-field dependences of rf absorption of granular HTS samples in a decreasing magnetic field are characterized by a lower absorption as compared to the values obtained in an increasing field for the same values of H. However, near $H=0$ the situation changes in all cases: the absorption in a decreasing field is stronger than in an increasing field. A transition from one situation to the other naturally determines the intersection of

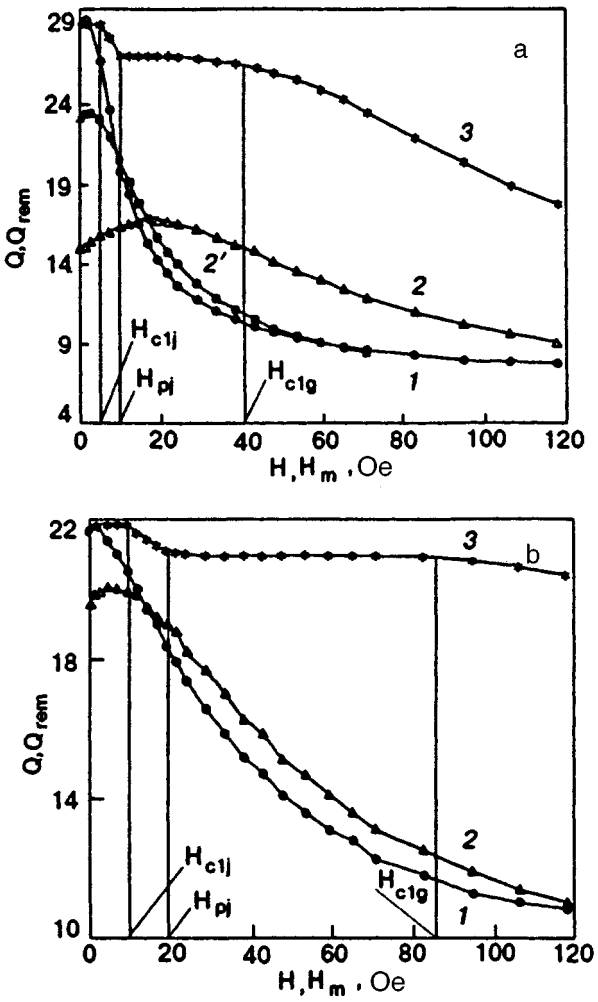

FIG. 1. Magnetic-field dependences of the Q-factor and $Q_{\rm rem}$ of an rf circuit loaded with a ceramic sample prepared according to the standard ceramic technology (a) and with partial melting (b) in an increasing magnetic field (curve *1*) and in a decreasing magnetic field for $H_m=165$ Oe (curve *2*) and 70 Oe (curve *2′*), and in a sample with trapped magnetic flux (curve *3*).

the curves describing the magnetic field dependences in increasing and decreasing fields at the point $H=H_c$. The value of the external magnetic field $H=H_{\rm ex}$ corresponding to the maximum value of critical current density on the dependence in a decreasing magnetic field normally exceeds the value $H=H_c(H_{\rm ex}>H_c)$.[1–5] This peculiarity is also observed for the magnetic-field dependences of rf absorption.

It is remarkable that the reverse situation, i.e., $H_{\rm ex}<H_c$, is clearly manifested in the experiment[9] aimed at the determination of the effect of the fields trapped in the intergranular space by closed circular currents embracing several granules. However, this peculiarity was disregarded in Ref. 9 as well as in other publications.

Figure 1a shows a typical field dependence of the Q-factor in a decreasing magnetic field for a sample synthesized according to the classical technology (curve *2*). For $H_m=165$ Oe, $H_{\rm ex}>H_c$ on this curve. The condition of equality of absorption in increasing and decreasing fields for $H=H_c$ in the case when $H_{\rm ex}>H_c$ can be easily explained in the model proposed in Refs. 2 and 4 and taking into account

the critical state of the subsystem of granules alone. This condition can be written in the form

$$|B| = |2B_g|, \tag{1}$$

where $B = \mu H$, μ is the permeability, and B_g the local value of the magnetic field in the intergranular space, which is associated with the dissipated field of the magnetic flux trapped by granules. It should be recalled that, according to the concepts of the model,[2,4] the magnetic field vectors **B** and $\mathbf{B}_g$ in the intergranular space are opposite. The peak on the curve *2* observed at the point $H_{\rm ex}$ is determined by the equality of local fields in the intergranular space:

$$|B| = |B_{\rm g}|. \tag{2}$$

However, as the maximum value of the magnetic field H_m for which the hysteresis cycle takes place decreases, the value of H_c on the magnetic field dependences of rf absorption is larger than $H_{\rm ex}$ in some cases (see Ref. 9). Curve *2′* in Fig. 1a obtained for $H_m = 70$ Oe is a typical example of the magnetic-field dependence in this case. Moreover, the condition $H_c > H_{\rm ex}$ can be also observed for higher values of H_m in the case when the technological conditions of synthesis of HTS materials are changed. By way of an example, Fig. 1b shows the magnetic-field dependence of rf absorption in a decreasing magnetic field (curve *2*) for an HTS sample whose synthesis was accompanied by partial melting, which made it possible to double the value of critical current density. For this sample, the condition $H_c > H_{\rm ex}$ is also fulfilled for $H_m = 165$ Oe, which is usually not observed for samples obtained by the standard method of solid-state synthesis.

In the electrodynamic model proposed in Refs. 2 and 4, the conditions of intersection of magnetic-field dependences of rf absorption in increasing and decreasing fields cannot be formulated for $H_c > H_{\rm ex}$, i.e., in the case when the total local value $B_{\rm eff}$ of magnetic field in the intergranular space does not change its direction to become antiparallel to the external magnetic field. For this purpose, we must modify the model of flux trapping[2,4] in order to take into account the flux trapping in the intergranular space.

DISCUSSION OF RESULTS

Before we take into account the influence of rf absorption of the magnetic field determined by the magnetic flux trapped by stable current loops embracing several granules, let us consider the main features of the electrodynamic model[2,4] applied for analysis of magnetic-field dependences of critical current J_c. We assume that J_c (as well as rf absorption) is mainly determined by the intergranular medium which can be often visualized as a network of Josephson junctions, and the influence of the external magnetic field on J_c (or absorption) is determined by the magnitude of the local magnetic field $B_{\rm eff}$ in the intergranular space. For this purpose, we consider the nature of variation of the components of the local magnetic field $B_{\rm eff}$ in the intergranular space as a function of a (decreasing) magnetic field H with the help of schematic diagram presented in Fig. 2. The variation of B in the intergranular medium is presented by the solid curve emerging from the origin, deviating from the straight line for small values of H and approaching it asymptotically for higher values of the magnetic field. The dot-and-dash line describes the change in the magnitude of the component B_g of the local magnetic field created by the dissipative field of the flux trapped by granules. The direction of this component in the intergranular medium is opposite to the direction of the external field component. However, the field B_g is presented in the first quadrant of the coordinate system for the sake of visualization of the total local field $B_{\rm eff}$ between granules.

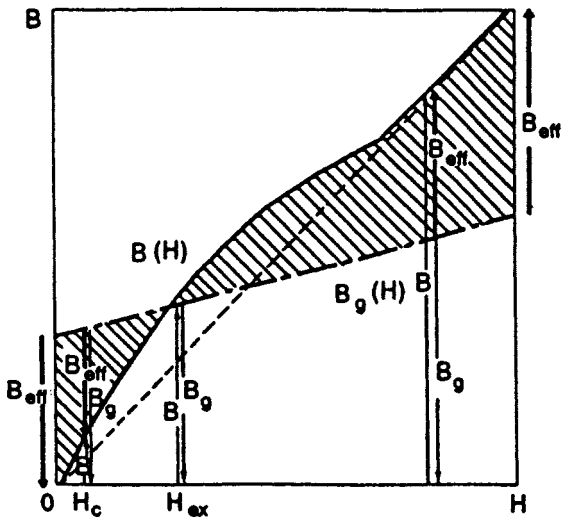

FIG. 2. Schematic representation of the dependences of local magnetic field components in the intergranular space on the applied decreasing magnetic field H in the field range $H < H_{c1g}$ for $H_m > H_{c1g}$, taking into account magnetic flux trapping only in grains (according to the model developed in Refs. 2 and 4).

On the diagram under consideration, the effective local magnetic field $B_{\rm eff}$ acting on the Josephson junctions between granules is determined by the sum of the vectors associated with the applied field B and the opposite field B_g. The variation of $B_{\rm eff}$ in a decreasing magnetic field is determined by the vertical size of the hatched region between the curves $B(H)$ and $B_g(H)$. Proceeding from this diagram, we cannot explain the fulfillment of the ''castling'' condition for the values of H_c and $H_{\rm ex}$, which is expressed in the form of the replacement of the inequality $H_{\rm ex} > H_c$ by the inequality $H_c > H_{\rm ex}$ (see Fig. 1b and curve *2′* in Fig. 1a).

These peculiarities of the magnetic-field dependences of rf absorption can be explained by introducing additional local fields B_j induced by the magnetic flux trapped in the intergranular space by stable closed currents passing through the system of granules and containing Josephson junctions in their circuit. We assume that superconductivity of the intergranular subsystem is weaker (the value of critical current density for this subsystem is much lower than for the subsystem of granules). However, it is also a type II superconductor which exhibits in static magnetic fields a transition to the critical state described by the simplest Bean's model. Naturally, this medium exists in the critical state only in very weak fields until intergranular junctions are broken by the applied field which affects the variation of the local field B_j more strongly than the variation of the local field B_g.

Proceeding from these assumptions, we can present

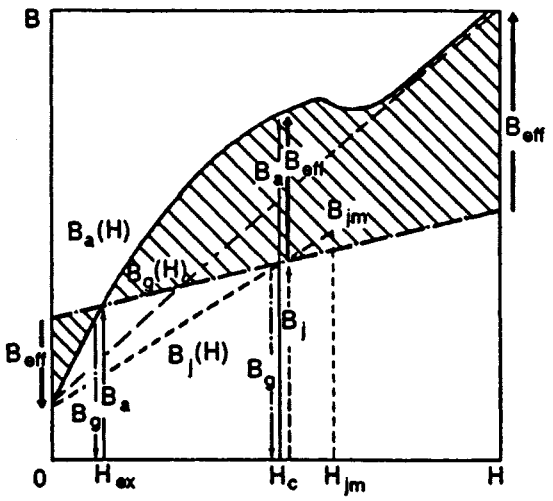

FIG. 3. Schematic representation of the dependences of local magnetic field components in the intergranular space on the applied decreasing magnetic field H in the field range $H<H_{c1g}$ for $H_m>H_{c1g}$, taking into account magnetic flux trapping not only in grains, but also in the intergranular space (modified model).

schematically the pattern of variation of the local magnetic field components in the intergranular space in a decreasing field as a function of the applied field (Fig. 3). The nature of variation of the local magnetic field component B_j associated with the trapped magnetic flux in the intergranular space is presented by a segment of the dashed curve with a slope larger than that of the dot-and-dash curve describing the variation of the field component B_g. This curve terminates at the point B_{jm} determining complete rupture of intergranular junctions. The direction of the magnetic field component B_j coincides with the direction of the applied magnetic field B in the medium.

In contrast to Fig. 2, the solid curve in Fig. 3 shows the total value of the local fields $B_a(H)$ in the intergranular medium which coincides in direction with the applied magnetic field component $B_a=B+B_j$, and not the component associated with the applied magnetic field B. However, the component $B_j=0$ for $H>H_{jm}$.

An analysis of the points of intersection of the dependence $B_g(H)$ with the dependence $B_j(H)$ and the nature of variation of $B_a(H)$ indicates the possibility of ''castling'' of the points H_c and $H_{\rm ex}$ on the magnetic-field dependence. For small H_m, the following condition is satisfied at the point H_c:

$$|B_g|=|B_j|, \tag{3}$$

which ensures mutual compensation of these fields. The role of the effective local field $B_{\rm eff}$ acting on intergranular junctions is played, as before, by the component associated with the applied field B subjected to a certain compression. If the inequality $H_c>H_{\rm ex}$ is satisfied, the condition

$$|B_g|=|B_a|=|B+B_j|. \tag{4}$$

is satisfied at the point $H_{\rm ex}$ corresponding to the extremal point on the magnetic-field dependence of rf absorption in a decreasing field.

With increasing H_m, i.e., for an ascending dot-and-dash curve describing the variation of $B_g(H)$, the conventional condition $H_{\rm ex}>H_c$ is satisfied in the case when it does not intersect with the segment of the dashed curve $B_j(H)$ in accordance with the diagram presented in Fig. 2 and corresponding to the model[2,4] disregarding magnetic flux trapping in the intergranular space. The effective local field acting on the intergranular medium is determined from the hatched region as in the diagram in Fig. 2.

The increase in the critical current density is reflected in a decrease in the slope of the dependence $B_j(H)$ and an increase in the value of B_{jm}. This leads to an increase in the value of H_c (the inequality $H_c>H_{\rm ex}$ being preserved), leading to an expansion of the magnetic field range in which rf absorption in a decreasing field exceed rf absorption in an increasing field. The validity of the inequality $H_c>H_{\rm ex}$ in fields up to $H_m=165$ Oe is illustrated by curve *2* in Fig. 1b, which was obtained on YBCO samples with partial melting. The peculiarities in the reversal of magnetic-field dependences of rf absorption in increasing and decreasing fields observed in Ref. 19 on texturized samples can probably be explained by a large abscissa of the point of intersection of the dependences $B_j(H)$ and $B_g(H)$, i.e., by a higher value of H_c in the inequality $H_c>H_{\rm ex}$.

The peculiarities in the magnetic-field dependences which are manifested in magnetic fields $H<H_{\rm c1g}$ and cannot be explained in the electrodynamic model[2,4] can be easily explained by taking into account the peculiarities of magnetic flux penetration and trapping in the intergranular medium of the samples. These peculiarities include an additional peak on the field dependence of rf absorption in samples with a trapped magnetic flux upon a change in the direction of the applied magnetic field,[14] a manifestation of the effect of magnetic field orientation on qualitative changes in the field dependence of absorption[20] under the same conditions, and manifestation of anisotropy.[21] It is also known that minima and maxima can appear on the virtually horizontal dependence $Q_{\rm rem}(H_m)$ in the field interval $H_{pj}\leqslant H_m\leqslant H_{c1g}$ for samples with a trapped magnetic flux upon a change in the conditions of thermal treatment of the samples.[15] This effect can also be explained easily by attributing it to changes in the system of Josephson junctions that determine the peculiarities in the magnetic flux trapping in the intergranular space, which is confirmed by direct measurements of magnetic flux.[22]

CONCLUSION

An analysis of peculiarities in magnetic-field dependences of rf absorption in HTS ceramic samples of the $YBa_2Cu_3O_{7-x}$ type in magnetic fields lower than the lower critical field H_{c1g} for granules indicates a noticeable influence of the magnetic fields created by the flux trapped in the intergranular space on the electrodynamics of the medium. These peculiarities imply that the standard model of critical state proposed in Refs. 2 and 4 and taking into account the magnetic flux trapping only in granules is inapplicable and requires a modification. The condition $H_{\rm ex}<H_c$ serves as the

criterion of manifestation of the effects of the field trapped in the intergranular medium on the magnetic-field dependences of rf absorption.

The model proposed here makes it possible to describe qualitatively all the peculiarities in the observed dependences of rf absorption on the external magnetic field both for $H<H_{c1g}$ and for $H>H_{c1g}$. The model takes into account the possibility of magnetic flux trapping in both subsystems: in grains in the intergranular medium.

[1] L. S. Kokhanchik, V. A. Marchenko, T. V. Nikiforova, and A. V. Nikulov, Fiz. Nizk. Temp. **14**, 872 (1988) [Sov. J. Low Temp. Phys. **14**, 479 (1988)].
[2] J. E. Evetts and B. A. Glowacki, Cryogenics **28**, 641 (1988).
[3] M. E. McHenry, P. Maley, and J. O. Willis, Phys. Rev. **B40**, 2666 (1989).
[4] Y. Yang, C. Beduz, and S. P. Ashworth, Cryogenics **30**, 618 (1990).
[5] P. K. Mishra, G. Ravikumar, P. Chaddan *et al.*, Jpn. J. Appl. Phys. **29**, L1612 (1990).
[6] A. I. D'yachenko and V. V. Chabanenko, Fiz. Nizk. Temp. **18**, 826 (1992) [Sov. J. Low Temp. Phys. **18**, 581 (1992)].
[7] K. H. Muller and D. N. Matthews, Physica **C206**, 275 (1993).
[8] H. Zhang, S. S. Yan, H. Ma *et al.*, Solid State Commun. **65**, 1125 (1988).
[9] K. Y. Chen and Y. I. Gian, Physica **C159**, 131 (1989).
[10] A. M. Dolgin and S. N. Smirnov, Sverkhprovodimost': Fiz., Khim, Tekhn. **2**, 104 (1989).
[11] Y. Yang, C. Beduz, and R. G. Scurlock, Physica **C201**, 325 (1992).
[12] Y. Maniva, A. Grupp, F. Hentsch, and M. Mehring, Physica **C156**, 755 (1988).
[13] I. E. Aronov, A. Ya. Kirichenko, A. A. Krokhin, and N. T. Cherpak, in *Problems of High-Temperature Superconductivity* [in Russian], Naukova Dumka, Kiev (1989).
[14] A. Ya. Kirichenko and N. T. Cherpak, Pis'ma Zh. Tekh. Phys. **18**, 85 (1992) [Sov. Tech. Phys. Lett. **18**, 758 (1992)].
[15] G. V. Golubnichaya, A. Ya. Kirichenko, N. T. Cherpak *et al.*, Sverkhprovodimost': Fiz., Khim. Tekh. **5**, 486 (1992).
[16] A. A. Zhukov, V. V. Moshchalkov, D. A. Komarkov *et al.*, Jpn. J. Appl. Phys. **29**, L760 (1990).
[17] E. Altshuler, S. Garcia, and J. Barroso, Physica **C177**, 61 (1991).
[18] E. V. Blinov, È. B. Sonin, A. K. Tagantsev, and K. B. Traito, Sverkhprovodimost': Fiz., Khim., Tekh. **4**, 503 (1991).
[19] A. I. D'yachenko, V. V. Chabanenko, M. V. Zalutskii, and E. M. Rozenblat, Fiz. Nizk. Temp. **20**, 167 (1994) [Low Temp. Phys. **20**, 134 (1994)].
[20] M. G. Semenchenko and V. G. Fleisher, Sverkhprovodimost': Fiz., Khim., Tekh. **3**, 240 (1990).
[21] G. V. Golubnichaya, V. T. Zagoskin, A. Ya. Kirichenko *et al.*, Dokl. NAN Ukr. No. 2, 63 (1996).
[22] Kh. R. Rostami, A. A. Sukhanov, and E. V. Mantarov, Fiz. Nizk. Temp. **22**, 58 (1996) [Low Temp. Phys. **22**, 42 (1996)].

Translated by R. S. Wadhwa

LOW-DIMENSIONAL AND DISORDERED SYSTEMS

Acoustic transparency of layered conductors

O. Galbova and G. Ivanovski

Faculty of Natural Sciences and Mathematics, Physical Institute, 9100 Skopje, Republic of Macedonia

O. V. Kirichenko and V. G. Peschansky

*B. Verkin Institute for Low Temperature Physics and Engineering, National Academy of Sciences of the Ukraine, 310164 Kharkov, Ukraine**

(Submitted September 2, 1996)
Fiz. Nizk. Temp. **23**, 173–179 (February 1997)

The method for investigating the electron properties of metals, which was developed by I. M. Lifshits under the assumption that the form of the energy–momentum relation for charge carriers is known *a priori*, and for reconstructing the electron energy spectrum from experimental data is applied for studying acoustoelectronic effects in layered conductors with a strongly anisotropic conductivity of the metallic type. It is shown that the attenuation of acoustic waves propagating along the layers can become much weaker in strong magnetic fields. The conditions for acoustic transparency of layered conductors with a quasi-two-dimensional electron spectrum are obtained, and the oscillatory dependence of acoustic damping decrement on the magnetic field is analyzed for various orientations of the acoustic wave vector and the magnetic field. © *1997 American Institute of Physics.* [S1063-777X(97)00602-6]

An analysis of acoustic waves propagating in metals in a magnetic field resulted in the successful solution of the inverse problem of reconstructing of the electron energy spectrum from experimental data, which was formulated by I. M. Lifshits. The concept of quasiparticles, viz., elementary excitations above the ground state of condensed media, is undoubtedly effective in an analysis of physical properties of various conductors, including low-dimensional ones. This is associated with a long lifetime of conduction electrons with the energy close to the Fermi energy, which makes it possible to study in detail the Fermi branch of the energy spectrum in detail without resorting to specific models of the energy–momentum relation for charge carriers. Such an approach developed by I. M. Lifshits[1] has made it possible to investigate thoroughly the electronic properties of layered conductors with a strong anisotropy in the electrical conductivity. Most of these conductors are layered structures of organic origin, whose electrical conductivity along the normal **n** to the layers is considerably smaller than the conductivity along the layers. The quasi-two-dimensional nature of the energy spectrum of charge carriers in such conductors leads to a number of specific effects[2–9] which are not observed in ordinary metals. The most impressive effect is associated with acoustic transparency of layered conductors in a magnetic field **H**, when the radius of curvature r of the trajectory of a conduction electron is much smaller than its mean free path l, but much larger than the acoustic wave length $1/k$. The damping decrement $\Gamma(H)$ for acoustic waves in metals in this magnetic field range is l/k times larger than $\Gamma(0)$. On the other hand, the electron energy absorption for acoustic waves propagating along the layers in quasi-two-dimensional conductors decreases with increasing magnetic field. The only exception are the resonant values of the magnetic field satisfying the condition $kr=\pi(n+1/4)$ under which $\Gamma(H)$ is again proportional to l/r.[5]

The current interest in low-dimensional structures is mainly due to the need in new superconducting materials for practical applications. However, the specific properties of such superconductors in the normal (nonsuperconducting) state can undoubtedly be used in various fields of electronics (e.g., acoustoelectronics). Galvanomagnetic phenomena in layered conductors have been studied experimentally by many authors, but acoustoelectronic effects have not been investigated experimentally to our knowledge. The presence of an additional parameter (wave frequency) can undoubtedly be used for studying the properties of charge carriers in layered conductors in greater detail and can probably help to find the reason behind some discrepancies between the theory of galvanomagnetic effects and experiments.

In addition to acoustic wave damping in conducting crystals, which is associated with the interaction of thermal phonons with coherent phonons having the acoustic frequency ω, many mechanisms of electron absorption of acoustic waves also exist. The most significant (deformation) mechanism[10] is associated with the energy renormalization for charge carriers under the action of crystal deformation

$$\delta\varepsilon=\lambda_{ij}u_{ij}. \tag{1}$$

In a magnetic field, this mechanism competes with the inductive mechanism, i.e., Joule losses associated with the

generation of electromagnetic fields by an acoustic wave. These fields can be determined with the help of Maxwell's equations

$$\text{curl curl } \mathbf{E}=(4\pi i\omega/c^2)\mathbf{j}; \tag{2}$$

$$\text{div } \mathbf{E}=4\pi\rho', \tag{3}$$

while the relation between the current density

$$\mathbf{j}=2(2\pi h)^{-3}\int d^3p e\mathbf{v}f(\mathbf{p},\mathbf{r},t), \tag{4}$$

and the strain tensor $u_{ij}=\partial u_i/\partial x_j$ and the electric field

$$\tilde{\mathbf{E}}=\mathbf{E}+[\dot{\mathbf{u}}\times\mathbf{H}]/c+m\ddot{\mathbf{u}}/e, \tag{5}$$

in a concomitant reference frame moving with the velocity of ions $\dot{\mathbf{u}}=\partial\mathbf{u}/\partial t$ can be determined by using Boltzmann's kinetic equation for the charge carrier distribution function $f(\mathbf{p},\mathbf{r},t)$:

$$\partial f/\partial t+\mathbf{v}\partial f/\partial\mathbf{r}+\{e(\tilde{\mathbf{E}}+[\mathbf{v}\times\mathbf{H}]/c-\partial\delta\varepsilon/\partial\mathbf{r}\}\partial f/\partial\mathbf{p} = W_{\text{col}}\{f\}. \tag{6}$$

Here ρ' and $\mathbf{v}=\partial\varepsilon/\partial\mathbf{p}$ are the noncompensated density and velocity of charge carriers, c the velocity of light, and e and m are the charge and mass of a free electron. The last term in formula (5) is associated with the Stewart–Tolman effect. The collision integral $W_{\text{col}}\{f\}$ vanishes upon the substitution of the equilibrium Fermi distribution function $f_0(\varepsilon-\mathbf{p}\cdot\dot{\mathbf{u}})$ for charge carriers in the concomitant reference frame.

Maxwell's equations and the kinetic equation should be supplemented with the equation from the theory of elasticity, taking into account the reciprocal effect of the system of electrons whose equilibrium is disturbed by the crystal deformation on the ionic vibrations. Such a system of equations in the case of small deformations was obtained for the first time by Silin[11] for an isotropic metal, by Kontorovich[12,13] for an arbitrary energy–momentum relation for charge carriers, and by Andreev and Pushkarov[14] for arbitrary deformations.

In the case of small ionic displacements $\mathbf{u}$, it is sufficient to use only the linear approximation in u_{ij} and to assume that the deformation potential tensor components λ_{ij} in Eq. (1) are functions of the momentum $\mathbf{p}$ of a conduction electron alone, while the magnitudes of these components can apparently be assumed to be of the order of the characteristic energy of charge carriers, i.e., the Fermi energy. In this case, the tensor components $\lambda_{ij}(\mathbf{p})$, as well as the electron energy $\varepsilon(\mathbf{p})$ in an undeformed crystal, i.e.,

$$\varepsilon(\mathbf{p})=\sum_{n=0}^{\infty}\varepsilon_n(p_x,p_y)\cos(anp_z/h), \tag{7}$$

are also strongly anisotropic functions of the momentum of charge carriers. We assume that the coefficients of cosines in expression (7) for $\varepsilon(\mathbf{p})$ decrease rapidly with increasing n so that $A_1=\eta A_0\ll A_0$ and $A_{n+1}\ll A_n$, where A_n is the maximum value of the function $\varepsilon_n(p_x,p_y)$ on the Fermi surface, $\varepsilon(\mathbf{p})=\varepsilon_F$.

In the linear approximation in a small perturbation of the electron system by crystal deformation, the kinetic equation for the function $f=f_0(\varepsilon-\mathbf{p}\cdot\dot{\mathbf{u}})-\psi(\mathbf{p},\mathbf{r})\exp(-i\omega t)\partial f_0/\partial\varepsilon$ assumes the form

$$\partial\psi/\partial t_H+\mathbf{v}\partial\psi\partial\mathbf{r}+\nu\psi=e\mathbf{v}\cdot\tilde{\mathbf{E}}-i\omega\Lambda_{ij}(\mathbf{p})u_{ij}, \tag{8}$$

where $\nu=(-i\omega+1/\tau)$; we assume that the wave is monochromatic with frequency ω; the collision integral in Eq. (8) is taken into account in the τ-approximation, i.e., as the operator of multiplication of the function f_0-f by the collision frequency $1/\tau$ of conduction electrons, and t_H is the time of motion of a charge in the magnetic field according to the equation

$$\partial\mathbf{p}/\partial t=e[\mathbf{v}\times\mathbf{H}]/c. \tag{9}$$

Here and below, the subscript "H" on t is be omitted, and $\Lambda_{ij}(\mathbf{p})=\lambda_{ij}(\mathbf{p})-\langle\lambda_{ij}\rangle/\langle 1\rangle$, where

$$\langle g\rangle=2(2\pi h)^{-3}\int g(\mathbf{p})d^3p\,\delta(\varepsilon-\varepsilon_F). \tag{10}$$

The solution of the linearized kinetic equation

$$\psi=\hat{R}\{\Lambda_{ij}(\mathbf{p})u_{ij}+e\tilde{\mathbf{E}}\cdot\mathbf{v}\}, \tag{11}$$

where $\hat{R}$ is the resolvent of Eq. (8), makes it possible to find the acoustoelectric coefficients connecting the electron fluxes due to the crystal deformation with the ionic displacement $\mathbf{u}$.

The conditions for the existence of a nontrivial solution of the complete system of linearized equations of the problem has the form of the energy–momentum relation between the wave vector $\mathbf{k}$ and the wave frequency ω. The imaginary component of the wave vector determines the damping decrements for the acoustic wave and the electromagnetic wave generated by sound, while the real component of the wave vector takes into account the renormalization of velocity of their propagation associated with the interaction of these waves with conduction electrons.

However, the acoustic damping decrement Γ can also be determined with the help of the dissipative function Q proportional to the time variation of entropy of the conductor.[10] Taking into account only the electron energy absorption for acoustic waves, we can write the dissipative function in the form

$$Q=\langle\psi\hat{W}_{\text{col}}\{\psi\}\rangle, \tag{12}$$

while the acoustic damping decrement is defined as

$$\Gamma=\langle|\psi|^2/\rho\dot{u}^2 s\tau\rangle, \tag{13}$$

where ρ is the crystal density and s the velocity of sound.

Using Maxwell's equation in the Fourier representation, we obtain the following relation connecting the electric field with the ionic displacement:

$$\{\mu_{ij}-\xi\sigma_{ij}(k)\}\tilde{E}_j=\{\xi k\omega a_{ij}(k)+\mu_{im}\varepsilon_{mnj}i\omega H_n/ck^2 - \mu_{ij}m\omega^2/e\}u_j;$$

$$\mathbf{j}\cdot\mathbf{k}=0, \tag{14}$$

where $\xi=4\pi i\omega/(k^2c^2-\omega^2)$; $\mu_{ij}=\delta_{ij}-k_ik_j/k^2$; δ_{ij} is the Kronecker delta, ε_{inj} the antisymmetric rank-three tensor ($\varepsilon_{123}=1$), and the acoustoelectric coefficients

$$\sigma_{ij}(k)=\langle e^2 v_i \hat{R} v_j\rangle, \quad a_{ij}(\mathbf{k})=\langle e v_i \hat{R}\Lambda_{jn}(\mathbf{p})\rangle u_j k_n/k \tag{15}$$

in the Fourier representation connect the current density

$$j_i(k)=\sigma_{ij}(k)\tilde{E}_j(k)+a_{ij}(k)k\omega u_j(k) \tag{16}$$

with the electric field and the displacement of ions.

Let us suppose that an acoustic wave propagates along the layers at right angles to the magnetic field $\mathbf{H}=(0, H\sin\theta, H\sin\theta)$. In this case, the solution of Eq. (14) in the main approximation in the small parameter η has the form

$$\tilde{E}_y(k)=\{1-\xi\tilde{\sigma}_{yy}(k)\}^{-1}[i\omega u_x H\cos\theta/ck^2 + \xi k\omega\tilde{a}_{yj}(k)u_j]; \tag{17}$$

$$\tilde{E}_z(k)=-i\omega u_x H\sin\theta/ck^2+m\omega^2 u_z/e, \tag{18}$$

where $\tilde{\sigma}_{ij}(k)=\sigma_{ij}(k)-\sigma_{ix}(k)\sigma_{xj}(k)/\sigma_{xx}(k)$ and $\tilde{a}_{ij}(k)=a_{ij}(k)-a_{xj}(k)\sigma_{ix}(k)/\sigma_{xx}(k)$.

Equation (18) is valid only for very small values of η, when $\eta^2\ll\beta=(\omega c/\omega_0 s)^2/\omega\tau$, where ω_0 is the frequency of plasma oscillations of the electron gas. In the opposite limiting case, for determining $\tilde{E}_z$ we must also take into account the terms depending on η in the power expansion of j_z in the small parameter η. However, $v_z E_z$ is always small for $\eta\ll 1$, and the electric field has to be taken into account in the calculation of the asymptotic expression for the dissipative function only in the cases when Q vanishes for $\eta=0$.

In ordinary metals, Joule losses are significant only in the region of strong magnetic fields, when the radius of curvature of the electron trajectory is smaller than not only its mean free path, but also the acoustic wave length, i.e., $kr\ll 1$. If the magnetic field bends the trajectory of charge carriers not very strongly, so that

$$1\ll kr\ll kl, \tag{19}$$

the energy absorption for acoustic waves in metals is mainly determined by the deformation mechanism. In low-dimensional conductors, the role of electromagnetic fields generated by an acoustic wave is very significant over a much wider range of magnetic fields including the magnetic fields satisfying condition (19). This is due to the fact that the acoustoelectric coefficients a_{ij} and σ_{ij} in such fields for $kr\ll 1/\eta$ and $r\ll l$ experience giant oscillations upon a change in the reciprocal magnetic field. As a result, the asymptotic behavior of the dissipative function differs significantly from that in ordinary metals, and the inclusion of electromagnetic fields leads to compensation of the deformation mechanism of energy absorption for acoustic waves, and hence to acoustic transparency of the layered conductor. The asymptote of acoustoelectric coefficients in this range of magnetic fields has the form

$$\tilde{\sigma}_{yy}(k)=(G/kD)(1-\sin kd);$$

$$\tilde{a}_{yj}(k)=-i(G\Lambda_{jx}/evkD)\cos kD, \tag{20}$$

where $D=cD_p/eH\cos\theta$, and D_p being the diameter of the Fermi surface along the p_y-axis, v and Λ_{jx} are the electron velocity and the value of $\Lambda_{jx}(\mathbf{p})$ at the reference point of the Fermi surface along the same axis p_y, and $G=4vD_p e^2\tau/ac(2\pi h)^2$.

The asymptotic expression for the dissipative function for $1\ll kD\ll 1/\eta$ and for the longitudinal polarization of the acoustic wave assumes the form

$$Q=\frac{eH\tau\cos\theta\{g_1^2(1+\sin kD)+g_2^2(1-\sin kD)-2g_1g_2\cos kD\}}{\pi^2h^2akvc\{1+|\xi\sigma_{yy}|^2\}}, \tag{21}$$

where $g_1=\Lambda_{jx}u_j k\omega$, and $g_2=av\omega u_x eHc^{-1}\cos\theta$.

It can be easily seen that the asymptotic form of the electroacoustic coefficients $\tilde{\sigma}_{yy}$ and $\tilde{\sigma}_{yj}$ changes significantly for $kD=2\pi(n+1/4)$, which leads to a sharp increase in the dissipative function. However, under nonresonant conditions, when $\cos kD$ differs significantly from zero, and there is no need to take into account small corrections in formulas (20) for acoustoelectric coefficients, the denominator in formula (21) for the dissipative function increases in proportion to H^2, and the damping decrement

$$\Gamma\cong(\omega/v)r/l \tag{22}$$

decreases upon an increase in the magnetic field and the mean free path of charge carriers. For the longitudinal polarization of sound, the tensor component Λ_{xx} is obviously of the order of the Fermi energy, and the value of $g_1\approx g_2 kD$ is much larger than g_2. In this case, acoustic transparency is optimal for the values of magnetic field for which kD is close to $2\pi(n-1/4)$, and anomalous acoustic transparency of the layered conductor must be observed between the resonant values of magnetic field, which are repeated with the period

$$\Delta(1/H)=2\pi e\cos\theta/cD_p, \tag{23}$$

(the anomalous acoustic transparency must have the same period).

In pure conductors, the mean free path of charge carriers at low temperatures can be so large that the condition $kl\eta\gg 1$ is observed. In this case, there exists a range of magnetic fields for which $1/\eta\ll kr\ll kl$, and oscillations of acoustoelectric coefficients are due to a small fraction of charge carriers of the order of $(kr\eta)^{-1/2}$ on the Fermi surface near its cross section by the extremal diameter D_p^{extr}. The magnetoacoustic resonance for $\mathbf{k}\perp\mathbf{H}$ is absent in this situation, and the acoustic damping decrement

$$\Gamma(H)=\{1+(kr\eta)^{-1/2}\sin(kD_0-\pi/4)\}\omega l/vr \tag{24}$$

has the same order of magnitude as in ordinary metals. Insignificant numerical factors of the order of unity are omitted in formulas (22) and (24), and $D_0 = cD_p^{\rm extr}/(eH\cos\theta)$.

Magnetoacoustic resonance for $\mathbf{k}\perp\mathbf{H}$ is possible only for $kr\eta \ll 1$, and small corrections in the parameters r/l and $1/(kr)$ must be taken into account in the expression for $\tilde{\sigma}_{yy}$ near the resonant values of the magnetic field. Simple calculations lead to the following interpolation formula for $\Gamma(H)$:

$$\Gamma(H) = \frac{\omega l/vr}{1+(l/kr^2)^2}, \tag{25}$$

and the absorption of acoustic wave energy by conduction electrons increases with the magnetic field in proportion to H for $l \ll kr^2$.

Attenuation of transverse waves in a layered conductor considerably depends on the form of nondiagonal components of the deformation potential tensor $\Lambda_{ij}(\mathbf{p})$. In the cases when $\Lambda_{yx}(\mathbf{p})$ and $\Lambda_{zx}(\mathbf{p})$ are much smaller than Λ_{xx} in the region of effective interaction of charge carriers with the wave, where $\mathbf{k}\cdot\mathbf{v} = \omega$, the order of magnitude of the acoustic damping decrement changes significantly. However, for shear waves with the polarization in the plane of the layers, periodic alteration of transparency and resonant absorption of acoustic wave energy is of the same nature as for longitudinal waves, i.e., resonant peaks in the dependence of acoustic damping decrement on $1/H$ are repeated with period (23), although the order of magnitude of acoustic wave energy absorption can differ considerably from that in the case of longitudinal waves.

Acoustic waves polarized along the normal to the layers attenuate over considerably longer distances if the component Λ_{zx} is small and vanishes as η tends to zero. In this case, the asymptotic solution of Maxwell's equations for $\mathbf{u} = (0,0,u)$ has the form

$$\begin{aligned} \tilde{E}_y &= \frac{k\omega\tilde{a}_{yz} + m\omega^2\tilde{\sigma}_{yz}/e}{1-\xi\tilde{\sigma}_{yy}}\,\xi u; \\ \tilde{E}_z &= \frac{\tilde{a}_{zz}k\omega\xi + m\omega^2/e}{1-\xi\tilde{\sigma}_{zz}}\,u. \end{aligned} \tag{26}$$

It can be easily verified that the components of the matrix a_{ij} as well as σ_{ij} do not contain terms linear in the parameter η if at least one of the indices i and j coincides with z. While calculating the dissipative function, we should not take into account the electric field $\tilde{E}_y$ proportional to η^2 since $ev_z\tilde{E}_z$ contains the term proportional to the first power of η. As a result of simple calculations, we obtain the following expression for the dissipative function for $1 \ll kr \ll 1/\eta$ and for arbitrarily small γ:

$$\begin{aligned} Q = \frac{\omega^3\tau u^2 eH\cos\theta}{acsv(2\pi h)^2}\Bigg| \Lambda_{zx} \\ + \frac{iA_1 am\omega}{hk(1-\xi\tilde{\sigma}_{zz})}\cos\left(\frac{aD_\rho}{h}\tan\theta\right)\Bigg|^2 (1+\sin kD). \end{aligned} \tag{27}$$

In the calculation of Q, we confined ourselves to only the first two terms in expression (7) for the energy–momentum relation for charge carriers. Acoustic transparency takes place when kD is strictly equal to $2\pi(1-1/4)$, and we must take into account small corrections in γ and $1/kr$ in the expression for the dissipative function. If $\sin kD$ differs significantly from -1, attenuation of acoustic waves increases with magnetic field as in ordinary crystals and is mainly determined by the first term in the brackets in formula (27), except in some exotic models of deformation potential for which $\Lambda_{zx} \ll \eta\varepsilon_F$. The amplitude of oscillations of Γ with period (23) associated with the periodic dependence of σ_{zz} on $1/H$, i.e.,

$$\sigma_{zz} = \frac{\eta^2\sigma_0}{kr}\left[1+\sin kD\,\cos\left(\frac{aD}{h}\tan\theta\right)\right], \tag{28}$$

has an order of magnitude that is v/s times smaller than the acoustic decrement component varying monotonically with the magnetic field if $\Lambda_{zx} \approx \eta\varepsilon_F$. In addition to these oscillations, the damping decrement of acoustic waves oscillates with a change in the angle θ with the period

$$\Delta(\tan\theta) = 2\pi h/aD_p. \tag{29}$$

Angular oscillations in magnetic fields satisfying condition (19) take place over the entire range of angles between the magnetic field and the normal to the layers.

If a conduction electron drifts along the acoustic wave vector (for example, the sound propagates along the y-axis), the acoustic damping decrement decreases by a factor of $(kl\eta)^2$ for $r/l \ll kr\eta \ll 1$. The solution of the kinetic equation in this case has the form

$$\begin{aligned} \psi = \{\exp(\nu T + i\overline{\mathbf{k}\cdot\mathbf{v}}T) - 1\}^{-1}\int_t^{t+T} dt'\,g(t') \\ \times\exp\{i\mathbf{k}\cdot[\mathbf{r}(t') - \mathbf{r}(t)]\}, \end{aligned} \tag{30}$$

where $g(t) = \omega\Lambda_{ji}(t)k_i u_j + e\mathbf{v}(t)\tilde{E}$.

For $1 \ll kl\eta \ll l/r$, the term proportional to $k\cdot\mathbf{v}T$ plays the leading role in the power series expansion of the factor in front of the integral in νT and $\overline{\mathbf{k}\cdot\mathbf{v}}T = \int_0^T dt\,\mathbf{k}\cdot\mathbf{v}(t)$. For this reason, the term νT in the expression for the dissipative function in the case of charge carrier drift along $\mathbf{k}$ with the velocity $\overline{v_y} = \overline{v_z}\tan\theta \cong \eta vt\tan\theta$ should be replaced by $kr\eta\tan\theta$. If $kr\eta\tan\theta \gg 1$, i.e., an electron can move during its mean free time over a distance much longer than the acoustic wave length, we have the magnetoacoustic resonance predicted and studied theoretically in Ref. 15. [This resonance is sometimes called in the literature the Doppler-shifted acoustic cyclotron resonance (DSACR).] The resonance sets in for $\overline{\mathbf{k}\cdot\mathbf{v}}T = 2\pi n$; in contrast to the case of ordinary metals, the amplitude of resonant oscillations is determined by the parameter $kr\eta$ rather than by kr.

The above formulas are valid when $\cos\theta \gg cD_p/eHl$. If the value of θ is close to $\pi/2$, i.e., $\cos\theta$ is so small that an electron cannot complete a revolution in its orbit in a magnetic field during its mean free time, the electrical conductivity tensor components $\tilde{\sigma}_{yy}$ and $\tilde{\sigma}_{zz}$ are close to their values in zero magnetic field. This is due to the fact that only the magnetic field component along the z-axis affects the dy-

namics of charge carriers in a two-dimensional conductor, and for $\eta \ll 1$ the role of magnetic field component H_y becomes noticeable in magnetoacoustic effects only in small corrections in the parameter η. For $\theta = \pi/2$, the magnetic-field dependence of the acoustic damping decrement is present only in the terms that vanish as η tends to zero, and magnetoacoustic effects are manifested most clearly only if a wave propagates with a displacement of ions along the normal to the layers.

The oscillatory dependence of Γ on $1/H$ takes place for $\theta = \pi/2$ only for not very weak corrugation of the Fermi surface, when $kr\eta \gg 1$. The period of oscillations

$$\Delta(1/H) = 4\pi e/kc\Delta D_{px}, \tag{31}$$

of the damping decrement of an acoustic wave propagating along the normal to the layers can be used to determine the intensity of Fermi surface corrugation to a high degree of accuracy. Here ΔD_{px} is the difference between the maximum and minimum diameters of the Fermi surface along the p_x-axis for $p_y = 0$.

The damping decrement for an acoustic wave polarized along the normal to the layers in a strong magnetic field for which $kr \ll 1$ depends considerably on the magnitude and orientation of the magnetic field relative to the layers, and the dependence of Γ on θ acquires sharp peaks or deeps which are repeated with period (29) only for $\tan\theta \gg 1$.

For an acoustic wave propagating along the normal to the layers, Maxwell's equations have the form

$$\begin{aligned} &\{1-\xi\tilde{\sigma}_{xx}(k)\}\tilde{E}_x - \xi\tilde{\sigma}_{xy}(k)\tilde{E}_y = \xi\tilde{a}_{xj}(k)u_j - (u_y H_z \\ &\quad - u_z H_y) i\omega/c - m\omega^2 u_x/e; \qquad (32) \\ &-\xi\tilde{\sigma}_{yx}(k)\tilde{E}_x + \{1-\xi\tilde{\sigma}_{yy}(k)\}\tilde{E}_y = \xi\tilde{a}_{yj}(k)u_j + u_x H_z i\omega/c \\ &\quad - m\omega^2 u_y/e. \end{aligned}$$

If the components Λ_{iz} are proportional to η, to a high degree of accuracy we can put $\tilde{a}_{\alpha j} = a_{\alpha j}$ and $\tilde{\sigma}_{\alpha\beta} = \sigma_{\alpha\beta}$, where $\alpha, \beta = x, y$, and the energy absorption of the acoustic wave propagating along the normal to the layers is mainly associated with Joule losses. In this case, the damping decrement of the wave can be calculated easily. However, magnetoacoustic effects can be manifested only under rather stringent conditions, when $r \ll l$ and $kr\eta \gg 1$ simultaneously, i.e., either in very pure samples, or for not very strong quasi-two-dimensionality. Although these conditions can hardly be satisfied in the layered conductor synthesized at present, we still write here the explicit form of the acoustic damping decrement in a magnetic field oriented in the plane of the layers, i.e., orthogonal to the wave vector of sound:

$$\Gamma(H) = \frac{\eta\omega\tau}{r}\{1-(kr\eta)^{-1/2}\beta\,\sin(kc\Delta D_{p1}/2eH + \pi/4)\}, \tag{33}$$

where ΔD_{p1} is the difference between the maximum and minimum diameters of the section of the Fermi surface by the plane $p_z = \text{const}$ in the direction orthogonal to the magnetic field. For such an experimental geometry, charge carriers do not drift along the acoustic wave vector, and the oscillations of Γ due to variation of the magnetic field are similar to Pippard oscillations,[16] but their amplitude is suppressed due to the presence of the small factor β.

This research was carried out under partial financing by the International Soros Foundation (Grants No. USP 042051 and K5X 100) and by the Ministry of Sciences of Macedonia.

*E-mail: peschansky@ilt.kharkov.ua

[1] I. M. Lifshits, *Selected Works. Electron Theory of Metals. Physics of Polymers and Biopolymers* [in Russian], Nauka, Moscow (1994).
[2] V. G. Peschansky, J. A. Roldan Lopez, and Toyi Gnado Yao, J. Phys. (Paris) **1**, 1469 (1991).
[3] V. G. Peschansky, S. N. Savel'eva, and Kh. Kheir Bek, Fiz. Tverd. Tela (St. Petersburg) **34**, 1640 (1992) [Sov. Phys. Solid State **34**, 871 (1992)].
[4] V. G. Peschansky, Kh. Kheir Bek, and S. N. Savel'eva, Fiz. Nizk. Temp. **18**, 1012 (1992) [Sov. J. Low Temp. Phys. **18**, 711 (1992)].
[5] O. V. Kirichenko and V. G. Peschansky, J. Phys. (Paris) **4**, 823 (1994).
[6] O. V. Kirichenko and V. G. Peschansky, Fiz. Nizk. Temp. **20**, 574 (1994) [Low Temp. Phys. **20**, 453 (1994)].
[7] V. G. Peschansky, G. Espeho, and D. Tesgera Bedassa, Fiz. Nizk. Temp. **21**, 971 (1995) [Low Temp. Phys. **21**, 748 (1995)].
[8] V. M. Gokhfeld, O. V. Kirichenko and V. G. Peschansky, Zh. Éksp. Teor. Fiz. **108**, 2147 (1995) [JETP **81**, 1171 (1995)].
[9] O. Galbova, G. Ivanovski, O. V. Kirichenko and V. G. Peschansky, Fiz. Nizk. Temp. **22**, 425 (1996) [Low Temp. Phys. **22**, 331 (1996)].
[10] A. I. Akhiezer, Zh. Éksp. Teor. Fiz. **8**, 1338 (1938).
[11] V. P. Silin, Zh. Éksp. Teor. Fiz. **38**, 977 (1960) [Sov. Phys. JETP **11**, 703 (1960)].
[12] V. M. Kontorovich, Zh. Éksp. Teor. Fiz. **45**, 1633 (1963) [*sic*].
[13] V. M. Kontorovich, in *Conduction Electrons* [in Russian], Nauka, Moscow (1985).
[14] A. F. Andreev and D. I. Pushkarov, Zh. Éksp. Teor. Fiz. **89**, 1883 (1985) [Sov. Phys. JETP **62**, 1087 (1985)].
[15] E. A. Kaner, V. G. Peschansky, and I. A. Privorotskii, Zh. Éksp. Teor. Fiz. **40**, 214 (1961) [Sov. Phys. JETP **13**, 147 (1961)].
[16] A. B. Pippard, Phil. Mag. **2**, 1147 (1957).

Translated by R. S. Wadhwa

Bose fluctuations and paramagnetic susceptibility of normal 2*D* metal with attraction between carriers: spin gap?

V. M. Loktev and S. G. Sharapov

*N. Bogoliubov Institute of Theoretical Physics, National Academy of Sciences of the Ukraine, 252143 Kiev, Ukraine**

(Submitted August 9, 1996; revised September 23, 1996)
Fiz. Nizk. Temp. **23**, 180–189 (February 1997)

The paramagnetic susceptibility of a $2D$ metal with attraction between charge carriers is obtained, proceeding from the simple theoretical field model. The temperature dependence of the magnetic susceptibility is calculated for various concentrations of fermions. It is shown that the paramagnetic susceptibility can be reduced significantly in view of the presence of a finite number of decoupling fermion pairs in the normal phase. The relation of the proposed model to the marginal behavior of the Fermi liquid in high-T_c superconductors, in particular, with the effects associated with the formation of a spin gap, is considered. © *1997 American Institute of Physics.* [S1063-777X(97)00702-0]

1. INTRODUCTION

Normal properties of high-temperature superconductors (HTS materials), including the spin gap manifested in a low-frequency spectral weight of quasiparticle Fermi excitations, [which is smaller than predicted by the Landau theory of Fermi liquid at temperatures T exceeding significantly (by a factor of 1.5–2) the superconducting transition temperature T_c], are undoubtedly one of the most acute and disputable problems in the HTS theory (see the reviews in Refs. 1–5). The decrease in spectral weight is observed most clearly in magnetic measurements (NMR,[1] neutron scattering,[2] etc.) and is attributed to the emergence, or opening of a gap in the spectrum of *spin* excitations at certain values of T. Above this temperature region (i.e., at $T>(1.5-2)T_c$), the spin gap is not manifested (or is closed) according to experimental data, and the Fermi subsystem of the HTS material becomes similar to the standard subsystem in many respects. No indications of a phase transition are observed in this case either.

Many attempts have been made[2,5–9] to attribute the observed behavior of HTS materials to peculiarities of their magnetic dynamics. Among other things, the authors of these publications assumed that magnetic anomalies of the normal phase of HTS materials, e.g., the temperature dependence of uniform paramagnetic susceptibility (PMS) χ differing from the Pauli dependence ($d\chi/dT>0$), are consequences of interaction of quasiparticle excitations of an AFM metal with overdamped spin waves which strongly attenuate according to the Landau mechanism, due to the formation of electron–hole pairs (see also Refs. 3, 10). The conclusions of the theory (which do not contradict the experiments)[1,4,5] are determined to a considerable extent by the charge carrier concentration: the anomalies for weakly doped compounds are manifested more clearly than for strongly doped samples, for which the Landau theory is more or less applicable.

Even disregarding the magnetism of HTS compounds as such, we can speak of two (equivalent to a certain extent) physical factors facilitating the ordinary behavior of the normal HTS phase, i.e., high values of T and a relatively high number density n_f of delocalized (free) charge carriers. As regards the second factor, $2D$ (and quasi-$2D$) metals including copper-based HTS materials (copper oxides) are clearly characterized by a parameter separating the regions of low and high values of n_f, i.e., by the energy ε_b of the bound two-fermion state formed as a result of attraction of any origin (direct[11,12] or indirect[13]). For example, if the Fermi energy $\varepsilon_F \ll |\varepsilon_b|$, the value of n_f can be regarded as small, and the behavior of the Fermi system[1)] differs significantly from the ordinary behavior[14,15] (e.g., the fermion chemical potential $\mu \neq \varepsilon_F$, attaining negative values $\mu<0$). A high number density n_f corresponds to the opposite inequality $\varepsilon_F \gg |\varepsilon_b|$ which leads to the ''restoration'' of the normal properties of the Fermi liquid. Finally, the range of $\varepsilon_F \gtrsim |\varepsilon_b|$ (with $\mu \approx \varepsilon_F$) is known as the ''crossover'' region in which we can expect a noticeable deviation of the temperature dependences of various parameters of a $2D$ metal from those predicted by the Landau theory without assuming that its Fermi sphere of the metal is broken (the latter is clearly detected in HTS materials).[3–5]

For this reason, the assumption that the anomalous (including magnetic) behavior of the normal phase of HTS compounds (their ''strangeness'') is probably due to lower dimensions of their electronic properties and a relatively low (as compared to ordinary metals) number density n_f rather than due to the structure of their magnetic ground state exhibiting strong AFM correlations appears quite plausible. The numerical calculations[16] (see also the review in Ref. 17) made for the $2D$ Hubbard model with attraction ($U<0$) at a lattice site also speak in favor of such an assumption. These calculations proved that, in view of fluctuational formation of noncorrelated pairs above T_c, anomalous temperature dependences can be traced even for not very large ratios $|U|/t$ (t is the one-particle hopping parameter). In this case, the PMS of fermions and the low-temperature spectral weight measured from NMR signals[1,4–6] (whose decrease was noted above) behave similarly.

At the same time, analytical calculations that would demonstrate the nature of and the reason behind the deviations in the behavior of the normal phase of a $2D$ metal from the predictions of the Landau theory as well as the temperature T at which these deviations are observed have not yet been carried out. For this reason, we shall make an attempt here to calculate the static PMS of a $2D$ electron system with attraction between particles. On one hand, the calculation of χ for the normal phase has the simplest form for such a gap, and on the other hand, it allows a tracing of the complex dynamic processes occurring in a fluctuating low-dimensional system. We deliberately disregard the contribution to the PMS from the magnetic subsystem proper which obviously plays a significant role in the case of copper oxides. It should only be noted that the Hubbard model with $U<0$ was investigated in recent publications,[18,19] through the solution of self-consistent equations for the T-matrix with the help of the method of moments (in the two-pole approximation, taking into account the two Hubbard subbands), and it was proved that such a model gives another example of the behavior differing from that typical of a Landau Fermi liquid.

We shall consider the field model of a $2D$ Fermi system with attraction (which is closer to an ordinary system) without presuming strong correlations between charge carriers. We proceed from a physical situation[3] in which strong correlations form the ground state of an HTS material and do not affect significantly free charge carriers appearing due to doping. Nevertheless, the spectrum of a low-dimensional (including $2D$) systems contains (see above) an additional discrete state (energy ε_b) or (depending on T) a continuum of such states which makes a significant contribution to the observed properties of the system.

2. MODEL AND GENERAL DISCUSSION

The simplest field Hamiltonian of a $2D$ Fermi system with a local attraction in an external magnetic field $\mathbf{H}$ has the form

$$\mathscr{K}=-\int d^2\mathbf{r}\Big\{\psi_\sigma^+(\mathbf{r})\left(\frac{\nabla^2}{2m}+\mu\right)\psi_\sigma(\mathbf{r}) + V\psi_\uparrow^+(\mathbf{r})\psi_\downarrow^+(\mathbf{r})\psi_\downarrow(\mathbf{r})\psi_\uparrow(r)+\mu_B H[\psi_\uparrow^+(\mathbf{r})\psi_\uparrow(\mathbf{r}) - \psi_\downarrow^+(\mathbf{r})\psi_\downarrow(\mathbf{r})]\Big\}, \tag{1}$$

where m is the effective mass of a particle, $V>0$ the attraction constant, μ_B the Bohr magneton, and it is assumed that $\hbar=k_B=1$. In accordance with the problem formulated above, we have omitted in (1) the vector potential which is known to be associated with diamagnetic susceptibility.[2)] It should be noted that model (1) was considered long ago by many authors (see, for example, Ref. 20), but only the superconducting phase ($T<T_c$) of a $3D$ system in strong fields (the PM limit) was studied comprehensively for large values of n_f (which, in other words, corresponds to the BCS theory).

Returning to model (1), we write the uniform PMS which can be expressed in terms of the thermodynamic potential $\Omega(v,\mu,T,\mathbf{H})$ (v is the volume):

$$\chi=-\frac{1}{v}\left.\frac{\partial^2\Omega}{\partial H^2}\right|_{H=0}. \tag{2}$$

In the approximation taking into account Gaussian fluctuations of the order parameter (which is equal to zero in the normal phase), we can obtain, by using the functional integration formalism,[21] the following expression for the thermodynamic potential:

$$\Omega(v,\mu,T,\mathbf{H})=-T(\mathrm{Tr\ Ln}\ G_0^{-1}-\mathrm{Tr\ Ln}\ \Gamma^{-1}), \tag{3}$$

in which

$$G_0(i\omega_n,\mathbf{k},\mathbf{H})=\frac{(i\omega_n+\mu_B H)\hat{I}+\xi(\mathbf{k})\tau_Z}{(i\omega_n+\mu_B H)^2-\xi^2(\mathbf{k})}\exp(i\delta\omega_n\tau_Z), \quad \delta\to+0 \tag{4}$$

and

$$\Gamma^{-1}(i\Omega_n,\mathbf{K},\mathbf{H})=\frac{1}{V}-\frac{1}{2}\int\frac{d\mathbf{k}}{(2\pi)^2}[\xi(\mathbf{k}+\mathbf{K}/2)+\xi(\mathbf{k}-\mathbf{K}/2)-i\Omega_n]^{-1}\Big\{\tanh\frac{1}{2T}[\xi(\mathbf{k}+\mathbf{K}/2)+\mu_B H]+\tanh\frac{1}{2T}[\xi(\mathbf{k}-\mathbf{K}/2)-\mu_B H]\Big\} \tag{5}$$

are the temperature Green's functions (GF) of an ideal Fermi gas and of fluctuations of the order parameter in the external field. Green's functions (4) and (5) are written in the following notation: τ_Z is the Pauli matrix, $\hat{I}$ is the unit matrix, $\xi(\mathbf{k})\equiv\mathbf{k}^2/2m-\mu$; $\omega_n\equiv(2n+1)\pi T$ and $\Omega_n\equiv 2n\pi T$. We assume that the energy–momentum relation is quadratic, and hence $n_f=m\varepsilon_F/\pi$ for $2D$ metals. The chemical potential can be determined from (3) according to the relation

$$n_f=-\frac{1}{v}\frac{\partial\Omega}{\partial\mu}, \tag{6}$$

whose role increases as the value of ε_F approaches $|\varepsilon_b|$, and accordingly the difference between the value of μ and ε_F increases.[3,17]

Taking into account the explicit form of (3), we obtain the following equation from (6) for the number of particles (we put $\mathbf{H}=0$ in it):

$$n_f=n_F(\mu,T)+2n_B(\mu,T), \tag{7}$$

where

$$n_F(\mu,T)=T\sum_{n=-\infty}^{\infty}\int\frac{d\mathbf{k}}{(2\pi)^2}\,\mathrm{tr}[G_0(i\omega_n,\mathbf{k},\mathbf{H}=0)\tau_Z] \tag{8}$$

and

$$n_B(\mu,T)=T\sum_{n=-\infty}^{\infty}\int\frac{d\mathbf{K}}{(2\pi)^2}\,\Gamma(i\Omega_n,\mathbf{K},\mathbf{H}=0) \tag{9}$$

are the effective average numbers of fermions and compound bosons (fluctuating pairs) for given μ and T. After the substitution of the GF (4) into expression (8) for the number of unpaired fermions, the latter expression can easily be summed over ω_n[22] and integrated over $\mathbf{k}$:

$$n_F(\mu,T)=\int\frac{d\mathbf{k}}{(2\pi)^2}\,n_F[\xi(\mathbf{k})]$$

$$=\frac{m}{\pi}\,T\,\ln[1+\exp(\mu/T)], \tag{10}$$

since $n_F(\omega)\equiv[\exp(\omega/T)+1]^{-1}$ is the Fermi distribution function.

In analogy with (7), we can also split the expression for the PMS so that

$$\chi(\mu,T)=\chi_F(\mu,T)-\chi_B(\mu,T), \tag{11}$$

i.e., we have two contributions: the fermion contribution

$$\chi_F(\mu,T)=\chi_{\text{Pauli}}[1+\exp(-\mu/T)]^{-1};$$

$$\chi_{\text{Pauli}}\equiv\mu_B^2 m/\pi \tag{12}$$

and the boson contribution

$$\chi_B(\mu,T)=\chi_b(\mu,T)n_B(\mu,T), \tag{13}$$

in which

$$\chi_b(\mu,T)=\chi_{\text{Pauli}}\frac{1}{8T^2}\int_{-\mu/2T}^{\infty}x^{-1}\sinh x\,\cosh^{-3}x\,dx \tag{14}$$

describes the contribution from the compound boson. It can be seen that the fluctuating Bose component makes a finite (and negative) contribution to PMS. It should be noted, however, that the quantities $n_B(\mu,T)$ defined by (6) and (9) generally do not coincide [the PMS (13) is associated with (9)]. However, in the case considered below, when the role of Eq. (7) becomes significant indeed, these definitions are identical.

Boson fluctuations taken into account in (3) can correspond to relatively stable as well decaying (short-lived) compound particles. In the general case, their lifetime depends on the relation between ε_F and ε_b, but for large n_f (i.e., for $\varepsilon_F\gg|\varepsilon_b|$), it depends on the relation between $\mu\approx\varepsilon_F$ and T_c (see below), which is more convenient and natural to use. (It should only be noted that expressions (13) and (14) can be obtained most easily by expanding (5) in powers of H; the corresponding expansion contains only even powers since compound singlet bosons do not perceive the direction of the field.)

As a result, the calculation of PMS for various densities of fermions can be reduced to an analysis of the self-consistent system of equations (7) and (11), the actual case of relatively high values of n_f corresponding to the formal substitution $\mu\to\varepsilon_F$ or to the solution of only one (second) equation. Even such a simple (at first sight) problem is actually complicated in view of a complex frequency–momentum (or, which is the same, space–time) behavior and temperature distribution of fluctuations. It should be noted in this connection that although potential (3) was obtained by taking these fluctuations into account, we used the lowest (Gaussian) approximation in which the interaction between fluctuations is neglected. This approximation is completely identical to the one used in Refs. 23 and 24, where the equality $\mu=\varepsilon_F$ was not presumed, and Eq. (7) was solved together with another equation, viz., the so-called Thouless condition. In the case of $3D$ systems, such an approach has made it possible to trace directly the crossover from the local pair mode to Cooper pairing.

On the other hand, an attempt was made[14] to use the same approach for analyzing the normal phase of $2D$ systems. Among other things, the $\mu(T)$ dependence for different initial charge carrier concentrations was determined from the solution of Eq. (7), and an astonishing conclusion was drawn that the system always contains a finite number of stable bound fermions for $T>T_c$ irrespective of n_f.

One way or another, we encounter here the problem of T_c of $2D$ systems. Indeed, phase fluctuations of the order parameter disturb long-range correlations so that either $T_c=0$,[25] or this temperature is much lower than its mean-field value T_c^{MF},[26] if we identify with this value the temperature T_{BKT} corresponding to the establishment of algebraic order[27,28] due to confinement of vortices.

All these stimulated the authors of Refs. 15 and 29 to revise the justification of the Gaussian approximation in the case when fluctuations are taken into account. It was found that the existence of stable pairs above T_c depends on n_f: there exists a critical concentration n_f^{cr} separating[3)] the Fermi-like ($n_f>n_f^{\text{cr}},\mu>0$) and Bose-like ($n_f<n_f^{\text{cr}},\mu<0$) behavior of the system. In other words, a new (Fermi-like) class of solutions, which did not exist in Ref. 14 and for which it is meaningless to speak of real bosons above T_c, was obtained in Refs. 15, 29.

At the same time, it was found in Ref. 29 that $T_c\neq 0$ in the Gaussian approximation, which, strictly speaking, cannot be regarded as a satisfactory result since, as soon as we go beyond this approximation (or take fluctuations into account), the result $T_c=0$ for $2D$ systems is restored immediately.[30] Thus, we have to decide whether we can calculate the PMS for an idealized $2D$ system or we must take into account the fact (on the basis of purely physical considerations) that real so-called $2D$ metals are actually quasi-$2D$ systems (as in the case of HTS compounds) and that a transition to the three-dimensional case (taking into account the coupling between conducting layers) always stabilizes T_c.[31,32]

We will stick to the second alternative and will henceforth assume that, on one hand, real densities are such that $\mu\approx\varepsilon_F$ in actual practice, and on the other hand, $T_c\approx T_c^{\text{MF}}$ for some reason or another. This allows us to calculate consistently (naturally, under the assumptions made above) the contribution of Gaussian fluctuations to the PMS of a strongly anisotropic ($2D$ in the limit) metal with high values of n_f. Moreover, we must admit that such assumptions are common for virtually all publications on the HTS theory, but as a rule, they are not formulated explicitly.

3. GREEN'S FUNCTION FOR COMPOUND BOSONS

If we continue $i\Omega_n \to \omega + i0$ analytically to the GF (5), we arrive at the retarded GF for bosons:

$$\Gamma^{-1}(\omega,\mathbf{K}) \equiv \Gamma^{-1}(\omega + i0,\mathbf{K},\mathbf{H}=0) = \frac{1}{V} - \frac{1}{2}\int \frac{d\mathbf{k}}{(2\pi)^2}\left[\xi(\mathbf{k}+\mathbf{K}/2) + \xi(\mathbf{k}-\mathbf{K}/2) - \omega - i0\right]^{-1}\left[\tanh\frac{1}{2T}\,\xi(\mathbf{k}+\mathbf{K}/2) + \tanh\frac{1}{2T}\,\xi(\mathbf{k}-\mathbf{K}/2)\right], \tag{15}$$

which is more convenient for analysis. Expression (15) was written for the first time in the pioneering work by Aslamazov and Larkin[33] (see also Ref. 34) devoted to investigation of fluctuation effects in $3D$ superconductors. In spite of its long history and apparent simplicity, a comprehensive analysis of the boson GF for arbitrary ω, $\mathbf{K}$, μ, and T has not been carried out yet. Such an analysis normally presumes the standard BCS mode in which $T_c/\varepsilon \sim 10^{-4}$, the fluctuation range is narrow (i.e., $|T-T_c| \ll T_c$), and ω and $\mathbf{K}$ are so small that the lowest expansion in derivatives in the Ginzburg–Landau effective potential is valid.

The attempts to study this GF for arbitrary (including negative) values of μ were made in Refs. 15, 21, and 35; it was proved, for example, that the following expansion holds in the region of small ω and $\mathbf{K}$:

$$\mathrm{Re}\,\Gamma^{-1}(\omega,\mathbf{K}) \equiv a + b\,\frac{\mathbf{K}^2}{4m} - c\,\omega, \tag{16}$$

whose coefficients in the $2D$ case can be represented by the formulas[21]

$$a = \frac{m}{4\pi}\left[\ln\frac{\pi T}{|\varepsilon_b|\gamma} - \int_0^1 dx\; x^{-1}\tanh\frac{\mu}{2T}\,x\right]; \tag{17}$$

$$b = \frac{m}{8\pi\mu}\left[\tanh\frac{\mu}{2T} + \frac{\mu}{2T} + \left(\frac{\mu}{2T}\right)^2 \int_{-\mu/2T}^{\infty} dx x^{-2}\,\tanh^2 x\right]; \tag{18}$$

$$c = \frac{m}{8\pi\mu}\int_1^{\infty} dx x^{-2}\,\tanh\frac{\mu}{2T}\,x \tag{19}$$

and $\ln\gamma = 0.577$ is the Euler constant. In contrast to $\mathrm{Re}\,\Gamma^{-1}(\omega,\mathbf{K})$, we can obtain the following closed expression for $\mathrm{Im}\,\Gamma^{-1}(\omega,\mathbf{K})$:

$$= -\frac{m}{4}\tanh\frac{\omega}{4T}\left[1 - f\left(\omega + 2\mu - \frac{K^2}{4m}, \frac{K^2}{4m}\right)\right]\theta\left(\omega + 2\mu - \frac{K^2}{4m}\right), \tag{20}$$

where

$$f(x,y) \equiv \frac{2}{\pi}\int_0^{\pi/2} d\varphi \times \frac{\cosh(\sqrt{xy}\,\cos\cdot\,\varphi/T) - 1}{\cosh[x+y-2\mu)/2T] + \cosh(\sqrt{xy}\,\cos\,\varphi/T)}, \tag{21}$$

which, however, virtually cannot be used in such a general form and also requires approximations.

In this case, the condition $a=0$, or the equation

$$\ln\frac{\pi T_c^{\mathrm{MF}}}{|\varepsilon_b|\gamma} = \int_0^1 dx x^{-1}\,\tanh\frac{\mu}{2T_c^{\mathrm{MF}}}\,x \tag{22}$$

for the critical line is just the implicit dependence $T_v^{\mathrm{MF}}(\mu)$ for all values of μ. If, however, we consider the available experimental data on HTS materials (see Refs. 1, 4, and 5), it can be easily seen that peculiarities of the problem are reflected in the possibility of expanding the range of T up to $T - T_c \gtrsim T_c$ rather than in the knowledge of the behavior of $\Gamma^{-1}(\omega,\mathbf{K})$ for an arbitrary μ.

Indeed, the relations $\mu/\varepsilon_F \lesssim 1$ and $T_c/\varepsilon_F \simeq (1-3)\cdot 10^{-2}$ are fulfilled for most of investigated HTS materials in the region of optimal doping.[36] These relations (especially the second one) imply that, even if a mode close to the BCS conditions is realized in an HTS material, it cannot be regarded as standard (this was emphasized more than once). In our opinion, it is important indeed that it is obviously insufficient to use the expansion of $\mathrm{Im}\,\Gamma^{-1}(\omega,0)$ in ω as well as the expansion of $\mathrm{Re}\,\Gamma^{-1}(\omega,\mathbf{K})$ (16) in order to find $n_B(\mu,T)$ [see Eqs. (9) and (15)] in the range of T values far from $T_c (\equiv T_c^{\mathrm{MF}})$ since it would ultimately be equivalent to the application of the Ginzburg–Landau theory which cannot be used directly[37,38] in view of a large contribution of short-wave and high-frequency fluctuations for $T - T_c \sim T_c$. Consequently, a correct description of fluctuations (including those under consideration) can be obtained by taking into account the dependence of the GF (15) on ω and $\mathbf{K}$ with the maximum possible accuracy. For this purpose, it would be expedient to use first of all a more accurate expression for $\mathrm{Im}\,\Gamma^{-1}(\omega,\mathbf{K})$ (expression (16) being preserved), which is physically due to dynamic decay processes for compound bosons, which are intense for $T > T_c$ and strongly affect the properties of the $2D$ system. The parameters of this decay are mainly determined by $\mathrm{Im}\,\Gamma^{-1}(\omega,\mathbf{K})$. It is also important that the approximate expression for $\mathrm{Im}\,\Gamma^{-1}(\omega,\mathbf{K})$ proposed below for calculating PMS is within the limits of applicability of representation (16).

Thus, when μ is indistinguishable from ε_F and simultaneously much larger an the actual values of T, the solution of Eq. (22) has the form

$$T_c^{\mathrm{MF}} = \frac{\gamma}{\pi}\sqrt{2|\varepsilon_b|\varepsilon_F} \approx T_c, \tag{23}$$

which immediately leads to the following relation for the corresponding actual values of n_f:

$$\frac{\varepsilon_F}{T_c} = \frac{\pi}{\sqrt{2}\,\gamma}\sqrt{\frac{\varepsilon_F}{|\varepsilon_b|}}. \tag{24}$$

This relation allows us to describe the extent of deviation of the behavior of the system from the predictions of the BCS theory by using the value of T_c which is more accessible for direct measurements than the energy ε_b. As regards expressions (17)–(19), they can be simplified significantly, for example, for the region $\mu/T \gtrsim 10$ and assume the form

$$a = \frac{m}{2\pi} \ln \frac{T}{T_c}; \quad b = \frac{m}{2\pi} \frac{7\zeta(3)}{(2\pi)^2} \frac{\mu}{T^2};$$

$$c = \frac{m}{2\pi} \frac{1}{4\mu} \tag{25}$$

[$\zeta(x)$ is the zeta-function]. It follows hence that when $T - T_c \sim T_c$, the approximate nature of the definition of $T_c = T_c^{\mathrm{MF}}$ used in (23) becomes immaterial. Moreover, using (25), we can transform (16) to

$$\mathrm{Re}\ \Gamma^{-1}(\omega, \mathbf{K}) = \frac{m}{2\pi} \left(\ln \frac{T}{T_c} + \alpha \mathbf{K}^2 - \frac{\omega}{4\mu} \right);$$

$$\alpha \equiv \frac{1}{4m} \frac{7\zeta(3)}{(2\pi)^2} \frac{\mu}{T^2}, \tag{26}$$

while the coefficient $m/2\pi$ in fact specifies the density of $2D$ fermion states. To within the factor 2/3 in the coefficient α, which is associated with the $2D$ nature of the system, expression (26) coincides with that derived by Aslamazov and Larkin[38] (it should be noted that they considered only the region close to T_c, replacing the quantity T by T_c; in our case, the retaining of current values of T and α is of fundamental importance).

It should also be noted that the term $\omega/4\mu$ in (26) is associated with the absence of complete electron–hole symmetry[39] in the model under investigation; this term describes the undamped component of the boson GF. In Ref. 33, this term was omitted since the value of ω was regarded as small, while, on the contrary, the ratio μ/T_c was assumed to be large. In our case, this term is not small and affects the behavior and value of PMS considerably.

We complete the calculation of $\mathrm{Im}\,\Gamma^{-1}(\omega, \mathbf{K})$ by deriving an expression for the region of small frequencies and momenta defined by the inequalities $\omega < T$ and $\mathbf{K}^2/4m \ll (T/\mu)T$. In this case, we obtain from (20) and (21)

$$\mathrm{Im}\ \Gamma^{-1}(\omega, \mathbf{K}) = -\frac{m}{4} \tanh\left(\frac{\omega}{4T} \right) (1 - \delta \mathbf{K}^2)\, \theta(\omega + 2\mu)\, \theta(1 - \delta \mathbf{K}^2), \tag{27}$$

where $\delta \equiv (1/16m)(\mu/T^4)$. Using formulas (26) and (27), we can write the sought GF for compound bosons appearing in (9) as well as its imaginary component used by us:

$$\mathrm{Im}\ \Gamma(\omega, \mathbf{K}) = -\frac{\mathrm{Im}\ \Gamma^{-1}(\omega, \mathbf{K})}{\left(\ln \frac{T}{T_c} + \alpha \mathbf{K}^2 - \frac{\omega}{4\mu} \right)^2 + \left(\frac{\pi}{2} \right)^2 (1 - \delta \mathbf{K}^2) \tanh^2\left(\frac{\omega}{4T} \right)}, \tag{28}$$

which is proportional to the boson spectral density. This expression differs basically from that obtained form the expansion in derivatives[33] in that large momenta in (28) are ''cut'' per se,[4)] which corresponds to the suppression of the contribution from short-wave Bose fluctuations. It should be noted that earlier such a cutting was introduced artificially[40] in order to expand the temperature (fluctuation) region of applicability of the Ginzburg–Landau approach.

The form of $\mathrm{Im}\,\Gamma^{-1}(\omega, \mathbf{K})$ given above allows us to use analytical calculations virtually to the end and to carry out numerical integration only at the last stage, which is very important in view of lack of analytical results. It should only be noted that henceforth we will have to use expression (28) in the region of $\omega \sim \mu$ also, i.e., beyond the above-mentioned limits where this expression [as well as (27)] holds directly. Nevertheless, the concordance between this algorithm and the approach developed in Ref. 40 indicates that the inaccuracy introduced by us is rather of quantitative than of qualitative nature.

4. TEMPERATURE BEHAVIOR OF PARAMAGNETIC SUSCEPTIBILITY

The summation over frequencies in (9) is carried out after the substitution of the spectral representation (28) into this expression:

$$n_B(\mu, T) = \frac{1}{\pi} \int_{-\infty}^{\infty} d\omega \int \frac{d\mathbf{K}}{(2\pi)^2}\, n_B(\omega)\, \mathrm{Im}\ \Gamma(\omega, \mathbf{K}), \tag{29}$$

where $n_B(\omega) \equiv [\exp(\omega/T) - 1]^{-1}$ is the Bose distribution function.

Before analyzing the behavior of $n_B(\mu, T)$ (29) for relatively large values of n_f, we write for comparison the solution of Eq. (7) in the case of small n_f, when $\mu < 0$ and $|\mu|/T \gg 1$ (the limit of local compound pairs). The required solution is the value $\mu \approx -|\varepsilon_b|/2$; it follows directly from formulas (11)–(14) that $\chi(\mu, T) = O[\exp(-|\varepsilon_b|/T).]$ The obtained result has a simple meaning: the contribution from fermions to the total PMS is exponentially small in view of their absence; the contribution from compound singlet bosons is suppressed by the large binding energy and zero spin [$\chi_b(-|\varepsilon_b|/2, T) \simeq 0$; see (14)] in spite of the fact that their number is relatively large [$n_B(-|\varepsilon_b|/2,\ T) \approx n_f/2$]. Among other things, this simple physical situation is important because it can be considered analytically, although Bose-like Fermi systems are apparently of theoretical interest only.

As regards PMS in the region of optimal concentrations, we can write [see (14)]

$$\chi_b(\mu, T) = 2\chi_{\mathrm{Pauli}} \alpha \frac{m}{\varepsilon_F}, \tag{30}$$

where χ_{Pauli} and α are defined in (12) and (26) respectively, and we assume, as before, that $\varepsilon_F/T \gg 1$. Integrating (29) with respect to $\mathbf{K}$ and using (28), we obtain

$$\int \frac{d\mathbf{K}}{(2\pi)^2}\,\mathrm{Im}\,\Gamma(\omega,\mathbf{K})$$

$$=\frac{1}{2\alpha m}\,\theta(\omega+2\varepsilon_F)\,\frac{1}{1+\kappa^2 t^2(\omega)}$$

$$\times\left\{\arctan\frac{1}{\kappa t(\omega)}-\arctan\frac{1}{\kappa t(\omega)}\right.$$

$$\times\left[1-\frac{1+\kappa^2 t^2(\omega)}{\kappa\left(\frac{1}{\kappa}+\ln\frac{T}{T_c}-\frac{\omega}{4\varepsilon_F}\right)}\right]$$

$$\left.-\frac{\kappa t(\omega)}{2}\ln\left|\frac{\left(\frac{1}{\kappa}+\ln\frac{T}{T_c}-\frac{\omega}{4\varepsilon_F}\right)^2}{\left(\ln\frac{T}{T_c}-\frac{\omega}{4\varepsilon_F}\right)^2+t^2(\omega)}\right|\right\}, \qquad (31)$$

where $t(\omega)\equiv(\pi/2)\tanh(\omega/4T)$, and the parameter $\kappa\equiv\delta/\alpha=\pi^2/7\zeta(3)\simeq 1.18$ can be used as a fitting parameter in view of the approximate nature of (27).

In order to complete the derivation of the expression for the density $n_B(\varepsilon_F,T)$, we must substitute (31) into (28), but before that we consider its another representation, i.e.,

$$n_B(\varepsilon_F,T)=\frac{1}{\pi}\int_0^\infty d\omega\int\frac{d\mathbf{K}}{(2\pi)^2}\,[\mathrm{Im}\,\Gamma(\omega,\mathbf{K})$$

$$-\mathrm{Im}\,\Gamma(-\omega,\mathbf{K})]n_B(\omega)$$

$$-\frac{1}{\pi}\int_0^\infty d\omega\int\frac{d\mathbf{K}}{(2\pi)^2}\,\mathrm{Im}\,\Gamma(-\omega,\mathbf{K}). \qquad (32)$$

This simple division is actually not formal, but has a certain physical meaning. Indeed, the first integral in (32) is singular at $T=T_c$ in view of the presence of the function $n_B(\omega)$ in it, while the second integral remains finite at this point. This means that the first integral corresponds to thermally excited decaying bosons which become coherent and stabilize in the form of Cooper pairs at $T=T_c$ (if we proceed from the region $T>T_c$). On the contrary, the second integral describes incoherent metastable Bose particles whose number is always finite.

The simplest estimates of the dependences on ε_F indicate that the order of magnitude of the first term in (32), or the boson density component depending on T, is proportional to T/ε_F; in the range of n_f under investigation, this term is small if the value of T is not close to T_c. The estimation of the second term gives $O(1)$, i.e., the contribution of compound bosons to PMS is always negative and can be comparable with the fermion contribution even if the fermion density in the system is large, and the fraction of compound bosons is relatively small. In other words, a finite number of short-lived [in view of the relatively large value of $\mathrm{Im}\,\Gamma^{-1}(\omega,\mathbf{K})$] and noncorrelated Bose particles, which depends on T_c weakly [only through $\mathrm{Im}\,\Gamma^{-1}(\omega,\mathbf{K})$], is always present in the normal phase of $2D$ Fermi systems with attraction between charge carriers irrespective of ε_F. Their correlation between these particles and their number increase as we approach the critical temperature. It should be borne in mind that the above statement concerning the large boson contribution to PMS is determined to a considerable extent by the dimensionality ($2D$ in our case). For $3D$ systems, the situation is different. For example, taking the same value of $\mathrm{Im}\,\Gamma(\omega,\mathbf{K})$ (which coincides[17] with that for a $2D$ system only for small ω and $\mathbf{K}$, but is much smaller for $\omega\sim-2\varepsilon_F$), we can find that $n_B(\varepsilon_F,T)\sim(T/\varepsilon_F)^{1/2}$ only due to the root dependence of the density of states on energy. This means that the boson contribution to the PMS of $3D$ systems decreases with increasing ε_F, instead of being constant as in the $2D$ case.

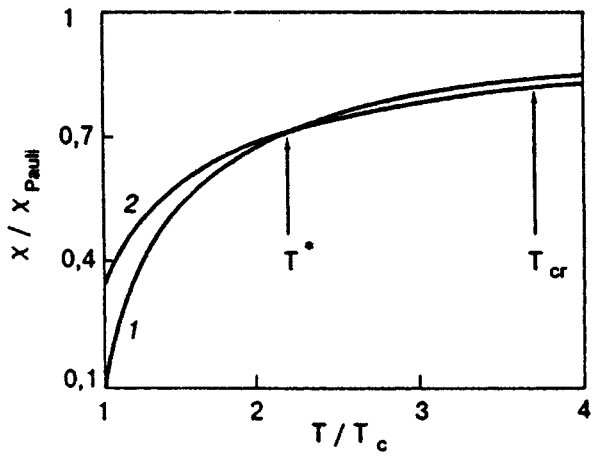

FIG. 1. Behavior of PMS as a function of T: $\varepsilon_F/T_c=10$ (curve *1*) and $\varepsilon_F/T_c=50$ (curve *2*). Characteristic temperatures T^* and $T_{\rm cr}$ are indicated approximately, and the intersection of the curves is due to the coefficients a, b, and c used in the form (25), for which the inequality $\mu/T>10$ used for calculating curve *1* is violated with increasing T.

In order to obtain the required temperature dependence of PMS, we integrated expression (31) numerically with respect to ω. The corresponding results are shown in Fig. 1. The calculations were made for $\chi(\varepsilon_F,T)$ determined from (11), where we assumed that $\chi_F(\varepsilon_F,T)\approx\chi_{\rm Pauli}$, and on the whole confirmed the above estimates. For example, for $T\gtrsim 2T_c$, the main contribution to $\chi_B(\varepsilon_F,T)$ indeed comes from the second [see (32)] term, and the dependence $\chi(\varepsilon_F,T)$ on T is close to linear. The contribution from the first term becomes significant in the region $T\lesssim 2T_c$; it can be seen that this contribution for $\varepsilon_F/T_c\simeq 10$ is naturally larger than for $\varepsilon_F/T_c\simeq 50$.

A comparison of theoretical curves with experimental dependences (see, for example, Refs. 1 and 5) indicates that they are close qualitatively. For example, two characteristic temperature intervals are usually distinguished on the experimental temperature dependences of PMS: the first interval, where PMS decreases linearly, and the second interval, where $\chi(\varepsilon_F,T)$ decreases more rapidly. In the case of HTS materials, this is explained by the formation of a gap in their spin excitation spectrum. The region $T^*\lesssim T\lesssim T_{\rm cr}$ corresponds to the first interval and the region $T_c\lesssim T\lesssim T^*$ to the second interval; here $T_{\rm cr}$ and T^* are some empirically determined temperatures (see Fig. 1). Although we could not estimate the values of these temperatures, it can be seen that

the temperature dependence obtained for PMS convincingly demonstrates the same behavior. In our opinion, this casts a shade of doubt on the theories and models in which such a behavior of PMS is attributed exclusively to the magnetic ground state of an HTS materials or to the magnetism of their cuprate planes, while the role and properties of the Fermi subsystem of a lower dimensionality is actually neglected. We believe that the latter can also be manifested in experiments (at any rate, its role cannot be disregarded).

CONCLUSION

The results of above calculations confirm the peculiar properties of $2D$ Fermi systems with attraction between particles. We considered direct nonretarded attraction by using the BCS model, but in all probability, the indirect interaction in a $2D$ system will necessarily lead to the same behavior of PMS, although this statement requires additional verification.

An interesting physical result obtained by us is the discovery of a significant role of noncorrelated fluctuating Bose pairs above T_c. They are responsible for the anomalous behavior of the normal phase associated, for example, with the formation of a pseudogap in it. A decrease in T leads to the emergence of correlations, and the behavior of the system near T_c is determined to a considerable extent by ordinary superconducting fluctuations like those in the Aslamazov–Larkin theory. The conclusion that the presence of the Fermi surface does not rule out a peculiar behavior of the Fermi system if its electron properties have lower (quasi-$2D$) dimensionality also appears to us as important. In the theories with real (and not virtual) local pairs (e.g., in the form of bipolarons), the Fermi surface does not exist.[41] The problem of the presence or absence of pairs above T_c can be solved if we assume that the pairs are not stable, but decaying formations whose role is especially important in systems with a lower dimensionality.

At the same time, our calculations did not reveal a tendency of PMS to the Pauli susceptibility at $T>2T_c$ upon an increase in the ratio ε_F/T_c. We can assume that this is due to the fact that we actually analyzed a $2D$ rather than quasi-$2D$ model since it was shown that the required behavior of PMS is observed for $3D$ systems. For this reason, a generalization of the model considered here to this more realistic (quasi-$2D$) case would be undoubtedly interesting (not to mention the inclusion of intrinsic magnetic subsystem, viz. localized spins in the model) in order to find out with the maximum possible certainty whether a spin gap is actually present in HTS materials, or the temperature behavior of their PMS can be described proceeding only from the presence of holes moving over cuprate layers and experiencing attraction according to a certain mechanism.

The authors are grateful to È. V. Gorbar and V. P. Gusynin for numerous stimulating discussions of the problems considered here and for valuable remarks.

Addendum made in proofs

In the publications appearing after this article was submitted (including A. C. Loester *et al.*, *Physica* **C203**, 208 (1996); H. Ding *et al.*, Phys. Rev. Lett. **76**, 1533 (1996) and *Nature* **382**, 51 (1996); D. S. Marshall *et al.*, *Phys. Rev. Lett.* **76**, 4841 (1996), and V. E. Kataev *et al.*, *Usp. Phys. Nauk* **166**, 213 (1996)), the results of measurements of one-particle photoemission spectra with angular resolution (ARPES) for cuprates are reported. These results indicate that the gap observed above T_c (to be more precise, a pseudogap as correctly indicated in these publications), is transformed more of less smoothly into a superconducting gap. Both gaps exhibit anisotropy, but their relation to the magnetism of HTS materials is not discussed.

In our opinion, these measurements confirmed qualitatively (and quite reliably) the pattern described above, according to which compound bosons exist in low-dimensional metals not only below T_c, but also at temperatures considerably higher than critical. The only difference lies in the lifetime and correlation of these particles: above T_c, the former is very short (bosons are overdamped), and the latter is absent (in the global sense). However, the indirect nature of fermion–fermion attraction, or, in other words, the inclusion or delay effects in the model, is an important circumstance which should be consistently taken into account in the model in order to compare (at least semiquantitatively) its physical properties with experimentally observed parameters. In this case, the formation of a gap (see Ref. 13) as well as a pseudogap under BCS-type conditions will obviously occur predominantly at the expense of ''corrosion'' of fermions just in the ''phonon (magnon, etc.) strip'' near the Fermi surface, which is observed in experiments.

*E-mail: vloktev@gluk.apc.org

[1)] In this case, it would be more appropriate to refer to it as a Bose system since all the fermions are coupled in individual (local) pairs, and the Fermi surface is absent (i.e., the spectral weight of quasiparticle Fermi excitations is equal to zero).

[2)] It can easily be seen that when the field **H** lies in the plane, the diamagnetic contribution to the total magnetic susceptibility is excluded altogether.

[3)] This quantity is in complete agreement with the criterion formulated in Introduction, the only difference being that the value of n_f^{cr} obtained in Ref. 15 corresponds to finite values of T.

[4)] For this reason, expression (27) is valid within the limits of applicability of expansion in momenta used for deriving (16).

[1] M. Mehring, Appl. Magn. Res. **3**, 383 (1992).
[2] A. Sokol, in *Proc. of the Stanford Conf. on Spectroscopics in Novel Superconductors*, Stanford (1995).
[3] V. M. Loktev, Fiz. Nizk. Temp. **22**, 3, 490 (1996) [Low Temp. Phys. **22**, 1, 376 (1996)].
[4] P. W. Anderson, *Theory of Superconductivity in High-T_c Materials*, Preprints of Princeton Univ. (1995).
[5] D. Pines, in *Invited Talks at the Bilkent Summer School on Condensed Matter Physics*, Ankara, Turkey (1996).
[6] B. G. Levi, Physics Today, June, 17 (1996).
[7] A. V. Chubikov and S. Sachdev, Phys. Rev. Lett. **71**, 169 (1993).
[8] A. Sokol and D. Pines, Phys. Rev. Lett. **71**, 2813 (1993).
[9] V. Bazykin, D. Pines, A. Sokol, and D. Thelen, Phys. Rev. **B49**, 1544 (1994).
[10] V. M. Loktev, Sverkhprovodimost': Fiz., Khim., Tekh. **4**, 2293 (1991); Fiz. Nizk. Temp. **19**, 375 (1993) [Low Temp. Phys. **19**, 263 (1993)].
[11] M. Randeira, J. Duan, and L. Shieh, Phys. Rev. Lett. **62**, 981 (1989); Phys. Rev. **B41**, 327 (1990).
[12] È. B. Gorbar, V. P. Gusynin, and V. M. Loktev, Sverkhprovodimost': Fiz., Khim., Tekh. **6**, 483 (1992); Fiz. Nizk. Temp. **19**, 1771 (1993) [Low Temp. Phys. **19**, 832 (1993)].
[13] V. M. Loktev and S. G. Sharapov, Fiz. Nizk. Temp. **22**, 271 (1996) [Low Temp. Phys. **22**, 211 (1996)].
[14] S. Schmitt-Rink, C. M. Varma, and A. E. Ruckenstein, Phys. Rev. Lett. **63**, 445 (1989).

[15] A. Tokumitu, K. Miyake, and K. Yamada, Progr. Theor. Phys. Suppl. **106**, 63 (1991); Phys. Rev. **B47**, 11988 (1993).
[16] M. Randeria, N. Trivedi, A. Moreo, and R. T. Scaletar, Phys. Rev. Lett. **69**, 2001 (1992).
[17] M. Randeria, in *Bose–Einstein Condensation* (ed. by A. Griffin, D. W. Snoke, and S. Stringari), Cambridge U.P., New York (1995).
[18] R. Micnas, M. N. Pedersen, S. Schafroth *et al.*, Phys. Rev. **B52**, 16223 (1995).
[19] T. Schneider, M. H. Pedersen, and J. J. Rodriguez-Nunez, Z. Phys. **257**, 257 (1996).
[20] K. Maki and T. Tsuneto, Progr. Theor. Phys. **31**, 945 (1964).
[21] V. P. Gusynin, V. M. Loktev, and I. A. Shovkovy, Preprint ITP, NAS Ukraine, No. ITP-95, 23E (1995).
[22] A. A. Abrikosov, L. P. Gor'kov, and I. E. Dzyaloshinskii, *Methods of Quantum Field Theory in Statistical Physics*, Prentice-Hall, Englewood Cliffs, NJ, 1963.
[23] P. Nozieres and S. Schmitt-Rink, J. Low Temp. Phys. **59**, 195 (1985).
[24] C. A. R. Sa de Melo, M. Randeira, and S. R. Engelbrecht, Phys. Rev. Lett. **71**, 3203 (1993).
[25] P. C. Hohenberg, Phys. Rev. **158**, 383 (1967).
[26] R. Mackenzie, P. K. Panigrahi, and S. Sakhi, Int. J. Mod. Phys. **A9**, 3603 (1994).
[27] V. L. Berezinskii, Zh. Eksp. Teor. Fiz. **59**, 907 (1970) [Sov. Phys. JETP **32**, 493 (1970)].
[28] J. Kosterlitz and D. Thouless, J. Phys. **C6**, 1181 (1973).
[29] J. Serene, Phys. Rev. **B40**, 10873 (1989).
[30] A. Tokumitu, K. Miyake, and K. Yamada, J. Phys. Soc. Jpn. **60**, 380 (1991).
[31] E. V. Gorbar, V. M. Loktev, and S. G. Sharapov, Physica **C257**, 355 (1996).
[32] S. G. Sharapov, Ukr. Fiz. Zh. **41**, 212 (1996).
[33] L. G. Aslamazov and A. I. Larkin, Fiz. Tverd. Tela (Leningrad) **10**, 1104 (1968) [Sov. Phys. Solid State **10**, 875 (1968)].
[34] A. V. Svidzinskii, *Spatially Inhomogeneous Problems in the Theory of Superconductivity* [in Russian], Nauka, Moscow (1982).
[35] M. Drechsler and W. Zwerger, Ann. Phys. (Leipzig) **1**, 15 (1992).
[36] M. Casas, J. M. Getino, M. de Llano *et al.*, Phys. Rev. **B50**, 15945 (1994).
[37] E. M. Lifshitz and L. P. Pitaevskii, *Statistical Physics* [in Russian], Nauka, Moscow (1978).
[38] M. Tinkham, *Introduction to Superconductivity*, McGraw-Hill, NY, 1975.
[39] H. Ebisawa and H. Fukuyama, Progr. Theor. Phys. **46**, 1042 (1971).
[40] B. R. Patton, V. Ambegaokar, and J. W. Wilkins, Solid State Commun. **7**, 1287 (1969).
[41] P. W. Anderson and N. F. Mott, Physics World **9**, 16 (1996).

Translated by R. S. Wadhwa

Crystal phase formation and growth in rare-gas clusters

S. I. Kovalenko, D. D. Solnyshkin, E. A. Bondarenko, and È. T. Verkhovtseva

*B. Verkin Institute for Low Temperature Physics and Engineering, National Academy of Sciences of the Ukraine, 310164 Kharkov, Ukraine**

(Submitted July 24, 1996)
Fiz. Nizk. Temp. **23**, 190–196 (February 1997)

The structure of clusters formed in supersonic jets of heavy rare gases is studied by the methods of electron diffractometry. It is found that a crystalline fcc structure with ''deformation-type'' stacking faults (SF) is formed in aggregates consisting of $N \geqslant 2 \cdot 10^3$ atoms/cluster. The SF density is a linear function of $N^{-1/3}$. The number of ''defective'' planes does not depend on the cluster size and is equal to four in all cases. Such a number of intersecting SF leads to the formation of nonvanishing atomic steps ensuring a rapid and subsequently defectless growth of the cluster on all densely packed planes facing the cubooctahedron. The obtained results confirm experimentally the important role of the kinetic factor in the formation of the atomic structure of a cluster. © *1997 American Institute of Physics.* [S1063-777X(97)00802-5]

The interest of fundamental science in the structure and physical properties of clusters is due to their intermediate position between individual atoms (molecules) and a macroscopic system (solid or liquid). The information on the properties of clusters is also important for solving problems in the physics of phase transitions, surface, and surface processes. The mechanisms of formation of cluster structure, kinetics of cluster growth, and the establishment of stages at which the formation of a certain property of a solid is completed are of considerable interest.

In recent years, experiments on clusters free of substrates and formed as a result of homogeneous nucleation in a gas jet expanding at constant entropy became very popular. At the last stage of growth, such clusters have a high temperature, facilitating a high rate of relaxation processes and the attainment of the equilibrium state.

The maximization of the binding energy of particles forming a cluster served as the main criterion in the choice of the optimal model of cluster structure until recently. Van de Waal[1] constructed the diagram of the dependence of the structure of a cluster consisting of Lennard-Jones particles on its size N on the basis of vast theoretical material obtained by using this approach. According to this diagram, icosahedron is most advantageous from the energy point of view for $N \leqslant 1.5 \cdot 10^3$ atoms/cluster, while decahedron is advantageous for larger N. The minimum size of a stable cubooctahedral fcc cluster must exceed 10^5 atoms/cluster. However, electron diffraction studies[2–4] confirmed the formation of an fcc structure even for $N \sim 10^3$ atoms/cluster. Van de Waal[1] proposed a considerable effect of kinetic processes (such as aggregation growth) on the structure formation and proved theoretically that a less advantageous fcc structure can be realized in argon clusters in the presence of stacking faults (SF), facilitating a rapid and defectless aggregation growth. Preliminary experimental data confirming this assumption for argon clusters were reported by us in a brief communication.[5] The present research is a detailed electron diffraction study of argon, krypton, and xenon clusters aimed at detection, identification, and determination of the number of SF in small crystalline aggregations of heavy rare gases. A detailed description of some methodical aspects of these investigations is also included.

EXPERIMENTAL TECHNIQUE

The experiments were carried out on a setup consisting of a generator of the supersonic cluster beam and an electron diffractometer EMR-100M. A detailed description of the setup was given in Ref. 4 The supersonic gas jet was created by a conical nozzle with the critical cross section diameter 0.34 mm, the cone angle 8.6°, and the ratio of the inlet and critical cross sectional areas 36.7. The gas flow was collimated with the help of a conical diaphragm of diameter 1.09 mm. The distance between the end face of the nozzle and the diaphragm was 5 mm. The point of intersection of the cluster jet and the electron beam was separated from the nozzle exit section by 110 mm. The size distribution of clusters, and hence the average size N were determined by the gas pressure P_0 at the nozzle entrance at a constant temperature $T_0 = 200$ K. The value of P_0 was varied from 0.027 to 0.6 mPa. The construction of the electron diffractometer allowed us to record diffraction patterns both electrometrically, and photographically. In the former case, a considerable fraction of incoherently scattered electrons could be removed by a counterfield, which improved the accuracy in determining the shape of diffraction peaks significantly. The photographic recording was used for precision measurements of the diameters of diffraction rings. A typical electron diffraction pattern from coarse crystalline clusters of inert gases is shown in Fig. 1. The diffraction pattern was obtained from an argon cluster jet formed under pressure $P_0 = 0.6$ mPa at $T_0 = 150$ K. The positions and relative intensities of diffraction peaks correspond to an fcc structure of aggregations. Reliable detection, identification, and calculation of packing defect density involves the precision measurement of the in-

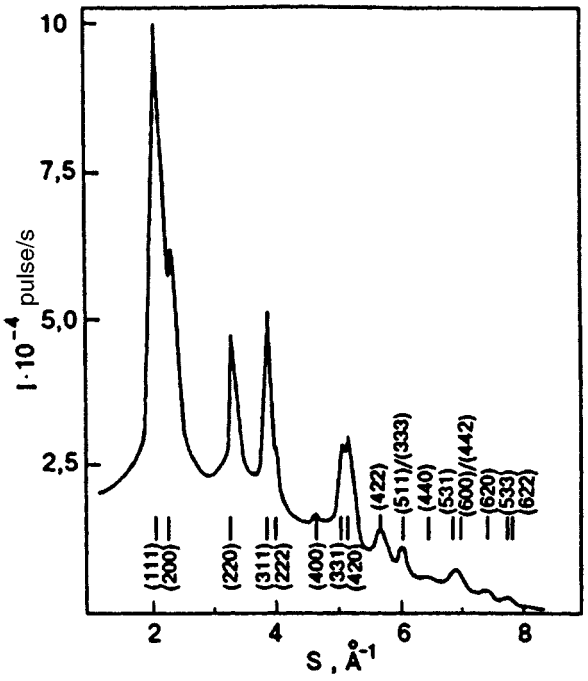

FIG. 1. Electron diffraction pattern for an argon cluster beam: $\overline{N} \simeq 2.5 \cdot 10^4$ atoms/cluster, $s = 4\pi \sin \Theta/\lambda$, where θ is the Bragg angle.

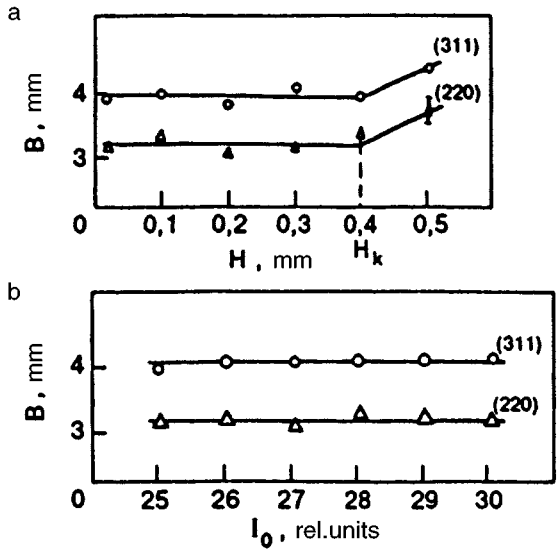

FIG. 2. Dependences of half-widths of diffraction peaks (220) and (311) on the electron diffraction patterns for an argon cluster beam ($\overline{N} \simeq 2 \cdot 10^4$ atoms/cluster) on the scanning gap width (a) and on the intensity I_0 of the primary beam (b).

strumental width b_0 of the electron beam and the instrument constant $L_{\text{eff}}\lambda$, where L_{eff} is the effective distance from the sample to the electron collector and λ the electron wave length. These quantities were determined by using a standard island thallium chloride film deposited on a substrate transparent for electrons. The values of b_0 and $L_{\text{eff}}\lambda$ were measured before the gas jet was exhausted to vacuum. The standard film was fixed in the region of intersection of the cluster and electron beams, and the value of b_0 was determined from the half-width of diffraction peaks of the standard. The correctness of such a method of measurement of b_0 was ensured by a large size of coherent scattering regions (CSR) for thallium chloride. According to electron-microscopic observations,[6] its value ranges from 400 to 500 Å. The value of $L_{\text{eff}}\lambda$ was determined according to the experimental technique described in detail in Ref. 7.

Peculiarities of the problems considered here require not only precision measurements of the positions of the centers of gravity in diffraction peaks, but also an analysis of their shape in order to eliminate instrumental factors (such as the gap diaphragm width H relative to which the diffraction pattern is scanned) as well as the intensity I_0 of the electron beam forming the diffraction pattern, which affect the peak width and profile. In order to determine the value of $H = H_k$ below which a change in the gap width of the entrance diaphragm does not affect the shape of the peak, the dependence of half-width B_{hkl} of diffraction peaks on H was recorded. The gap width varied from 0.02 to 0.5 mm. The results are presented in Fig. 2a, where the gap width is plotted along the abscissa axis and the half-width of (220) and (311) peaks on the diffractogram from an argon cluster jet with $\overline{N} \simeq 2 \cdot 10^4$ atoms/cluster along the ordinate axis. It can be seen from the curves that the values of B_{hkl} are virtually independent of H for $H < H_k = 0.4$ mm. As diffraction peaks become blurred, the value of H_k is shifted toward higher values, and vice versa. In the case of the sharpest peaks a on electron diffraction patterns from the TlCl standard film, $H_k = 0.3$ mm. For this reason, the gap width in our experiments did not exceed 0.25 mm. In Fig. 2b, the intensity of the primary electron beam is plotted along the abscissa axis and the half-widths of the (220) and (311) peaks for Ar_N along the ordinate axis. The maximum value of I_0 satisfied the requirements of reliable detection of diffraction peaks with intermediate intensity. It can be seen from the curves that the half-width of diffraction peaks are virtually independent of the intensity of the primary beam for reasonable values of I_0.

The determination of the average size of clusters constitutes a central problem in the physics of cluster jets. Here we determined the characteristic average size $\delta \sim N^{1/3}$ of crystalline clusters with the help of the Selyakov–Scherrer (SS) relation from the results on complete broadening of diffraction peaks as well as broadening caused by stacking faults. The correctness of application of the SS relation for crystalline clusters with the fcc structure and average size $N > 10^3$ atoms/cluster was based on the calculations carried out in Ref. 8. In addition, we compared the size of CSR obtained by two independent methods, i.e., electron diffractometry using the SS relation and electron microscopy. Reference measurements were made on gold island films obtained by thermal evaporation of Au in a high vacuum followed by its deposition on an amorphous carbon substrate film. The values of δ obtained by the two methods were in good agreement. The difference was smaller than 10%, i.e., did not exceed the error in the measurements of δ by electron diffraction method.

According to the theory of x-ray scattering,[9] the characteristic size of clusters was calculated by the formula

$$1/\delta = 1/\delta^* - 1/\delta_s, \tag{1}$$

where δ^* is the effective size determined from the total diffraction peak broadening with the help of the SS relation, and $1/\delta_s$ is the broadening due to SF. According to the theory, we have

$$\delta_d = \frac{d_{111}}{1.5\alpha + \beta} \frac{1}{j \cos \varphi}, \tag{2}$$

where d_{111} is the separation between densely packed layers, $j \cos \varphi$ the parameter typical of a given family of planes, α the density of a SF of the ''deformation'' type, and β the density of twin (growth) SF.

The presence of stacking faults of the ''deformation'' type in fcc clusters can be determined from a certain regularity in the displacement of diffraction peaks relative to their position in a defect-free crystal.[9] In addition, the blurring and considerable displacement of certain closely-spaced peaks toward one another leads to their poor resolution. This refers, for example, to (111) and (200) peaks as well as (331) and (420). The presence of twinned SF does not cause a displacement of diffraction peaks and only leads to their insignificant asymmetric broadening. An analysis of the obtained diffraction patterns did not reveal any asymmetry of the peaks, which implies a low density of twinned SF. The value of β was determined as follows. In the case of an isomeric cluster (this assumption is justified for an aggregation formed in an expanding gas jet), the difference in complete broadenings of two diffraction peaks (hkl) and $(h'k'l')$ according to relations (1) and (2) is $C(1.5\alpha + \beta)$, where

$$c = L_{\text{eff}} \lambda [(j \cos \varphi)_{hkl} - (j \cos \varphi)_{h'k'l'}]/d_{111}.$$

Since the value of α can be found from independent measurements of the position of diffraction peaks, this difference determines the value of β unambiguously. Our experiments proved that the density of SF of the ''twinning'' type was equal to zero to within experimental error for all the cases under investigation. The value of α was calculated from the displacement of the centers of gravity of diffraction peaks relative to their position in a defect-free crystal. The value of this quantity was determined by using a standard diffraction ring (311) of the object under investigation, whose diameter did not change in the presence of SF. The values of α were calculated by using the Patterson formulas.[10] In the case of diffraction of fast electrons, these formulas can be transformed, in view of the smallness of Bragg's angles, to[11]

$$\Delta D_{\text{SF}}/D = G j \alpha^*/2, \tag{3}$$

where $\Delta D_{\text{SF}}/D$ is the relative change in the diameter of a diffraction ring under the effect of SF, G is a constant quantity for a given family of planes $\{hkl\}$ averaged over all the groups of (hkl) planes with the same displacement, j the fraction of planes of the family $\{hkl\}$ affected by SF, and α^* the parameter connected with the SF density through the relation

$$\alpha^* = \frac{4\pi}{3\sqrt{3}} \left[\frac{1}{2} - \frac{3}{2\pi} \arctan \sqrt{3}(1 - 2\alpha) \right]. \tag{4}$$

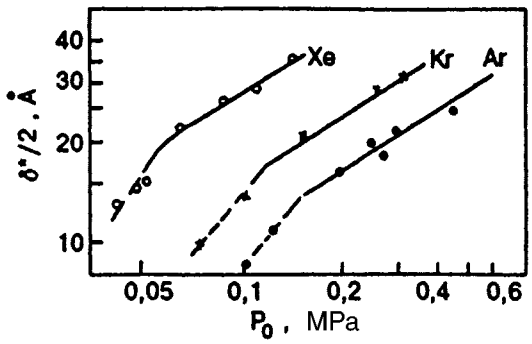

FIG. 3. Dependence of the effective radius $\delta^*/2$ of clusters on the pressure at the nozzle entrance ($T_0 = 200$ K): Ar_N(●), Kr_N(×), and Xe_N(○).

In order to find the value of α, the diameters of diffraction rings (111) and (220) were measured with the help of a precision comparator IZA-2. The relatively high intensity and sharpness of the chosen peaks ensured a quite admissible precision of measurements. In most cases, the relative error in the measurements of α did not exceed 20%.

DISCUSSION OF RESULTS

It was mentioned above that our task was the detection and measurement of the SF density in crystalline clusters of rare gases. The primary stage in the solution of this problem was the determination of the range of pressures P_0 under which the cluster beams are predominantly formed by crystalline aggregations. For this purpose, we used the following arguments. According to the calculations[8] confirmed by the results of electron diffractometry,[3,4] a transition from a fcc structure to an icosahedral structure causes a strong broadening of diffraction peaks, followed by a change in the form of the dependence of the peak half-width on the size of scattering aggregations. Figure 3 shows the dependence of the effective radius $\delta^*/2$ of the clusters on pressure P_0 plotted on the basis of an analysis of obtained diffraction patterns for the three gases under investigation. The values of these quantities are plotted on the logarithmic scale. It should be recalled that the value of δ^* was determined on the basis of the SS relation from the half-width of diffraction peaks ($\delta^* \propto B_{hkl}^{-1}$). It can be seen from the figure that above a certain pressure range, the experimental points obtained for Ar_N, Kr_N, and Xe_N clusters fit to a straight line corresponding to the dependence $\delta^* \propto P_0^{0.61}$. For lower values of P_0, δ^* decreases rapidly (more rapid peak blurring), indicating, according to Ref. 4, the predominance of icosahedral aggregations in the cluster beam. Subsequent experiments were made with pressures P_0 under which crystalline clusters are preferentially formed.

Figures 4a, b, and c show diffraction patterns of Ar, Kr and Xe cluster beams respectively. The diffraction patterns observed experimentally for all the three types of cluster beams display peculiarities typical of fcc structures with ''deformation'' stacking faults: displacement of (111) and (220) peaks toward large diffraction angles, and poor resolution of (111) and (200) as well as (331) and (420) peaks associated with their broadening and displacement toward

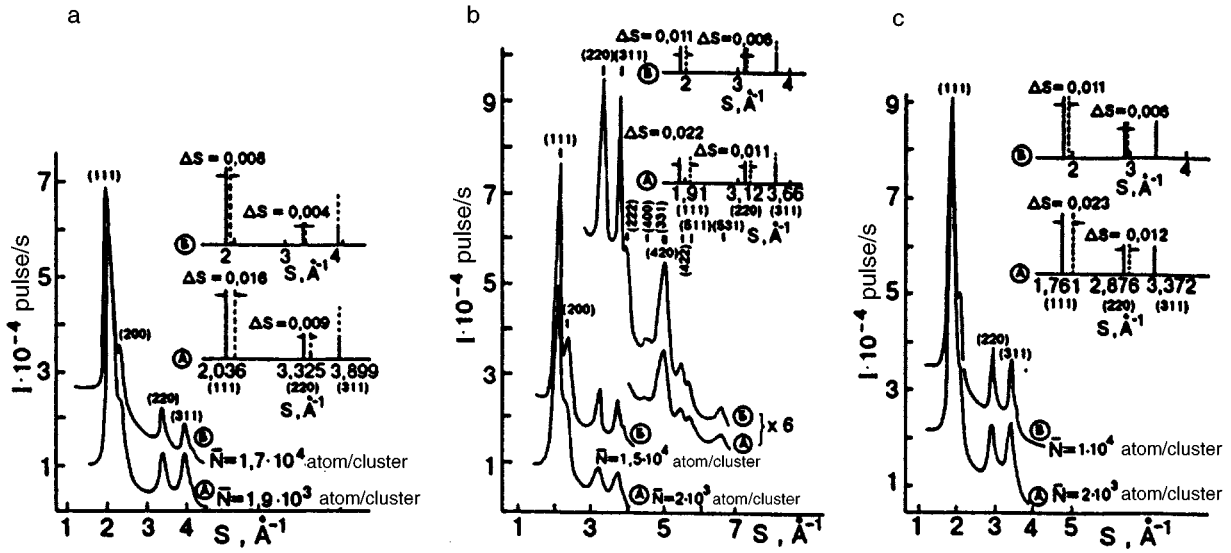

FIG. 4. Electron diffraction patterns for Ar_N (a), Kr_N, (b) and Xe_N (c) clusters. The insets show the calculated positions of peaks for defect-free clusters (solid lines) and experimentally observed positions (dashed lines); $s=4\pi\sin\theta/\lambda$.

each other. The insets on these figures give an idea as to the magnitude and nature of these displacements: solid lines show the positions of diffraction peaks for defect-free fcc clusters, while dashed lines indicate the experimental values. It can be seen from the figure that as the average size of clusters increases, the discrepancy between the calculated, positions of peaks for defect-free aggregations and the experimentally observed peaks decreases, and the splitting of (111) and (200) peaks increases. It should be noted that a decrease in the average size of crystalline clusters increases the contribution to the diffraction pattern both from the surface, and from the quasi-crystalline structure. However, possible changes in the intensity distribution of diffracted beams initiated by these contributions do not affect the peculiarities which makes it possible to detect and identify SF. The results of observations were subsequently used for determining the true (taking into account SF) radius $\delta/2$ of crystalline clusters. The results obtained for Ar_N, Kr_N, and Xe_N are shown in Fig. 5. The values of $\delta/2$ are plotted along the ordinate axis and the values of P_0 along the abscissa axis on the logarithmic scale. The scales of pressure for different rare gases are shifted relative one another according to the law of ''corresponding jets.'' [12] It can be seen from the figure that the experimental points corresponding to Ar_N, Kr_N, and Xe_N clusters fit to the same straight line with the slope equal to 0.61. The same slope was obtained in Refs. 12 and 13 for argon clusters in a wide range of average size by using the acoustic nozzle and with the same object for supersonic nozzle.[4,14] An analysis of the curves in Figs. 3 and 5 showed that crystalline clusters prevail in cluster beams with an average radius of aggregations exceeding 26–30 Å (its value depends on the gas). This means that crystalline clusters prevail in atomic beams with $N\geqslant 2\cdot 10^3$ atoms/cluster. It should be noted in this connection that the value $N\simeq 800$ atoms/cluster, for which crystalline aggregations prevail in argon cluster beams according to our earlier results[4] is underestimated since we did not take into account stacking faults.

The SF density as a function of the characteristic size of crystalline cluster is shown in Fig. 6. It can be seen from the figure that the value of α for clusters of all the gases under investigation fits to the same straight line to within experimental error, and the SF density decreases monotonically with increasing size of crystalline aggregations, and hence the total number n of densely packed planes. If we consider that

$$\alpha=n_{\mathrm{SF}}/n, \tag{5}$$

where n_{SF} is the number of stacking faults, the observed regularity indicates that the value of n_{SF} remains constant or changes insignificantly during the cluster growth.

In order to determine n_{SF}, we will use relation (5) as well as the fact that

$$n=3\delta/d_{111}. \tag{6}$$

This gives

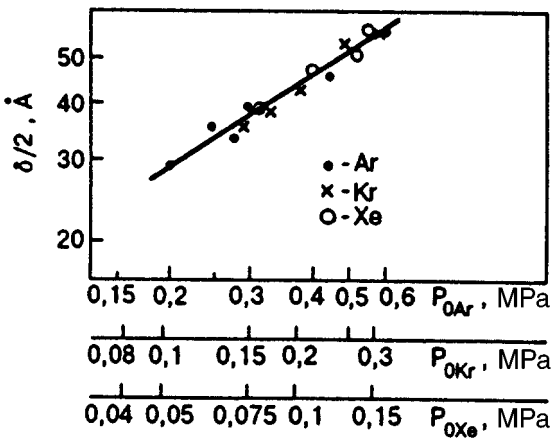

FIG. 5. Dependence of the true radius $\delta/2$ of clusters on the gas pressure P_0 at the nozzle entrance at a constant temperature $T_0=200$ K: Ar_N(●), Kr_N(×), and Xe_N(○).

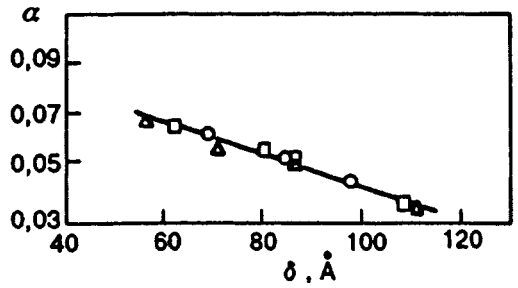

FIG. 6. Variation of the SF density with the cluster size: $Ar_N(\triangle)$, $Kr_N(\bigcirc)$, and $Xe_N(\square)$.

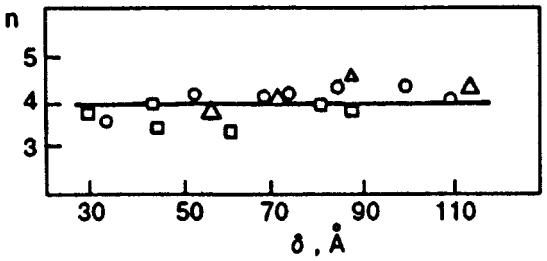

FIG. 7. The number n_{SF} of ''defective'' planes in crystalline clusters of various size: $Ar_N(\triangle)$, $Kr_N(\bigcirc)$, and $Xe_N(\square)$.

$$n_{SF}=3\sqrt{3}\,\alpha\,\delta/a, \tag{7}$$

where a is the crystalline cluster lattice constant for the corresponding inert gas. Figure 7 shows the results of calculation of the $n_{SF}(\delta)$ dependence by formula (7). According to the figure, clusters of different sizes contain the same number of stacking faults, equal to 4. The obtained result is valid for all the gases under investigation and indicates that SF are formed at early stages of formation of fcc clusters whose subsequent growth is defectless.

Thus, the analysis of the obtained results shows that an fcc structure with stacking faults of the ''deformation'' type is formed in clusters of heavy rare gases with a size $N \geqslant 2\cdot 10^3$ atoms/cluster ($\delta/2 \geqslant 26-30$ Å). Stacking faults can be regarded as small regions of the hcp phase intruded into the fcc structure. The formation of the fcc phase is apparently facilitated by a vanishingly small difference between hcp and fcc packings in the case of rare gas atoms. Moreover, the calculations taking into account only paired interaction between particles[15] predicted a higher stability of the hcp structure for solidified rare gases. According to theoretical analysis,[16] local cluster regions with a fifth-order symmetry can serve as sources of intersecting SF. The results of calculations show that the number of stacking faults does not depend on the size of the atomic complex and is equal to four in all cases. Such a number of intersecting stacking faults piercing the entire volume of a cluster leads to leads to the formation of nonvanishing steps of the same type as in the case when a screw dislocation emerges at the surface on all densely packed planes facing a cubooctahedron. A further growth of the cluster does not require the formation of new nuclei on densely packed faces since it occurs due to trapping of newly arriving atoms by the formed steps. The regularity of atomic packing is not violated in this case, which rules out the formation of new stacking faults. As a result, the SF density decreases as the aggregation grows. Thus, our results of observations indicate a significant role of the kinetic factor in the formation of the cluster structure and serve as a convincing experimental proof of the hypothesis put forth by van de Waal.[1] The obtained experimental results also indicate the important role of stacking faults in the formation of the crystalline structure of the cluster. The realization of an fcc structure in solidified heavy inert gases is apparently determined to a considerable extent by the presence of intersecting SF which can ensure a rapid and subsequently defectless crystal growth only in the fcc (but not in the hcp) lattice.

*E-mail: sktb@ilt.kharkov.ua

[1] B. W. van de Waal, J. Chem. Phys. **98**, 4909 (1993).
[2] J. Farges, M. F. de Feraudy, B. Raoult, and G. Torchet, Adv. Chem. Phys. **70**, 45 (1988).
[3] J. W. Lee and G. D. Stein, Surface Sci. **156**, 112 (1985).
[4] S. I. Kovalenko, D. D. Solnyshkin, É. T. Verkhovtseva, and V. V. Erementko, Fiz. Nizk. Temp. **20**, 961 (1994) [Low Temp. Phys. **20**, 758 (1994)].
[5] S. I. Kovalenko, D. D. Solnyshkin, É. T. Verkhovtseva, and V. V. Eremenko, Chem. Phys. Lett. **250**, 309 (1996).
[6] S. I. Kovalenko and P. E. Toryanik, Kristallografiya **35**, 1303 (1990).
[7] B. K. Vainshtein, *Structural Electron Diffractometry* [in Russian], Izd. Akad. Nauk SSSR, Moscow (1956).
[8] J. W. Lee and G. D. Stein, J. Chem. Phys. **91**, 2450 (1987).
[9] V. I. Iveronova and G. P. Revkevich, *The Theory of X-Ray Scattering* [in Russian], Izd. MGU, Moscow (1972).
[10] M. S. Patterson, J. Appl. Phys. **23**, 805 (1952).
[11] Yu. F. Komnik, Fiz. Tverd. Tela (Leningrad) **6**, 873 (1964) [Sov. Phys. Solid State **6**, 672 (1964)].
[12] O. F. Hagena and W. Obert, J. Chem. Phys. **56**, 1793 (1972).
[13] J. Farges, M. F. de Feraudy, B. Raoult, and G. Torchet, J. Chem. Phys. **84**, 3491 (1986).
[14] R. Karnbach, M. Joppien, J. Stapelfeldt *et al.*, Rev. Sci. Instrument **64**, 2838 (1993).
[15] T. H. K. Barron and C. Domb, Proc. Roy. Soc. **A227**, 447 (1955).
[16] B. W. van de Waal, J. Cryst. Growth **158**, 153 (1996).

Translated by R. S. Wadhwa

DYNAMICS OF THE CRYSTAL LATTICE

Dynamics and stability of localized modes in nonlinear media with point defects

M. M. Bogdan and A. S. Kovalev

*B. Verkin Institute for Low Temperature Physics and Engineering, National Academy of Sciences of the Ukraine, 310164 Kharkov, Ukraine**

I. V. Gerasimchuk

Kharkov State University, 310077 Kharkov, Ukraine
(Submitted July 25, 1996)
Fiz. Nizk. Temp. **23**, 197–207 (February 1997)

The soliton states localized at a point defects are investigated by using the nonlinear Schrödinger equation for various signs of the nonlinearity and for different types of defects. The quantum interpretation of these nonlinear localized modes is given in terms of bound states of a large number of Bose particles. The dynamic properties and stability of these states for different types of interaction between elementary excitations with one another and with the defect are investigated. The boundaries of the region of existence and stability of ''impurity'' solitons are determined depending on the ''intensity'' of the defect, and the frequency of small oscillations of a soliton near the defect is calculated. © *1997 American Institute of Physics.* [S1063-777X(97)00902-X]

INTRODUCTION

The states localized near an impurity were studied for the first time 50 years ago by I. M. Lifshits.[1,2] In recent years, this problem was considered on a new, ''nonlinear'' level. New experimental data on low-temperature diffusion and internal friction served as an impetus for theoretical investigations of local vibrational states in ideal and defective anharmonic elastic media.[3–10] Such excitations were considered for the first time in Refs. 11 and 12 in which long-lived vibrational states of molecules were studied in simple molecular crystals. The stability of such localized vibrations was associated with anharmonism of intramolecular oscillations. The frequencies of these oscillations lie outside the continuous spectrum band and depend on the amplitude of vibrations.

On the other hand, a medium with defects can also exhibit local vibrations (which, however, are localized near an impurity) even in the linear limit. The frequency of these vibrations is fixed and is determined by the sign and ''intensity'' of the defect (e.g., by the sign and magnitude of the mass defect). For this reason, it would be interesting to analyze local vibrations, taking into account anharmonisms and defects simultaneously. Zavt and Reitman[13] were the first to study this problem by considering the effect of anharmonisms on the behavior of an isotopic defect in quantum crystals (the emergence of local vibrations with low frequencies in the case of a heavy impurity).

In Refs. 14 and 15, this problem was considered in a one-dimensional model using the soliton approach. In the case of an isotropic impurity in an anharmonic chain, soliton solutions whose frequencies lied above as well as below the continuous band spectrum of linear waves were found by the asymptotic method. It was proved that nonlinearity can lead to the formation of specific local modes in crystals with defects even for the defect sign for which local vibrations are absent in the linear limit. In these publications, however, the stability of local modes of various types was not discussed, and the semiclassical interpretation of these states was not used. Semiclassical quantization of self-trapped elastic vibrations in an ideal (defect-free) one-dimensional anharmonic chain was carried out in Ref. 16, where the concept of elastic solitons of the envelope as a bound state of a large number of phonons was formulated (see also Ref. 17).

Later,[18] a somewhat different model (sine-Gordon equations) was used for semiclassical quantization of small-amplitude nonlinear oscillations localized near an impurity for a fixed sign of anharmonisms and for a certain sign of the defect, and a hypothesis concerning the nature of stability for local modes of various types was formulated. Finally, the interaction of a soliton with an impurity was considered in Ref. 19 in the model described by a nonlinear Schrödinger equation with a δ-shaped potential simulating the defect.

Here we will analyze excitations localized near point defects of various signs by using a one-dimensional nonlinear Schrödinger equation (NSE) with an arbitrary sign of anharmonisms and carry out the semiclassical quantization of all types of obtained solutions. It will be shown that the result can be interpreted in terms of quasiparticles interacting with one another and with a defect.

Following the technique described in Ref. 20, we shall carry out a stability test for the obtained soliton solutions and show that the presence of an attracting impurity is a factor stabilizing a soliton. In this case, a soliton exists and is stable both for attraction between quasiparticles, and for their re-

pulsion. In the former case (attraction), the vibrational mode of the soliton center of gravity relative to an impurity is present in the spectrum of small excitations of the soliton. In the latter case (repulsion), such an ''intrinsic mode'' does not exist, and we have only the continuous excitation spectrum corresponding to free quasiparticles.

A repulsive impurity does not disturb a soliton self-trapped due to attraction between quasiparticles, but only deforms and repels it. This process is described by a linear mode of the unstable soliton.

Thus, we shall carry out a complete analysis of stability of a soliton localized at a defect for an arbitrary type of interaction of quasiparticles with one another and with an impurity.

The application of our results is not limited to the theory of anharmonic crystals since NSE with attraction and repulsion are widely used in the theory of magnetically ordered media, nonlinear optics, dynamics of superfluid liquid helium, etc.

1. SOLITON SOLUTIONS OF NONLINEAR SCHRÖDINGER EQUATION IN THE PRESENCE OF IMPURITY

In the theory of a crystal lattice, the term ''local defect'' is applied to a defect whose size is of the order of atomic spacing. In an analysis of soliton solutions whose size is determined by the soliton frequency and can vary over a wide range, it is natural to apply the term local (or point) defect to a perturbation of the characteristics of the medium, which is concentrated over distances much smaller than the soliton width.

In the presence of a point defect, the NSE for the field variable u has the form

$$i\partial u/\partial t+\partial^2 u/\partial z^2-\omega_0 u+\beta u|u|^2=Q\delta(z)u, \tag{1.1}$$

where β is the interaction constant for elementary excitations ($\beta>0$ corresponds to their mutual attraction and $\beta<0$ to repulsion), ω_0 is the minimum frequency of elementary excitations in the linear system, and Q the characteristic of the magnitude of the defect (its ''intensity''). For $Q>0$, elementary excitations are ''repelled'' by a defect, while for $Q<0$ they are effectively attracted to it.

In the linear limit for $Q<0$, vibrations localized at an impurity atom are present in the system. The frequency of these vibrations $\omega_l=\omega_0-Q^2/4$. For $Q>0$, such local vibrations are absent.

The equation of motion (1.1) is the Euler equation for the Lagrangian with the following density:

$$L=\sqrt{2}[u^*\partial u/\partial t-u\partial u^*/\partial t]-|\partial u/\partial z|^2-\omega_0|u|^2 +(\beta/2)|u|^4-Q\delta(z)|u|^2. \tag{1.2}$$

The solution of Eq. (1.1) is reduced to the solution of the homogeneous equation

$$i\partial u/\partial t+\partial^2 u/\partial z^2-\omega_0 u+\beta u|u|^2=0 \tag{1.3}$$

in the regions $z>0$ and $z<0$ with the following boundary condition for $z=0$:

$$u|_{+0}=u|_{-0}, \tag{1.4}$$

$$\partial u/\partial z|_{+0}=\partial u/\partial z|_{-0}+Qu|_0. \tag{1.5}$$

We will seek steady-state solutions of Eq. (1.3) in the form

$$u(z,t)=u(z)\exp(-i\omega t), \tag{1.6}$$

where $u(z)\to 0$ for $|z|\to\infty$. As a result, for $\beta>0$ we obtain the following expression for the solution satisfying the boundary conditions:

$$\tilde{u}(z,t)=(2/\beta)^{1/2}\varepsilon\ \cosh^{-1}\{\varepsilon(|z|-z_0)\}\exp(-i\omega t), \tag{1.7}$$

where the parameter $\varepsilon\equiv(\omega_0-\omega)^{1/2}$ characterizes the excitation frequency, while the parameters ε and z_0 are connected through the relation following from the boundary condition:

$$2\varepsilon\ \tanh(\varepsilon z_0)=Q. \tag{1.8}$$

It can be seen from this relation that $\mathrm{sgn}(z_0)=\mathrm{sgn}\,Q$, and the maximum possible frequency of the solution with any sign of Q coincides with the frequency of local vibrations in the corresponding linear system:

$$\omega_l=\omega_0-Q^2/4, \tag{1.9}$$

and the interval of admissible frequencies is not bounded from below.

In the case of negative values of the parameter β, the solution satisfying the boundary conditions has the form

$$\tilde{u}(z,t)=(2/|\beta|)^{1/2}\varepsilon\ \sinh^{-1}\{\varepsilon(|z|-z_0)\}\exp(-i\omega t). \tag{1.10}$$

In this case, the quantity z_0 can assume only negative values, and the relation between the parameters ε and z_0 now has the form

$$2\varepsilon\ \coth(\varepsilon z_0)=Q. \tag{1.11}$$

Thus, the quantity Q for $\beta<0$ can only be negative, i.e., the bound state localized at an impurity exists only in the case of an attracting defect.

The interval of admissible frequencies now has the upper and lower boundaries: the minimum value corresponds to the frequency ω_l of local vibrations of the linear system, while the maximum value corresponds to the boundary ω_0 of the linear wave spectrum.

Thus, nonlinear localized states exist for the following relations between the parameters β and Q: (1) $\beta>0$, $Q<0$; (2) $\beta>0$, $Q>0$, and (3) $\beta<0$, $Q<0$. Let us consider the structure of these solutions in these three cases in greater detail.

(1) For $\beta>0$, $Q<0$, the maximum of the vibration amplitude is at the point of location of the impurity ($z_0<0$), and the solution has the form presented in inset *1* to Fig. 1a. In the small-amplitude limit, when $\omega_l-\omega\ll\omega_l$, the parameter z_0 tends to infinity [$z_0\approx -Q^{-1}\ \ln(\omega_l-\omega)$], and the amplitude of a local excitation depends on frequency according to the law typical of solitons:

$$u(z=0)|_{\omega\to\omega_l}\approx(2/\beta)^{1/2}(\omega_l-\omega)^{1/2}. \tag{1.12}$$

For $\omega=\omega_l$, the nonlinear local mode is transformed into conventional vibrations in the linear theory.

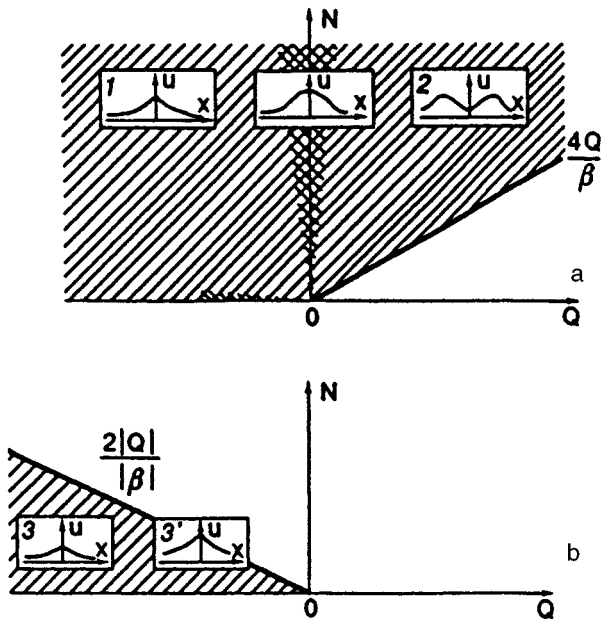

FIG. 1. Regions of existence of nonlinear localized states (hatched) for different types of nonlinearity: $\beta>0$ (a) and $\beta<0$ (b). Double hatching marks the regions of applicability of perturbation theory in the stability test for solutions. The insets show characteristic profile of the envelope of localized soliton states.

In the opposite limiting case $\omega\to-\infty$, the parameter z_0 tends to zero ($z_0\approx -Q/\omega$), and the solution becomes singular.

(2) For $\beta>0$, $Q>0$, the vibration amplitude maximum does not coincide with the point of location of the defect, and the local excitation is a bound state of two solitons located symmetrically on both sides of the defect with the centers at points $\mp z_0$ (see inset *2* to Fig. 1a). In this case, the limit $\omega\to-\infty$ virtually coincides with the previous case, but the form of the solution at the maximum possible frequency ω_l is essentially different. For $\omega_l-\omega\ll\omega_l$, the separation between the bound solitons tends to infinity: $2z_0\approx -2Q^{-1}\ln(\omega_l-\omega)$, and the vibrational amplitude of the defect tends to zero in accordance with (1.12). However, the amplitude of solitons tends to a finite quantity

$$A|_{\omega=\omega_l}=(2/\beta)^{1/2}Q/2, \tag{1.13}$$

and this limit is not a small-amplitude limit.

(3) In the case $\beta<0$, $Q<0$, the localized excitation profile has approximately the same shape as for $\beta>0$, $Q<0$ (case (1)), and the maximum of the vibrational amplitude is at the point of location of the defect (see inset *3* to Fig. 1b), but the frequency range of the local mode is completely different. In the case (1), the frequency changes in the interval $-\infty<\omega<\omega_l$, while in the present case $\omega_l<\omega<\omega_0$.

The linear limit corresponds to the transition $\omega\to\omega_l$, for which the parameter z_0 tends to infinity as in the case (1): $z_0\approx -Q^{-1}\ln(\omega-\omega_l)$, and the amplitude tends to zero in analogy with (1.12):

$$u(z=0)|_{\omega\to\omega_l}\approx(2/\beta)^{1/2}(\omega-\omega_l)^{1/2}. \tag{1.14}$$

The limiting transition to the frequency value $\omega=\omega_0$ is more interesting. In this case, $\varepsilon\to0$, and relation (1.11) implies that the parameter z_0 tends to a finite value $z_0=2/Q$, while the solution (1.10) is transformed into a function with power asymptotic forms at infinity, i.e., into an algebraic soliton (see inset $3'$ to Fig. 1b)

$$\tilde{u}(z,t)=(2/|\beta|)^{1/2}\{|z|+2/|Q|\}^{-1}\exp(-i\omega t) \tag{1.15}$$

with the impurity vibration amplitude

$$u(z=0)|_{\omega\to\omega_0}=(2/|\beta|)^{1/2}|Q|/2. \tag{1.16}$$

It is well known[17] that the possibility of existence of power solitons is associated with the inclusion of competing nonlinearities in the evolution equations or with the presence of many-particle interactions of various types. For example, the inclusion of paired repulsion of particles and their three-particle attraction (i.e., of the terms of the $u|u|^4$ type in Eq. (1.1) with $\beta<0$) leads to the formation of algebraic solitons at the edge of the linear wave spectrum. Such solitons are unstable.[21] In the case of an impurity under consideration, the situation is similar in many respects: we have two types of interactions, viz., the paired interaction between particles described by the term $\beta u|u|^2$, and the one-particle interaction of elementary excitations with an inhomogeneity. In this case, paired solitons exist for paired repulsion of quasiparticles and their attraction to the defect. It will be shown below, however, that these solitons are stable.

In order to clarify the physical origin of the states considered above, we will carry out their semiclassical quantization.

2. INTEGRALS OF MOTION AND SEMICLASSICAL QUANTIZATION OF SOLITONS

Equation (1.1) describes the dynamics of a conservative system, and hence possesses an obvious integral of motion, viz., the total energy

$$E=\int_{-\infty}^{+\infty}\varepsilon(z)dz, \tag{2.1}$$

whose density has the form

$$\varepsilon(z)=|\partial u/\partial z|^2+\omega_0|u|^2-(\beta/2)|u|^4+Q\,\delta(z)|u|^2. \tag{2.2}$$

Moreover, it has an additional integral of motion, viz., the total number of elementary excitations, of field quanta[15]

$$N=\int_{-\infty}^{+\infty}n(z)dz=\int_{-\infty}^{+\infty}|u|^2dz, \tag{2.3}$$

where $n(z)$ is the number density of quasiparticles.

Till now, we characterized a soliton solution by its frequency ω. In order to clarify the quantum-mechanical nature of the soliton, it is convenient to go over from frequency as a dynamic characteristic to the number N of excitations bound in the soliton.

Let us first consider the case when $\beta>0$. We express the integrals of motion E and N in terms of frequency (or the parameter ε associated with it). Using the explicit form of

the solution (1.7) in formulas (2.1)–(2.3) and taking into account the dependence $z_0(\varepsilon)$ [see (1.8)], we obtain the following relations:

$$E=\beta^{-1}[-4\varepsilon^3/3+4\varepsilon\omega_0+2Q\omega_0-Q^3/6], \tag{2.4}$$

$$N=4\beta^{-1}[\varepsilon+Q/2]. \tag{2.5}$$

It should be noted that for a small intensity Q of the defect and for small values of the parameter ε, expression (2.4) leads to the following relation for energy:

$$E=4\omega_0\beta^{-1}(\varepsilon+Q/2), \tag{2.6}$$

which is similar to the energy of a local vibration of a point isotopic impurity in a one-dimensional crystal (see Ref. 15).

For $\beta<0$, we substitute solution (1.10) and $z_0(\varepsilon)$ from relation (1.11) into formulas (2.1)–(2.3) and obtain the dependences $\mathbf{E}=(\omega)$ and $N=N(\omega)$ which are completely identical to formulas (2.4) and (2.5).

The positiveness of the integral of motion N implies that $\varepsilon>-Q/2$ for positive values of β, while the boundary condition (1.8) leads to a more stringent inequality determining the range of the solution:

$$\varepsilon>|Q|/2 \quad \text{for} \quad \beta>0. \tag{2.7}$$

For $\beta<0$ (when the solution exists only for $Q<0$), the positive value of N [or relation (1.11)] means that the parameter ε must satisfy the following condition:

$$0<\varepsilon<|Q|/2 \quad \text{for} \quad \beta<0. \tag{2.8}$$

The critical value of $\varepsilon=|Q|/2$ corresponds to the frequency ω_l of the local linear mode.

Using relations (2.5) and (2.7), we find that all positive values of N are admissible for positive β and $Q<0$, while for $Q>0$ the following constraint is imposed on N:

$$N>4Q/\beta \quad \text{for} \quad Q>0,\ \beta>0. \tag{2.9}$$

The value $N_*=2Q/\beta$ corresponds to the frequency ω_l at which a local vibration splits into two solitons separated by infinitely large distances from the impurity and incorporating $2Q/\beta$ bound elementary excitations in each. For $Q<0$, the minimum value of N is zero, which corresponds to zero amplitude of the solution at the frequency ω_l. In Fig. 1a, the region of existence of the solitons in the plane of parameters (N,Q) for $\beta>0$ is hatched.

In the case of negative β, relations (2.5) and (2.8) lead to the following constraint on possible values of N:

$$N<2|Q|/|\beta| \quad \text{for} \quad Q<0,\ \beta<0. \tag{2.10}$$

In this case, the critical value $N_0=2|Q|/|\beta|$ corresponds to a power soliton at the frequency ω_0. The minimum value $N=0$ is attained at the frequency ω_l. The region of admissible values of parameters (N,Q) for $\beta<0$ is hatched.

Using expressions (2.4) and (2.5) and eliminating the parameter ω, we find the following relation between the total energy and the number of bound excitations:

$$\begin{aligned}E(N)&=N\omega_0-NQ^2/4-\beta^2N^3/48+\beta QN^2/8\\&=N\omega_l-\beta^2N^3/48+\beta QN^2/8.\end{aligned} \tag{2.11}$$

For $\beta>0$, the interpretation of the obtained expression is obvious. The first term in (2.11) describes the energy of N noninteracting elementary excitations and corresponds to the description of the system in the linear approximation. In this case, the intrinsic energy of these excitations changes as a result of their interaction with the impurity: $\omega_0\to\omega_l=\omega_0-Q^2/4$. The frequency ω_l corresponds to the frequency of linear local impurity vibrations. The second terms in (2.11) describes the energy of interaction of elementary excitations in a soliton and has the same form as in the case of solitons in a homogeneous medium. Finally, the last term describes the interaction of bound particles through an impurity. It should be noted that the sign of the defect (the sign of Q) determines only the last term: for $Q<0$, the energy decreases, i.e., the impurity ''attracts'' the particles and the soliton as a whole, while for $Q>0$ the presence of impurity increases the soliton energy, i.e., the impurity ''repels'' the soliton.

Expression (2.11) implies that the energy at the boundary of the region of existence of nonlinear localized vibrations is $E=2(N_0\omega_0-\beta^2N_0^3/48)$ for $\beta>0$, with $N_0=2Q/\beta$, i.e., is equal to doubled energy of a soliton with N_0 bound elementary excitations. It is interesting to note that, for $\beta<0$, the relation $E=N_0\omega_0-\beta^2N_0^3/48$ coinciding with the expression for a soliton in a homogeneous medium is satisfied at the boundary of the region of existence of localized solutions (for $N_0=2|Q|/|\beta|$) for power solitons at the impurity. (For ordinary power solitons, we have $E=N\omega_0$, i.e., the binding energy of quasiparticles vanishes.)[17]

Expression (2.11) also shows that the energy per elementary excitation in a local state is lower than the energy of a free quasiparticle:

$$E/N=\omega_0-(Q/2-\beta N/8)^2-\beta^2N^2/192<\omega_0. \tag{2.12}$$

This relation makes it possible to interpret a soliton solution as a bound state of a large number of elementary excitations.[17]

Differentiating expression (2.11) with respect to N and using relation (2.5) for $N(\varepsilon)$, we can easily verify the fulfillment of the conventional relation

$$\partial E/\partial N=\omega, \tag{2.13}$$

which takes place for solitons in conservative nonlinear systems with the quantity N as an integral of motion.

Thus, the frequency of a nonlinear local vibration plays the role of chemical potential for elementary excitations bound in it.

We shall use relation (2.11) to write the explicit expression for frequency ω:

$$\omega=\partial E/\partial N=\omega_0-(\beta^2/16)(N-2Q/\beta)^2. \tag{2.14}$$

For $Q=0$, this expression is identical to the dependence $\omega=\omega(N)$ for a soliton in a homogeneous system.

Since the inequality $\partial^2E/\partial N^2=\partial\omega/\partial N<0$ usually defines the region of stability for soliton solutions, we shall calculate the derivative $\partial\omega/\partial N$. According to (2.14), in our case we have

$$\partial\omega/\partial N=-(\beta^2/8)(N-2Q/\beta). \tag{2.15}$$

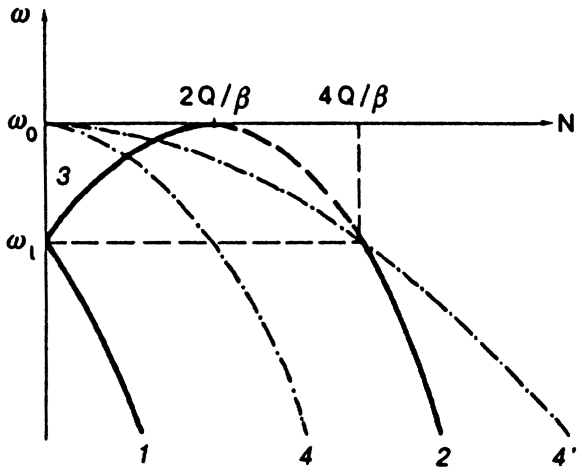

FIG. 2. Dependences $\omega=\omega(N)$ for various types of nonlinear localized states: $\beta>0$, $Q<0$ (curve *1*), $\beta>0$, $Q>0$ (curve *2*), and $\beta<0$, $Q<0$ (curve *3*). The curves *4* and *4′* describe the dependences $\omega=\omega(N)$ for a soliton and two noninteracting solitons in an ideal system free of defects.

It hence follows that the inequality

$$\partial\omega/\partial N=\partial^2E/\partial N^2<0 \quad \text{for} \quad \beta>0, \tag{2.16a}$$

holds for positive values of the parameter β in the entire region of existence of nonlinear localized states, while in the case of negative values of β, the opposite inequality holds:

$$\partial\omega/\partial N=\partial^2E/\partial N^2>0 \quad \text{for} \quad \beta<0. \tag{2.16b}$$

Usually (in spatially-homogeneous nonlinear systems), dynamic solitons are modulation-stable for the negative sign of the derivative $\partial\omega/\partial N$ and unstable for the positive sign of the derivative.[17,20,22] It will be shown below that for spatially-heterogeneous systems with defects, the situation is different: a soliton solution localized at a defect is stable only for $Q<0$ (for any sign of β) and unstable for $Q>0$.

The dependence $\omega=\omega(N)$ (2.14) for various signs of Q and β is shown in Fig. 2. Curve *1* corresponds to case (1) ($\beta>0$,$Q<0$), curve *2* describes the $\omega=\omega(N)$ dependence in case (2) ($\beta>0$, $Q>0$), and curve *3* corresponds to negative values of β [case (3)].

The dot-and-dash curves in same figure show the $\omega=\omega(N)$ dependences for a solitary soliton in an ideal medium (curve *4*):

$$\omega=\omega_0-\beta^2N^2/16, \tag{2.17a}$$

and for two noninteracting solitons separated by an infinitely large distance from one another (curve *4′*):

$$\omega=\omega_0-(\beta^2/16)(N/2)^2. \tag{2.17b}$$

At the point $\omega=\omega_l$, $N_*=4Q/\beta$, curves *2* and *4′* intersect, i.e., bifurcation of the $\omega=\omega(N)$ dependence is observed: for $N=N_*$, the dependence *2* for a solution localized near the impurity splits from curve *4′* for two noninteracting solitons, i.e., two solitons are ''coupled'' through the defect.

3. STABILITY OF NONLINEAR IMPURITY STATES

Let us analyze the stability of the obtained solutions relative to small perturbations of amplitude and phase. We shall solve this problem by following the algorithm proposed in Ref. 20.

Representing the solution of Eq. (1.1) in the form

$$u(z,t)=\tilde{u}(z,t)+\theta(z,t)=u(z)\exp(-i\omega t) + v(z,t)\exp(-i\omega t), \tag{3.1}$$

where $\tilde{u}(z,t)$ is the solution of Eq. (1.1) for a stationary soliton and $|\theta(z,t)|\ll|\tilde{u}(z,t)|$, we linearize Eq. (1.1) in small corrections $v(z,t)$ and obtain the following equation for $v(z,t)$:

$$i\partial v(z,t)/\partial t+\partial^2v(z,t)/\partial z^2-\varepsilon^2v(z,t)+2\beta v(z,t)u^2(z) + \beta v^*(z,t)u^2(z)=Q\delta(z)v(z,t). \tag{3.2}$$

Writing the solution of Eq. (3.2) in the form

$$v(z,t)=(A(z)+iB(z))\exp(\Omega t), \tag{3.3}$$

we obtain the following system of two ordinary linear differential equations for the functions A and B:

$$\mathbf{L}_0B=\Omega A,$$
$$\mathbf{L}_1A=-\Omega B, \tag{3.4}$$

where the operators $\mathbf{L}_0$ and $\mathbf{L}_1$ are defined as

$$\mathbf{L}_0=-d^2/dz^2+\varepsilon^2-\beta u^2(z)+Q\delta(z), \tag{3.5}$$

$$\mathbf{L}_1=-d^2/dz^2+\varepsilon^2-3\beta u^2(z)+Q\delta(z), \tag{3.6}$$

and the function $u(z)$ (in the notation introduced above) must satisfy the equation

$$\mathbf{L}_0u(z)=0. \tag{3.7}$$

Eliminating the function B from the system of equations (3.4), we arrive at the following eigenvalue problem:

$$\mathbf{L}_0\mathbf{L}_1A=-\Omega^2A. \tag{3.8}$$

It should be noted that although the operator L_0L_1 is not Hermitian, the real-valuedness of its eigenvalues Ω^2 can be proved easily by reducing the initial eigenvalue problem (3.4) to an equivalent problem for the Hermitian operator $\mathbf{L}^-\mathbf{L}_1\mathbf{L}^+W=-\Omega^2W$, where $\mathbf{L}^\pm=\pm d/dz+(du/dz)/u$, $W=\mathbf{L}^-B$ and $\mathbf{L}_0=\mathbf{L}^+\mathbf{L}^-$.

Since the function u does not vanish anywhere, there exists a positive-definite operator $\mathbf{L}_0^{-1}$ inverse to operator $\mathbf{L}_0$ on the subspace of functions orthogonal to u. Consequently, we can apply the variational principle to Eq. (3.8), according to which the minimum eigenvalue $-\Omega_0^2$ is given by

$$-\Omega_0^2=\min[\langle\varphi|\mathbf{L}_1|\varphi\rangle/\langle\varphi|\mathbf{L}_0^{-1}|\varphi\rangle], \quad \langle u|\varphi\rangle=0. \tag{3.9}$$

In this case, the problem can be reduced to an analysis of the conditional minimum of the functional $F=\langle\varphi|\mathbf{L}_1|\varphi\rangle$.

Using the Lagrangian method of undeterminate multipliers, we can obtain the following equation for the function ψ minimizing the functional F for $\langle u|\psi\rangle=0$:

$$\mathbf{L}_1\psi=\lambda\psi+\alpha u. \tag{3.10}$$

The minimum value of F is determined by the minimum value of λ for which Eq. (3.10) has a solution. Taking into account the condition $\langle u|\psi\rangle=0$, we obtain from (3.10) the following equation for λ (see Ref. 20):

$$\alpha\sum_{n=1}^{\infty} C_n^2/(\lambda_n-\lambda)=\alpha f(\lambda)=0, \tag{3.11}$$

where $C_n=\langle u_0|\psi_n\rangle$, and ψ_n and λ_n are the eigenfunctions and the eigenvalues of the operator $\mathbf{L}_1$, respectively.

Let us first analyze the stability of solutions for a positive parameter β (cases (1) and (2)).

In the absence of a defect, the stability test for solution (1.7) corresponds completely to the scheme described in Ref. 20. In this case, the operator $\mathbf{L}_1$ is defined as

$$\mathbf{L}_1^{(0)}=-d^2/dz^2+\varepsilon^2-6\varepsilon^2\ \cosh^{-2}(\varepsilon z). \tag{3.12}$$

The eigenfunction of the ground state of this operator and the corresponding eigenvalue have the form

$$\psi_1^{(0)}=(3\varepsilon)^{1/2}\ \cosh^{-2}(\varepsilon z)/2,\quad \lambda_1^{(0)}=-3\varepsilon^2, \tag{3.13}$$

while the eigenfunction and the eigenvalue of the next state are given by

$$\psi_2^{(0)}=(3\varepsilon/2)^{1/2}\ \sinh(\varepsilon z)\cosh^{-2}(\varepsilon z),\quad \lambda_2^{(0)}=0. \tag{3.14}$$

It is well known that, in the absence of impurity, the soliton solution of the NSE is stable. The presence of a defect complicates the analysis of the stability of the solution since in this case the operators $\mathbf{L}_0$ and $\mathbf{L}_1$ have a more complex form than in the case when $Q=0$. Let us prove, however, that for values of $\varepsilon|z_0|\ll 1$, the operator $\mathbf{L}_1$ has the form $\mathbf{L}_1=\mathbf{L}_1^{(0)}+\hat{\eta}$, where $\hat{\eta}$ is a perturbation linear in small corrections. In this case, we can take into account the variation of eigenfunctions and eigenvalues of the operator $\mathbf{L}_1^{(0)}$ in perturbation theory.

If the inequality $\varepsilon|z_0|\ll 1$ is satisfied, it follows from the boundary condition (1.8) that

$$\varepsilon z_0\approx Q/(2\varepsilon),\quad \varepsilon\gg|Q|/2. \tag{3.15}$$

In this case, formula (2.5) leads to the relation between the parameters N and Q, which determines the region on the plane (N,Q), where the solution of the above-formulated problem in the perturbation theory exists:

$$N\gg 2|Q|/\beta. \tag{3.16}$$

This region is shown by double hatching in Fig. 1a (the sector near the N-axis). It should be noted that the smallness of the soliton amplitude is generally not required, and the role of small perturbation is played by the defect whose ''intensity'' plays the role of the expansion parameter $Q/(2\varepsilon)$.

Expanding solution (1.7) into a power series in the small parameter εz_0 and taking into account dependence (3.15) in the expansion, we obtain the following relation accurate to within first-order terms in $Q/(2\varepsilon)$:

$$u(z)=(2\beta)^{1/2}\varepsilon\ \cosh^{-1}(\varepsilon z)\{1+[Q/(2\varepsilon)]\tanh(\varepsilon|z|)\}. \tag{3.17}$$

Substituting the expression obtained for $u(z)$ into formula (3.6) and taking into account the terms of the order not higher that the first power of $Q/(2\varepsilon)$, we obtain the expression for the operator $\mathbf{L}_1$:

$$\begin{aligned}\mathbf{L}_1&=-d^2/dz^2+\varepsilon^2-6\varepsilon^2\ \cosh^{-2}(\varepsilon z)+[Q/(2\varepsilon)]\\&\quad\times\{-12\varepsilon^2\ \sinh(\varepsilon|z|)\cosh^{-3}(\varepsilon z)+2\varepsilon\,\delta(z)\}\\&\equiv\mathbf{L}_1^{(0)}+\hat{\eta},\end{aligned} \tag{3.18}$$

where $\overline{\eta}\propto Q/(2\varepsilon)$ is the perturbation of the operator $\mathbf{L}_1^{(0)}$.

In perturbation theory, we obtain the following corrections to eigenvalues of the operator $\mathbf{L}_1^{(0)}$:

$$\lambda_n^{(1)}=\eta_{nn}=\langle\psi_n^{(0)}|\,\hat{\eta}\,|\psi_n^{(0)}\rangle=\int_{-\infty}^{+\infty}dz\,\psi_n^{(0)*}\hat{\eta}\psi_n^{(0)}. \tag{3.19}$$

In this case, the eigenfunctions of the operator $\mathbf{L}_1$ assume the form $\psi_n=\psi_n^{(0)}+\zeta(z)$, where $\zeta(z)\sim Q/(2\varepsilon)$ is a correction of the same parity as the function $\psi_n^{(0)}$.

The correction to the eigenvalue corresponding to the ground state of the operator $\mathbf{L}_1^{(0)}$ has the form

$$\begin{aligned}\lambda_1^{(1)}&=Q/(2\varepsilon)(3\varepsilon/4)\int_{-\infty}^{+\infty}dz\ \cosh^{-2}(\varepsilon z)\\&\quad\times\{-12\varepsilon^2\ \sinh(\varepsilon|\hat{z}|)\cosh^{-3}(\varepsilon z)\\&\quad+2\varepsilon\,\delta(z)\}\cosh^{-2}(\varepsilon z)\\&=-(3\varepsilon/4)Q,\end{aligned} \tag{3.20}$$

while the correction to the eigenvalue $\lambda_2^{(0)}$ of the next level is given by

$$\begin{aligned}\lambda_2^{(1)}&=Q/(2\varepsilon)(3\varepsilon/2)\int_{-\infty}^{+\infty}dz\ \sinh(\varepsilon z)\cosh^{-2}(\varepsilon z)\\&\quad\times\{-12\varepsilon^2\ \sinh(\varepsilon|z|)\cosh^{-3}(\varepsilon z)\\&\quad+2\varepsilon\,\delta(z)\}\sinh(\varepsilon z)\cosh^{-2}(\varepsilon z)\\&=-(3\varepsilon/2)Q.\end{aligned} \tag{3.21}$$

Thus, taking into account the expressions for $\lambda_1^{(0)}$ and $\lambda_2^{(0)}$, we obtain approximate (to within Q/ε) expressions for eigenvalues of the two lowest states of the operator $\mathbf{L}_1$:

$$\lambda_1=-3\varepsilon^2-3\varepsilon Q/4, \tag{3.22a}$$

$$\lambda_2=-3\varepsilon Q/2. \tag{3.22b}$$

It can be seen that $\lambda_1<\lambda_1^{(0)}<0$ and $\lambda_2<0$ for $Q>0$; $\lambda_1^{(0)}<\lambda_1<0$ and $\lambda_2>0$ for $Q<0$. In view of different signs of the eigenvalue λ_2 for $Q>0$ and $Q<0$, these cases must be considered separately.

The case of $\beta>0$, $Q>0$. For $\alpha=0$ (see Eq. (3.10)), ψ is an eigenfunction of the operator $\mathbf{L}_1$, while λ coincides with one of its eigenvalues. Since the eigenfunction ψ_1 cannot be orthogonal to u (see Ref. 20), and $\langle u|\psi_2\rangle=0$, the minimum eigenvalue $-\Omega_0^2$ is determined by the value λ_2. Thus, the conditional minimum of the functional F is equal to $\lambda_2=-3\varepsilon Q/2<0$, and hence Ω is real-valued.

Thus, positive values of Q correspond to exponentially increasing perturbations, and the soliton solution is unstable. Instability is manifested in an exponential increase in the

spatially antisymmetric correction (the symmetric function ψ_1 corresponds to the principal eigenvalue λ_1). Soliton dynamics in this case can be presented as follows: quasiparticles are ''pumped'' from one half-space to another. For large values of time, we cannot solve the problem, but complete ''pumping'' of particles to one half-space will take place; the formed soliton ''repelled'' by the defect will go to infinity.

The solution, taking into account small corrections to the form of a soliton for $Q>0$, is given by

$$u(z,t)=u_0(z,t)+v(z,t)\exp(-i\omega t)\cong\left[\left(\frac{2}{\beta}\right)^{1/2}\varepsilon\ \cosh^{-1}(\varepsilon z)+\frac{Q}{2\varepsilon}\left(\frac{2}{\beta}\right)^{1/2}\varepsilon\ \sinh(\varepsilon|z|)\cosh^{-2}(\varepsilon z)\right]\exp(-i\omega t)+\xi\left(\frac{3\varepsilon}{2}\right)^{1/2}\sinh(\varepsilon z)\cosh^{-2}(\varepsilon z)\exp(\Omega t)\times\exp(-i\omega t)$$
$$\cong\left(\frac{2}{\beta}\right)^{1/2}\varepsilon\ \cosh^{-1}\left\{\varepsilon\left[z-\mathrm{sgn}(z)\ \frac{Q}{2\varepsilon^2}-\frac{\xi}{2\varepsilon}\left(\frac{3\beta}{\varepsilon}\right)^{1/2}\times\exp(\Omega t)\right]\right\}\exp(-i\omega t), \tag{3.23}$$

where $\xi\ll 1$. (Here we have used the main approximation in expression (3.3) for the small correction $v(z,t)$: $A\approx\xi\psi_2^{(0)}$, $B\simeq 0$.)

Thus, in this approximation the amplitude of the solution does not change, but a synchronous shift towards one of the centers of two solitons located on different sides of the defect and associated with it takes place:

$$z_0^{\pm}\cong\mathrm{sgn}(z)Q/(2\varepsilon^2)+(\xi/2\varepsilon)(3\beta/\varepsilon)^{1/2}\exp(\Omega t). \tag{3.24}$$

In order to find the increment of this shift instability Ω, we will use formula (3.8) ''encased'' by the antisymmetric function ψ_2 corresponding to the second level of the operator $\mathbf{L}_1$. In the main order in the small parameter $Q/(2\varepsilon)$, expression (3.9) assumes the form

$$\Omega^2\cong-\langle\psi_2^{(0)}|\hat{\eta}|\psi_2^{(0)}\rangle/\langle\psi_2^{(0)}|\mathbf{L}_0^{(0)-1}|\psi_2^{(0)}\rangle=-\lambda_2/\langle\psi_2^{(0)}|\mathbf{L}_0^{(0)-1}|\psi_2^{(0)}\rangle, \tag{3.25}$$

where the operator $\mathbf{L}_0^{(0)}$ is defined by expression (3.5), and the function $\psi_2^{(0)}$ is defined by (3.14). It can easily be verified that

$$\mathbf{L}_0^{(0)}[z/\cosh(\varepsilon z)]=2\varepsilon\ \sinh(\varepsilon z)/\cosh^2(\varepsilon z), \tag{3.26}$$

and hence

$$\mathbf{L}_0^{(0)-1}\psi_2^{(0)}=[3/(8\varepsilon)]^{1/2}z/\cosh(\varepsilon z). \tag{3.27}$$

Thus, the denominator in formula (3.25) is equal to $3/(4\varepsilon^2)$, and the increment of instability is given by

$$\Omega\cong(2Q\varepsilon^3)^{1/2}. \tag{3.28}$$

The case of $\beta>0$, $Q<0$. Since $\lambda_2>0$ in this case, the conditional minimum of the functional F is positive for $\alpha=0$. For a nonzero Lagrangian multiplier α, the conditional minimum of the functional F is determined by the smallest root of Eq. (3.11). We can prove[20] that in this case (as well as for $Q=0$), the sign of $\lambda_{\min}$ is determined by the sign of the quantity $f(\lambda=0)$: we have $\lambda_{\min}\geqslant 0$ for $f(0)\leqslant 0$ and a negative $\lambda_{\min}$ for $f(0)>0$.

For $\lambda=0$, formula (3.11) can be easily written in the form $f(0)=\langle u|\mathbf{L}_1^{-1}|u\rangle$. In order to calculate the value of this quantity, it is sufficient to differentiate Eq. (3.7) with respect to ε^2 and, using the form of the operators $\mathbf{L}_0$ and $\mathbf{L}_1$ (see (3.5) and (3.6)), to verify the relation $\mathbf{L}_1\partial u/\partial\varepsilon^2+u=0$. This gives

$$f(0)=\langle u|\mathbf{L}_1^{-1}|u\rangle=-\langle u|\partial u/\partial\varepsilon^2\rangle=-(1/2)\partial/\partial\varepsilon^2\langle u|u\rangle=-(1/2)\partial N/\partial\varepsilon^2=(1/2)\partial N/\partial\omega, \tag{3.29}$$

where N is the number of quasiparticles defined by formula (2.5).

Thus, the sign of the conditional minimum of the functional F for $\alpha\neq 0$ is determined by the sign of the derivative $\partial\omega/\partial N$ (i.e., by the sign of the quantity $\partial^2E/\partial N^2$: the conditional minimum of the functional F is positive for $\partial\omega/\partial N\leqslant 0$, and according to (3.9), $\Omega^2<0$.

It was proved earlier (see (2.16a)) that, in the case of negative Q and positive β, the derivative $\partial\omega/\partial N<0$. This indicates the absence of exponentially increasing perturbations (Ω is a purely imaginary quantity) and the stability of the solution in the approximation linear in perturbation. Thus, antisymmetric corrections to the solution $\tilde{u}(z,t)$ describe small oscillations of a soliton relative to the impurity.

Solution (3.1) for $Q<0$ and $\beta>0$ can be reduced to the form

$$u(z,t)\cong(2/\beta)^{1/2}\varepsilon\ \cosh^{-1}\{\varepsilon[z-\mathrm{sgn}(z)Q/(2\varepsilon^2)-(\xi/2\varepsilon)(3\beta/\varepsilon)^{1/2}\cos(\nu t)]\}\exp(-i\omega t), \tag{3.30}$$

where $\xi\ll 1$ is a small (arbitrary) amplitude of oscillations of the center of the soliton relative to the region of localization of the impurity, and $\nu\equiv-i\Omega$ is the frequency of these oscillations.

In order to find the frequency ν, we use formula (3.25), where $\lambda_2=3\varepsilon|Q|/2>0$ in our case [see (3.22b)]. Thus, the frequency of oscillations is given by

$$\nu=(2|Q|\varepsilon^3)^{1/2}. \tag{3.31}$$

It should be noted that in the case of a ''smeared'' impurity, when the region of its localization is much larger than the soliton width, the oscillatory frequency of the soliton in the external potential field $U(z)$ simulating the impurity ($Q=\int U(z)dz$) is connected with the intensity Q of the potential through the relation

$$\nu=(|Q|/L^3)^{1/2}, \tag{3.32}$$

where L is the characteristic spatial size of the inhomogeneity.[17] This is in qualitative agreement with the result (3.31) obtained for a δ-shaped impurity, but the role of characteristic linear size is now played by the size L of the defect instead of the soliton width $1/\varepsilon$. It should be recalled that our analysis is valid only when the inequality (3.16) is satisfied.

In Ref. 18, another limiting case was analyzed in detail in the case of the sine-Gordon equation for an attractive impurity ($Q<0$): $\varepsilon-|Q|/2\ll|Q|/2$, i.e., $\omega_l-\omega\ll\omega_0-\omega_l$. It was assumed that $|Q|\ll 1$. It can be easily seen from relation (2.5) that the following limitations are imposed on the values of parameters N and Q: $N\ll 2|Q|/\beta$, $|Q|\ll 1$ (the sector with double hatching near the negative semiaxis Q in Fig. 1a). It was shown in Ref. 18 that in this limiting case a soliton localized at the impurity is stable and performs small oscillations relative to the center of the impurity at a frequency

$$\nu\cong[3(\omega_{\max}-\omega)]^{1/2}. \tag{3.33}$$

Taking into account the results obtained by us and in Ref. 18, we can assume that nonlinear local excitations are stable for all values of $Q<0$ and $N>0$.

Let us go over to an analysis of stability of solution (1.10) describing a nonlinear excitation localized at the impurity in the case of negative β and Q.

Following the algorithm described above, we can show that for $\beta<0$ and $Q<0$, the operator $\mathbf{L}_1$ is positive definite. Let us first consider the operator $\mathbf{L}_0$. When $Q,\beta<0$, it assumes the following form [see (3.5)]:

$$\mathbf{L}_0=-d^2/dz^2+\varepsilon^2+|\beta|u^2(z)-|Q|\,\delta(z), \tag{3.34}$$

where $u(z)$ is defined by (1.10). Solution $u(z)$ is an eigenfunction of the ground state of the operator $\mathbf{L}_0$ with zero eigenvalue [see (3.7)]. Thus, the operator $\mathbf{L}_0$ is nonnegative. The potential energy corresponding to the operator $\mathbf{L}_0$ has the form

$$U_0(z)=\varepsilon^2+|\beta|u^2(z)-|Q|\,\delta(z). \tag{3.35}$$

It is significant that in contrast to the case when $\beta>0$ and $Q<0$, the correction to the δ-shaped potential is now positive. The potential well (3.35) contains the only discrete level corresponding to the ground state of the operator $\mathbf{L}_0$, while the next energy level coincides with the lower boundary of the continuous spectrum band.

The potential energy corresponding to the operator $\mathbf{L}_1$ now has the form [cf. (3.6)]

$$U_1(z)=\varepsilon^2+3|\beta|u^2(z)-|Q|\,\delta(z). \tag{3.36}$$

Thus, in contrast to case (1) with $\beta>0$ and $Q<0$, when the inequality

$$\int U_0(z)dz>\int U_1(z)dz,$$

holds, for $\beta<0$ we have

$$\int U_0(z)dz<\int U_1(z)dz. \tag{3.37}$$

Consequently, upon a transition from the operator $\mathbf{L}_0$ to the operator $\mathbf{L}_1$, the entire system of eigenvalues is shifted upwards, which indicates the absence of negative eigenvalues and a second discrete energy level for the operator $\mathbf{L}_1$. Hence we can draw a conclusion on the stability of the bound state for $\beta<0$ and $Q<0$ in the entire range of its existence and the absence of an intrinsic vibrational mode in this nonlinear localized excitation.

CONCLUSION

It has been proved that the states localized at an impurity in a nonlinear medium with point defects are possible for any sign of anharmonisms (the sign of β) in the case of attraction of quasiparticles to the defect ($Q<0$). In the case of mutual attraction between quasiparticles ($\beta>0$), a nonlinear excitation can be localized at the impurity even in the case of the repulsive nature of the defect ($Q>0$).

For $\beta>0$ (attraction between quasiparticles) and $Q<0$ (attractive impurity), a point defect plays the role of a potential well for a bound many-particle state, and soliton is localized near the defect and oscillates near its center at a frequency $(2\varepsilon^3|Q|)^{1/2}$. In this case, localized soliton solutions are stable.

For $\beta>0$ and $Q>0$, the soliton solution localized near a repulsive quasiparticle of the impurity is unstable. This instability is manifested in an exponential increase of antisymmetric corrections to the solution: quasiparticles are ''pumped'' from one half-space to another and form a soliton localized on one side of the impurity, which is repelled from it and goes to infinity.

In the case when $\beta<0$ (repulsion between quasiparticles), nonlinear local excitations are possible only for $Q<0$, and the state bound to the defect is stable.

This research was partly financed by the International Soros Program Supporting Education in Science (grant No. GSU052252) and by the International Science Foundation (grant No. U21200).

*E-mail: kovalev@ilt.kharkov.ua

[1] I. M. Lifshitz, Nuovo Cimento Suppl. **3**, 716 (1956).
[2] I. M. Lifshitz and A. M. Kosevich, Repts. Progr. Phys. **29**, 217 (1966).
[3] A. J. Sievers and S. Takeno, Phys. Rev. Lett. **61**, 970 (1988).
[4] S. Takeno and A. J. Sievers, Solid State Commun. **67**, 1023 (1988).
[5] V. M. Burlakov, S. A. Kiselev, and V. N. Pyrkov, Solid State Commun. **74**, 327 (1990).
[6] A. J. Sievers and S. Takeno, Phys. Rev. B **39**, 3374 (1989).
[7] J. B. Page, Phys. Rev. B **41**, 7835 (1990).
[8] S. R. Bickham and A. J. Sievers, Phys. Rev. B **43**, 2339 (1991).
[9] K. W. Sandusky, J. B. Page, and K. E. Schmidt, Phys. Rev. B **46**, 6161 (1992).
[10] S. A. Kiselev, S. R. Bickham, and A. J. Sievers, Phys. Lett. A **184**, 255 (1994).
[11] A. A. Ovchinnikov, Zh. Éksp. Teor. Fiz. **57**, 263 (1969) [Sov. Phys. JETP **30**, 147 (1969)].
[12] A. A. Ovchinnikov and N. S. Èpikhman, Usp. Fiz. Nauk **138**, 289 (1982) [Sov. Phys. Uspekhi **25**, 738 (1982)].
[13] G. S. Zavt and S. P. Reifman, Pis'ma Zh. Éksp. Teor. Fiz. **15**, 738 (1972) [JETP Lett. **15**, 523 (1972)].
[14] A. M. Kosevich and A. S. Kovalev, Zh. Éksp. Teor. Fiz. **67**, 1793 (1974) [Sov. Phys. JETP **40**, 89 (1974)].
[15] A. M. Kosevich and A. S. Kovalev, Fiz. Nizk. Temp. **1**, 1544 (1975) [Sov. J. Low Temp. Phys. **1**, 742 (1975)].
[16] M. M. Bogdan and A. M. Kosevich, Fiz. Nizk. Temp. **2**, 794 (1976) [Sov. J. Low Temp. Phys. **2**, 391 (1976)].
[17] A. M. Kosevich and A. S. Kovalev, *Introduction to Nonlinear Mechanics* [in Russian], Naukova Dumka, Kiev (1989).
[18] Y. Kivshar and B. Malomed, J. Phys. A **21**, 1553 (1988).
[19] D. I. Pushkarov and R. D. Atanasov, Phys. Lett. A **149**, 287 (1990).
[20] N. G. Vakhitov and A. A. Kolokolov, Izv. Vuzov: Radiofizika **XVI**, 1020 (1973).
[21] M. M. Bogdan and A. S. Kovalev, Pis'ma Zh. Éksp. Teor. Fiz. **31**, 213 (1980) [JETP Lett. **31**, 195 (1980)].
[22] V. A. Ivanov and A. I. Sukstanskii, Solid State Commun. **50**, 523 (1984).

Translated by R. S. Wadhwa

Localized vibration spectra of crystals with intercalated plane

M. A. Ivanov, Yu. V. Skripnik, and N. N. Gumenchuk

Institute of Metal Physics, National Academy of Sciences of the Ukraine, 252142 Kiev, Ukraine
(Submitted April 16, 1996; revised June 24, 1996)
Fiz. Nizk. Temp. **23**, 208–217 (February 1997)

Additional symmetric and antisymmetric localized branches of the vibrational spectrum of a crystal, associated with the presence of intercalated (interstitial) planes in strongly anisotropic crystals, are investigated by using the discrete model and taking into account the interaction between nearest neighbors. Energy–momentum relations for such vibrations are analyzed, and the values of parameters for which local vibrations are excited above and below the energy band in the continuous spectrum of the crystal corresponding to the given value of the wave vector component in this plane are determined. Special attention is paid to an analysis of the possibility of formation of well-defined resonant modes of the spectrum, which are located within the allowed band and are polarized along and across the interstitial plane. © *1997 American Institute of Physics.* [S1063-777X(97)01002-5]

INTRODUCTION

The analysis of vibrational spectra of crystals with various planar defects (such as phase boundaries, twinning planes, and intercalated planes) is an important problem in solid state physics. The existence of special elastic waves propagating near the surface of a medium was predicted for the first time by Rayleigh.[1] Various types of waves emerging in the presence of interfaces between different media were subsequently studied in the theory of elasticity.[2–4]

In the case of the discrete lattice model, a general approach to an analysis of spectra of crystals with planar defects was proposed by Lifshits and Kosevich,[5] who analyzed the possibility of the formation of an additional two-dimensional branch of the spectrum for the simplest type of perturbations. The spectra of vibrational states localized near a plane defect in a crystal were studied in many publications, including those where numerical methods were used.[6–8] Special attention was paid to vibrations whose energies are separated from the main spectrum by a gap, and the amplitudes decrease exponentially with increasing distance from the defect. Moreover, it was noted in Ref. 8 that the impurity monolayer at the crystal surface can lead under certain conditions to the emergence of resonant modes. It should be emphasized, however, that a consistent theory which would describe all possible spectral branches of crystals with various types of planar defects (including energy–momentum relation and attenuation of resonant modes) taking into account a variation of the atomic masses as well as the force constants for crystals with such defects has not been constructed yet.

It was shown in Refs. 9–11 by using the two-parameter model of an impurity center taking into account the change in masses as well as in force constants that well-defined resonant modes can emerge even in low-dimensional ($1D$ or $2D$) systems in the case of a weak coupling between an impurity and the matrix. Considering that the problem of determining the vibration spectrum of a crystal with a planar defect is essentially one-dimensional,[5] it would be interesting to use this approach for an analysis of the spectra of crystals with two-dimensional defects. An interstitial (intercalated) plane can serve as a general form of a $2D$ defect for which the two-parametric form of perturbation is significant. An analysis of various properties (including the vibrational spectrum) of the intercalated plane in layered crystals is of special importance. If we also take into account the strong anisotropy of the energy–momentum relation for phonons in these crystals, including the presence of flexural spectral modes, we can expect a large variety in the nature of the emerging two-dimensional impurity states and in the corresponding energy–momentum relations in such systems.

For this reason, we shall consider here the spectrum of localized and resonant vibrational states with different symmetries, which is associated with the presence of the intercalated plane in layered crystals with arbitrary values of atomic masses in this plane and force constants determining the coupling between the atoms in the plane and the matrix. Considerable attention will be paid to an analysis of conditions for the emergence of resonant spectral modes, their energy–momentum relations, and damping.

MODEL OF INTERCALATED PLANE IN A LAYERED CRYSTAL

In the harmonic approximation, the equations of motion of atoms in a layered crystal have the form

$$\omega^2 \chi^{\alpha}_{n,N} - \sum L^{\alpha\beta}_{nn',NN'} \chi^{\beta}_{n'N'} = 0, \tag{1}$$

where $\chi^{\alpha}_{n,N}$ is the α-component ($\alpha = x,y,z$) of the displacement of the nth atom in the Nth plane and $\hat{L}$ the dynamic matrix of the initial crystal. We assume that the initial layered crystal can be described by the model proposed in Refs. 12 and 13. In this model, the crystal has a hexagonal symmetry, and it is sufficient to take into account only the interaction of nearest neighbors in the direction perpendicular to the layers:

$$L_{nn,NN+1}=-\begin{bmatrix}\alpha_1/m & 0 & 0\\ 0 & \alpha_1/m & 0\\ 0 & 0 & \alpha_2/m\end{bmatrix},\quad \alpha_1\ll\alpha_2, \quad (2)$$

where α_1 and α_2 are the force constants for noncentral and central interaction between the planes, respectively. We assume that the above assumptions are valid for a crystal with an intercalated plane also, but the force constants of its interaction with the nearest layers of the crystal (for definiteness, we denote them by $N=0$ and 1) have different values: α_1' and α_2'. In this case, $\alpha_1'\ll\alpha_2'\ll\alpha_3$, where α_3 is the constant of atomic interaction in the layers of the initial crystal.

In crystals with a two-dimensional defect, the translational invariance is violated only in the direction perpendicular to it. For this reason, we seek the solution of this problem in the form $\chi^{\alpha}_{n,N}=\chi^{\alpha}_N(\mathbf{k}_\perp)\exp(i\mathbf{k}_\perp\cdot\mathbf{r}_n)$, where the z-axis is perpendicular to the crystal layers in the impurity plane, $\mathbf{k}_\perp=k_x\mathbf{e}_x+k_y\mathbf{e}_y$, and $\mathbf{r}_n$ is the radius vector of the nth atom in the layer.

It follows from the symmetry of the system that we can write three different types of equations of motion: (1) for displacements of atoms of the intercalated plane, (2) for displacements of atoms of the first and zeroth planes, and (3) for all the remaining planes. From symmetry considerations, it is also convenient to go over to new variables for the components of the displacements of atoms in the plane:

$$\chi_N^{(1)}=\frac{k_x\chi_N^x+k_y\chi_N^y}{k_\perp},\quad \chi_N^{(2)}=\frac{k_x\chi_N^y-k_y\chi_N^x}{k_\perp},$$
$$\xi_1=\frac{k_x\xi^x+k_y\xi^y}{k_\perp},\quad \xi_2=\frac{k_x\xi^y-k_y\xi^x}{k_\perp}, \quad (3)$$

where ξ^α is the α-component of atomic displacement in the impurity plane. In these variables, we obtain the following equations describing atomic displacements in the plane for small values of k_x and k_y:

$$\left(\omega^2-\frac{2\alpha_1}{m}-\omega_{\|j}^2(k_\perp)\right)\chi_{-1}^{(j)}+\frac{\alpha_1}{m}(\chi_{-2}^{(j)}+\chi_0^{(j)})=0,$$
$$\left(\omega^2-\frac{2\alpha_1}{m}-\widetilde{\omega}_{\|j}^2(k_\perp)\right)\chi_0^{(j)}+\frac{\alpha_1}{m}(\chi_{-1}^{(j)}+\chi_1^{(j)})$$
$$=-\frac{\alpha_1'\xi_j}{m}+\left(\frac{\alpha_1'}{m}-\frac{\Delta\alpha_1}{m}\right)\chi_0^{(j)}+\frac{\Delta\alpha_1}{m}\chi_1^{(j)},$$
$$\left(\omega^2-\frac{2\alpha_1'}{M}-\omega_{\|j}'^2(k_\perp)\right)\xi_j+\frac{\alpha_1'}{M}(\chi_0^{(j)}+\chi_1^{(j)})=0, \quad (4)$$
$$\omega_{\|j}^2(k_\perp)=c_jk_\perp^2,\quad \widetilde{\omega}_{\|j}^2(k_\perp)=\widetilde{c}_jk_\perp^2,$$
$$\omega_{\|j}'^2(k_\perp)=c_j'k_\perp^2,\quad j=1,2,$$

where c_j, $\widetilde{c}_j$, and c_j' are the squares of the velocities of sound in the layers of the initial crystal, in the layers adjoining the defect, and in the intercalated plane itself respectively, m and M are the masses of atoms of the initial crystal and of the intercalated plane respectively, and $\Delta\alpha_1=\alpha_1-\widetilde{\alpha}_1,\widetilde{\alpha}_1$ being the second-order force constant for a noncentral interaction of crystal layers closest to this plane.

The strong anisotropy of the crystal under investigation is manifested, in particular, in that the velocity of acoustic vibrations polarized in the plane is determined by the maximum coupling parameter:

$$c_j\sim\frac{\alpha_3a^2}{m},\quad \alpha_3\gg\alpha_2\gg\alpha_1, \quad (5)$$

where a is the lattice constant of the layers.

It can be seen from (4) that the equations describing vibrations with different polarizations j within the layer (longitudinal and transverse vibrations in the long-wave limit) can be separated. An analysis of these vibrational branches is the same so that we can henceforth omit the subscript j.

In this model, the vibrations polarized across the layers do not interact with other modes. Consequently, for these components of displacements of atoms we can immediately write

$$\left(\omega^2=\frac{2\alpha_2}{m}-\omega_\perp^2(k_\perp)\right)\chi_{-1}^z+\frac{\alpha_2}{m}(\chi_{-2}^z+\chi_0^z)=0,$$
$$\left(\omega^2-\frac{2\alpha_2}{m}-\widetilde{\omega}_\perp^2(k_\perp)\right)\chi_0^z+\frac{\alpha_2}{m}(\chi_{-1}^z+\chi_1^z)$$
$$=-\frac{\alpha_2'\xi_z}{m}+\left(\frac{\alpha_2'}{m}-\frac{\Delta\alpha_2}{m}\right)\chi_0^z+\frac{\Delta\alpha_2}{m}\chi_1^z,$$
$$\left(\omega^2-\frac{2\alpha_2'}{M}=\omega_\perp'^2(k_\perp)\right)\xi_z+\frac{\alpha_2'}{M}(\chi_1^z+\chi_0^z)=0, \quad (6)$$

where $\Delta\alpha_2=\alpha_2-\widetilde{\alpha}_2$; $\widetilde{\alpha}_2$ and $\widetilde{\omega}_\perp(k_\perp)$ are the corresponding force constant and the frequency of vibrations in the planes adjacent to the intercalated plane.

It is well known that layered crystals can exhibit flexural vibrations of the layers due to a strong (as compared to the interaction between the layers) noncentral interaction of atoms in the layer.[14,15] For these vibrations, for small values of $k_\perp$ we have

$$\omega^2(k_\perp)=c_\perp k_\perp^2+Aa^2k_\perp^4,\quad A\sim c_j,\quad A\gg c_\perp. \quad (7)$$

The vibrational frequencies $\omega_\perp'(\mathbf{k}_\perp),\widetilde{\omega}_\perp(\mathbf{k}_\perp)$ of the intercalated plane and of the adjacent planes in the matrix are defined by similar expressions with corresponding values of $c_\perp'$, $\widetilde{c}_\perp$, A', and $\widetilde{A}$. The invariance of the crystal relative to an infinitely small rotation implies that

$$c_\perp=\frac{\alpha_1b^2}{m}, \quad (8)$$

where b is the separation between the layers. We can prove that the rule of sums is fulfilled when the following relations hold for a crystal with an intercalated plane:

$$2\Delta\alpha_1=\alpha_1'>0,\quad \alpha_1'<2\alpha_1, \quad (9)$$
$$Mc_\perp'=2m(c_\perp-\widetilde{c}_\perp). \quad (10)$$

Eliminating the components of atomic displacements in the intercalated plane from the equations of motion, we can easily find that the two-dimensional matrix of perturbation introduced by the defect and depending on the wave vector $\mathbf{k}_\perp$ can be written in the form

$$V_{NN}^{\parallel}(\omega,k_\perp)=(\delta_{N0}+\delta_{N1})(\delta_{N'0}+\delta_{N'1})\left[\frac{\alpha_1'}{2m}+\frac{(\alpha_1')^2/(mM)}{\omega^2-\omega_\parallel'^2(k_\perp)-2\alpha_1'/M}+(\tilde{\omega}_\parallel^2(k_\perp)-\omega_\parallel^2(k_\perp))\delta_{NN'}\right] \tag{11}$$

for vibrations polarized in the plane and

$$V_{NN'}^{\perp}(\omega,\mathbf{k}_\perp)=(\delta_{N0}+\delta_{N1})(\delta_{N'0}+\delta_{N'1})\times\left[\frac{(\alpha_2')^2/(mM)}{\omega^2-(\omega_\perp')^2(k_\perp)-2\alpha_2'/M}+\left(\tilde{\omega}_\perp^2(k_\perp)-\omega_\perp^2(k_\perp)+\frac{\alpha_2'}{m}-\frac{\Delta\alpha_2}{m}\right)\delta_{NN'}+\frac{\Delta\alpha_2}{m}(1-\delta_{NN'})\right] \tag{12}$$

for vibrations polarized across the plane.

In this case, the frequencies of new vibrations associated with the presence of the defect can be determined form the condition

$$\det(\hat{l}-\hat{V}^{\perp,\parallel}(\omega,\mathbf{k}_\perp)\hat{g}^{\perp,\parallel}(\omega,\mathbf{k}_\perp))=0, \tag{13}$$

where $\hat{g}^{\perp,\parallel}$ is the unperturbed one-dimensional Green's function for a layered crystal:

$$\hat{g}^{\perp,\parallel}=\begin{pmatrix} g_{00}^{\perp,\parallel} & g_{01}^{\perp,\parallel} \\ g_{10}^{\perp,\parallel} & g_{00}^{\perp,\parallel}\end{pmatrix};$$

$$g_{NN'}^{\perp,\parallel}(\omega,\mathbf{k}_\perp)\equiv g_{NN'}^{\perp,\parallel}(\varepsilon_{\perp,\parallel})\equiv g_{NN'}^{\perp,\parallel}=\frac{1}{N_0}\sum_{k_z}\frac{\exp(ik_z r_{NN'}^z)}{\varepsilon_{\perp,\parallel}-\omega_{2,1}^2\sin^2(k_z b/2)};$$

$$\varepsilon_{\perp,\parallel}=\omega^2-\omega_{\perp,\parallel}^2(k_\perp); \tag{14}$$

$\omega_{1,2}^2=4\alpha_{1,2}/m$, and N_0 is the number of planes in the crystal. Since we take into account here only the interaction between the nearest planes, and the atomic displacements in the intercalated plane are taken into account in expressions (11) and (12), it was sufficient to consider only 2×2 matrices for determining the frequencies of localized vibrations associated with the intercalated plane.

For the perturbations of the type under investigation, Eq. (13) naturally splits into the symmetric and antisymmetric components corresponding to inphase and antiphase vibrations of the adjacent planes. In this case, the equations defining the frequencies of symmetric vibrations polarized across the layers assume the form

$$1=\left(\frac{\alpha_2'}{m}+\frac{2(\alpha_2')^2/(mM)}{\omega^2-\omega_\perp'^2(k_\perp)-2\alpha_2'/M}+\tilde{\omega}_\perp^2(k_\perp)-\omega_\perp^2(k_\perp)\right)\times(g_{00}^{\perp}+g_{01}^{\perp}),$$

$$1=\left(\frac{\alpha_1}{m}+\frac{2(\alpha_1')^2/(mM)}{\omega^2-\omega_\parallel'^2(k_\perp)-2\alpha_1'/M}+\tilde{\omega}_\parallel^2(k_\perp)-\omega_\parallel^2(k_\perp)\right)\times(g_{00}^{\parallel}+g_{01}^{\parallel}). \tag{15}$$

The frequencies of antisymmetric vibrations are accordingly defined by the equations

$$1=\left(\frac{\alpha_2'}{m}-\frac{2\Delta\alpha_2}{m}+\tilde{\omega}_\perp^2(k_\perp)-\omega_\perp^2(k_\perp)\right)(g_{00}^{\perp}-g_{01}^{\perp}),$$

$$1=(\tilde{\omega}_\parallel^2(k_\perp)-\omega_\parallel^2(k_\perp))(g_{00}^{\parallel}-g_{01}^{\parallel}). \tag{16}$$

Using relations (14), we can obtain the following expressions for the matrix elements of unperturbed Green's functions appearing in (15) and (16):

$$g_{00}^{\parallel,\perp}+g_{01}^{\parallel,\perp}=2g_{00}^{\parallel,\perp}\left(1-\frac{\varepsilon_{\parallel,\perp}}{\omega_{1,2}^2}\right)+\frac{2}{\omega_{1,2}^2},$$

$$g_{00}^{\parallel,\perp}-g_{01}^{\parallel,\perp}=2(\varepsilon_{\parallel,\perp}g_{00}^{\parallel,\perp}-1)/\omega_{1,2}^2, \tag{17}$$

while the diagonal elements of these functions for arbitrary values of the parameter $\varepsilon_{\parallel,\perp}$ have the form[16]

$$g_{00}^{\parallel,\perp}=\begin{cases}\operatorname{sgn}(\varepsilon_{\parallel,\perp})/\sqrt{\varepsilon_{\parallel,\perp}(\varepsilon_{\parallel,\perp}-\omega_{1,2}^2)}, & \varepsilon_{\parallel,\perp}<0,\ \varepsilon_{\parallel,\perp}>\omega_{1,2}^2,\\ i/\sqrt{\varepsilon_{\parallel,\perp}(\omega_{1,2}^2-\varepsilon_{\parallel,\perp})}, & 0<\varepsilon_{\parallel,\perp}<\omega_{1,2}^2.\end{cases} \tag{18}$$

In the subsequent analysis of the frequencies of vibrations associated with the intercalated plane, we shall consider localized vibrations whose frequencies lie outside the corresponding band of the continuous spectrum of the initial crystal for given values of $\mathbf{k}_\perp$, and the amplitudes decrease exponentially with increasing distance from the defect, as well as resonant vibrations whose frequencies lie within the energy band corresponding to bulk modes of the initial crystal.

SYMMETRIC VIBRATIONS

We begin the analysis of the vibrational spectra of a crystal with an intercalated plane with the most interesting case of symmetric vibrations. It can be seen from (15) that the impurity plane actively participates in vibrations of this type of symmetry so that its intralayer parameters and accordingly the frequencies $\omega_\parallel'^2(\mathbf{k}_\perp)$ produce an appreciable effect on the energy–momentum relation of localized vibrations associated with the defect.

In the analysis of vibrations polarized in the plane, we neglect (for simplicity) the change in the properties of the crystal layers nearest to the defect. In this case, the following condition holds: $\tilde{\omega}_\parallel^2(k_\perp)=\omega_\parallel^2(k_\perp)$, and the second expression in (15) [on account of (18)] assumes the form

$$\frac{\varepsilon_\parallel-\Delta\omega_\parallel^2(k_\perp)-2\alpha_1'/M}{\gamma[\varepsilon_\parallel-\Delta\omega_\parallel^2(k_\perp)]}=1+\begin{cases}-\left(\dfrac{\varepsilon_\parallel-\omega_1^2}{\varepsilon_\parallel}\right)^{1/2}, & \varepsilon_\parallel<0,\ \varepsilon_\parallel>\omega_1^2,\\ i\left(\dfrac{\omega_1^2-\varepsilon_\parallel}{\varepsilon_\parallel}\right)^{1/2}, & 0<\varepsilon_\parallel<\omega_1^2,\end{cases} \tag{19}$$

where

$$\Delta\omega_{\parallel}^2(k_\perp)=\omega_{\parallel}'^2(k_\perp)-\omega_{\parallel}^2(k_\perp);\quad \gamma=\frac{\alpha_1'}{2\alpha_1}<1. \tag{20}$$

It should be noted that the expression on the right-hand side of Eq. (19) has a typical one-dimensional singularity (divergence) at the lower boundary ($\varepsilon_\parallel=0$) of the band for bulk modes corresponding to the given value of $\mathbf{k}_\perp$ and a root singularity typical of three-dimensional crystals at the upper boundary ($\varepsilon_\parallel=\omega_1^2$). The absence of one-dimensional singularity at the upper boundary in formula (19) is associated with the choice of the model of the crystal and intercalated plane: the atoms from adjacent layers of the crystal and in the impurity plane are located exactly above one another and interact only with nearest neighbors.

It follows from Eq. (19) that, for any value of $\Delta\omega_{\parallel}^2(\mathbf{k}_\perp)<0$, i.e., in the case when atoms in the impurity plane are coupled with one another more strongly than in the matrix layers, a low-frequency branch of local vibrations, which is typical of two-dimensional effects and which was described for the first time in Ref. 5, splits from the unperturbed band. The frequencies of this branch corresponding to a given value of $\mathbf{k}_\perp$ lie below the edge of the acoustic band (i.e., $\varepsilon_\parallel<0$) and tend to zero as $\mathbf{k}_\perp\to 0$. For the crystal model with a plane defect considered here, the energy–momentum relation for this branch for $k_\perp\to 0$ has the form

$$\omega_{\parallel,l}^2(k_\perp)\approx\omega_{\parallel}^2(k_\perp)-\frac{(\Delta\omega_{\parallel}^2(k_\perp))^2}{\omega_1^2(m/M)^2}. \tag{21}$$

As in Ref. 6, we have $\omega_{\parallel}^2(k_\perp)-\omega_{\parallel,l}^2(k_\perp)\propto k_\perp^4$. It can be seen that the obtained energy–momentum relation does not depend on the coupling between the intercalated plane and the matrix. Such a behavior is quite unexpected (especially in the case of a weakly bound defect). This question will be analyzed in greater detail below.

Apart from the low-frequency branch of local vibrations, the given system can also exhibit resonant vibrations whose frequencies (for a given value of $\mathbf{k}_\perp$) lie in the band of corresponding bulk modes of the continuous spectrum of the unperturbed as well as local vibrations with frequencies lying above this band.

Let us consider in greater detail the possibility of emergence of well-defined resonant vibrations. Neglecting the second (imaginary) term on the right-hand side of Eq. (19), we obtain the following expression of the energy–momentum relation for vibrations polarized in the plane:

$$\omega_{\parallel,r}^2(k_\perp)=\omega_{\parallel}'^2(k_\perp)+\omega_{\parallel,r}^2(0), \tag{22}$$

$$\omega_{\parallel,r}^2(0)=\frac{2\alpha_1'/M}{1-\gamma}=\frac{\gamma}{1-\gamma}\frac{m}{M}\,\omega_1^2<\omega_1^2. \tag{23}$$

Here $\omega_{\parallel,r}^2(0)$ is the square of the limiting frequency of resonant vibrations. According to (23), the value of $\omega_{\parallel,r}^2(0)$ lies in the energy band of the continuous spectrum when the parameters of the intercalated plane satisfy the following condition:

$$\gamma<\frac{1}{1+m/M}. \tag{24}$$

Expression (22) shows that the dependence of the frequency of resonant vibrations on the wave vector $\mathbf{k}_\perp$ is determined only by the magnitude of $\omega_{\parallel}'^2(\mathbf{k}_\perp)$, i.e., is the same as for an isolated intercalated plane, and does not depend on the coupling of this plane with the matrix. Consequently, if atoms in the given plane are coupled with one another more strongly than in the layers of the initial crystal [$\Delta\omega_{\parallel}^2(\mathbf{k}_\perp)>0$], the frequency of a resonant vibration gradually moves away with increasing $\mathbf{k}_\perp$ from the lower boundary of the band corresponding to bulk modes and approaches this boundary if the coupling between atoms in the intercalated plane is weaker than in the matrix.

Using Eq. (19), we can also derive the following expression for the broadening of the squared frequency $\omega_{\parallel,r}^2(\mathbf{k}_\perp)$ of resonant vibrations:

$$\Gamma_{\parallel,r}(k_\perp)=\frac{\gamma}{1-\gamma}\,\omega_{\parallel,r}^2(0)\left(\frac{\omega_1^2+\omega_{\parallel}^2(k_\perp)-\omega_{\parallel,r}^2(k_\perp)}{\omega_{\parallel,r}^2(k_\perp)-\omega_{\parallel}^2(k_\perp)}\right)^{1/2}. \tag{25}$$

The condition for a resonant vibration to be well defined has the form

$$|\omega_{\parallel,r}^2(k_\perp)-\omega_{\parallel,e}^2(k_\perp)|\gg\Gamma_{\parallel,r}(k_\perp), \tag{26}$$

where $\omega_{\parallel,e}^2(\mathbf{k}_\perp)$ are the vibrational frequencies corresponding to the upper and lower edges of the band for a given value of $k_\perp$. Instead of two inequalities (26), we can write, taking into account the explicit expression (25) for damping, the following interpolation criterion:

$$\frac{M\omega_{\parallel,r}^4(0)}{m[\omega_{\parallel,r}^2(k_\perp)-\omega_{\parallel}^2(k_\perp)]^{3/2}}\,[\omega_1^2+\omega_{\parallel}^2(k_\perp)-\omega_{\parallel,r}^2(k_\perp)]^{-1/2}\ll 1. \tag{27}$$

Expressions (26) and (27) imply that the necessary condition for the emergence of resonant states is that the intercalated plane must be weakly coupled with the matrix. Indeed, in the case of low-frequency resonant vibrations ($\omega_{\parallel,r}^2(0)\ll\omega_1^2$) for small values of $\mathbf{k}_\perp$ we find that conditions (26) and (27) can be reduced to the following inequality for the coupling parameters:

$$\gamma\ll(1+M/m)^{-1}. \tag{28}$$

Condition (28) can also be written in the form

$$\omega_{\parallel,r}^2(0)\ll\left(\frac{m}{M}\right)^2\omega_1^2. \tag{29}$$

Consequently, for $m\gg M$, well-defined resonant states can lie at the middle of the continuous spectral band or at its upper edge. In the latter case, the criterion for the existence of resonant states has the form

$$(\omega_1^2-\omega_{\parallel,r}^2(0))\gg\omega_1^2(M/m)^2.$$

As the resonant vibration branch approaches the boundary of the band corresponding to bulk modes, the expression on the right-hand side of (27) diverges, the conditions for the existence of resonant vibrations are violated, and the corresponding branch is interrupted. In this case, the broadening of resonant states at the lower edge of the spectrum also diverges,

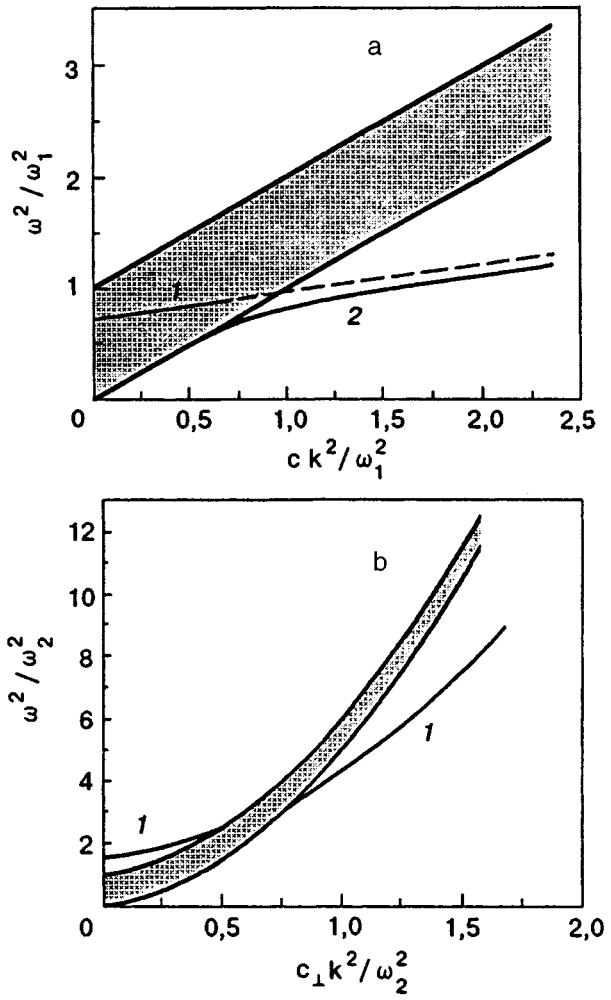

FIG. 1. Energy–momentum relations (*a*) $\omega^2_{\parallel,r}(k_\perp)$ for symmetric resonant (curve *1*) and $\omega^2_{\parallel,l}(k_\perp)$ for local (curve *2*) vibrations of a crystal with an intercalated plane described by formula (19) for $\gamma=0.1$, $m/M=6.5$, and $c'/c=0.25$, and (*b*) $\omega^2_{\perp,l}(\mathbf{k}_\perp)$ for antisymmetric local vibrations of the crystal with an intercalated plane (curve *1*) described by (35) for $\nu_\perp=1.5$, $(\tilde{c}_\perp-c_\perp)/c_\perp=-0.8$, $(\tilde{A}-A)/A=-0.85$, and $(Aa^2\omega_2^2)/c_\perp^2=4$. The regions of continuous spectrum of the crystal are hatched.

Let us consider in greater detail the behavior of low-frequency of resonant vibrations, for which the condition $\Delta\omega^2_\parallel(\mathbf{k}_\perp)<0$ is fulfilled. As the wave vector increases, the frequency $\omega^2_\parallel(\mathbf{k}_\perp)$ of such vibrations, which is defined in (22), approaches the lower edge of the unperturbed spectral band and terminates in this region. On the other hand, a low-frequency branch of local vibrations is formed for such values of $\Delta\omega^2_\parallel(\mathbf{k}_\perp)$ (see above). The frequency of these vibrations is described by formula (21) as long as the condition $|\Delta\omega^2_\parallel(k_\perp)| \leqslant \omega^2_{\parallel,r}(0)$ is satisfied. As the wave vector increases further, the vibrational frequency of this branch approaches asymptotically the continuation of the energy–momentum relation (22) for resonant vibrations [see expression (31) for details]. The general form of the energy–momentum relation for resonant and local vibrations in the case of weakly coupled intercalated plane considered here is presented in Fig. 1a.

In the general case, the square of the frequency of localized vibrations polarized in the plane for a given value of $\mathbf{k}_\perp$ is defined by the solution of the equation

$$\omega^2_{\parallel,l}(k_\perp)=\omega'^2_\parallel(k_\perp)+\frac{2\alpha_1'}{M}\times\left\{1-\gamma\left[1-\left(\frac{\omega^2_{\parallel,l}(k_\perp)-\omega^2_\parallel(k_\perp)-\omega_1^2}{\omega^2_{\parallel,l}(k_\perp)-\omega^2_\parallel(k_\perp)}\right)^{1/2}\right]\right\}^{-1}. \quad (30)$$

Such local vibrations lying above the upper edge of the band can be either a continuation of resonant spectral branches, or an independent branch starting at $\mathbf{k}_\perp=0$. It should be noted that in contrast to the lower edge, localized vibrations do not split from the upper edge for arbitrarily small values of the quantity $\Delta\omega^2_\parallel(\mathbf{k}_\perp)>0$.

The necessary condition for the emergence of a localized state for $\mathbf{k}_\perp=0$ is that the parameters of the intercalated plane must satisfy the condition opposite to (24). Since the parameter $\alpha_1'<2\alpha_1$ in view of the conditions of crystal invariance to rotations, the masses of atoms from the intercalated plane in the case of local vibrations whose frequencies lie much higher than the energy band corresponding to bulk modes for $\mathbf{k}_\perp=0$ must be much smaller than the masses of matrix atoms ($M\ll m$). In the general case, the energy–momentum relation for high-frequency local vibrations of the given symmetry assumes the form

$$\omega^2_{\parallel,l}(k_\perp)=\omega^2_{\parallel,l}(0)+\omega'^2_\parallel(k_\perp),$$
$$\omega^2_{\parallel,l}(0)=2\alpha_1'/M. \quad (31)$$

Expressions (22) and (31) show that the energy–momentum relation for low-frequency resonant and high-frequency local vibrations is positive and is determined by the intralayer vibrational frequencies only in the intercalated plane itself. In the intermediate cases, matrix vibrations can also affect the energy–momentum relation.

It also should be noted that in the case two branches of such modes are present in all cases when resonant and localized vibrations polarized in the plane are excited, . The difference in their frequencies is due to the fact that the quantities $\omega^2_\parallel(k_\perp)$ and $\omega'^2_\parallel(k_\perp)$ in expressions (19)–(31) depend on the type of polarization j. At the same time, the limiting frequencies $\omega^2_{\parallel,l}(0)$ and $\omega^2_{\parallel,r}(0)$ do not depend on the index j so that both these branches converge at the point $\mathbf{k}_\perp=0$.

Let us now consider the vibrations polarized perpendicularly to the planes of the crystal. An analysis of the corresponding symmetric vibrations is in general similar to that carried out above for the vibrations in the planes of the layers. The main difference (apart from the fact that the energy–momentum relations $\omega^2_\perp(k_\perp)$, $\omega'^2_\perp(k_\perp)$, $\tilde{\omega}^2_\perp(k_\perp)$ themselves change significantly is that in formula (15) we cannot in principle assume that $\tilde{\omega}^2_\parallel(k_\perp)=\omega^2_\parallel(k_\perp)$ in view of the sum rule. As a result, the explicit dependence of frequencies of localized vibrations on the wave vector can change slightly. For example, instead of formula (21), in the case of low-frequency local vibrations, we obtain

$$\omega^2_{\perp,l}(k_\perp)=\omega^2_\perp(k_\perp)$$
$$-\frac{\{c_\perp k_\perp^2+a^2k^4[A(1+2m/M)-A'-\widetilde{A}2m/M]\}^2}{\omega_2^2(m/M)^2},$$

$$\omega'^2_\perp(k_\perp)-\omega^2_\perp(k_\perp)+(\widetilde{\omega}^2_\perp(k_\perp)-\omega^2_\perp(k_\perp)2m/M<0. \quad (32)$$

The limitations on the variation of the velocity of sound [see (10)] in layers adjacent to the intercalated plane affect the energy–momentum relation and attenuation of the corresponding localized vibrations insignificantly since the condition $|\widetilde{\omega}^2_\perp(k_\perp)-\omega^2_\perp(k_\perp)|\leqslant a_2'/m$ is valid in the range of wave vectors where a linear energy–momentum relation is observed. However, the changes in the spectrum can be stronger for large values of wave vectors for which this condition becomes invalid in view of the possible change in flexural rigidity in the planes adjacent to the defect.

It should be noted that the ratios of the parameters α_1' and α_2' (which determine the frequencies of localized vibrations associated with the presence of the interstitial plane) to the corresponding values of the matrix parameters can be arbitrary and generally do not correlate with one another. For this reason, the three types of localized modes do not necessarily appear (or disappear) simultaneously.

ANTISYMMETRIC VIBRATIONS

In the case of vibrations associated with the intercalated plane and transformed according to the antisymmetric representation, the layers nearest to the defect move in antiphase, and the atoms of the impurity plane do not participate in these vibrations. Localized vibrations in this case can emerge only due to a change in the parameters of the layers nearest to the intercalated plane.

Expressions (17) and (18) show that the characteristic difference $g^{\parallel,\perp}_{00}-g^{\parallel,\perp}_{01}$ between lattice Green's functions, which defines, according to Eqs. (16), the frequencies of localized antisymmetric vibrations, has a root divergence at the upper boundary of the spectral band for the unperturbed crystal, corresponding to a given value of $\mathbf{k}_\perp$, while the singularity at the lower boundary is of the conventional three-dimensional type (in contrast to the case of symmetric vibrations).

Over the entire frequency range, and taking into account the explicit form of lattice Green's functions (17) and (18), Eq. (16) can be written in the form

$$1=f_{\parallel,\perp}(k_\perp)\left[\left(\frac{\varepsilon_{\parallel,\perp}}{\varepsilon_{\parallel,\perp}-\omega^2_{1,2}}\right)^{1/2}-1\right], \quad (33)$$

$$f_{\parallel,\perp}(k_\perp)=\nu_{\parallel,\perp}+\frac{\widetilde{\omega}^2_{\parallel,\perp}(k_\perp)-\omega^2_{\parallel,\perp}(k_\perp)}{\omega^2_{1,2}},$$

$$\nu_\parallel=0,\quad \nu_\perp=\frac{2\widetilde{\alpha}_2+\alpha_2'-2\alpha_2}{2\alpha_2}>-1. \quad (34)$$

In the allowed energy band of the vibrational spectrum for an unperturbed crystal ($0<\varepsilon_{\parallel,\perp}<\omega^2_{1,2}$), the radical in expression (33) becomes imaginary, and Eq. (33) in this spectral region has no physical solutions since the function $f_{\parallel,\perp}(k_\perp)$ does not depend on frequency, i.e., antisymmetric resonant modes do not appear for any polarization.

In the frequency range where $\varepsilon_\perp<0$ or $\varepsilon_\perp>\omega_2^2$, Eq. (33) can be easily solved in explicit form:

$$\omega^2_{\parallel,\perp,l}(k_\perp)=\left(1+\frac{f^2_{\parallel,\perp}(k_\perp)}{1+2f_{\parallel,\perp}(k_\perp)}\right)\omega^2_{1,2}+\omega^2_{\parallel,\perp}(k_\perp). \quad (35)$$

Since $\nu_\parallel=0$ for vibrations polarized in the plane, only localized vibrations lying above the upper edge of the continuous spectrum band can exist for small values of the wave vector. In this case, it is necessary that the intralayer rigidity in the planes nearest to the intercalated plane be higher than in the matrix $[(\widetilde{\omega}^2_\parallel(k_\perp)-\omega^2_\parallel(k_\perp)>0]$. The corresponding frequency of vibrations tends to ω_1 as $\mathbf{k}_\perp\to 0$ according to the same law $[\omega^2_{\parallel,l}(k_\perp)-\omega^2_\parallel(k_\perp)-\omega_1^2\propto k_\perp^4]$ as for symmetric vibrations near the lower band boundary[5] in view of the one-dimensional nature of the singularity of the unperturbed spectrum in this region.

For modes polarized across the plane, local vibrations above the edge of the energy band can also exist for $\mathbf{k}_\perp=0$ if the parameter $\nu_\perp>0$, i.e., when the effective transverse coupling associated with the presence of the intercalated plane becomes tighter the possibility of the emergence of similar antisymmetric vibrations was indicated earlier in Ref. 6 for another model of the impurity plane). If, for example, the elastic constant remains unchanged upon a transition to the plane adjacent to the intercalated one ($\widetilde{\alpha}_2=\alpha_2$), such local vibrations appear for arbitrary values of the parameter α_2' determining the elastic coupling between the intercalated plane and the matrix. The dispersion of frequencies $\omega^2_{\perp,l}(\mathbf{k}_\perp)$ of the emerging local vibrations is always positive. If, however, the condition $\widetilde{\omega}^2_\perp(k_\perp)-\omega^2_\perp(k_\perp)<0$, is satisfied, the value of $f_\perp(k_\perp)$ decreases with increasing wave vector $\mathbf{k}_\perp$, and the frequency $\omega_{\perp,l}(k_\perp)$ approaches the upper boundary of the allowed energy band. Finally, for $f_\perp(k_\perp)=0$, this spectral branch of localized transverse vibrations disappears. With a further increase in the wave vector (for $f_\perp(k_\perp)<-1$), this spectral branch can appear again below the allowed energy band. The general form of the energy–momentum relation for localized states is presented in Fig. 1b.

Localized transverse vibration can also be excited in the case when the parameter $\nu_\perp$ is negative ($-1<\nu_\perp<0$). In this case, the corresponding localized states will be formed for finite values of the wave vector $\mathbf{k}_\perp$ (above the allowed spectral band for $\widetilde{\omega}^2_\perp(k_\perp)-\omega^2_\perp(k_\perp)>0$ and $f_\perp(k_\perp)>0$. and below this band for $\widetilde{\omega}^2_\perp(k_\perp)-\omega^2_\perp(k_\perp)<0$ and $f_\perp(k_\perp)<-1$; the latter case can also be realized for vibrations polarized in the plane).

CONCLUSION

The analysis of the conditions for the emergence of additional branches of local and resonant vibrations in strongly anisotropic crystals with an intercalated interstitial plane shows that such spectral branches can exist in a wide and quite realistic range of the parameters of the system. We can assume that these results will also be valid in general for

weakly anisotropic crystals with an intercalated plane as well as in the case of a substitutional plane. However, the energy–momentum relations for localized impurity vibrations in strongly anisotropic crystals can be much more diversified in view of a relatively small width of the allowed band for bulk modes in the two-dimensional Brillouin zone (as compared to the maximum frequency of acoustic vibrations).

It should be noted, however, that some of the obtained results require additional analysis in order to verify their stability in the case of other models. This concerns above all the form of the spectrum of various vibrations near the upper boundary of the allowed spectral band. Also, we have analyzed only the energy–momentum relations and attenuation of various types of vibrations induced by a planar defect, but the influence of such vibrations on the thermodynamic and optical parameters of the crystal being measured require a further investigation.

This research was carried out under the support of ISSEP grant No. 042026.

Remark. After this manuscript had been submitted, the editorial board kindly acquainted the authors with the article ''Acoustic shear waves localized near a plane defect in a fcc crystal'' prepared for publication by A. M. Kosevich, E. S. Syrkin, and A. V. Tutov,[17] in which similar problems are considered. In both papers, the vibrational spectra of the crystal with a planar defect are considered on the basis of the discrete (atomic) model. The main difference lies in the types of crystal lattice (a layered crystal of hexagonal symmetry) and in the method of analysis of vibrations, in which the law of decrease in the vibrational amplitude with increasing distance from the defect was not specified by us beforehand. This allowed us, for example, to determine the energy–momenta relations for not only local, but also resonant oscillations. Moreover, we considered the spectra of longitudinal as well as transverse vibrations with the components of the wave vector with arbitrary directions and with small magnitudes. Nevertheless, some qualitative results obtained by using these two approaches are similar. The closest case for comparison is that considered in Sec. 1 of Ref. 17, where the role of the defect is played by the change in force constants for two adjacent planes of the crystal. In our analysis, this corresponds to the limiting case of zero values of the parameter α' (i.e., in fact, the absence of an intercalated plane), but the parameters $\tilde{\alpha}$ are generally assumed to be other than α. As in Ref. 17, the branches of symmetric vibrations (however, polarized not only in the plane, but also at right angles to it) split from the lower edge of the energy band for small values of $\mathbf{k}_\perp$ if the corresponding values of frequencies $\tilde{\omega}_{\perp,\parallel}(k_\perp)$ are smaller than the frequencies $\omega_{\perp,\parallel}(k_\perp)$ of the unperturbed crystal, i.e., for a weaker interplanar coupling. As the coupling becomes stronger, symmetric modes can appear, according to Ref. 17 only above the band edge and for finite values of $\mathbf{k}_\perp$. Transverse antisymmetric modes are on the whole in agreement with the results obtained in Ref. 17 for longitudinal vibrations. However, for longitudinal antisymmetric modes we observe a qualitative difference: the energy–momentum relation for local modes emerging above the band edge upon an increase in the interplanar coupling always tends to the upper edge of the energy band for $\mathbf{k}_\perp \to 0$ in view of the fulfillment of the sum rule for the crystal model under consideration, while in the case of a weaker coupling such local vibrations can emerge only below the band edge and for finite values of $\mathbf{k}_\perp$. It would be interesting to carry out a more detailed comparison of our results and the results obtained in Ref. 17 on the basis of the same crystal model.

[1] Lord Rayleigh, London Math. Soc. Proc. **17**, 4 (1885).
[2] Yu. A. Kosevich and E. S. Syrkin, Kristallografiya **33**, 1339 (1988).
[3] A. M. Kosevich and A. V. Tutov, Fiz. Nizk. Temp. **19**, 1273 (1993) [Low Temp. Phys. **19**, 905 (1993)].
[4] Yu. A. Kosevich and E. S. Syrkin, Fiz. Tverd. Tela (Leningrad) **31**, 127 (1989) [*sic*].
[5] I. Lifshitz and A. Kosevich, Rep. Prog. Phys. **29**, 217 (1966).
[6] T. G. Petrova and E. S. Syrkin, Fiz. Nizk. Temp. **17**, 411 (1991) [Sov. J. Low Temp. Phys. **17**, 215 (1991)].
[7] I. M. Gelfgat and E. S. Syrkin. Fiz. Nizk. Temp. **3**, 899 (1977) [Sov. J. Low Temp. Phys. **3**, 437 (1977)].
[8] E. S. Syrkin and I. M. Gelfgat, Fiz. Nizk. Temp. **12**, 525 (1986) [Sov. J. Low Temp. Phys. **12**, 295 (1986)].
[9] M. I. Ivanov and Yu. V. Skripnik, Fiz. Tverd. Tela (Leningrad) **32**, 2965 (1990) [Sov. Phys. Solid State **32**, 1722 (1990)].
[10] M. I. Ivanov and Yu. V. Skripnik, Fiz. Nizk. Temp. **16**, 1171 (1990) [Sov. J. Low Temp. Phys. **16**, 677 (1990)].
[11] M. A. Ivanov, A. M. Kosevich, E. S. Syrkin, *et al.*, Fiz. Nizk. Temp. **19**, 434 (1993) [Low Temp. Phys. **19**, 305 (1993)].
[12] A. M. Kosevich, *Physical Mechanics of Real Crystals* [in Russian], Naukova Dumka, Kiev (1981).
[13] L. I. Glazman and A. M. Kosevich, Fiz. Nizk. Temp. **6**, 527 (1980) [Sov. J. Low Temp. Phys. **6**, 253 (1980)].
[14] I. M. Lifshitz, Zh. Éksp. Teor. Fiz. **22**, 471 (1952).
[15] I. M. Lifshitz, Zh. Éksp. Teor. Fiz. **22**, 475 (1952).
[16] A. Maradudin, E. Montroll *et al.*, *Theory of Lattice Dynamics in the Harmonic Approximation*, New York (1965).
[17] Yu. A. Kosevich and E. S. Syrkin, Fiz. Nizk. Temp. **22**, 804 (1996) [Low Temp. Phys. **22**, 617 (1996)].

Translated by R. S. Wadhwa

Solute segregation at grain boundaries in polycrystals with dominating mass transport by complexes

V. V. Slezov

National Science Center ''Kharkov Institute of Physics and Technology,'' 310108 Kharkov, Ukraine

O. A. Osmayev

*Kharkov State University, 310077 Kharkov, Ukraine**

V. V. Rogozhkin

Central Research Institute ''Prometej,'' St. Petersburg, Russia

(Submitted June 12, 1996)
Fiz. Nizk. Temp. **23**, 218–232 (February 1997)

Isothermal segregation of an impurity from a finite-size grain to the interface or the external free surface under predominant mass transfer by (vacancy–impurity atom) complexes is studied at low temperatures. A modified equation is obtained for an impurity with the effective diffusion coefficient containing the diffusion coefficients of the impurity and complexes with different weights. The temporal evolution of the impurity concentration is determined for planar, spherical, and cylindrical grains (which are close in shape to conventional grains) in the case of a dilute solution at an arbitrary temperature. Simple algebraic equations are obtained for the impurity concentration at the interface as a function of time. These equations are also valid for a concentrated solution of the impurity at the interface. The kinetics of impurity redissolution, i.e., the enrichment or depletion of the interface with the impurity (the departure of impurity to the bulk of the grain) is considered. [S1063-777X(97)01102-X]

INTRODUCTION

Many properties of polycrystalline materials are determined by the presence of an impurity at the interface between grains. As a result of segregation, the atomic concentration of impurity atoms at the interface can become much higher than in the bulk of a grain. The formation of a concentrated solution of the impurity at the interface and the emergence of precipitates at the grain boundaries deteriorates the mechanical properties of the material and can lead to temper brittleness of the metal.

The theory of segregation is based, as a rule, on the Mac Lean approach[1] which is applicable if the diffusion length of the impurity is much smaller than the grain size (i.e., the grain is approximated by a semi-infinite medium). In the case of a fine-grain structure of the substance or a high mobility of impurities (e.g., under irradiation), the diffusion length can become comparable with or larger than the characteristic grain size. In this paper, we consider segregation of an impurity from a finite-size grain to the interface. According to some experimental data, the diffusion rate for an impurity in a complex with a point defect is much higher than in the free state.[2] For this reason, we consider the general case when mass transfer can be accomplished by the diffusion of individual impurity atoms as well as impurity atoms in a complex with a point defect (vacancy). Starting from the Girifalco publications,[3,4] the latter mechanism was called the ''vacancion pump.'' However, a number of assumptions made in Ref. 3 (such as the local equilibrium relative to the complex formation) as well as in subsequent publications[2,4–6] were not substantiated rigorously.

In this research, we analyze the conditions under which an impurity in complexes plays a significant role in diffusion processes on account of different time scales in these processes and at low temperatures. An analysis of such phenomena extends the scope of concepts associated with diffusion processes, which were formulated by Academician I. M. Lifshits at the beginning of the seventies.

1. FORMULATION OF THE PROBLEM AND BASIC SYSTEM OF EQUATIONS

Impurity–vacancy or impurity–interstitial atom complexes can play a significant role at low temperatures (at $T<Q$, where T is the temperature in energy units and Q the binding energy of a complex). The latter complexes play an important role only in materials under irradiation since the number of such complexes is small under normal conditions. If the diffusion coefficient for complexes is much larger than the diffusion coefficient for an impurity, the complexes play the major role in mass transfer.

Following Ref. 7, we consider here a grain of a typical size and symmetric shape (plane-parallel, spherical, or cylindrical). Such an approach is justified since similar processes occur in all grains in polycrystals, and the grains are under identical conditions on the average. This means that we can neglect the flows of point defects and impurity atoms through the middle of the interface between the grains, and

accumulation of the impurity in the grain is obviously determined by the flows of impurity atoms to the grain boundary. Consequently, both the formation and disintegration of complexes must be taken into account in the diffusion equations for point defects (vacancies), impurity atoms, and complexes. Internal sinks (dislocations) should also be taken into account in the case of vacancies.

Let us write the system of diffusion equations for determining the concentrations c_v, c_s, and c_{vs} of vacancies, impurity atoms, and vacancy–impurity atom complexes, respectively. For this purpose, we must supplement the right-hand side of diffusion equations with sources and sinks of impurities, vacancies, and complexes. This gives

$$\frac{\partial c_v}{\partial t} = D_v \Delta c_v + \alpha(k c_{vs} - c_v c_s) - D_v \rho (c_v - c_v^e), \tag{1}$$

$$\frac{\partial c_{vs}}{\partial t} = D_{vs} \Delta c_{vs} - \alpha(k c_{vs} - c_v c_s), \tag{2}$$

$$\frac{\partial c_s}{\partial t} = D_s \Delta c_s + \alpha(k c_{vs} - c_v c_s). \tag{3}$$

We denote

$$\varepsilon = \alpha(k c_{vs} - c_v c_s), \tag{4}$$

where c_v^e is the equilibrium concentration of vacancies, k the equilibrium constant relative to disintegration and formation of complexes, D_v, D_s, and D_{vs} are the volume diffusion coefficients for vacancies, impurity atoms, and vacancy–impurity complexes respectively, and α is the frequency with which an impurity atom is combined with a vacancy to form a complex:

$$\alpha = p \frac{(D_v + D_s)}{a'^2}.$$

Here a is the atomic spacing, p a coefficient of the order of unity, and ρ the density of dislocations in a grain.

It is well known that the chemical potentials of complexes, impurity atoms and vacancies in equilibrium are connected through the relation $\mu_{vs} = \mu_s + \mu_v$. If, in addition, we assume that the solution in a grain is dilute in c_v, c_s, and c_{vs}, we obtain

$$\frac{c_v c_s}{c_{vs}} = k = \exp\left\{ \frac{\psi_{vs} - \psi_s - \psi_v}{T} \right\},$$

where ψ_{vs}, ψ_s, and ψ_v are the excess energy of a complex, an impurity atom, and a vacancy respectively.

The term $\alpha k c_{vs}$ in Eqs. (1)–(4) describes the decay, and the term $\alpha c_v c_s$ the formation of complexes. It should be noted that in order to find the steady-state flow of vacancies to dislocations, we must solve the problem for the entire ensemble of dislocations since a stationary solution of such a problem in an infinite two-dimensional space does not exist. Such a self-consistent solution, obtained in Ref. 8 for an ensemble, leads to the expression $\eta D_v \rho (c_v - c_v^e)$, where the coefficient η is of the order of unity. For estimates, we can put $\eta = 1$.

We choose the initial conditions in an obvious way (since the sample is prepared, as a rule, by cooling from melt, when complexes virtually do not form, and the time of sample preparation is shorter than the time of a significant segregation of impurity at the grain boundaries under the given conditions). In this case,

$$\begin{aligned} &c_s|_{t=0} = c_s(0) = c_s^0, \quad c_{vs}|_{t=0} = 0, \\ &c_v|_{t=0} = c_v^e, \quad c_s^b|_{t=0} = c_s^b(0), \end{aligned} \tag{5}$$

where the superscript **b** indicates that the value of the quantity is taken in the bulk of the grain.

Let us determine the boundary conditions for vacancies, complexes, and impurity atoms. It is well known that the boundaries of the general form for vacancies are powerful sources and sinks of vacancies. For this reason, the concentration of vacancies at the grain boundary is maintained in equilibrium:

$$c_v|_f = c_v^e, \tag{6}$$

where f is an arbitrary point at the grain surface.

We assume that the parameters of the process under investigation are such that the characteristic time $a^2/\beta D_s$ required for an atoms to go over from a grain to the interface[9] is much shorter than the characteristic time t_0 of variation of the impurity concentration in the grain, which will be defined below (it should be noted that $\beta = D_s'/D_s < 1$, where D_s is the diffusion coefficient of the last hop of an impurity atom to the interface; if $D_s' > D_s$, the last but one jump will be a ''bottleneck,'' and hence we must have $0 < \beta < 1$). This means that the chemical potential of the impurity at the interface and in the bulk of the grain is the same:

$$\mu_s^b|_f = \mu_s|_f. \tag{7}$$

Henceforth, we shall specify the conditions when the equilibrium relative to the decay of complexes accompanied by a transition of an impurity to the grain boundary is observed to a high degree of accuracy. This means that the relaxation time (i.e., the time t_{vs}^p of equalization of the decay and formation rates for complexes) is much shorter than t_0. In this case, we can write the following condition at the grain boundary:

$$\mu_{vs}|_f = \mu_s^b|_f + \mu_v|_f = \mu_s|_f + \mu_v|_f. \tag{8}$$

Considering that the impurity concentration at the interface can be high, we find that the chemical potential of the impurity at the interface has the form

$$\mu_s^b = \psi^b + \tilde{\beta} c_s^b + T \ln \frac{c_s^b}{1 - c_s^b}. \tag{9}$$

The second term on the right-hand side of this expression takes into account the interaction of impurity atoms at neighboring lattice sites, while the third term takes into account a strong short-range interaction, i.e., the fact that only one particle can be at a lattice site. As a rule, the interaction of impurity atoms at neighboring sites is weak as compared to the contribution from the remaining terms in (9).

It follows from (7) and (9) that the Langmuir relation[11] holds at the interface:

$$\left.\frac{c_s^b(t)}{1-c_s^b(t)}\right|_f = \gamma c_s|_f = \gamma\lambda(t), \tag{10}$$

where $\lambda(t)$ is the concentration of impurity atoms at the interface, $\gamma=\exp(\Delta G/T)$ the redistribution coefficient, $\Delta G=(\psi_s-\psi_s^b)/T$, and ψ_s^b is the excess energy of dissolution of the impurity at the interface. Assuming that the solution at the interface is dilute ($c_s^b \ll 1$), we obtain the Henry relation

$$c_s^b|_f = \gamma c_s|_f = \gamma\lambda(t). \tag{11}$$

Integrating (2) and (3) over the entire volume, summing up the equations, and going over from the volume integral to the integral over the surface on the right-hand side of the equation, we arrive at the following relations:

$$V\left(\frac{d\overline{c_s}}{dt}+\frac{d\overline{c_{vs}}}{dt}\right)=\int_S(\mathbf{j}_s+\mathbf{j}_{vs})d\cdot\mathbf{S}=(j_s+j_{vs})|_f S,$$

$$\overline{c_s}=\frac{1}{V}\int_V c_v dV, \quad \overline{c_{vs}}=\frac{1}{V}\int_V c_{vs}dV, \tag{12}$$

where $\overline{c_s}$ and $\overline{c_{vs}}$ are the values of the concentrations of impurity atoms and complexes averaged over the volume.

In relations (12), we have assumed that the grains are symmetric, and hence the flow at the interface does not depend on the point on the grain surface. The positive direction of the normal to the surface is the inward direction from the surface to the bulk of the grain. The law of conservation for the impurity gives

$$V\left(\frac{d\overline{c_s}}{dt}+\frac{d\overline{c_{vs}}}{dt}\right)=-dS\,\frac{dc_s^b}{dt}, \tag{13}$$

where $2d$ is the width of the interface between two neighboring grains. Consequently, we obtain the following condition at the boundary from (12) and (13):

$$-(j_{vs}+j_s)|_f=\frac{dc_s^b}{dt}\,d. \tag{14}$$

Here we assume that the grain boundary is narrow, and the diffusion coefficient in the boundary is large, and hence diffusion processes rapidly level out the concentration of impurity. This means that c_s^b at the interface is a function of time alone.

Thus, we have obtained a complete system of diffusion equations (1)–(3) with the initial conditions (5) and boundary conditions (6)–(8), (10), and (14). It should be noted that if the local equilibrium at the interface cannot be stabilized over a time much shorter than the duration of the process under consideration, conditions of a more general form are satisfied at the interface. In this case, we must write the boundary condition of the third kind, which has the form

$$j_s|_f=\beta\,\frac{D_s}{a}\,(c_s|_f-\widetilde{c}_s), \tag{15a}$$

$$j_{vs}|_f=p\,\frac{D_v}{a}\,k(c_{vs}|_f-\widetilde{c}_{vs}), \tag{15b}$$

where $\widetilde{c}_s$ is the equilibrium concentration of impurity, which can be determined from the condition (7) of equality of the values of chemical potential at the interface and in the bulk of the grain, and $\widetilde{c}_{vs}$ the equilibrium concentration for the decay of complexes at the interface, which can be determined from the condition of equilibrium between the decay and formation of complexes at the interface: $\widetilde{c}_{vs}=c_v^e c_s/k$. It should be noted that c_s^b and current quantities c_s and c_{vs} have the same characteristic time of variation t_0 (since they are connected through the conservation law for the impurity). As a rule, the process occurs with a small deviation from local equilibrium, and hence $\widetilde{c}_{vs}$ and $\widetilde{c}_s$ have the same characteristic time t_0 of their variation.

The first term in Eq. (15a) for the impurity flow to the interface is the impurity flux to the boundary, while the second term characterizes the flux from the boundary. The coefficient $D_s'/a=\beta D_s/a\,(0<\beta<1)$ is the effective rate of a transition of an impurity atom to the grain boundary. While determining the flux through the interface for complexes, we take into account in Eq. (15b) the fact that a vacancy at the interface overcomes a barrier, and then an impurity atom goes over to the prepared vacancy. The first term ($\gamma k c_{vs}$) in Eq. (15b) describes the flow of complexes to the interface. As a result of decay, the complexes carry the impurity through the interface (i.e., the disintegration of complexes and the transition of the impurity to the interface occur simultaneously). The second term ($\gamma k\widetilde{c}_{vs}$) describes the flow of complexes from the interface. The difference between the fluxes in (15b) is absorbed by the boundary. The coefficient $D_v'/a=pD_v/a$ is the effective rate of transition of a vacancy through the interface. Thus, if the characteristic time t_0 (i.e., the time during which the substance is supplied to the interface, which is found to equal to the time of variation of $\widetilde{c}_{vs}$ and c_s), is much longer than the maximum time of the transition ($a^2/\beta D_s$ or a^2/pD_v), the condition of local equilibrium is satisfied to a sufficiently high degree of accuracy, i.e., the boundary conditions (7) and (8) are valid and lead to

$$c_s|_f=\widetilde{c}_s \quad \widetilde{c}_{vs}|_f=\widetilde{c}_{vs}=c_v^e\widetilde{c}_s/k. \tag{16}$$

2. CHARACTERISTIC TIME t_p OF VACANCY CONCENTRATION TUNING TO ITS EQUILIBRIUM VALUE

In Eqs. (17)–(19), we go over from t to $\tau=(D_v/a^2)t$, which gives

$$\frac{\partial c_v}{\partial\tau}=\dot{c}_v=a^2\Delta c_v+\varepsilon-\rho a^2(c_v-c_v^e), \tag{17}$$

$$\frac{\partial c_{vs}}{\partial\tau}=\dot{c}_{vs}=\frac{D_{vs}}{D_v}\,\Delta c_{vs}-\varepsilon, \tag{18}$$

$$\frac{\partial c_s}{\partial\tau}=\dot{c}_s=\frac{D_s}{D_v}\,\Delta c_s+\varepsilon, \tag{19}$$

$$\varepsilon=kc_{vs}-c_s c_v\,. \tag{20}$$

In these equations, the terms $\Delta c\approx\mathrm{div}\,j$ are proportional to the flux of point defects (vacancies, complexes, or impurity atoms) from an arbitrarily chosen small macroscopic volume (physical point). It should be noted that these terms in (17)–(19) have the same order of magnitude as

$(a^2/D_v t)c_v$, $(a^2/D_v t)c_{vs}$, $(a^2/D_v t)c_s$ respectively (taking into account diffusion lengths for the corresponding defects). Let us consider the values of time for which the first terms in (17)–(19) are smaller than any of the remaining terms of Eqs. (17)–(19). In this case, these first terms can be neglected, which actually means that the process can occur in two stages for such values of time. At the first stage, for $t_p \ll \Delta t \ll t$ and on a small time scale (interval), when we can neglect the outflow of point defects from a small macroscopic volume, the rearrangement of concentrations of complexes and impurity atoms takes place so that their total number is conserved. In view of the presence of sources, the vacancy concentration tends to its equilibrium value, i.e., the processes of formation and disintegration complexes are levelled out, and the concentration of vacancies tends to its equilibrium value at each point.

It should be noted that he characteristic size l of a physical point belongs to the interval $a/c_s^{1/3} \ll l \ll L_D$ (L_D is the impurity diffusion length and $a/c_s^{1/3}$ the separation between impurity atoms). Thus, at the first stage (small time scale), the process is described by Eqs. (17)–(19) without Laplace operators, with certain boundary conditions at the time instant t, which have the form

$$c_v|_{\tau=0} = c_v^*, \quad c_s|_{\tau=0} = c_s^*, \quad c_{vs}|_{\tau=0} = c_{vs}^*, \tag{21}$$

where τ is measured from t.

As a result of relaxation ($t_p \ll \Delta t \ll t$), certain relations will be established between the quantities c_v, c_{vs}, and c_s. These relations virtually do not change in the subsequent description of the process, when the exchange between small macroscopic volumes becomes significant, while the concentration appearing in these relations change slowly with the characteristic time of exchange between small macroscopic volumes, which is naturally much longer than the relaxation time.

Equations (17)–(19) show that, with such a partial relaxation, the impurity conservation law is satisfied at an arbitrary physical point: $c_s + c_{vs} = c_s^* + c_{vs}^*$. In this case, $\varepsilon = k(c_s^* + c_{vs}^*) - c_s(k + c_v)$; $\varepsilon|_{\tau=0} = kc_{vs}^* + c_s^* c_v^*$. Taking these expressions into account, we can simplify Eqs. (17)–(19) and write them in the form

$$\dot{c}_s = \varepsilon = k(c_s^* + c_{vs}^*) - c_s(k + c_v), \tag{22}$$

$$\dot{c}_v = k(c_s^* + c_{vs}^*) - c_s(k + c_v) - \rho a^2(c_v - c_v^e) = \varepsilon - \rho a^2(c_v - c_v^e). \tag{23}$$

Let us write Eq. (22) in integral form:

$$c_s = c_s^* \left[\exp\left\{ -\int_0^\tau [k + c_v(\tau')]d\tau' \right\} + k\,\frac{c_s^* + c_{vs}^*}{c_s^*} \times \exp\left\{ -\int_0^\tau [k + c_v(\tau')]d\tau' \right\} \int_0^\tau \times \exp\left\{ \int_0^{\tau'} [k + c_v(\tau'')]d\tau'' \right\} d\tau' \right]. \tag{24}$$

Substituting this equation into the expression for ε, we obtain

$$\varepsilon = k(c_s^* + c_{vs}^*) - (k + c_v)c_s^* \left\{ 1 + k\,\frac{c_s^* + c_{vs}^*}{c_s^*} \times \int_0^\tau \exp\left[\int_0^{\tau'} [k + c_v(\tau'')]d\tau'' \right] d\tau' \right\} \times \exp\left[-\int_0^\tau [k + c_v(\tau')]d\tau' \right]. \tag{25}$$

Let us prove that $c_v > 0$ and has a single minimum. Indeed, if the minimum $c_v = \tilde{c}_v$ is attained for $\tau = \tau_0$, we have $\dot{c}_v|_{\tau=\tau_0} = 0$. Denoting $c_v|_{\tau=\tau_0} = \tilde{c}_v$, $c_s|_{\tau=\tau_0} = \tilde{c}_s$ we obtain from (23)

$$\dot{c}_v|_{\tau=\tau_0} = 0 = k(c_s^* + c_{vs}^*) - \tilde{c}_s(k + \tilde{c}_v) - \rho a^2(\tilde{c}_v - c_v^e), \tag{26}$$

for $\tau = \tau_0 \neq 0$. Considering that $c_s^* + c_{vs}^* > \tilde{c}_s$ (since impurity sources are absent), we obtain the relation $\tilde{c}_v/c_v^e > \rho a^2/(\tilde{c}_s + \rho a^2)$ from (26). An analysis of this relation shows that the value of c_v belongs to the interval

$$0 < \tilde{c}_v \leqslant c_v. \tag{27}$$

Using this inequality for $\tilde{c}_v$, we can simplify relation (25) to a high degree of accuracy. For this purpose, we consider the expression in the brackets of (25). The integral in (25) acquires its value (with an exponential accuracy) mainly at the upper limit $\tau' = \tau$, and hence

$$(k + c_v)\int_0^\tau \exp\left\{ \int_0^{\tau'} [k + c_v(\tau'')]d\tau'' \right\} d\tau' \cong \int_0^\tau (k + c_v(\tau'))\exp\left\{ \int_0^{\tau'} (k + c_v[\tau''])d\tau'' \right\} d\tau' = \exp\left\{ \int_0^\tau [k + c_v(\tau')]d\tau' \right\} - 1. \tag{28}$$

Taking this relation into account, we can write (25) in the form

$$\varepsilon = (kc_{vs}^* - c_s^* c_v)\exp\left\{ -\int_0^\tau [k + c_v(\tau')]d\tau' \right\}. \tag{29}$$

Using this relation for ε, we obtain the closed equation for c_v:

$$\dot{c}_v = (kc_{vs}^* - c_s^* c_v)\exp\left\{ -\int_0^\tau [k + c_v(\tau')]d\tau' \right\} - \rho a^2(c_v - c_v^e), \quad c_v|_{\tau=0} = c_v^*. \tag{30}$$

Introducing the new variable $\Delta (\Delta = c_v - c_v^e)$, we obtain the following equation for Δ:

$$\dot{\Delta} = (kc_{vs}^* - c_s^* c_v^e)\exp\left\{ -\int_0^\tau [k + c_v(\tau')]d\tau' \right\} - \left[\rho a^2 + c_s^* \exp\left\{ -\int_0^\tau [k + c_v(\tau')]d\tau' \right\} \right]\Delta, \quad \Delta|_{\tau=0} = c_v^* - c_v^e. \tag{31}$$

This equation can be slightly simplified:

$$\dot{\Delta}=(kc_{vs}^*-c_s^*c_v^e)\exp\{-(k+\tilde{c}_v)\}\tau-[\rho a^2+c_s^*\exp\{-(k+\tilde{c}_v)\}\tau]\Delta,$$

$$\Delta|_{\tau=0}=c_v^*-c_v^e,\quad \overline{c_v}=\frac{1}{\tau}\int_0^\tau c_v(\tau')d\tau'. \tag{32}$$

Representing Eq. (32) in integral form, we obtain

$$\Delta=(kc_{vs}^*-c_s^*c_v^e)\exp\left\{-\rho a^2\tau+\frac{c_s^*}{k+\overline{c_v}}\times\exp[-(k+\overline{c_v})\tau]\right\}\int_0^\tau\exp[-(k+\overline{c_v})\tau']\times\exp\left\{\rho a^2\tau'-\frac{c_s^*}{k+\overline{c_v}}\exp[-(k+\overline{c_v})\tau']\right\}d\tau'+(c_v^*-c_v^e)\exp\left\{-\rho a^2\tau+\frac{c_s^*}{k+\overline{c_v}}\times\exp[-(k+\overline{c_v})\tau]\right\}. \tag{33}$$

Let us analyze this expression. For

$$k+\overline{c_v}\gg\rho a^2 \tag{34}$$

we have

$$\Delta\propto(kc_{vs}^*-c_s^*c_v^e)\exp\{-\rho a^2\tau\}+(c_v^*-c_v^e)\exp\{-\rho a^2\tau\}. \tag{35}$$

Here we have taken into account the fact that under the condition (34), the integral appearing in (33) tends to a constant as $\tau\to\infty$. The obtained expression (35) shows that the time of relaxation of c_v to c_v^e is given by

$$\tau_p\to 1/(\rho a^2), \tag{36}$$

or, in dimensional units,

$$t_p\propto 1/(D_v\rho).$$

In the case when

$$k+\overline{c_v}\ll\rho a^2 \tag{37}$$

we take into account the fact that the integral in (33) acquires its value mainly at the upper limit, and the slowly varying multiplier can be factored out of the integral at the upper limit. This gives

$$\Delta\propto\frac{(kc_{vs}^*-c_s^*c_v^e)}{\rho a^2}\exp\{-(k+\overline{c_v})\tau\}+(c_v^*-c_v^e)\times\exp\{-\rho a^2\tau\}. \tag{38}$$

In this case, the relaxation time is given by

$$\tau_p\propto\frac{1}{k+\overline{c_v}}\ \text{ or }\ t_p\propto\frac{a^2}{D_v}\frac{1}{k+\overline{c_v}}=\frac{1}{\alpha(k+\overline{c_v})}. \tag{39}$$

It can be seen from (29) that the characteristic relaxation time ε has the form

$$\frac{a^2}{D_v}\frac{1}{k+\overline{c_v}}=\frac{1}{\alpha(k+\overline{c_v})}.$$

Thus, if $k+\overline{c_v}\gg\rho a^2$, the value of ε first tends to zero over the time $1/[\alpha(k+c_v)]$, and then c_v approaches c_v^e during the characteristic time $1/(D_v\rho)$. If $k+c_v\ll\rho a^2$, c_v is tuned to c_v^e over the time $1/(D_v\rho)$, and the value of ε simultaneously tends to zero during the time $1/[\alpha(k+c_v)]$. Consequently, the relaxation time for $\varepsilon\to 0$ and $c_v\to c_v^e$ is equal to $1/(D_v\rho)$ under condition (34) and to $(a^2/D_v)(k+c_v)^{-1}$ for (37). Moreover, we can replace (for estimates) $\overline{c_v}$ by c_v^e under condition (37) if $k\geqslant c_v^e$ (i.e., if the decay of complexes is significant).

3. REDUCED SYSTEM OF EQUATIONS

After partial relaxation on a large time scale (when the exchange of point defects between small macroscopic volumes, viz., physical points, is significant), we can use a reduced system of equations for c_v, c_{vs}, and c_s, in which the relation obtained for relaxation time are taken into consideration. This system of equations has the form

$$c_v\cong c_v^e, \tag{40a}$$

$$\varepsilon=\alpha(kc_{vs}-c_sc_v^e)\cong 0, \tag{40b}$$

$$\frac{\partial}{\partial t}(c_{vs}+c_s)=D_{vs}\Delta c_{vs}+D_s\Delta c_s. \tag{40c}$$

Thus, we arrive at a simpler system of equations for the most important time interval $t_0\geqslant t\gg t_p$ in which the segregation to the grain boundary actually takes place. Relations (40a) and (40b) are approximate (to within the above accuracy). Equation (40c) is an exact differential equation, in which we can put $\varepsilon=0$ while determining the relation between c_s and c_{vs} (the smallness of ε is defined as $\varepsilon/\alpha kc_{vs}\propto\varepsilon/\alpha c_v^e c_s\ll 1$). If we take into account the fact that ε differs from zero, Eq. (40c) acquires the terms giving small corrections to the solution in the zeroth approximation in ε (see Appendix).

Thus, in the zeroth approximation in ε, we obtain the following relations for c_s from (40c):

$$\frac{\partial c_s}{\partial t}=D_{\text{eff}}\Delta c_s,\quad D_{\text{eff}}=\frac{kD_s+c_v^eD_{vs}}{k+c_v^e},\quad c_{vs}=\frac{c_v^e}{k}c_s. \tag{41}$$

Since the system of reduced equations (40a)–(40c) is applicable starting not from the initial instant of time, but from $t\gg t_p$, we must determine the initial and the boundary conditions for this system in the zeroth approximation in ε also. Starting from the moment of time at which the process is described by the system of reduced equations, a fraction of impurity atoms goes over to complexes, and no appreciable segregation to the interface takes place since $t\gg t_p$. In this case, $c_s^0=c_s'^0+c_{vs}'^0$, $c_{vs}'^0=(c_v^e/k)c_s'^0$ [see (39)], which gives

$$c_s|_{t=0}=c_s'^0=\frac{k}{k+c_v^e}c_s^0,$$

$$c_{vs}|_{t=0}=c'^{0}_{vs}=\frac{c_v^e}{k+c_v^e}\,c_s^0,\quad c_s^b|_{t=0}=c_s^b(0). \tag{42}$$

It should be noted that the initial condition for $c_s^b(0)$ has not changed since, by hypothesis, complexes do not exist at the grain boundary, and the impurity concentration does not change during the relaxation time. The fluxes at the grain boundary in the zeroth approximation in ε are given by $j_{vs}=D_{vs}\nabla c_{vs}=(c_v^e/k)D_{vs}\nabla c_s$, $j_s=D_s\nabla c_s$. In this case, Eq. (14) assumes the form

$$-D_{\text{eff}}\nabla c_s|_f=d_{\text{eff}}\frac{dc_s^b}{dt},$$

$$d_{\text{eff}}=\frac{k}{k+c_v^e}\,d. \tag{43}$$

Thus, we have obtained a system of equations (41) with the initial conditions (42) and with the boundary conditions (11), (15b), (16), and (43) which describe impurity segregation at the grain boundary taking into account complexes.

It should be noted that the impurity can be in the free state with a probability w_s or in a complex with the probability w_{vs}, $w_s+w_{vs}=1$. The ratio of the probabilities is the ratio of the corresponding relaxation times (i.e., the lifetimes in the corresponding states) τ_s and τ_{vs}, where $\tau_s=1/(\alpha c_v^e)$, $\tau_{vs}=1/(\alpha k)$. In this case, $w_s/w_{vs}=\tau_s/\tau_{vs}=k/c_v^e$, whence $w_s=k/(k+c_v^e)$, $w_{vs}=c_v^e/(k+c_v^e)$. In terms of probabilities, the effective diffusion coefficient assumes the form $D_{\text{eff}}=w_sD_s+w_{vs}D_{vs}$. It has the form of a superposition of the diffusion coefficients of impurity atoms and complexes with different weights, corresponding to the probability of the impurity occupying a definite state.

As $k\to 0$, the diffusion coefficient $D_{\text{eff}}\to D_{vs}$ (i.e., the complexes in the system do not disintegrate, and all of free impurity atoms in a grain become coupled in complexes after a certain time).

For $k\to\infty$, the diffusion coefficient $D_{\text{eff}}\to D_{vs}$ (i.e., the lifetime of complexes tends to zero, and a formed complex decays immediately, so that complexes do not exist. Thus, complexes dominate in mass transfer under the condition $D_{\text{eff}}\gg D_s$.

It should be noted that a further analysis is similar to that in Ref. 7. Using the system of equations (41) derived above for c_s derived above (in the zeroth approximation in ε), we consider the diffusion of an impurity atom for a plane-parallel grain with the characteristic size $L=2l$. In this case, we have

$$\frac{\partial c_s}{\partial t}=D_{\text{eff}}\Delta c_s,\quad \Delta=\partial^2/\partial x^2, \tag{44}$$

$$-D_{\text{eff}}\nabla c_s|_{x=\pm l}=d_{\text{eff}}\frac{dc_s^b}{dt} \tag{45}$$

with the following initial and boundary conditions:

$$c_s|_{t=0}=c'^{0}_{s}=\frac{k}{k+c_v^e}\,c_s^0,\quad c_s^b|_{t=0}=c_s^b(0)=\gamma\lambda(0), \tag{46}$$

$$c_s^b|_{x=l}=\gamma c_s=\gamma\lambda(t). \tag{47}$$

We seek the solution of Eq. (44) in the form $\tilde{c}_s(x,t)=c_s(x,t)-\lambda(t)$. In this case, Eq. (44) and conditions (46) and (47) assume the form

$$\frac{\partial\tilde{c}_s}{\partial t}=D_{\text{eff}}\frac{\partial^2\tilde{c}_s}{\partial x^2}-\frac{\partial\lambda}{\partial t}, \tag{48}$$

$$\tilde{c}_s(\pm l,t)=0,\quad \tilde{c}_s(x,0)=c'^{0}_{s}-\lambda(0). \tag{49}$$

The solution of Eq. (48) [which obviously should be sought in the form of a series in $\cos k(x/l)$] has the same form as in Ref. 7:

$$\tilde{c}_s(x,t)=c_s(x,t)-\lambda(t)=2\sum_{n=0}^{\infty}\frac{(-1)^n}{k_n^2}\exp\left[-\frac{D_{\text{eff}}t}{l^2}k_n^2\right]\times\left\{c'^{0}_{s}-\lambda(0)-\int_0^t\frac{d\lambda}{dt'}\exp\left[\frac{D_{\text{eff}}t'}{l^2}k_n^2\right]dt'\right\}\times\cos k_n(x/l),$$

$$k_n=\pi\left(n+\frac{1}{2}\right). \tag{50}$$

Substituting this expression into (45), we obtain

$$\frac{d_{\text{eff}}l}{D_{\text{eff}}}\frac{dc_s^b}{dt}=2\sum_{n=0}^{\infty}\exp\left[-\frac{D_{\text{eff}}t}{l^2}k_n^2\right]\left\{c'^{0}_{s}-\lambda(0)-\int_0^t\frac{d\lambda}{dt'}\exp\left[\frac{D_{\text{eff}}t'}{l^2}k_n^2\right]dt'\right\}. \tag{51}$$

Integrating (51) between 0 and t and changing the order of integration in the double integral, we obtain

$$\frac{d_{\text{eff}}}{l}[c_s^b(t)]-c_s^b(0)]=[c'^{0}_{s}-\lambda(0)]S(t)-\int_0^t\frac{d\lambda}{dt'}S(t-t')dt', \tag{52}$$

$$S(t)=\sum_{n=0}^{\infty}\frac{2}{k_n^2}\left\{1-\exp\left[-\frac{D_{\text{eff}}t}{l^2}k_n^2\right]\right\}. \tag{53}$$

Integrating by parts the last term in (52), we find that

$$\frac{d_{\text{eff}}}{l}[c_s^b(t)-c_s^b(0)]=c'^{0}_{s}S(t)+\int_0^t\lambda(t')\frac{\partial S(t-t')}{\partial t'}dt'. \tag{54}$$

The function appearing in the integrand of (54) contains two cofactors, one of which $[\lambda(t')]$ is smooth, and the other $[\partial S(t-t')/\partial t')]$ attains its maximum value at the upper limit, and $\partial S(t-t')/\partial t'|_{t'\to t}\to\infty$. The main contribution to the integral comes from the region of large values of t' close to t; consequently, we replace the smoothly varying function $\lambda(t')$ by its value at the upper limit. As a result, we obtain instead of the integral equation, an ordinary algebraic equation

$$\frac{d_{\text{eff}}}{l}[c_s^b(t)-c_s^b(0)]=[c'^{0}_{s}-\lambda(t)]S(t). \tag{55}$$

It should be noted that if $t\to\infty$, in equilibrium we have $\lambda(\infty)=c_s(\infty)=c_s^b(\infty)/\gamma$ and[7]

$$S(t)|_{t\to\infty}=S(\infty)=\sum_{n=0}^{\infty}\frac{2}{k_n^2}=\sum_{n=0}^{\infty}\frac{2}{\pi^2(n+1/2)^2}=1$$

In this case, Eq. (55) leads to

$$\frac{d_{\text{eff}}}{l}\,[c_s^b(\infty)-c_s^b(0)]=\left[c_s'0-\frac{c_s^b(\infty)}{\gamma}\right], \tag{56}$$

or, taking into account the equalities $c_s^b(\infty)/\gamma = c_s(\infty)$, $c_s'^0 =(k/(k+c_v^e))c_s^0$,

$$d[c_s^b(\infty)-c_s^b(0)]=\frac{k+c_v^e}{k}\left[\frac{k}{k+c_v^e}\,c_s^0-c_s(\infty)\right]l. \tag{57}$$

Considering that $[(k + c_v^e)/k]c_s(\infty) = c_s(\infty) + c_{vs}(\infty)$, we obtain (as expected) the exact law of impurity conservation for $t\to\infty$:

$$d[c_s^b(\infty)-c_s^b(0)]=[c_s^0-c_s(\infty)-c_{vs}(\infty)]l. \tag{58}$$

It should be noted that Eq. (55) is written in the general form for an arbitrary relation between λ and c_s^b irrespective of its complexity. For the Henry condition (11), we obtain, using (55),

$$\begin{aligned}c_s^b(t)&=c_s^b(0)+[\gamma c_s'^0-c_s^b(0)]\,\frac{S(t)}{\eta+S(t)}\\&=c_s^b(0)+\left[\gamma\,\frac{k}{k+c_v^e}\,c_s^0-c_s^b(0)\right]\frac{S(t)}{\eta+S(t)},\\ \eta&=\frac{d_{\text{eff}}\gamma}{l}=d\,\frac{k}{k+c_v^e}\,\frac{\gamma}{l}.\end{aligned} \tag{59}$$

Formula (59) describes segregation of impurity to the interface at any instant of time for the known diffusion coefficients of impurities, their equilibrium concentrations, initial concentrations and the coefficients of redistribution between the interface and the grain. The values of these phenomenological quantities must be known from other independent experiments. We can also assume that these quantities are parameters and, using the array of experimental curve (plotted at the same temperature, but for different values of initial concentrations and indifferent time intervals), select the parameters in the obtained formula so that experimental curves fit to the theoretical dependence to the required degree of accuracy. The values of these quantities can be regarded as the values of the corresponding parameters.

In the case of segregation in grain of an isotropic shape, it is convenient to use the spherical grain approximation. Taking into account the results obtained in Ref. 7, we can write the diffusion equation in the form

$$\begin{aligned}\tilde{c}_s(r,t)=2\sum_{n=1}^{\infty}\frac{(-1)^{n+1}}{k_n}\exp\left\{-\frac{D_{\text{eff}}t}{R^2}\,k_n^2\right\}\Bigg(c_s'^0-\lambda(0)\\-\int_0^t\frac{d\lambda}{dt'}\exp\left\{\frac{D_{\text{eff}}t'}{R^2}\,k_n^2\right\}dt'\Bigg)\,\frac{\sin(k_n\times r/R)}{r/R},\end{aligned} \tag{60}$$

where R is the grain radius and $k_n=\pi n$.

After similar transformations, we obtain

$$\begin{aligned}\frac{d_{\text{eff}}}{R}\,[c_s^b(t)-c_s^b(0)]&=[c_s'^0-\lambda(0)]S^s(t)\\&\quad-\int_0^t\frac{d\lambda}{dt'}\,S^s(t-t')dt'.\end{aligned} \tag{61}$$

Here the quantity d_{eff} is defined by (43), where d is the half-width of the interface, i.e., the width of the spherical layer absorbing impurity atoms, and the quantity $S^s(t)$ is defined in analogy with (53):

$$S^s(t)=\sum_{n=1}^{\infty}\frac{2}{k_n^2}\left[1-\exp\left(-\frac{D_{\text{eff}}t}{R^2}\,k_n^2\right)\right].$$

Using simple arguments (the same as in the case of a planar grain), we obtain

$$\begin{aligned}&\frac{d_{\text{eff}}}{R}\,[c_s^b(t)-c_s^b(0)]\\&=[c_s'^0-\lambda(t)]S^s(t)=\left(\frac{k'}{k+c_v^e}\,c_s^0-\lambda(t)\right)S^s(t).\end{aligned} \tag{62}$$

In the case when the Henry condition holds, we have

$$\begin{aligned}c_s^b(t)&=c_s^b(0)+[\gamma c_s'^0-c_s^b(0)]\,\frac{S^s(t)}{\eta'+S^s(t)}\\&=c_s^b(0)+\left(\gamma\,\frac{k}{k+c_v^e}\,c_s^0-c_s^b(0)\right)\frac{S^s(t)}{\eta'+S^s(t)},\\ \eta'&=\frac{\gamma d_{\text{eff}}}{R}.\end{aligned} \tag{63}$$

The solution of Eq. (62) satisfies the law of conservation of the amount of impurity for $t\to\infty$:

$$3d[c_s^b(\infty)-c_s^b(0)]=[c_s^0-c_s(\infty)-c_{vs}(\infty)]R, \tag{64}$$

since, according to Ref. 7, we have

$$S^s(t\to\infty)=\sum_{n=1}^{\infty}\frac{2}{k_n^2}=\sum_{n=1}^{\infty}\frac{2}{\pi^2n^2}=\frac{1}{3}$$

and $\lambda(\infty)=c_s(\infty)$

Let us carry out a similar analysis for a grain of a cylindrical shape, assuming that the condition along its axis are uniform. Using the results obtained in Ref. 7, we can write the solution of Eq. (44), where R is the radius of the cylinder, and the Laplacian is written in polar coordinates:

$$\begin{aligned}\tilde{c}_s(r,t)=2\sum_{k_n}\frac{1}{k_n}\exp\left\{-\frac{D_{\text{eff}}t}{R^2}\,k_n^2\right\}\Bigg(c_s'^0-\lambda(0)\\-\int_0^t\frac{d\lambda}{dt'}\exp\left\{\frac{D_{\text{eff}}t'}{R^2}\,k_n^2\right\}dt'\Bigg)\,\frac{J_0(k_n\times r/R)}{J_1(k_n)},\end{aligned} \tag{65}$$

where k_n are the zeroth of the zeroth-order Bessel function $J_0(k_n)=0$, and $J_1(k_n)$ is the first-order Bessel function.

After calculations, we obtain for $c_s^b(t)$ an equation similar to Eq. (61), where the quantity d appearing in d_{eff}, is the half-width of the boundary, i.e., of the cylindrical layer in which the impurity segregation from the grain takes place, and instead of $S^s(t)$ we have

$$S^c(t)=\sum_{k_n}\ \frac{2}{k_n}\left[1-\exp\left(-\frac{D_{\text{eff}}t}{R^2}\,k_n^2\right)\right]. \tag{66}$$

The summation is carried out over the zeroth of the function $J_0(k)$. As in the case of a plane-parallel grain (55), we can easily obtain the following equation for $c_s^b(t)$:

$$\frac{d_{\text{eff}}}{R}\,[c_s^b(t)-c_s^b(0)]=[c_s'^0-\lambda(t)]S^c(t)$$
$$=\left(\frac{k}{k+c_v^e}\,c_s^0-\lambda(t)\right)S^c(t). \tag{67}$$

Under Henry's condition, this relation assumes the form

$$c_s^b(t)=c_s^b(0)+[\gamma c_s'^0-c_s^b(0)]\,\frac{S^c(t)}{\eta'+S^c(t)}$$
$$=c_s^b(0)+\left(\gamma\,\frac{k}{k+c_v^e}\,c_s^0-c_s^b(0)\right)\,\frac{S^c(t)}{\eta'+S^c(t)}. \tag{68}$$

In order to satisfy the law of conservation of the amount of impurity for $t\to\infty$, i.e.,

$$2d[c_s^b(\infty)-c_s^b(0)]=[c_s^0-c_s(\infty)-c_{vs}(\infty)]R,$$

the following relation must hold[7]: $S^c(t\to\infty)=\Sigma_{k_n}2/k_n^2=1/2$ and $\lambda(\infty)=c_s(\infty)$.

It should be noted that expressions (59), (63), and (68) for the impurity concentration at the interface describe the process of depletion of a grain with impurity and its emergence at the interface as well as the inverse process of transition of impurity from the interface to the grain under certain conditions. As in Ref. 7, the specific process is determined by the value of the redistribution coefficient γ and the values of k and c_v^e at a given temperature T.

In the case of constant temperature T_0, the system with the initial value of $c_v^b(0)\neq 0$ evolves to the equilibrium state. Considering that $S(t)|_{t\to\infty}=1$, we obtain from (59)

$$c_s^b(\infty)|_{T_0}=\left[c_s^b(0)\Big|_{T_0}\eta(T_0)+\gamma(T_0)\,\frac{k(T_0)}{k(T_0)+c_v^e(T_0)}\,c_s^0\Big|_{T_0}\right]$$
$$\times[1+\eta(T_0)]^{-1}. \tag{69}$$

If we change the temperature from T_0 to T_1, the equilibrium is violated, and one of the following processes takes place, depending on the relation between T_0 and T:

for $T_0>T_1$ [i.e., $\gamma(T_0)<\gamma(T_1)$], and additional transition of impurity to the boundary takes place;

for $T_0<T_1$ [i.e., $\gamma(T_0)>\gamma(T_1)$], a fraction of impurity ions leaves the interface and is dissolved in the grain again. In this case, the new equilibrium (at T_1) level of impurity concentration is

$$c_s^b(\infty)|_{T_1}=c_s^b(0)|_{T_1}+\left[\gamma(T_1)\,\frac{k(T_1)}{k(T_1+c_v^e(T_1)}\,c_s^b\Big|_{T_1}-c_s^0\Big|_{T_1}\right]\frac{1}{1+\eta(T_1)}$$
$$=\frac{[k(T_0)+c_v^e(T_0)]/k(T_0)+[\gamma(T_0)d]/l}{1+\eta(T_0)}\,\frac{k(T_1)}{k(T_1)+c_v^e(T_1)}$$
$$\times\frac{\gamma(T_1)c_s^b(0)|_{T_0}\eta(T_0)+c_s^0|_{T_0}\gamma(T_0)k(T_0)/[k(T_0)+c_v^e(T_0)]}{\gamma(T_0)\qquad\qquad 1+\eta(T_1)}. \tag{70}$$

Here we consider that the initial impurity concentration $c_s^0|_{T_1}$ at T_1 includes the total amount of impurity (i.e., impurity atoms in the free form and in complexes $c_s^0|_{T_1}=c_s(\infty)|_{T_0}+c_{vs}(\infty)|_{T_0}$).

In addition, if we change the temperature from T_1 again to T_0, expression (70) is transformed into (69) after the corresponding relaxation time.

Reducing both sides of relation (59) to the common denominator, we obtain a very simple relation which exactly corresponds to the impurity conservation law in any state (both in the free form and in complexes):

$$\frac{d}{l}\,c_s^b(\infty)\Big|_T+c_s(\infty)|_T+c_{vs}(\infty)|_T=\frac{d}{l}\,c_s^b(0)\Big|_T+c_s^0|_T. \tag{71}$$

It should be noted that the obtained formula is valid for an arbitrary temperature.

Using formula (59) (and knowing all the parameters D, k, c_v^e, γ, and c_s^0), we can predict the time interval after which the impurity concentration at the interface attains the dangerous limit (as regards the strength of the material) if it was high at the initial instant. This means that after this time interval, the material cannot be used. It can be seen from (59), however, that the direction of impurity segregation can be reversed by elevating the temperature since in this case the redistribution coefficient decreases, and a new equilibrium state will be attained as impurity atoms move from the interface to the bulk of the grain.

Moreover, formula (59) can be used to determine the time after which the impurity concentration at the interface attains the safety limit. It is important to note that, since the impurity diffusion coefficient increases significantly with temperature, the time over which the impurity concentration at the interface decreases and reaches the safety limit is much shorter than the service life of the material after which the concentration at the interface attains the dangerous limit.

By way of an example, let us estimate the change in temperature for which the service life t_{ex} is 1000 times longer than the time t_{re} of recovery of the safety concentration of impurity. The ratio of these times can be estimated to a high degree of accuracy as the ratio of the corresponding

effective diffusion coefficients $D_{\rm eff}^{\rm ex}$ and $D_{\rm eff}^{\rm re}$ (it is well known that the preexponential factor weakly depends on temperature). Considering that $k \gg c_v^e$ and $D_{\rm eff} \propto (c_v^e/k) D_{vs} \propto D_s/k$, we obtain

$$\frac{t_{\rm ex}}{t_{\rm re}} = \frac{D_{\rm eff}^{\rm ex}}{D_{\rm eff}^{\rm re}} = \frac{D_{\rm eff}^{\rm ex} k_{\rm re}}{D_{\rm eff}^{\rm re} k_{\rm ex}} \approx \frac{e^{-Q_D/T_{\rm ex}}}{e^{-Q_D/T_{\rm re}}} \frac{e^{-Q_k/T_{\rm re}}}{e^{-Q_k/T_{\rm ex}}}$$
$$\approx \exp\left\{ \frac{Q_D - Q_k}{T_{\rm ex}} \frac{\Delta T}{T_{\rm ex}} \right\},$$

where $\Delta T = T_{\rm ex} - T_{\rm re}$, and Q_D and Q_k are the activation energies for diffusion and decay of a complex respectively.

On the other hand, $t_{\rm ex}/t_{\rm re} \simeq 10^3$, and hence we can take the characteristic value $(Q_D - Q_k)/T_{\rm ex} \simeq 15-20$ for estimates. Consequently, $\Delta T/T_{\rm ex} \simeq 1/2-1/3$, i.e., the recovery temperature must differ by 25–50% from the operation temperature. Using the above estimate and the experimental values of $t_{\rm ex}$, $t_{\rm re}$, ΔT, and $T_{\rm ex}$, we can estimate the difference $Q_D - Q_k$. Using the values of diffusion activation energy for specific materials, we can estimate Q_k, and hence the constant k of equilibrium relative to the decay and formation of complexes also.

CONCLUSIONS

(1) The kinetics of impurity segregation at grain boundaries is studied at low temperatures under conditions when vacancy–impurity complexes play a significant role in segregation dominate in mass transfer (the complexes can increase or decrease the mobility of an impurity).
(2) A modified equation is obtained for an impurity with the effective diffusion coefficient containing the diffusion coefficients for the impurity and complexes with different weights. The temporal evolution of the impurity concentration for planar, spherical, and cylindrical grains at an arbitrary temperature is traced in the case of a dilute solution.
(3) An analysis of the kinetics of impurity segregation can provide additional information on the chemical equilibrium constant k (in fact, an analysis of the effective diffusion coefficient shows that this constant is determined by two energies of diffusion activation and not by one).
(4) A simple algebraic equation describing the enrichment as well as depletion of the interface with an impurity (depending on external conditions) is obtained for the segregation of the impurity in a complex as well as in a free form at the grain boundary.
(5) It is important to note that the obtained basic algebraic equation does not depend on the form of chemical potential of impurity at the interface (i.e., is valid for a dilute as well as a concentrated solution at the interface; this problem will be considered in a separate article).
(6) A similar approach can be used in the case of irradiated materials, when radiation-induced point defects form mobile complexes with impurity atoms with a high probability.

This research was partly financed by ISSEP, grants No. SPU042062 (V. V. Slezov) and No. PSU052094 (O. A. Osmaev).

APPENDIX

Let us write the system of equations (38), (39), and (41) taking into account the terms containing ε and having the following order of smallness:

$$\frac{\partial c_s}{\partial t} = D_{\rm eff} \Delta c_s - \frac{1}{\alpha(k + c_v^e)} \left[\frac{\partial \varepsilon}{\partial t} - D_{vs} \Delta \varepsilon \right],$$
$$c_{vs} = \frac{c_v^e}{k} c_s + \frac{\varepsilon}{\alpha k}, \quad c_v \cong c_v^e, \tag{A1}$$

where

$$D_{\rm eff} = \frac{k D_s + c_v^e D_{vs}}{k + c_v^e}.$$

In order to describe the evolution of c_s and ε, we use Eqs. (A1) and (3) with the following initial and boundary conditions (while writing the boundary conditions, we must consider a grain of a definite shape; here we analyze a plane-parallel grain of size $L = 2l$). It was proved in Sec. 3 and in Ref. 7 that an analysis of spherical or cylindrical grains is carried out similarly. We choose the system of coordinates so that its origin coincides with the center of the grain. It should be noted that all the conditions at the grain boundaries ($\pm l$) are identical, and hence the fluxes from the left and from the right are equal, while the fluxes at the center of the grain ($x = 0$) are absent in view of the symmetry of the problem, and hence $\nabla c|_{x=0} = 0$. While deriving the conditions for ε, we must substitute into (4) the initial and boundary conditions for c_s and c_{vs}:

$$c_s|_{t=0} = c_s'^0, \quad \left.\frac{\partial c_s}{\partial t}\right|_{x=0} = 0, \quad c_s|_{x=l} = \lambda(t); \tag{A2a}$$

$$\varepsilon|_{t=0} = 0, \quad \left.\frac{\partial \varepsilon}{\partial x}\right|_{x=0} = 0, \quad \varepsilon|_{x=l} = 0. \tag{A2b}$$

Carrying out the substitution $c_s = \tilde{c}_s + \lambda(t)$, we transform Eqs. (A1) and (3) into equations with homogeneous boundary conditions:

$$\frac{\partial \tilde{c}_s}{\partial t} = D_{\rm eff} \Delta \tilde{c}_s - \frac{1}{\alpha(k + c_v^e)} \left(\frac{\partial \varepsilon}{\partial t} - D_{vs} \Delta \varepsilon \right) - \frac{\partial \lambda}{\partial t}, \tag{A3a}$$

$$\frac{\partial \tilde{c}_s}{\partial t} = D_{\rm eff} \Delta \tilde{c}_s + \varepsilon - \frac{\partial \lambda}{\partial t}. \tag{A3b}$$

The initial and boundary conditions for $\tilde{c}_s$ become

$$\tilde{c}_s|_{x=l} = 0, \quad \tilde{c}_s|_{t=0} = c_s'^0 - \lambda(0), \tag{A4}$$

while the conditions for ε remain unchanged.

In order to find solutions of Eqs. (A3a) and (A3b), we first solve the corresponding homogeneous equations. Taking into account the boundary conditions, we can write these solutions in the form

$$\tilde{c}_s=\sum_n \tilde{c}^{\,s}_n(t)\cos k_n x, \quad \varepsilon=\sum_n \varepsilon_n(t)\cos k_n x, \tag{A5}$$

where $k_n=(\pi/l)(n+1/2)$. Substituting (A5) into the homogeneous parts of (A3a) and (A3b) and integrating them with corresponding cosines, we obtain

$$\dot{\tilde{c}}^{\,s}_n=-D_{\rm eff}k_n^2\tilde{c}^{\,s}_n-\frac{1}{\alpha(k+c_v^e)}(\dot{\varepsilon}_n+D_{vs}k_n^2\varepsilon_n), \tag{A6a}$$

$$\dot{\tilde{c}}^{\,s}_n=-D_s k_n^2\tilde{c}^{\,s}_n+\varepsilon_n. \tag{A6b}$$

As usual, we have

$$\tilde{c}^{\,s}_n=A_n\exp(\lambda_n t); \quad \varepsilon_n=B_n\exp(\lambda_n t). \tag{A7}$$

Substituting (A7) into (A6a) and (A6b), we obtain

$$A_n(\lambda_n+D_{\rm eff}k_n^2)+\frac{1}{\alpha(k+c_v^e)}(\lambda_n+D_{vs}k_n^2)B_n=0, \tag{A8a}$$

$$A_n(\lambda_n+D_s k_n^2)-B_n=0. \tag{A8b}$$

Using the initial condition for $\tilde{c}_s$, we determine $A_n(0)$ [note that $\tilde{c}^{\,s}_n|_{t=0}=A_n(0)$]:

$$A_n(0)=(c_s'^0-\lambda(0))\frac{2}{lk_n}(-1)^n. \tag{A9}$$

Using (A9), we can easily find $B_n(0)$ from (A8b):

$$B_n(0)=\frac{2k_n}{l}(-1)^n(D_s-D_{\rm eff})[c_s'^0-\lambda(0)]. \tag{A10}$$

From the homogeneous system (A8a) and (A8b), we obtain

$$\frac{\lambda_n^2}{\alpha(k+c_v^e)}+\left(1+\frac{(D_s+D_{vs})k_n^2}{\alpha(k+c_v^e)}\right)\lambda_n+\frac{D_{vs}k_n^2k_n^2D_s}{\alpha(k+c_v^e)}+D_{\rm eff}k_n^2=0. \tag{A11}$$

This expression shows that all $\lambda_n<0$ (since we are dealing with a quadratic equation with positive coefficients). Consequently, in the general solution (A5), only the terms satisfying the condition $|\lambda_n|t\leqslant 1$ at any instant of time are significant. These terms determine solution (A5) with an exponential accuracy. The values of λ_n satisfying the condition $|\lambda_n|t\geqslant 1$ make an exponentially small contribution to (A5).

Let us determine the time starting from which the terms appearing in Eq. (A11) have considerably different order of smallness. Estimating the terms of Eq. (A11) and taking into account the condition $|\lambda_n|t\leqslant 1$ (we compare the third and fifth terms:

$$\frac{(D_s+D_{vs})k_n^2\lambda_n t}{\alpha(k+c_v^e)t}\frac{1}{(D_{\rm eff}k_n^2)}\propto\frac{1}{\alpha c_v^e t}\ll 1$$

for $|\lambda_n|t\leqslant 1$, $D_s\ll D_{vs}$), we find that for a time $t\gg 1/(\alpha c_v^e)$, Eq. (A11) assumes the form

$$y^2+y+C=0, \tag{A12}$$

where

$$y=\frac{\lambda_n}{\alpha(k+c_v^e)}; \quad C=\frac{D_{vs}k_n^2k_n^2D_s}{[\alpha(k+c_v^e)]^2}+\frac{D_{\rm eff}k_n^2}{\alpha(k+c_v^e)}.$$

The condition $|\lambda_n|t\leqslant 1$ implies that $y\ll 1$ (indeed,

$$y_n=\frac{\lambda_n}{\alpha(k+c_v^e)}\frac{t}{t}\propto\frac{1}{\alpha(k+c_v^e)t}\ll 1,$$

since we consider the system not from the beginning of segregation, but starting from the time interval $t_0\gg t\gg 1/(\alpha c_v^e)$ which is most important for segregation, and starting from which the system of diffusion equations is simplified significantly; this characteristic time is longer than the time of an individual diffusive jump $t_{\rm dif}\approx 1/(\alpha c_v^e)=a^2/D_s$). In addition, the condition $y\ll 1$ implies that $C\ll 1$. Solving the quadratic equation (A12) and taking into account the condition for C, we obtain the roots

$$y_n^{(1)}=-C \ \text{ or } \ \lambda_n^{(1)}=-\left[\frac{D_{vs}k_n^2D_sk_n^2}{\alpha(k+c_v^e)}+D_{\rm eff}k_n^2\right], \tag{A13}$$

$$y_n^{(2)}=-1 \ \text{ or } \ \lambda_n^{(2)}=-\alpha(k+c_v^e). \tag{A14}$$

While determining $y_n^{(2)}$, we neglect the term C as compared to -1. It can be seen from (A14) that the second solution corresponding to the root $\lambda_n^{(2)}$ gives an exponentially small quantity of the order of $\exp[-\alpha(k+c_v^e)t]$. Consequently, we have only one solution with $\lambda_n^{(1)}$ which has a finite value.

Let us prove that for $|\lambda_n|t\leqslant 1$ and $t\gg 1/(\alpha c_v^e)$, the terms appearing in the expression for $\lambda_n^{(1)}$ have different orders of smallness, i.e., $\lambda_n^{(1)}=-D_{\rm eff}k_n^2$. Indeed,

$$\frac{D_{vs}k_n^2D_sk_n^2}{\alpha(k+c_v^e)}\frac{1}{D_{\rm eff}k_n^2}=\frac{D_{vs}D_s}{D_{\rm eff}^2}\frac{D_{\rm eff}k_n^2t}{\alpha(k+c_v^e)t}\propto\frac{D_{vs}D_s}{D_{\rm eff}^2}\frac{1}{\alpha(k+c_v^e)t}\ll 1.$$

It should be noted that

$$\frac{D_{vs}D_s}{D_{\rm eff}^2}\propto\frac{D_s/D_{vs}}{(D_s/D_{vs}+c_v^e/k)^2}.$$

Testing this expression for extremum, we find that it attains its maximum value for $D_s/D_{vs}=c_v^e/k$. Substituting the maximum value, we arrive at the following expression:

$$\frac{c_v^e/k}{(c_v^e/k+c_v^e/k)^2}\frac{1}{\alpha(k+c_v^e)t}\propto\frac{1}{4\alpha c_v^e t}\ll 1.$$

Consequently, for time $t\gg 1/(\alpha c_v^e)$, we can neglect the first term as compared to the second term in the expression for $\lambda_n^{(1)}$, i.e.,

$$\lambda_n^{(1)}=-D_{\rm eff}k_n^2. \tag{A15}$$

It can be seen from the condition $|\lambda_n|t\leqslant 1$ that the main contribution to the solution for a set of values of $\lambda_n^{(1)}$ comes from the values of n satisfying the condition $D_{\rm eff}k_n^2t\leqslant 1$, while the remaining terms make an exponentially small contribution.

The total solution of the system (A3a) and (A3b) is the sum of the solutions of the homogeneous equation obtained above and of the nonhomogeneous equation with the right-hand side for zero initial conditions (and for characteristic time $t\gg 1/(\alpha c_v^e)$). Using the standard approach of variation of an arbitrary constant, we obtain

$$\sum_n \cos k_n x \dot{A}_n(t) e^{\lambda_n t} + \frac{\partial \lambda}{\partial t} = 0, \tag{A16a}$$

$$\sum_n \cos k_n x [\dot{A}_n(t) e^{\lambda_n t} + A_n(t) \lambda_n e^{\lambda_n t} + D_s A_n(t) e^{\lambda_n t} k_n^2 - B_n e^{\lambda_n t}] + \frac{\partial \lambda}{\partial t} = 0. \tag{A16b}$$

From (A16a) and (A16b), we obtain

$$A_n = -\int_0^t \frac{\partial \lambda}{\partial t'} e^{-\lambda_n t'} \frac{2}{l k_n} (-1)^n dt', \tag{A17a}$$

$$B_n = A_n(\lambda_n + D_s k_n^2). \tag{A17b}$$

Finally, B_n is given by

$$B_n = \frac{2k_n}{l}(-1)^n (D_s - D_{\text{eff}}) \left(-\int_0^t \frac{\partial \lambda}{\partial t'} e^{-\lambda_n t'} dt' \right). \tag{A18}$$

The total solution (A5) taking into account (A9), (A10), (A17a), and (A18) assumes the form

$$\tilde{c}_s = \sum_{n=0}^{\infty} \frac{2}{l k_n} (-1)^n \left[c_s'^0 - \lambda(0) - \int_0^t \frac{\partial \lambda}{\partial t'} e^{-\lambda_n t'} dt' \right] e^{\lambda_n t} \cos k_n x, \tag{A19a}$$

$$\varepsilon = \sum_{n=0}^{\infty} \frac{2k_n}{l} (-1)^n (D_s - D_{\text{eff}}) \left[c_s'^0 - \lambda(0) - \int_0^t \frac{\partial \lambda}{\partial t'} e^{-\lambda_n t'} dt' \right] e^{\lambda_n t} \cos k_n x. \tag{A19b}$$

Estimating ε from (A19b) (here we take into account the fact that $D_s - D_{\text{eff}} \propto D_{\text{eff}}$ and $\lambda_n = -D_{\text{eff}} k_n^2$), we obtain

$$\varepsilon \propto \sum_{n=0}^{\infty} \frac{2}{l k_n} (-1)^n \lambda_n \left[c_s'^0 - \lambda(0) - \int_0^t \frac{\partial \lambda}{\partial t'} e^{-\lambda_n t'} dt' \right] e^{\lambda_n t} \cos k_n x. \tag{A20}$$

It can be seen from (A20) and (A19a) that the differentiation of $\tilde{c}_s$ with respect to time [where $\tilde{c}_s = c_s + \lambda(t)$] gives the following relation accurate to $D_s / D_{\text{eff}} \ll 1$:

$$\varepsilon \propto \frac{\partial c_s}{\partial t} \cong -\frac{c_s}{t}. \tag{A21}$$

It will be shown below that, for a time $t < t_0$, the parameter c_s is described by a power function of time to a high degree of accuracy. For $t \approx t_0$ (i.e., for a time of the order of that corresponding to the end of segregation), the value of c_s depends on a small number of terms (see (A19a)), and the derivative $\partial c_s / \partial t \propto -c_s / t_0$. The same result can be obtained directly from (3) by using Eq. (A1). Thus, using Eq. (A1) and the estimate (A21) for ε, we can easily prove that all terms in Eq. (A1) with ε contains a small parameter $[\alpha(k + c_v^e)t]^{-1} \ll 1$ as compared to the terms containing c_s. Indeed, the Laplacian $\Delta \propto 1/D_{\text{eff}} t$; $\varepsilon \propto c_s / t$; $\partial \varepsilon / \partial t \propto c_s / t^2$; $\partial c_s / \partial t \propto c_s / t$; $D_{\text{eff}} \Delta \varepsilon \propto c_s / t^2$. Equation (A1) leads to

$$\frac{c_s}{t} \propto \frac{c_s}{t} - \frac{1}{\alpha(k + c_v^e)} \left[-\frac{c_s}{t^2} - \frac{c_s}{t^2} \right] \propto \frac{c_s}{t} \left[1 + \frac{2}{\alpha(k + c_v^e)t} \right].$$

Consequently, we obtain a closed equation for c_s accurate to terms of the order of $[\alpha(k + c_v^e)t]^{-1}$ as compared to unity, and Eq. (3) defines ε. Therefore, we can replace the second equation by the condition $\varepsilon \approx 0$ to within small terms indicated above.

Indeed, $\varepsilon \propto c_s / t \to \varepsilon / c_s \propto 1/t$ or $\varepsilon / \alpha c_v^e c_s \propto 1 / \alpha c_v^e \ll 1$, $(\alpha k c_{vs} - \alpha c_v^e c_s)(\alpha c_v^e c_s)^{-1} \propto (\alpha c_v^e t)^{-1} \ll 1$.

*E-mail: berezhnoy@pem.kharkov.ua

[1] D. McLean, *Grain Boundaries in Metals*, Clarendon Press, Oxford, 1957.
[2] L. Karlsson, Acta Met. **36**, 25 (1988).
[3] L. A. Girifalco, Acta Met. **13**, 583 (1965).
[4] H. Kahn and L. A. Girifalco, Acta Met. **14**, 749 (1966).
[5] R. M. Asimov, Acta Met. **14**, 1005 (1966).
[6] G. G. Samsonidze, A. N. Orlov, and Yu. V. Trushin, Fiz. Metal. Metalloved. **55**, 676 (1983).
[7] V. V. Slezov, L. N. Davydov, and V. V. Rogozhkin, Fiz. Tverd. Tela (St. Petersburg) **37**, 3565 (1995) [Solid State **37**, 1964 (1995)].
[8] V. V. Slyozov and P. A. Bereznyak, *Irradiation Creep of Metals in Physics of Radiation Effects in Crystals* (ed. by R. A. Johnson and A. N. Orlov), Elsevier Science Publ. (1986).
[9] V. V. Slezov and L. V. Tanatarov, Metallofizika **10**, 90 (1988).
[10] L. Landau and E. Lifshitz, *Theoretical Physics. Statistical Physics, Pts. 1 and 2*, 3rd ed., Pergamon, Oxford, 1980.
[11] B. S. Bokshtein, I. V. Kopetskii, and L. S. Shvindlerman, *Thermodynamics and Kinetics of Grain Boundaries in Metals* [in Russian], Metallurgiya, Moscow (1986).

Translated by R. S. Wadhwa

SHORT NOTES

The role of long-wave longitudinal phonons in kinetics of insulators

R. N. Gurzhi and A. V. Yanovskiĭ

*B. Verkin Institute for Low Temperature Physics and Engineering, National Academy of Sciences of the Ukraine, 310164 Kharkov, Ukraine**

(Submitted July 10, 1996)
Fiz. Nizk. Temp. **23**, 233–235 (February 1997)

It is shown that long-wave longitudinal phonons considerably affect heat transfer in most of existing crystals in spite of symmetry degeneracy of transverse vibrational branches. This is because of close values of phase velocity of transverse phonon modes in these crystals. Such effects are most pronounced in phonon hydrodynamics and in the propagation of second sound. It is shown that the thermal conductivity of bulk samples is a nonmonotonic function of the parameter characterizing the difference between the velocities of transverse modes. © *1997 American Institute of Physics.* [S1063-777X(97)01202-4]

1. Three-phonon processes involving at least one longitudinal partner can exist in the following two forms: (a) collisions $l+t\leftrightarrow l$, $l\leftrightarrow t+t$ (l is the longitudinal and $t\equiv t_{1,2}$ are transverse vibrational modes) in which the mean free path of long-wave longitudinal phonons (LLP) increases with decreasing frequency ω in proportion to ω^{-4} irrespective of the symmetry of the crystal lattice, and (b) collisions $l+t_{1,2}\leftrightarrow t_{2,1}$ in which the mean free path of LLP is proportional to ω^{-n}. Depending on crystal symmetry, the value of n can be equal to[1] 2, 3, or 4: $n=2$ corresponds to the tangency of transverse branches at the point of symmetry degeneracy, $n=3$ to their intersection, and $n=4$ to the absence of degeneracy or, on the contrary, to complete coincidence of transverse modes (the model of isotropic elastic medium).

The processes in which the mean free path $l(\omega)$ of LLP increases for $\omega\to 0$ in proportion to ω^{-n} with $n\geqslant 3$ alone cannot ensure a finite thermal conductivity. In this case, the thermal conductivity $\kappa\sim\int\omega^2 l(\omega)d\omega$ diverges (the so-called Pomeranchuk problem).[2] The Rayleigh scattering at impurities does not help either since $l(\omega)\propto\omega^{-4}$ in this case.

However, most crystals accessible to experimental investigations have a symmetry (and elastic properties) for which the processes $l+t_{1,2}\leftrightarrow t_{2,1}$ are allowed; in this case, $n=2$, and it may appear that the problem does not exist. It is usually assumed that the kinetic properties of insulators at low temperatures (excluding very dirty samples) are mainly determined by phonons.[3,4] In this connection, it is appropriate to mention the fact underlying the subsequent analysis: in most crystals, the transverse modes t_1 and t_2 differ insignificantly:

$$\delta=\max_{\mathbf{f}}\frac{|s_{t_1}(\mathbf{f})-s_{t_2}(\mathbf{f})|}{s_{t_1,t_2}(\mathbf{f})}\ll 1,$$

where s_{t_1,t_2} are the phase velocities of the corresponding transverse modes depending on the direction of the wave vector $\mathbf{f}$. These substances are close in their properties to an isotropic elastic medium (see Table I; metals can be of interest in the superconducting state).

In such crystals, the energy of transverse phonons participating in the processes $l+t_{1,2}\leftrightarrow t_{2,1}$ is considerably higher (by a factor of δ^{-1}) than the energy of longitudinal phonons according to the conservation laws: $\omega_{t_1}\sim\omega_{t_2}\sim\delta^{-1}\omega_l\gg\omega_l$. Consequently, the Herring mechanism has a threshold for high frequencies since the number of corresponding transverse phonons with energy $\omega_{t_{1,2}}>T$ is exponentially small for $\omega_l>\delta T$.[5] We can write the reciprocal relaxation time for LLP in such processes in the form ($x=\omega T^{-1}$)

$$\tau_H^{-1}(x)\equiv s_l l_H^{-1}(x)\sim\begin{cases}x^2\delta^{-1}, & x\ll\delta;\\ x^5\delta^{-4}\exp\{-x\delta^{-1}\}, & \delta\ll x\leqslant 1.\end{cases}\tag{1}$$

It is usually assumed that $\delta\sim 1$, and hence $\tau_H^{-1}(x)\sim x^2$.

2. In bulk samples, the processes $l+t_{1,2}\leftrightarrow t_{2,1}$ remove the divergence in thermal conductivity, confining the integration domain (lower limit) to the cutoff frequency ω_0 which can be determined from the equation

$$l_H^{-1}(x_0)=(l_N^{-1}+l_i^{-1})x_0^4,\quad x_0=\omega_0 T^{-1}.$$

Here $l_N\propto T^{-5}$ and $l_i\propto T^{-4}$ are the mean free paths for thermal phonons relative to scattering at one another and at ''impurities'' respectively.[1)]

Under the conditions when the LLP contribution dominates, and truncation takes place above the threshold for the Herring mechanism, we obtain the following expressions in the Callaway approximation:

$$\kappa\approx Cs_l(l_N^{-1}+l_i^{-1})^{-1}x_0^{-1}\left[1-\frac{5}{4}(R_1^{-2}+R_2^{-2})\frac{\delta}{x_0}+\left(2+\frac{l_i}{l_N}\right)x_0+\ldots\right];$$

TABLE I. Values of parameter δ for some materials.

	Substance									
	^{4}He	NaF	LiF	H_2	D_2	CdS	Al	BaF_2	Some quasi-crystals	W
δ	1/5	1/7	1/8	0.1	0.1	0.1	<0.1	$5\cdot10^{-2}$	$2\cdot10^{-2}$	$2\cdot10^{-3}$

$$x_0 \approx \delta \ln\left[\frac{e l_H^{-1}(\delta)}{\delta^4(l_i^{-1}+l_N^{-1})}\right]; \tag{2}$$

$$5\delta \ll x_0 \ll \min\left(\frac{l_N}{l_i},1\right). \tag{3}$$

Here $C\propto T^3$ is the heat capacity, $R_{1,2}$ are the main radii of curvature of the surface defined by the equation $\rho(\mathbf{f})=\delta^{-1}s_t^{-1}|s_{t_1}(\mathbf{f})-s_{t_2}(\mathbf{f})|$ at the point corresponding to the maximum value of ρ (ρ is the radius in the spherical system of coordinates; by definition, $\delta,\rho_{\max}=1$).

The obtained result can be interpreted easily: if the main contribution to thermal conductivity comes from phonons with a frequency $\omega_0 \ll T$, we have $\kappa \approx Cs_l l_{\rm tr}(x_0)x_0^3 \approx Cs_l(l_N^{-1}+l_i^{-1})^{-1}x_0^{-1}$, where x_0^3 reflects the statistical weight of LLP. Hence, it follows that, for $\delta \ll 1$, the thermal conductivity is anomalously large ($x_0 \ll 1$) and has a peculiar dependence on temperature T and point defect concentration η. For pure samples ($l_i \gg l_N$), the thermal conductivity $\kappa \propto T^{-2}$ (in a conventional analysis,[3] we have $\kappa \propto T^{-1}\eta^{-1}$), while for dirty samples ($l_i \ll l_N$) we have $\kappa^{-1}\propto T\eta\ln(T\eta\delta^{-3})$ (normally, $\kappa^{-1}\propto T^{3/2}\eta^{1/2}$).[8] It should be noted that for $\delta=1/5$, the contributions from thermal phonons to LLP are generally of the same order of magnitude.

It follows from (1) and (2) that with increasing δ, the cutoff frequency $\omega_0=x_0(\delta)T$ increases at a lower rate than the linear function of this parameter. As a result, the left inequality in (3) is violated. For dirty samples, this leads to a nonmonotonic dependence of thermal conductivity κ on δ. Indeed, according to (2), for $x_0 \ll \delta$ we have $\kappa^{-1}\sim\delta\ln(\delta^{-3})$, while for $x_0<\delta$, $\kappa\sim\delta^{1/2}$ according to calculations (see Fig. 1).

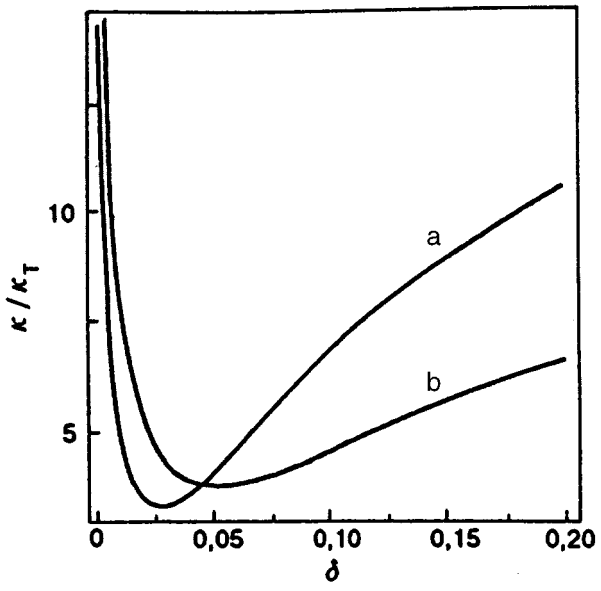

FIG. 1. Thermal conductivity of dirty samples as a function of the parameter δ reduced to the contribution from thermal phonons $\kappa_T=Cs_l l_i$ for $l_N/l_i=1000$ (a) and 100 (b).

3. In the case of hydrodynamic heat transfer, LLP in samples with a finite size are manifested in a different way: $l_N \ll d \ll \sqrt{l_N l_i}$.

(a) For thin samples, a specific nonlocal hydrodynamics is manifested. In this case, the interaction between the phonon gas layers moving with different velocities is realized through LLP whose mean free path is comparable with the size of the system.[5]

Let us consider the conditions required for this effect which have not been analyzed earlier and which are obtained from the requirement of smallness of the first corrections to thermal conductivity determined by the solution of the integral equation in nonlocal hydrodynamics (see Ref. 5) taking into account relation (1):

$$[dl^{-1}(x_0)]^{7/4}=[dl_N^{-1}x_0^4]^{7/4} \ll 1, \tag{4}$$

where

$$x_0 \simeq \delta \ln\left[\frac{e l_N}{\delta^4 l_H(\delta)}\right], \quad l(x)=l_N x^{-4}.$$

(b) For samples with a larger thickness, peculiar local hydrodynamics with the viscosity $\mu=s_l l_{\rm eff}$, where $l_{\rm eff}\approx x_0^3 l(x_0)=l_N x_0^{-1}$, is realized for $1<x_0^{-4}\ll dl_N^{-1}$. The viscosity is determined by LLP with the mean free path $l(x_0)\gg l_N$ (the factor x_0^3 reflects the number of such phonons, $l(x_0)\ll d$). As a result, for $\delta \ll 1/5$, we determine not l_N (as usually assumed), but a larger quantity $l_{\rm eff}\approx l_N x_0^{-1}$ from experiments on Poiseuille flow of a phonon gas.

Similar considerations are applicable for the problem of attenuation of second sound whose wavelength plays the role of d in this case.

Finally, it should be noted that nonlocal hydrodynamics is most suitable for determining the role of LLP since condition (4) contains the small parameter x_0 to the seventh power, while x_0 appears in condition (3) only to the first power.

*E-mail: gurzhi@ilt.kharkov.ua

[1)]The divergence can be removed if we take into account the finiteness of the lifetime of longitudinal thermal phonons, i.e., the Simons mechanism,[6] which makes the $l+l\leftrightarrow l$ processes involving LLP allowed. However, according to calculations,[7] the corresponding mean free path l_S is apparently too large: $l_S\approx 10^4 T^{-2} l_N$ for solid hydrogen and $l_S\approx 4\cdot10^6 T^{-2} l_N$ for NaCl, where T is measured in degrees Celsius.

[1] C. Herring, Phys. Rev. **95**, 954 (1954).
[2] I. Ya. Pomeranchuk, Zh. Eksp. Teor. Fiz. **11**, 246 (1941).
[3] R. Berman, *Thermal Conduction*, Oxford University Press, Oxford (UK) (1976).
[4] T. N. Antsygina and V. A. Slyusarev, Fiz. Nizk. Temp. **19**, 494 (1993) [Low Temp. Phys. **19**, 348 (1993)].
[5] R. N. Gurzhi and A. O. Maksimov, Pis'ma Zh. Éksp. Teor. Fiz. **27**, 252 (1978) [JETP Lett. **27**, 236 (1978); Fiz. Nizk. Temp. **4**, 1321 (1978) [Sov. J. Low Temp. Phys. **4**, 623 (1978)].
[6] S. Simons, Proc. Phys. Soc. **82**, 401 (1977).
[7] R. N. Gurzhi and A. O. Maksimov, Fiz. Nizk. Temp. **3**, 356 (1977) [Sov. J. Low Temp. Phys. **3**, 171 (1977)].
[8] V. L. Gurevich, *Kinetics of Phonon Systems* [in Russian], Nauka, Moscow (1980).

Translated by R. S. Wadhwa

Electron paramagnetic resonance measurements of static magnetic susceptibility

F. G. Cherkasov, I. V. Ovchinnikov, A. N. Turanov, S. G. L'vov, and V. A. Goncharov

*Kazan' Physicotechnical Institute, Russian Academy of Sciences, 420029 Kazan', Russia**

A. Ya. Vitols

Riga Technical University, LV-1656 Riga PDP, Latvija
(Submitted October 28, 1996)
Fiz. Nizk. Temp. **23**, 236–239 (February 1997)

It is shown that the total volume magnetic susceptibility of a substance can be measured in principle with the help of electron paramagnetic resonance (EPR). For this purpose, the conventional EPR technique can be used along with a known reference compound with a very narrow resonant absorption line. The accuracy of absolute susceptibility measurements is comparable to that of classical methods. © *1997 American Institute of Physics.*
[S1063-777X(97)01302-9]

Classical methods of measurement of static magnetic susceptibility have become conventional in everyday laboratory experiments. In recent years, high-sensitivity (SQUID) magnetometers are being used widely in the study of macroscopic properties of materials. At the same time, information on a nontraditional approach to the determining of volume magnetic susceptibility appeared in the literature. This approach is based on analysis of chemical shifts of protons (^{1}H) in the nuclear magnetic resonance (NMR) spectra and is intended for studying liquid media.[1,2] We propose that electron paramagnetic resonance be used for this purpose.

The volume susceptibilities of paramagnetic materials can be measured with the help of a conventional stationary EPR spectrometer. The detecting element of such a spectrometer plays the role of a magnetometer if we use the so-called reference compounds with a narrow high-intensity EPR line[1)] in our measurements (the arrangement of the reference sample and the substance under investigation in a measuring ampule for specimens will be given below). In the presence of the substance under investigation, a splitting of the narrow line of the reference material was observed; as expected, this splitting was proportional to the volume susceptibility of the substance under investigation. As a result, the procedure of experimental determining the susceptibility was reduced to the recording to the spectrum of the reference specimen. The EPR signals from the materials under investigation did not hamper the measurements since these signals actually were not detected in the mode for observation of the narrow line.[2)] Thus, we propose here a resonant method suitable for absolute measurements of the volume magnetic susceptibility of solid, liquid, and liquid-crystal materials.

EPR spectra were measured in the 3-cm wavelength range[3)] on the radiospectrometer BER-418S at room temperatures and under conventional requirements for correct recording of very narrow EPR signals.[3,4] The samples were placed in coaxial cylindrical glass or quartz ampules of diameter 5–6 mm. The objects under investigation were weakly magnetic substances with a low and high volume susceptibility. The reference sample was in the form of a LiF crystal with very small high-purity particles of metallic lithium.[5,6] Such particles with a typical size 0.6–1 μm were obtained in LiF single crystals exposed to a high-intensity neutron beams (after thermal annealing and tempering in liquid nitrogen). Such particles were also formed in LiF during solid-phase electrolysis. After irradiation (or electrolysis), the crystals were crushed and used for measurements in the form of granules with a diameter 0.1–0.2 mm. Any of such granules was characterized by a solitary symmetric EPR line (on conduction electrons) with a peak width ΔH_{pp}(300 K) $\simeq$40–70 mG. The signal was strong enough even at low levels of microwave power ($P\sim 10^{-4}$ W) in the resonator for a magnetic field modulation depth 10–30 mG. Precision measurements of the g-factor revealed that it is isotropic and differs from the value g_0 for a free electron by $\delta g = g - g_0 = (-3 \pm 4)\cdot 10^{-6}$ (where $g_0 = 2.00229$) in the temperature range 9–400 K. The magnetic susceptibility of the irradiated reference sample including the diamagnetic contribution from the LiF matrix and the paramagnetic contribution from coloring centers and the metal is[7] $\chi_n = -0.88\cdot 10^{-6}$ at 20 °C.[4)] The volume susceptibility χ_c of the sample obtained electrolytically is determined by the diamagnetic susceptibility in LiF and is close to the value $-1.07\cdot 10^{-6}$ (20 °C); consequently, such a sample is most convenient for susceptibility measurements in the temperature range from 4.2 to 800 K. The resonant properties of LiF with metallic Li and the prospects of its application in magnetic studies are considered in Refs. 5 and 6.

The method of magnetic susceptibility measurement is based on the measurement of splitting of the narrow EPR line for the reference sample in the case of the transverse orientation of the axis of the measuring ampule relative to the external constant magnetic field H_0 (in the resonator of the spectrometer). The ampule geometry and the observed EPR spectra are shown schematically in Fig. 1. The EPR spectrum of the reference sample contained a single narrow line for any arrangement of the sample in the ampule. If we

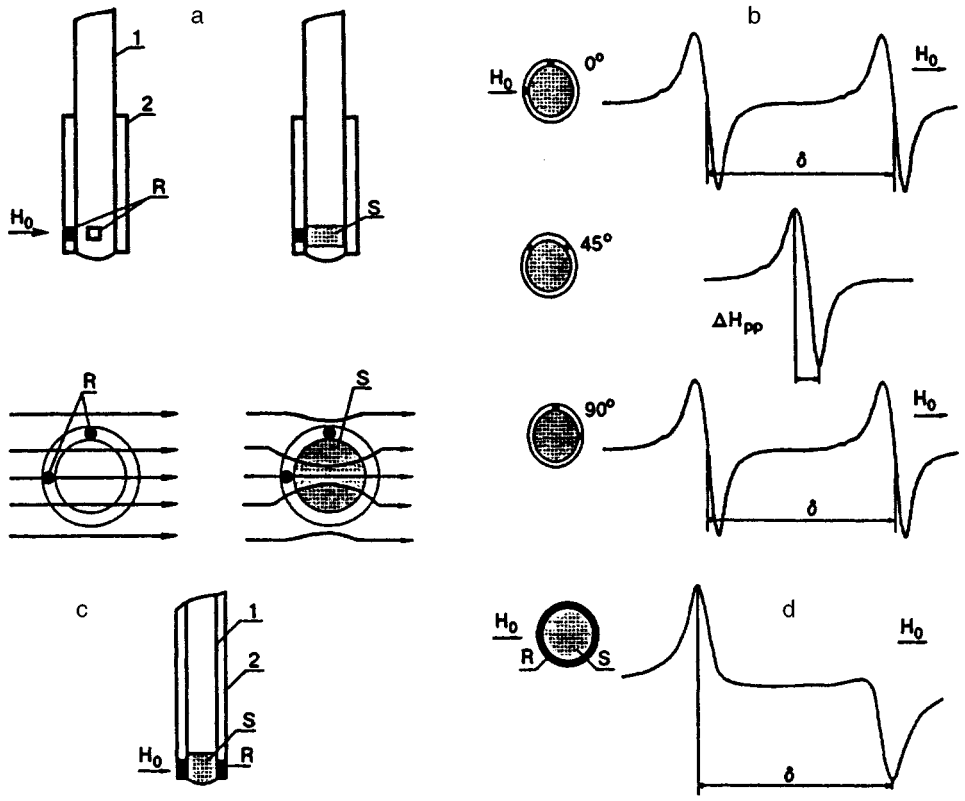

FIG. 1. Construction of the ampule for samples (a,c) and the observed maximum splitting δ of the EPR signal for the angles of rotation 0 and 90° ampule of the relative to the applied field H_0 for a pointlike reference sample (b) and for an arbitrary position of the ampule for an annular reference sample (d); central tube (*1*), outer tube of the ampule (*2*), reference sample (*R*), and the substance under investigation (*S*); the change in the magnetic flux density in the presence of a paramagnetic material is shown schematically in the lower part of a (on the right).

place a substance (in the form of a powder, single crystal, or liquid) with unknown susceptibility into the inner tube and fix two granules of the reference sample in the annular plane of the ampule as shown in Figs. 1a and b, the EPR spectrum will contain two narrow lines instead of one. In the case when a ''continuous'' annular reference sample was used, the EPR signal was smeared and had the form of a overmodulated line (see Figs. 1c and d). In both cases, the signal ''splitting'' occurs due to the nonuniformity of the magnetic field created by the substance under investigation and depends linearly on the susceptibility χ of the substance:

$$\delta = H_0(\alpha + \beta\chi), \tag{1}$$

where the coefficients α and β are different for different configurations of experiment and are determined by the geometrical parameters of the ampule and by the susceptibilities of the reference sample and the ampule material[1,8] ($\beta \sim 4\pi$ in the CGSM units and of the order of unity in the SI units). For substances under investigation with susceptibilities $(1-2)\cdot 10^{-5}$, the average splitting $\delta \simeq 0.5$ G for a pointlike reference sample is measured with an error 0.01–0.02 G in view of inaccuracy in the fixation of the ampule (to within $\pm 2.5°$). Consequently, the relative error in the determination of susceptibility on the basis of formula (1) is 2–3%. For substances with a high susceptibility, this error is accordingly smaller. It should be noted that the application of small reference samples makes it possible to operate with a very small amount of substance ($\sim$10–20 mg), and the ampule with an annular reference sample (Fig. 1c) is more convenient for measuring the temperature dependences of χ.

The EPR measurements which make it possible to determine χ from the gauge data for substances with known magnetic susceptibilities are most suitable and reliable. In this case, the coefficients α and β can be regarded as gauge constants which can be estimated from susceptibility data for two or three standard substances by using the ampule with a pointlike or annular reference sample (see Figs. 1a and c). It can be seen from Fig. 2 that a linear dependence of $\delta(\chi)$ is observed for most of paramagnetic materials. The magnetic susceptibilities of these substances were measured by the

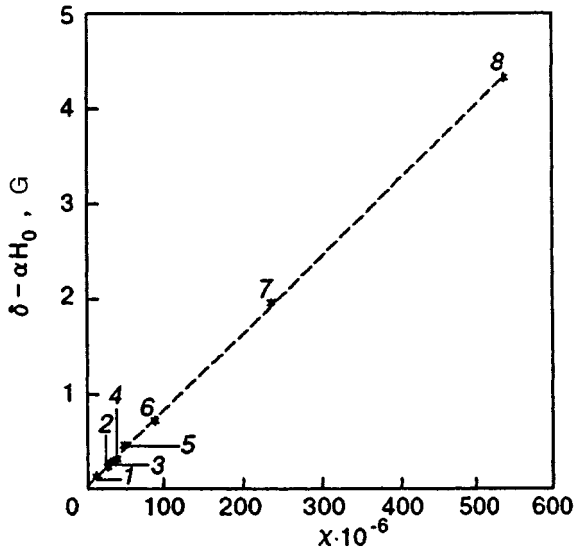

FIG. 2. Dependence of the splitting δ of the EPR signal on the volume susceptibility χ for some paramagnetic materials: $CuSO_4 \cdot 5H_2O$ (*1*); $NiSO_4 \cdot 7H_2O$ (*2*); $Cr_2(SO_4)_3 \cdot 18H_2O$ (*3*); $HgCo(CNS)_4$ (*4*); $FeCl_3$:C_2H_2OH (*5*); $Fe_2(SO_4)_3 \cdot 9H_2O$ (*6*); $MnSO_4 \cdot 7H_2O$ (*7*); Gd_2O_3 (*8*).

Faraday method to within 1%. The values of δ were measured with the help of an ampule with an annular reference sample of height 5–6 mm. It should be noted that powder samples were investigated in the form of pressed pellets since the accuracy in the measurements of χ was determined to a considerable extent by the homogeneity and reproducibility of ampule filling with the sample.

It should be noted in conclusion that the potentialities of an EPR magnetometer are determined to a considerable extent by the parameters and properties of the reference sample. At the present time, the EPR measurements for metallic lithium in LiF at frequencies up to 550 GHz, i.e., in magnetic fields of strength up to 195 kG, can be regarded as feasible; such experiments will make it possible to improve the accuracy of EPR measurements of susceptibility with the help of the given (Li–LiF) reference sample. It would be also practical to use this sample for studying the magnetic parameters of substances in the temperature range from 2 to 800 K. In this connection, the resonant method can be applied, for example, in the analysis of the total susceptibility of metals and superconductors and for studying anisotropy in the magnetic susceptibility and orientational dynamics of paramagnetic liquid crystals.[9]

The authors are grateful to G. B. Teitelbaum, Yu. V. Yablokov, and N. N. Garif'yanov for fruitful discussions and valuable comments.

This research was carried out under the support of the Russian Foundation of Fundamental Studies (Grants Nos. 96-02-18255 and 96-03-32725).

*E-mail: fred@dionis.kfti.kcn.ru

1) The absorption line characterized by the peak width $\Delta H_{pp} < 0.1$ G is observed in substances with a spin concentration of 10^{20} spins/cm^3 and higher.[3,4] Here ΔH_{pp} is the separation between nearest experimental points on the absorption curve.

2) The only exception is metal–ammonia solutions and other substances with a very narrow EPR line.[4]

3) That is, at a frequency of 9.4 GHz in a constant magnetic field of the order of 3.4 kG. The natural nonuniformity of the magnetic field in the volume ~ 1 cm^3 did not exceed 0.03 G/cm.

4) All values of susceptibility are given in the CGSM system of units.

[1] K. M. Emsley, J. Feeney, and L. H. Sutcliff, *High Resolution Nuclear Magnetic Resonance Spectroscopy*, vol. 1, Pergamon Press, Oxford (1965).
[2] S. G. Vul'fson, *Molecular Magnetochemistry* [in Russian], Nauka, Moscow (1991).
[3] C. P. Poole, *Electron Spin Resonance*, Wiley, New York (1967).
[4] C. P. Poole and H. A. Farach, *Handbook of Electron Spin Resonance*, Amer. Inst. of Phys., USA (1994).
[5] F. G. Cherkasov, G. A. Denisenko, A. Ya. Vitols *et al.*, in *Magnetic Resonance and Related Phenomena, Proc. of the 27th Congress AMPERE* (ed. by Salikhov), vol. 1, Kazan (1994).
[6] F. G. Cherkasov, S. G. L'vov, G. A. Denisenko *et al.*, in *4th Int. Symp. on ESR Dosimetry and Applications* (ed. by D. Regulla), Munich (1995).
[7] A. Van Den Bosch, Radiat. Effects **19**, 129 (1973).
[8] J. R. Zimmerman and M. R. Foster, J. Phys. Chem. **61**, 282 (1957).
[9] I. V. Ovchinnikov, I. G. Bikchantaev, and Yu. G. Galyametdinov, *Radiospectroscopy of Condensed Media* [in Russian], Nauka, Moscow (1990).

Translated by R. S. Wadhwa

Reflection and transformation of acoustic waves at the interface in superfluid ^{3}He-*A*

Sh. E. Kekutiya and N. D. Chkhaidze

Institute of Cybernetics, Georgian Academy of Sciences, 310086 Tbilisi, Georgia
(Submitted November 9, 1995; revised September 2, 1996)
Fiz. Nizk. Temp. **23**, 135–139 (February 1997)

The reflection and transformation of acoustic waves in ^{3}He-*A* and ^{3}He-A_1 is considered in two cases: (1) at the boundary of a solid impermeable wall for an arbitrary angle of incidence, and (2) for a normal incidence of waves at the interface between a free liquid and a system of periodic plane-parallel capillaries filling the half-space. In the first case, the reflection coefficient of first and second sounds, spin and spin–temperature waves, and the coefficients of mutual transformation of these waves are calculated. It is shown that a longitudinal spin wave is not transformed into other waves and experiences instead the total reflection at the solid wall. The angle of incidence for which the energy attenuation coefficient of first sound attains its maximum value is calculated as well as the angular interval corresponding to attenuation and total internal reflection of second sound. In the second case, the coefficients of excitation of fourth sound and of a magnetoacoustic wave by the first and second sounds, the reflection coefficients for the first and second sounds and for a longitudinal spin wave, the coefficient of transformation of first sound into second sound and vice versa, and the coefficient of reflection of fourth sound at the interface between the capillary system and the free liquid, and the coefficient of excitation of a longitudinal spin wave in free helium by the same wave in a capillary are calculated.
[S1063-777X(97)00102-3]

At temperatures of the order of millikelvins, quasiparticles in liquid ^{3}He in the triplet state with the relative orbital angular momentum $L=1$, experience Cooper pairing leading to a transition to the superfluid state. In zero magnetic field, liquid ^{3}He exists in two superfluid phases known as the *A*- and *B*-phases. In a strong magnetic field, another superfluid phase ^{3}He-A_1 exists in a certain temperature range between normal ^{3}He and ^{3}He-*A*.

We shall consider here the ^{3}He-*A* phase in zero magnetic field as well as the phase ^{3}He-A_1. In both phases, the unit vector **l** determines the direction along which the orbital angular momentum of Cooper pairs has a component $L_z=1$. The superfluid liquid ^{3}He-*A* is a coherent mixture of two superfluid components characterized by Cooper pairing in the spin configurations $s_z=\pm 1$ along the unit vector **s**, while ^{3}He-A_1 contains Cooper pairs in the single spin state $s_z=1$.

The MNR method is a powerful tool for studying the properties of superfluid ^{3}He. However, rich and valuable information on the properties of ^{3}He can also be extracted from an analysis of oscillations propagating in it.

Wave processes can be described by a system of hydrodynamic equations. Since the phases under investigation are anisotropic liquids, the phenomenological coefficients appearing in these equations are tensors. In order to simplify calculations, we shall not take into account this anisotropy explicitly. Moreover, the equilibrium texture of the vectors **l** and **s** is uniform in the problems under consideration. Consequently, we can use hydrodynamic equations given in Ref. 1. It should be noted here that the vector **l** can be considered to be rigidly fixed in acoustic processes.[2]

Superfluid phases of ^{3}He can transmit various types of waves. Normal acoustic modes in unbounded ^{3}He-*A* are the first and second sounds as well as a longitudinal spin wave, while in ^{3}He-A_1 such modes are first sound and a spin–temperature wave. In the case of complete stagnation of the normal component in capillaries, normal modes are the fourth sound and the longitudinal spin wave in ^{3}He-*A* and a magnetoacoustic wave in ^{3}He-A_1. In addition, a viscous diffuse mode in which only the normal component oscillates (if we neglect the tensor nature of kinetic coefficients appearing in the hydrodynamic equations) also exists in ^{3}He-*A* and ^{3}He-A_1.[3]

In this publication, we analyze the reflection and transformation of acoustic waves in ^{3}He-*A* and ^{3}He-A_1 in two different cases: (1) at the boundary with a solid impermeable wall for an arbitrary angle of incidence of a wave, and (2) for the normal incidence of waves at the interface between a free liquid and a system of plane-parallel periodic capillaries filling the half-space.

1. REFLECTION AND TRANSFORMATION OF WAVES IN ^{3}He-*A* AND ^{3}He-A_1 AT THE BOUNDARY WITH A SOLID IMPERMEABLE WALL

The reflection of waves at a solid wall in a superfluid liquid is peculiar since several types of waves can propagate in the liquid. When an acoustic wave is incident at the wall, the reflection of the sound is accompanied by the excitation of other types of acoustic waves as well as a viscous wave which is the main mechanism of acoustic energy dissipation in the given case.

Assuming that the wall is perfectly rigid, nonmagnetic, and perfectly heat insulating, we obtain the following boundary conditions: the equality to zero of the normal component (along the x-axis) of the total fluxes of mass, magnetization, and heat as well as the ''slippage'' condition for the velocity of normal flow (we use the same conditions as in Ref. 4). In the case of ^{3}He-A, these conditions have the form

$$v_{sx}=0, \quad w_{spx}=0, \quad v_{nx}=0,$$
$$v_{ny}=-\frac{1+P}{1-P}\,\xi\,\frac{\partial v_{ny}}{\partial x}, \tag{1}$$

where $\mathbf{v}_n$ is the normal velocity, $\mathbf{v}_s$ the conventional superfluid velocity, $\mathbf{w}_{sp}$ the superfluid spin velocity, ξ the slip length, and P the specular factor of quasiparticles.

We now consider the motion of the liquid as a superposition of the incident and reflected waves. In this case,

$$\begin{aligned}
&\mathbf{v}_n=\sum_{j=1}^{2}\nabla(Q_j+\widetilde{Q}_j)+\mathbf{v}_{\rm tr},\\
&\mathbf{v}_s=\sum_{j=1}^{2}P_j\nabla(Q_j+\widetilde{Q}_j),\\
&\mathbf{w}_{sp}=\nabla Q_3+\nabla\widetilde{Q}_3,\\
&P_1=1, \quad P_2=-\rho_n/\rho_s,
\end{aligned} \tag{2}$$

where Q_1, Q_2, and Q_3 are the velocity potentials for incident waves of first and second sounds and of the longitudinal spin wave respectively, $\widetilde{Q}_1$, $\widetilde{Q}_2$, and $\widetilde{Q}_3$ are the velocity potentials in reflected waves, $\mathbf{v}_{\rm tr}$ is the velocity of th normal component for the viscous wave generated upon reflection, and ρ_n and ρ_s are the densities of the normal and superfluid components.

In order to obtain quantitative relations between the intensities of incident and reflected waves, we write the velocity potentials for these waves in the form

$$\begin{aligned}
&Q_j=c_j\,\exp[i(k_j\,\cos\,\theta_j x+k_j\,\sin\,\theta_j y-\omega t)],\\
&v_{{\rm tr}\,x}=\frac{k_{\eta y}}{k_{\eta x}}\,v_{{\rm tr}\,y},\\
&v_{{\rm tr}\,y}=\widetilde{c}_\eta\,\exp[i(-k_{\eta x}x+k_{\eta y}y-\omega t)],\\
&k_{\eta x}^2=k_\eta^2-k_{\eta y}^2,\\
&\widetilde{Q}_j=\widetilde{c}_j\,\exp[i(-k_j\,\cos\,\theta_j x+k_j\,\sin\,\theta_j y-\omega t)],\\
&(j=1,2,3),
\end{aligned} \tag{3}$$

where c_1, c_2, and c_3 are the amplitudes of incident waves, $\widetilde{c}_1$, $\widetilde{c}_2$, $\widetilde{c}_3$, and $\widetilde{c}_\eta$ the amplitudes of reflected waves, k_1, k_2, k_3, and k_η the corresponding wave vectors of first and second sounds, the longitudinal spin wave, and the viscous wave, θ_1, θ_2, and θ_3 the angles of incidence and reflection of the corresponding waves, and ω the acoustic frequency.

Using the boundary conditions (1) and relations (2) and (3), we determine the ratio of the amplitudes of reflected and incident waves which can be used for finding the reflection coefficients R_{11}, R_{22}, and R_{33} of the first and second sound and of the spin wave respectively as well as the coefficients of mutual transformation of these waves (R_{12}, R_{21}, R_{13}, R_{32}, R_{23}, and R_{31}). These coefficients are defined as the ratio of energy fluxes in the reflected and incident waves normal to the surface:

$$\begin{aligned}
&R_{12}=R_{21}=8\,\frac{\rho_s}{\rho_n}\,\frac{k_1}{k_2}\,\frac{a^2\,\cos\,\theta_1}{(1+a+b+\gamma)^2+(a+b+\gamma)^2};\\
&R_{11}=\frac{(1+b+\gamma-a)^2+(b+\gamma-a)^2}{(1+a+b+\gamma)^2+(a+b+\gamma)^2};\\
&R_{13}=R_{31}=0; \quad R_{23}=R_{32}=0;\\
&R_{22}=\frac{(1+a-b+\gamma)^2+(a-b+\gamma)^2}{(1+a+b+\gamma)^2+(a+b+\gamma)^2};\\
&R_{33}=1,
\end{aligned} \tag{4}$$

where

$$\begin{aligned}
&a=\left(\frac{\rho_n}{2\rho}\right)\lambda_v k_1\,\sin\,\theta_1\,\tan\,\theta_1;\\
&b=\left(\frac{\rho_s}{2\rho}\right)\lambda_v\,\frac{k_1^2}{k_2}\,\sin^2\,\theta_1;\\
&\gamma=(1+P)\xi/(1-P)\lambda_v;
\end{aligned}$$

λ_v is the viscous wave length, and the angles θ_1 and θ_2 are connected through the relation $k_1\,\sin\,\theta_1=k_2\,\sin\,\theta_2$.

It follows from these relations that the longitudinal spin wave experiences total reflection. According to the energy conservation law, the energy absorption coefficients for the first and second sounds are defined as

$$D_1=1-R_{11}-R_{12}; \quad D_2=1-R_{22}-R_{21}.$$

For the angle of incidence

$$\theta_{1\,\max}=\pi/2-(\rho_n/\rho)k_1\lambda_v(\sqrt{2}/2)(1-\gamma),$$

the absorption coefficient for first sound attains its maximum value and then decreases rapidly since $R_1\lambda_v\ll 1$ and $\theta_{1\,\max}$ is close to $\pi/2$. The larger the value of γ, the closer $\theta_{1\,\max}$ to $\pi/2$. The second sound absorption associated with the viscous wave is observed in the angular interval $0<\theta_2<\theta_2'$ $=\arcsin(k_1/k_2)$. For $\theta_2=0$ and $\theta_2>\theta_2'$, total internal reflection of second sound takes place.

In a strong magnetic field H, the A-phase is transformed into the A_1-phase near the transition temperature $T_c\simeq 3$ mK. In order to obtain homogeneous textures of **l** and **s**, the magnetic field must be directed along the wall. In this case, the reflection and transformation of waves at the wall is similar to that in the case of ^{3}He-A with the only exception that, according to hydrodynamic equations,[1] the physical meaning in the case of ^{3}He-A_1 can be attached not to $\mathbf{v}_s$ and $\mathbf{w}_{sp}$ separately, but to the sum $\mathbf{v}_s+\mathbf{w}_{sp}$; besides, superfluid fluxes of mass and spin coincide, and the boundary conditions have the form

$$v_{sx}+w_{spx}=0; \quad v_{nx}=0; \quad v_{ny}=-\frac{1+P}{1-P}\,\xi\,\frac{\partial v_{ny}}{\partial x}, \tag{5}$$

while for the velocities we have

$$\mathbf{v}_n=\sum_{j=1}^{2}\nabla(Q_j+\widetilde{Q}_j)+\dot{\mathbf{v}}_{\rm tr},$$

$$\mathbf{v}_s+\mathbf{w}_{sp}=\sum_{j=1}^{2}P_j\nabla(Q_j+\widetilde{Q}_j), \tag{6}$$

where $P_1=1$ and $P_2=(-\rho_n/\rho_s)$ as before. The index $j=1$ corresponds to first sound, while $j=2$ to the spin–temperature wave. We have taken into account the fact that $M/M_s\ll 1$, where M is the equilibrium longitudinal magnetization and M_s the magnetization of a completely polarized liquid ^{3}He.

For R_{11}, R_{22}, R_{12}, and R_{21}, we obtain the same expressions as (4), but k_2 is the wave vector of the spin–temperature wave.

2. TRANSFORMATION OF SOUNDS IN ^{3}He-*A* AND ^{3}He-A_1 AT THE BOUNDARY WITH A SYSTEM OF PLANE-PARALLEL PERIODIC CAPILLARIES

An analysis of waves propagating in a confined geometry makes it possible to study simultaneously a complex of acoustic processes. An interesting object of investigations in this respect is a system consisting of a porous medium. The model of a porous medium was chosen in the form of identical plane-parallel capillaries of width d, formed by impermeable planes of thickness $D-d$, which are perpendicular to the interface between the free surface and the capillaries filled with superfluid helium.[5] We assume that d is much smaller than the wavelength λ_v and the dipole length ξ_d.

Let us consider the incidence of first and second sounds and of a longitudinal spin wave from the free liquid ^{3}He-*A* on a porous medium filled with the superfluid liquid ^{3}He-*A*. We assume that sound is incident along the normal to the interface ($y=0$) between the free liquid ($x<0$) and the system of capillaries ($x>0$) and propagates along the x-axis. Fourth sound is formed in the capillaries in this case. In addition to acoustic waves uniform in y, nonuniform waves are also excited when a sound wave is incident at the interface with the system of capillaries. Since we consider the system of capillary as a model of a porous medium, the period D of the system of capillaries is much smaller than the characteristic wavelengths:

$$k_1D\ll 1,\quad k_2D\ll,\quad k_3D\ll 1,$$

$$|k_\eta|D\ll 1,\quad k_4D\ll 1,$$

where k_4 is the wave vector of fourth sound. Under these conditions, all nonuniform waves attenuate over distances much shorter than the characteristic wavelengths, and we take into account only uniform waves. The following boundary conditions are observed at the interface between the free liquid and the capillaries: the heat flux continuity, the continuity of the normal component of the total mass flux, the continuity of magnetization flux, the continuity of chemical potential which is the potential of the retrieving force $\mathbf{v}_s$, and the continuity of the similar quantity for $\mathbf{w}_{sp}$, which is equal to $(M_s/\rho)h$, where h is the internal magnetic field. Consequently, the boundary conditions for ^{3}He-*A* can be written in the form

$$\begin{aligned}
&v_{nx}(x<0)=0,\\
&Dv_{sx}(x<0)=dv_{sx}(x>0),\\
&Dw_{spx}(x<0)=dw_{spx}(x>0),\\
&\mu(x<0)=\mu(x>0),\\
&\frac{M_s}{\rho}\,h(x<0)=\frac{M_s}{\rho}\,h(x>0).
\end{aligned} \tag{7}$$

while for oscillating quantities we have

$$\vec{v}_n(x<0)=\sum_{j=1}^{2}\nabla(Q_j+\widetilde{Q}_j),$$

$$\vec{v}_s(x<0)=\sum_{j=1}^{2}P_j(Q_j+\widetilde{Q}_j),$$

$$\vec{w}_{sp}(x<0)=\nabla Q_3+\nabla\widetilde{Q}_3,$$

$$\mu(x<0)=i\omega\sum_{j=1}^{2}P_j(Q_j+\widetilde{Q}_j),$$

$$\frac{M_s}{\rho}\,h(x<0)=i\omega(Q_3+\widetilde{Q}_3),\quad \vec{v}_s(x>0)=\nabla Q_4',$$

$$\vec{w}_{sp}(x<0)=\nabla\widetilde{Q}_3,\quad \mu(x>0)=i\omega Q_4',$$

$$\frac{M_s}{\rho}\,h(x>0)=i\omega Q_3', \tag{8}$$

where Q_j and $\widetilde{Q}_j$ are the potentials of the velocities of incident and reflected waves, Q_4' is the potential of superfluid velocity of fourth sound excited in capillaries, and Q_3' the potential of the spin superfluid velocity of the longitudinal spin wave excited in the capillaries. These potentials have the form

$$\begin{aligned}
&Q_j=c_j\,\exp[i(k_jx-\omega t)],\\
&\widetilde{Q}_j=\widetilde{c}_j\,\exp[i(-k_jx-\omega t)],\quad j=1,2,3,\\
&Q_3'=c_3'\,\exp[i(k_3x-\omega t)],\\
&Q_4'=c_4'\,\exp[i(k_4x-\omega t)].
\end{aligned} \tag{9}$$

Using relations (7)–(9), we can find the ratio of the amplitudes of the reflected wave and the wave excited in the capillaries. Then we can determine the coefficients A_1 and A_2 of excitation of fourth sound by first and second sounds, respectively as well as the coefficient A_3 of excitation of the longitudinal spin wave by another spin wave:

$$\begin{aligned}
&A_1=4\frac{d}{D}\sqrt{\rho_s/\rho}\left(1+\frac{d}{D}\sqrt{\rho_s/\rho}\right)^{-2};\\
&A_2=\frac{\rho_n}{\rho_s}\frac{k_1}{k_2}A_1;\\
&A_3=4\frac{d}{D}\left(1+\frac{d}{D}\right)^{-2}.
\end{aligned} \tag{10}$$

We can also calculate the reflection coefficients R_{11} and R_{22} for first and second sounds and R_{33} for a longitudinal spin wave:

$$R_{11}=1-A_1,$$

$$R_{22}=1-\frac{\rho_n}{\rho_s}\frac{k_1}{k_2}A_1\left(1+\frac{d}{D}\sqrt{\rho_s/\rho}\right); \tag{11}$$

$$R_{33}=\frac{(1-d/D)^2}{(1+d/D)^2}.$$

The coefficients R_{12} of transformation of first sound into second and R_{21} of transformation of second sound into first can be written in the form

$$R_{12}=R_{21}=4\left(\frac{d}{D}\right)^2\frac{k_1}{k_2}\frac{\rho_n}{\rho}\left(1+\frac{d}{D}\sqrt{\rho_s/\rho}\right)^{-2}. \tag{12}$$

As in the case of reflection of sounds at a solid wall, a longitudinal spin wave is not mixed with other waves. In contrast to analogous problem for HeII,[5] we obtained the values for A_3 and R_{33}.

Analyzing similarly the reflection of fourth sound at the interface between the system of capillaries filled with superfluid helium and the free liquid, the excitation of first and second sounds by fourth sound in free helium, and the reflection of a spin wave, we find that

$$R_1=R_{11};\quad F_1=A_1;\quad F_2=A_2;$$

$$F_3=A_3;\quad R_2=R_{33}, \tag{13}$$

where R_1 and R_2 are the reflection coefficients of fourth sound and of the longitudinal spin wave at the end of a capillary, F_1 and F_2 are the coefficients of excitation of first and second sounds by fourth sound, and F_3 the coefficient of excitation of a longitudinal spin wave in free helium by the same wave in a capillary.

It is also interesting to consider the reflection and transformation of acoustic waves in the case of superfluid ^{3}He-A_1. The boundary conditions in ^{3}He-A_1 are imposed not on $\mathbf{v}_s$, μ, $\mathbf{w}_{sp}$, and $(M_s/\rho)h$ separately, but on $\mathbf{v}_s+\mathbf{w}_{sp}$ and $\mu+(M_s/\rho)h$. The number of these conditions is reduced to three since we have the potentials of the velocities of first sound, spin–temperature wave, and magnetoacoustic wave. The expressions for A_1, A_2, R_{11}, R_{22}, R_{12}, and R_{21} remain the same as for superfluid ^{3}He-A, but the index ''2'' now corresponds to a spin–temperature wave.

Our calculations were made for homogeneous textures of **l** and **s** in an unbounded volume of helium in capillaries. Naturally, these conditions are observed for $D-d\ll d$. We believe that the results obtained by us are valid for any values of d and D (for D much smaller than the characteristic wavelengths). Naturally, the homogeneity of a texture will be violated near the boundary at a distance much smaller than the acoustic wavelengths, but this inhomogeneity should not affect the results of calculations.

[1] G. E. Baramidze, G. E. Gurgenishvili, and G. A. Kharadze, Fiz. Nizk. Temp. **9**, 122 (1983) [Sov. J. Low Temp. Phys. **9**, 60 (1983)].

[2] G. E. Volovik, Usp. Fiz. Nauk **143**, 73 (1984) [Sov. Phys. Uspekhi **27**, 363 (1984)].

[3] Sh. E. Kekutiya, D. G. Sanikidze, and N. D. Chkhaidze, Fiz. Nizk. Temp. **11**, 1127 (1985) [Sov. J. Low Temp. Phys. **11**, 619 (1985)].

[4] Sh. E. Kekutiya and D. G. Sanikidze, Fiz. Nizk. Temp. **11**, 572 (1985) [Sov. J. Low Temp. Phys. **11**, 312 (1985)].

[5] M. I. Kaganov, D. G. Sanikidze, O. G. Tkeshelashvili, and V. Ya. Yampol'skii, Zh. Éksp. Teor. Fiz. **59**, 812 (1970) [Sov. Phys. JETP **32**, 445 (1970)].

Translated by R. S. Wadhwa